A detailed study of streamer chambers

J. A. Lightfoot

Lightfoot, J. A. (1972) A detailed study of streamer chambers. Doctoral thesis, Durham University.

A DETAILED STUDY OF STREAMER CHAMBERS

by

J.A. LIGHTFOOT B.Sc.

A THESIS SUBMITTED TO THE UNIVERSITY OF DURHAM
FOR THE DEGREE OF DOCTOR OF PHILOSOPHY

BEING AN ACCOUNT OF WORK CARRIED OUT IN THE
UNIVERSITY OF DURHAM DURING THE PERIOD
OCTOBER 1969 to SEPTEMBER 1972

OCTOBER 1972

CONTENTS

ABSTRACT

This theis describes the construction and operation of a neon helium streamer chamber. The design of a fast high voltage pulsing system, which utilises the energy stored in a water dielectric capacitor and has been charged by a Marx generator, is discussed in detail.

The performance of the system is examined and its characteristics are investigated particularly where they are relevant to its use as a particle detector. A statistical model has been programmed and is used to predict and interpret the results obtained directly from the streamer chamber. The agreement between theory and practice is found to be good.

The spacial accuracy of the device is measured and its resolution estimated. No significant sensitivity to ionisation has been found but a time resolution of less than 1 μsec appears feasible.

Suggestions to improve the streamer chamber system are made and proposals for a second generation streamer chamber are given.

CHAPTER ONE

INTRODUCTION

Particle detectors which rely on the principle of a gaseous discharge for their operation form a range of instruments which find application in every branch of radiation physics. They fall into two main subdivisions but in all cases consist essentially of a volume of gas to which an electric field may be applied.

The constituents of the gas and the variation of the applied field both spatially throughout the gas and temporarily decide the nature of the detector.

1.1. Primary Detectors

Primary detectors are capable of responding independently to a particle which traverses their sensitive volume. The simplest type is the ionisation chamber in which the electron-ion pairs, created by the particle to be detected, are swept out of the volume of the detector by a clearing field of a few volts per centimetre and the ionisation current is measured directly.

If the applied field is increased, usually by making the anode from a fine wire or system of wires, then a controlled amount of gas amplification may take place and a current pulse, with its height proportional to the initial ionisation density, is produced. Although proportional counters have been known for many years, interest in this type of detector has been revived by the development of multiwire proportional chambers (1).

Increasing the field still further leads to breakdown of the gas around the anode. This propagates by ultra violet ionisation along the wire. The output pulses lose their proportionality but may be of several tens of volts and can be handled by very simple electronics. These Geiger counters have been perhaps the most important of all detectors until recently superceded by the scintillation counter.

1.2. Secondary Detectors

The secondary detectors to which the streamer chamber is the latest edition are incapable of detecting particles without first being triggered by a primary detector. The most significant difference between the two groups of detectors is that the electric field applied to the sensitive volume of a secondary detector is in the form of a pulse. The characteristics of the detector are decided principally by the amplitude and duration of this pulse and by the geometry of the electrodes.

In 1957 Cranshaw and de Beer (2) applied 7kV pulses of 1μ sec duration to a pair of parallel plate electrodes separated by 1 mm of air at NTP. If the pulse was applied within a few microseconds of the passage of an ionising particle through the plates, then a spark formed at the point of passage. Such a spark chamber is capable of fixing the coordinates of a particles trajectory in two dimensions to within 1 mm and the third may be found by using a stack of several chambers.

One significant advance since this prototype has been the use of noble gas fillings to replace the air. Neon is the most popular gas and has a breakdown voltage of only ~ 1.5 kV/cm. Chambers with interelectrode gaps of 1 cm may be constructed and driven by pulses of only 4 to 5 kV. The total ionisation produced in such a chamber by a minimum ionising particle is about 30 cm^{-1} which contributes to the high efficiency of such devices and the discharges produced have a usefully high visible light output. Helium has many of the electrical advantages of neon and is much cheaper but the ionisation density produced in it is about five times less than in neon. The manufacturing process of neon is such that a mixture of 70% neon and 30% helium is the most readily produced and it is this gas which is most used in spark chambers.

Several types of spark chamber have evolved from this basic form. These are summarised in Figure 1.1. Part a) of this figure shows the

(a) SPARK CHAMBER

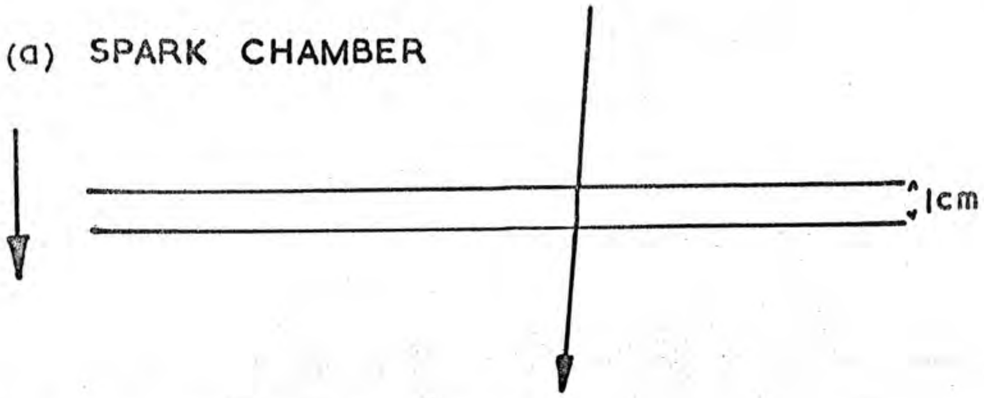

(b) WIDE GAP CHAMBER

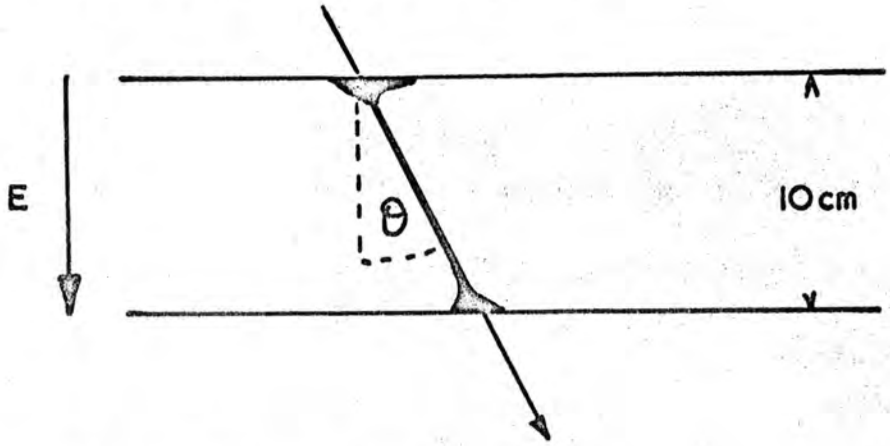

(c) PROJECTION CHAMBER

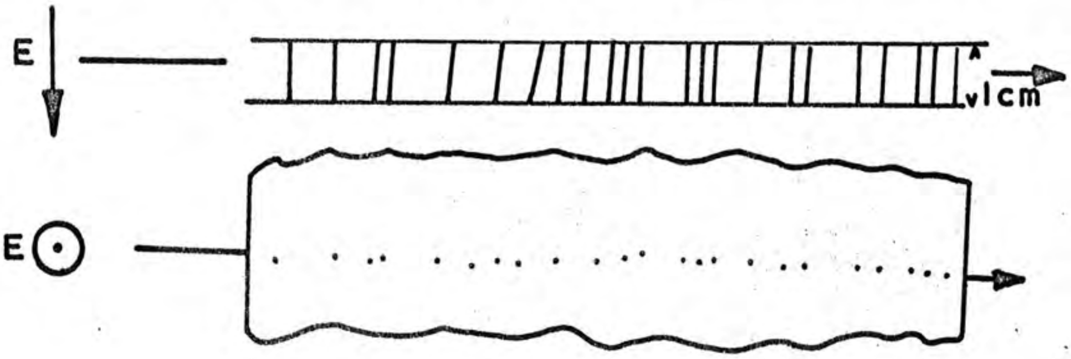

(d) STREAMER CHAMBER

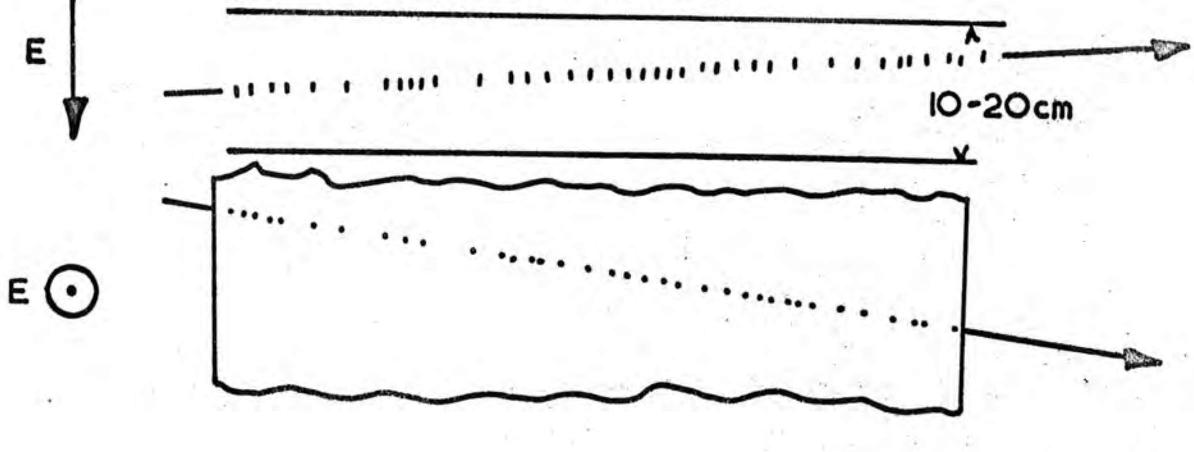

Figure 1.1

simple form described above. There are several ways of extracting the coordinates of the spark from such a chamber. The most obvious way is to photograph the spark but each frame must be analysed by hand at a later date. For real time analysis an on-line system is essential and may be of the closed circuit television type (3) the sonic type (4) or, as is more often the case in recent years, the magnetostrictive type (5). In the latter the electrodes are in the form of parallel wires about 1 mm apart. The spark causes a high current to be drawn along a pair of wires which induces a magnetostriction in a magnetostrictive wand placed under the ends of the wires..The constriction travels along the wand with the velocity of sound and its transit time is a measure of the coordinates of the wire.

If the gap between the electrodes of a conventional parallel plate spark chamber is increased to more than 10cm and the amplitude of the high voltage pulse is also increased to maintain the same field in the gas, information concerning the third coordinate of the particle's trajectory may be extracted (6). This device is known as the track spark chamber,Figure 1.1b. For angles θ less than about 45° the line of the spark will follow the trajectory of the particle but for angles greater than this the discharge breaks up into several sparks and the information is lost.

In the projection chamber Fig. 1.1c the electrode spacing is again about 1 cm but the particles are allowed to traverse the chamber at right angles to the applied field (7). A series of sparks form along the particle trajectory,each starting from a different group of electrons. The track is displayed in a two dimensional projection and yields a greater track length than a simple spark chamber of similar size but the acceptance of the device is much lower and a stack of chambers must again be used to produce three dimensional information. As many sparks are produced in a single chamber along one particle track, the projection chamber must have a high multi-track efficiency. This is achieved by insulating the gas, and hence the sparks, from the electrodes and so preventing the removal of the high voltage pulse by the first spark to cross the gap. In this chamber the electrodes must be made transparent, either by making them from closely spaced wires or a conducting thin film, to allow photography of the projected image.

The streamer chamber combines many of the features of the track and projection chamber. The electrode spacing is usually between 5 and 30 cms and the gas is enclosed in a transparent box placed between them. Particles are allowed to traverse the box in any direction as the streamers chamber is a true three dimensional track locator. Within a few microseconds of an event an electric field is applied to the gas but is removed after only 10 to 20 nsec while the discharges are only a few millimetres long and have not crossed the gap between the electrodes. The resultant track Figure 1.1d is seen as a series of streaks looking perpendicular to the line of the applied field and as a series of dots looking parallel to the field. Such a detector was first constructed by Chikovani (8) (and Dolgoshein (9)) who applied pulses of 200kV to a box measuring 100 x 100 x 19cm which contained neon at NTP. The pulse lasted about 40nsec and produced photographable streamers about 1 cm long.

Since then the development of streamer chambers has taken two main paths. The first of these is that followed by the large accelerator groups. These are intended primarily as replacements for the bubble chamber,tend to be large, complex and expensive and are used mainly for track location (10)(11). The high voltage pulse necessary to power such chambers is normally produced by a Blumlein line which has been pulse-charged from a Marx generator.

The second path has been towards much smaller devices driven by fast-discharge Marx generators (12). The streamers produced in these chambers are usually much shorter, and hence less bright, than those produced in the larger chambers and must be photographed via an image intensifier. Such chambers can be used to study the streamers themselves and the characteristics of particles other than their location, for example their ionisation. The considerable differences in size and photographic technique between the two types of chamber make the extrapolation of data, concerning the properties of streamers and particle tracks, from the smaller to the larger systems difficult and often inaccurate.

The streamer chamber which is the subject of this thesis was intended to bridge the gap between the two lines of development. As this was the first streamer chamber to be built within the department it was decided to use a neon helium gas mixture first, as many of its parameters are well known, and to use the information gained to proceed to more sophisticated systems and more complex gas mixtures in the future. This thesis describes the design, construction and performance of this first streamer chamber. Its size was chosen for it to be useful not only as a track detector for cosmic rays, with which the development is closely associated, but also as an instrument which would yield information concerning the formation of streamers along the trajectory of particles, in particular where it is relevant to its role as a detector. Efforts were made to reduce the size and complexity of the pulsing system and to develop an instrument which is both straight forward and reliable.

REFERENCES

1. CHARPAK, G. Nuc. Inst. Methods 62 (1968) 262.
2. CRANSHAW, T.E and de BEER J.F., Il Nuovo Cimento 5 (1957) 1107.
3. RUTHERGLEN, J.G. and PATERSON, J.M., Proc. Symp. Nuc. Inst. Harwell 1961.
4. BELETINI G., CERN 65-33.
5. GIANELLI, G., Nuc. Inst. Methods 31 (1964) 29.
6. CHARPAK, G., J. Phys. Rad. 18 (1957) 539.
7. FUKUI S. and MIYAMOTO, S., J. Phys. Soc. Japan 16 (1961) 2574.
8. CHIKOVANI, G.E., Nuc. Inst. Methods 29 (1964) 261.
9. DOLGOSHEIN, B.A., Nuc. Inst. Methods 29 (1964) 1970.
10. ECKARDT, V., and LADAGE, A., Proc. Int. Symp on Nuc. Elect. Versailles 1968 6 III p 10.1.
11 BULOS, F, SLAC 74 (1967)
12. GYGI, E. and SCHNEIDER, F. CERN 64-46.

CHAPTER TWO

THEORETICAL DESIGN

2.1 Introduction

Having decided to construct a neon helium streamer chamber the requirements of such a system must be evaluated. In the following chapter its mode of operation and the theoretical design of the relevant component parts is described.

2.2 The Basic Breakdown Process

To decide the duration and amplitude of the high voltage pulse which will drive a streamer chamber it is necessary to consider the processes involved in streamer generation (1), (2). Consider an electron in a volume of neon gas at NTP. Kinetic theory has shown that it is colliding with the neon atoms with a frequency of about 10^{13} collisions/second and moves with an average random velocity of about 10^{7} cm/sec. If an electric field is now applied to the gas the electron will acquire a drift component to its velocity towards the anode. If the field is large enough for the electron to aqquire sufficient energy from the field between collisions to ionise a neon atom then the number of electrons will increase. This increase is described by Townsend's first ionisation coefficient α , defined as the mean number of ion pairs created by one electron per centimeter of its path travelled in the direction of the field. Thus the number of electrons n grows as

$$n = \exp(\alpha x) = \exp(\alpha v t) \qquad 2.1$$

where x is the drift distance of the electron in the direction of the field, v is the drift velocity of the electron ($\sim 10^{7}$ cm/sec) and t is time. The values of α for both neon and helium are strong functions of field and are shown in Figure 2.1 and Figure 2.2 (3), (4). During this process (n-1) positive ions are produced which drift towards the cathode but with a velocity which is typically 10^{3} times slower than that of the electrons. Because of the short times involved in streamer generation, <20n sec, the positive ions will be considered stationary.

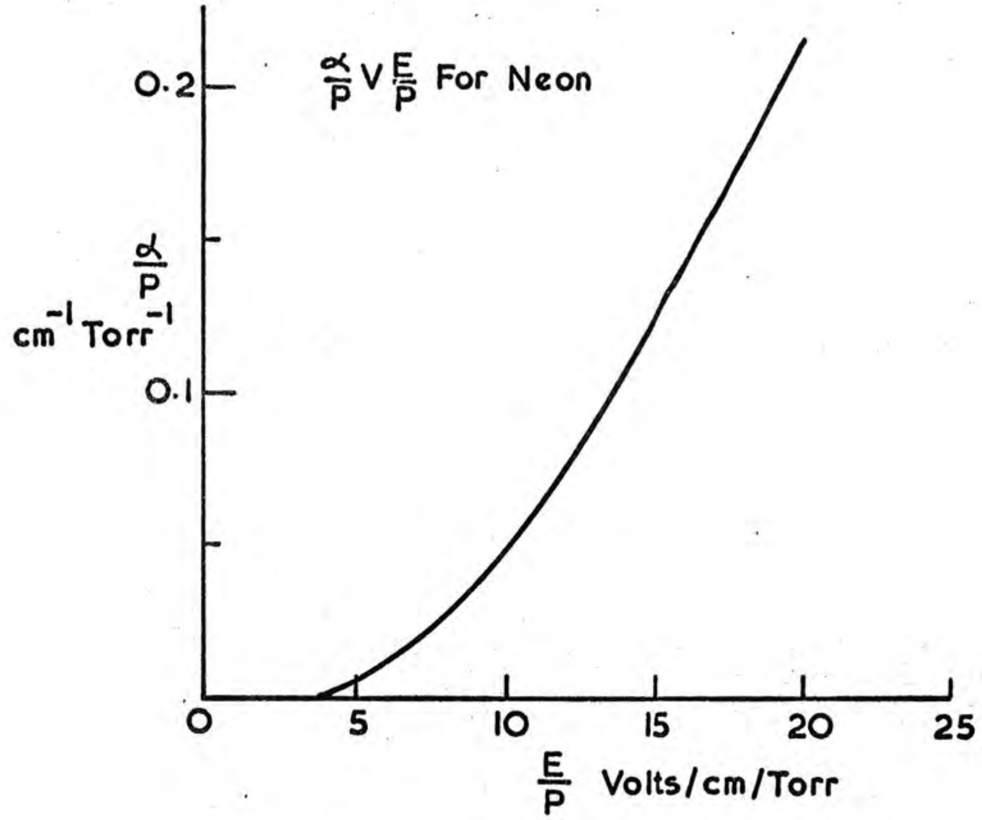

Figure 2.1

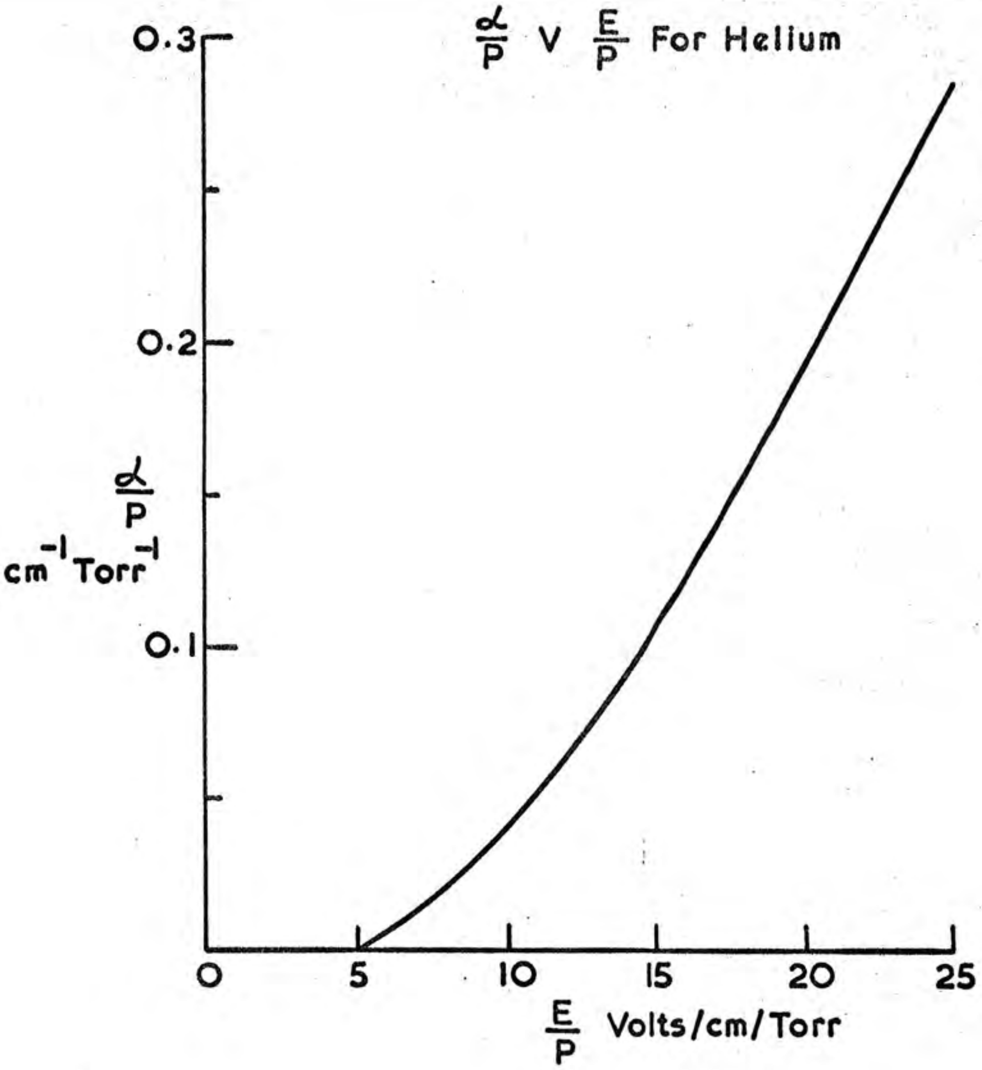

Figure 2.2

Thus the positive ions create a space charge behind the advancing electron avalanche.

As the electron cloud grows it also diffuses radially outward and 85% of the electrons can be shown to be contained within a sphere of radius r where

$$r = \sqrt{4Dt} \qquad 2.2$$

D is the diffusion constant for electrons in neon and has been shown to be 1800 cm^2/sec for zero field (1), (2) and this time. When the distance drifted by the avalanche approaches 1 mm, which occurs in <10 nsec for neon at NTP and applied fields of 20 kV/cm, the number of electrons approaches 10^8. At this point the magnitude of the field at the surface of the avalanche due to the electrons is of the same order as that of the applied field and constitutes the end of the avalanche phase of the discharge. The distance drifted by the electrons at this stage L_m is known as the Meek length, (5).

During the avalanche growth photons are produced from atoms which have been excited rather than ionised by the drifting electrons. Raather (1) has shown that the number of photons emitted by an avalanche is approximately equal to the number of electrons contained therein. Therefore 10^8 photons may be expected from an avalanche which has attained the Meek length. This is too few to permit conventional photography and so the discharge must be allowed to continue further.

The separation of the electrons from the positive ions produces a region of reduced field between them which retards the discharge, however a complementary region of high field is produced immediately in front of and behind the avalanche. The experiments of Mohler (20) and the theory of Lozanskii (21) have shown that ionisation may be produced by photons from an avalanche in the surrounding gas. Electrons which are produced in the high field region will multiply rapidly by collision and the photon flux will increase thus causing a rapid increase in the velocity of the discharge which now progresses towards both anode and cathode. This is known as the streamer mechanism. Figure 2.3 and

Figure 2.4 show the velocity of such streamers in neon as a function of applied field and streamer length obtained by Davidenko et al. (6), using an image intensifier and high speed photography. As the number of electrons contained in, and hence the number of photons emitted by, a streamer which is a few millimeters long is 10^2 to 10^3 times that of an avalanche, photography of such streamers is possible using conventional high speed film. Davidenko et al. have also shown (7) that in neon at 600 Torr and for an applied field of 10 kV/cm the brightness of a streamer is an increasing exponential function of streamer length. Also (8) for fixed streamer length the brightness increases with field in the range 10-20 kV/cm for neon 70%, helium 30% at 760 Torr. Hence for bright streamers which are short enough to permit accurate track location pulsed fields of 15-20 kV/cm and of < 20 nsec duration are required.

2.3 Linear Field Production

For reasons of convenience and availability the streamer chamber system was designed around a pair of sealed glass boxes containing 98% neon and 2% helium at 760 Torr. These measured 60x60x12.5 cm and were manufactured by the International Research and Development Company Limited of Newcastle upon Tyne, U.K. Chambers made from other materials but of the same dimensions were also investigated and will be described in detail in Chapter 3.

The two chambers are mounted on either side of a central high voltage electrode and between a pair of earth electrodes which are joined on two opposite sides to give a pseudo coaxial geometry, Figure 2.5. The advantages of this type of electrode system are:-

a) It doubles the effective gap width which can be driven by a given high voltage pulse.

b) It reduces the r.f. radiation from the device.

c) It improves the safety of the device by totally enclosing the high voltage electrode.

VELOCITY OF STREAMER (v) OF LENGTH 4.5mm AS A FUNCTION OF ELECTRIC FIELD IN NEON

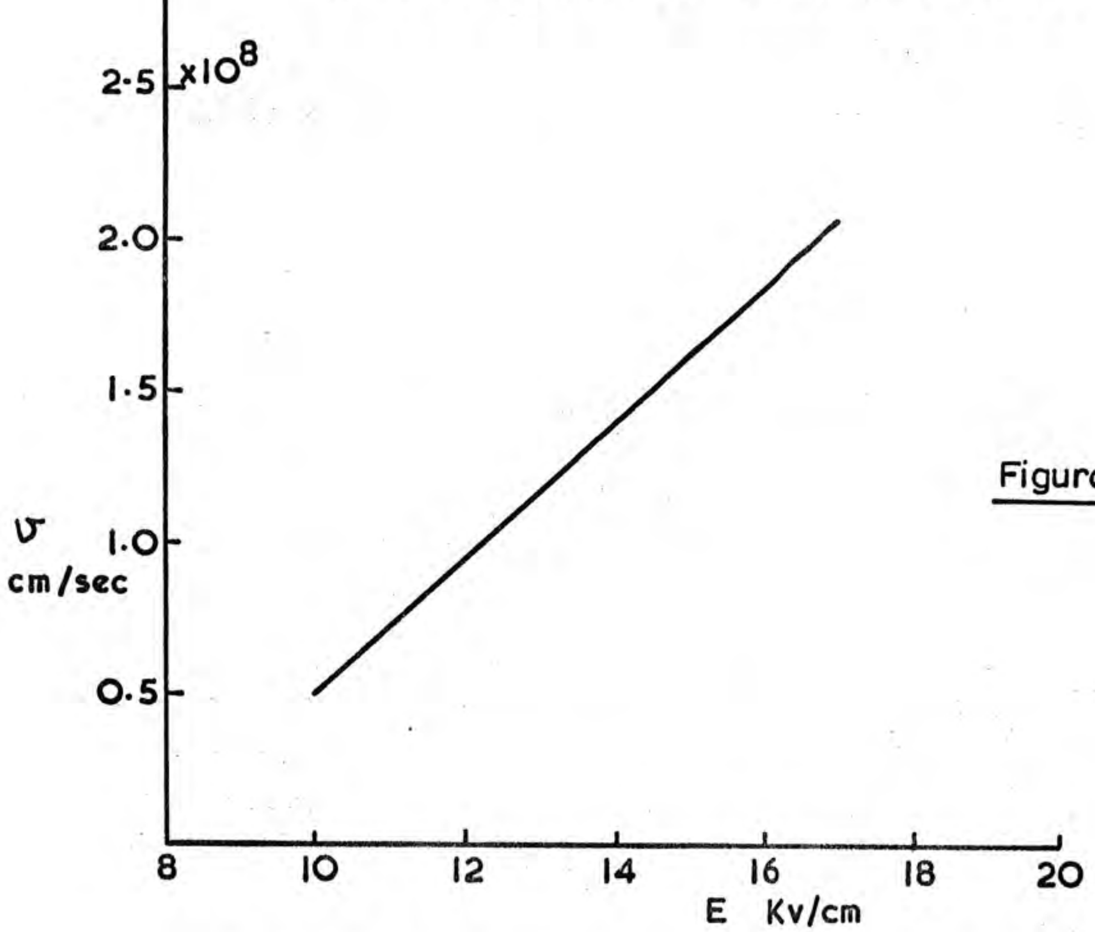

Figure 2.3

VELOCITY OF DIRECT (v^+) AND REVERSE (v^-) STREAMER AS A FUNCTION OF LENGTH IN NEON

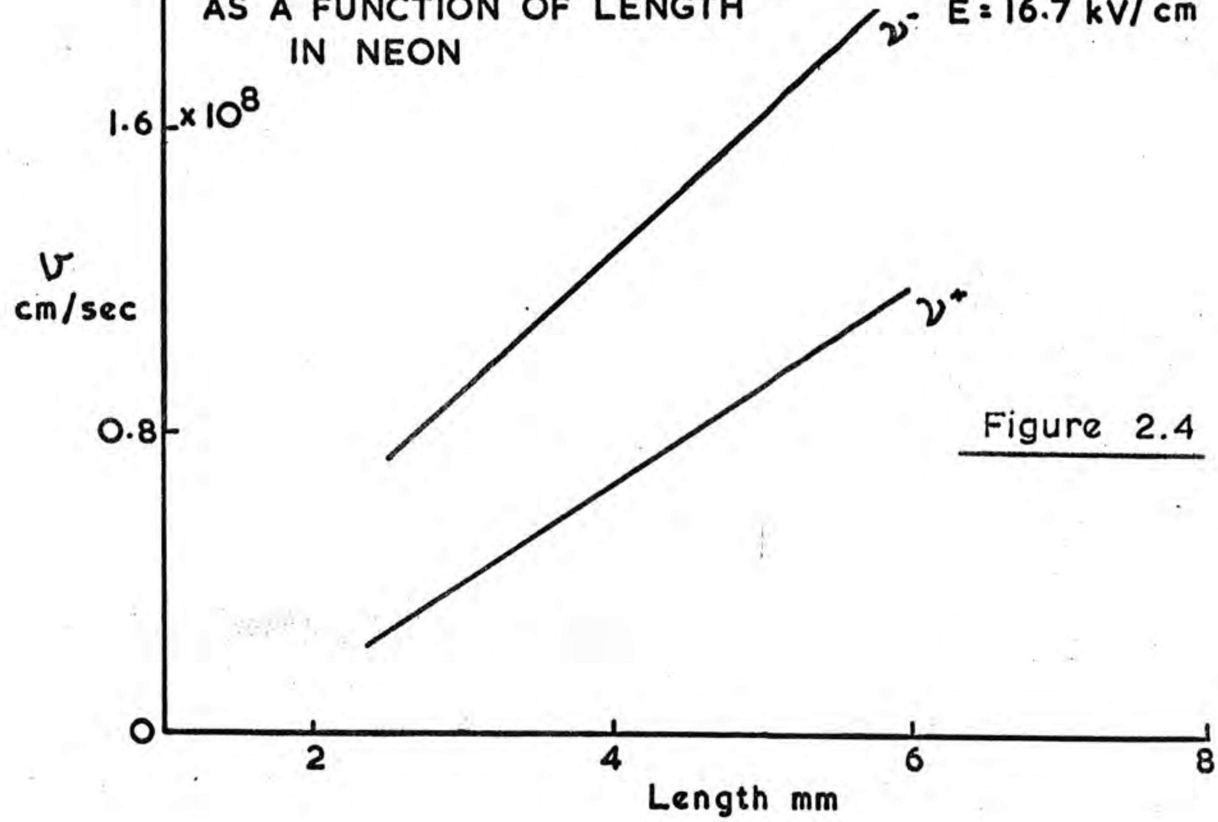

Figure 2.4

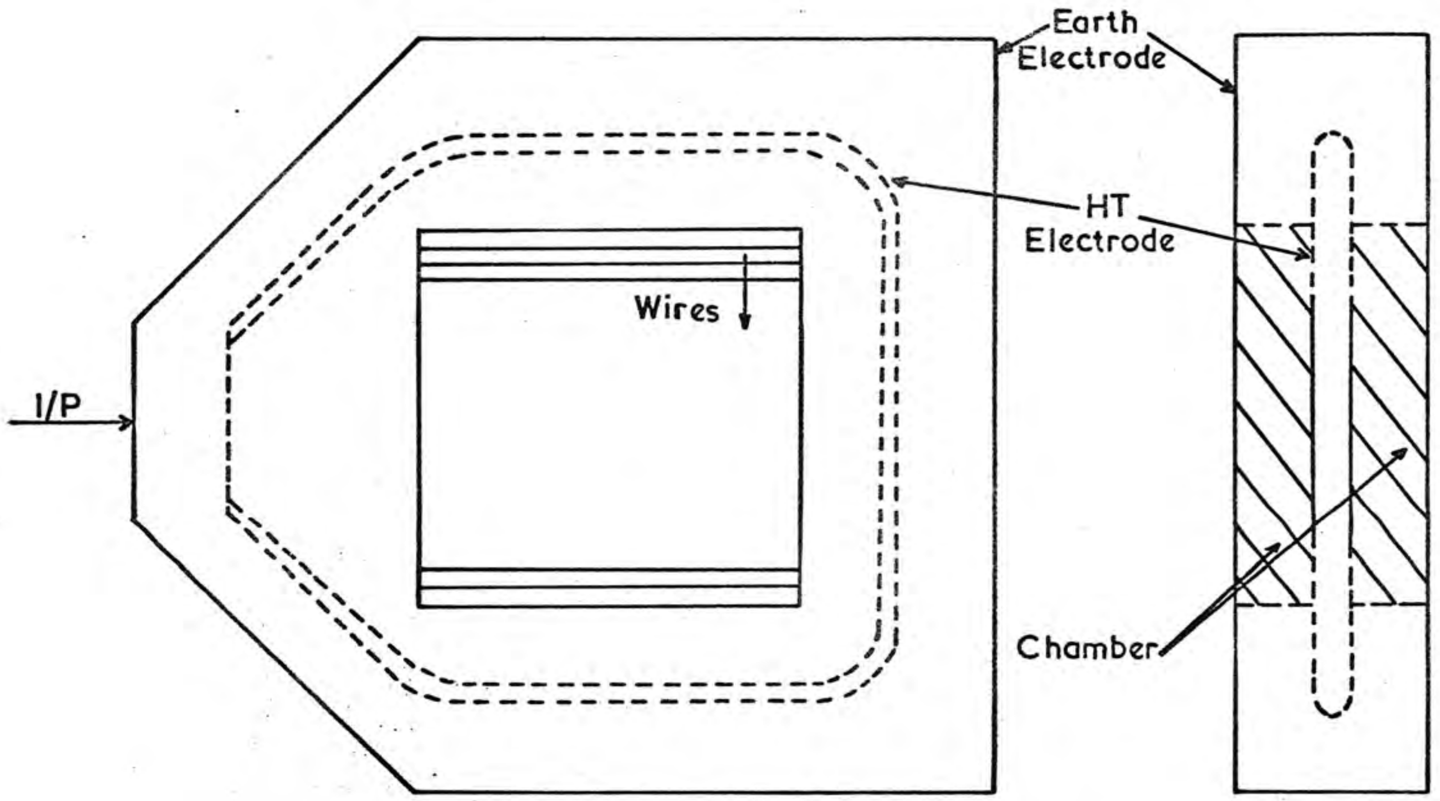

Figure 2.5 THE ELECTRODE STRUCTURE

d) It improves the linearity of the field near the edges of the electrodes.

However the electrode capacity is greater and the characteristic impedance less for this geometry than for chambers mounted side by side and hence require a lower impedance source for the high voltage pulse.

To facilitate easy manipulation of the chambers and to avoid contact of the electrodes with the chamber walls an electrode spacing of 15 cm was chosen. As the streamer velocity is a strong function of field, Figure 2.3, there must be a constant field throughout the volume of the chamber if isotropic sensitivity is to be achieved. Distortions of the field near the edges of the electrode structure make it necessary to extend the straight part of the electrodes beyond the chamber edges. The degree of extension necessary was determined by the method of numerical relaxation and Poissons equation was solved for this geometry and the potential distribution within the interelectrode gap obtained. The basis of this method is outlined in Appendix A. For this method to succeed the area for which the solution is required must be bound either by a line of known potential or a line of symmetry. Therefore, it was assumed that the field would become linear provided the straight region of the electrodes is extended far enough. The potential distribution is shown in Figure 2.6 and is normalised to a maximum of 100. For an electrode spacing of 15 cms and an overlap of the earth electrode of 15 cm the field is linear to within the limits of the calculation ($< 2\%$) 16 cms from the end of the high voltage electrode. The linearity of the field is also improved by the fitting of a corona guard to the edge of the high voltage electrode (Chapter 3) but it was not possible to take account of this using the above method.

To permit photography of the streamers in a direction parallel to the field the region of the electrodes covering the chambers must be transparent. This can be done by making electrodes of wires or meshes in this region or by coating the surface of the chambers with a transparent conducting film.

POTENTIAL DISTRIBUTION INSIDE THE ELECTRODE STRUCTURE

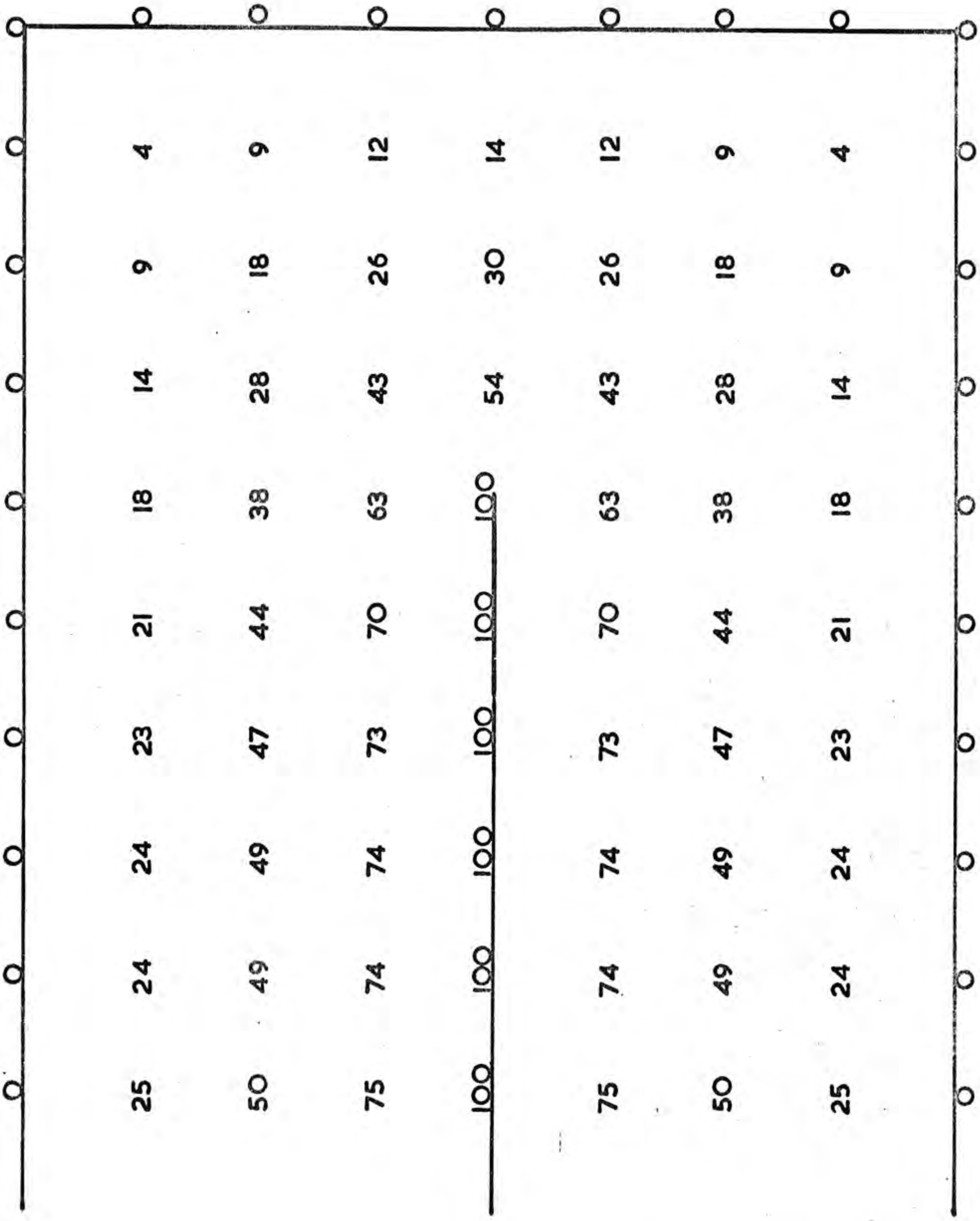

0	0	0	0	0	0	0	0	0
0	4	9	12	14	12	9	4	0
0	9	18	26	30	26	18	9	0
0	14	28	43	54	43	28	14	0
0	18	38	63	100	63	38	18	0
0	21	44	70	100	70	44	21	0
0	23	47	73	100	73	47	23	0
0	24	49	74	100	74	49	24	0
0	24	49	74	100	74	49	24	0
0	25	50	75	100	75	50	25	0

Figure 2.6

Wires were chosen for this purpose as they are of low cost and can easily be replaced when damaged.

The distortion of the potential distribution produced by a system of infinitely fine wires placed symmetrically between two earthed planes and separated from each other by 0.08 of the distance to the earth planes is shown in Figure 2.7. The potential on the wires is normalised to 1000. The potential distribution is seen to have relaxed to within 0.1% of that which would be produced by a plane electrode two wire spacings into the gap. As the wire used was of finite diameter and the ratio of wire spacing to gap width was 0.066, the distortion of the field produced by the wires is considered to be even less than that shown in Figure 2.7.

It can be seen from Figure 2.5 that the electrodes are tapered toward the input end. This is to improve the impedance match with the high voltage pulse generator and to ensure an isotropic distribution of the pulse. The angle of taper is 45^0 and is the smallest angle which can be accomodated in the available space. The resultant electrode is 180cms long, 120 cm high and 30 cms deep. The characteristic impedance of such a structure as given by the 'radio formulae' (9) is $30\,\Omega$ and its capacity is 200pf. As the pulse transit time of the electrodes, ~ 8nsec, is comparable with the applied pulse length they should exhibit both the properties of a transmission line and a capacity. In practice the latter was found to be the dominant parameter.

2.4 The High Voltage Source

With an interelectrode gap of 15 cms and a required field of up to 20 kV/cm a high voltage pulse of between 250 and 300 kV. is required. Sources of direct current at such amplitudes have been used to power pulsing systems (3), (10), but these tend to be large and expensive and were considered unsuitable in this case. The most convenient way of generating high voltages when the output is required in the form of a pulse is the Marx generator (11), (12), (13).

Figure 2.8a shows a simple three stage Marx generator. A number,

POTENTIAL DISTRIBUTION AROUND A WIRE ELECTRODE

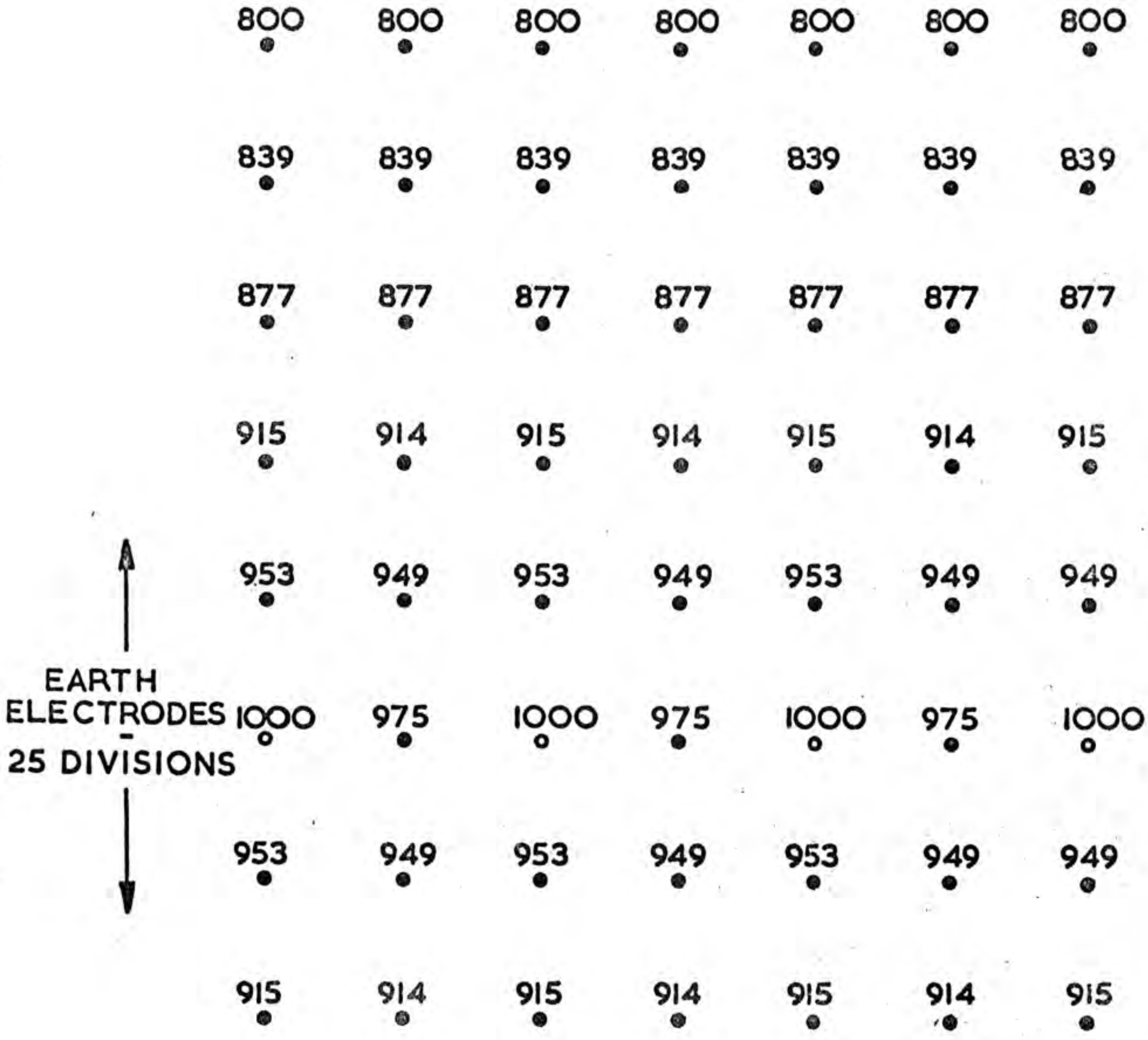

Figure 2.7

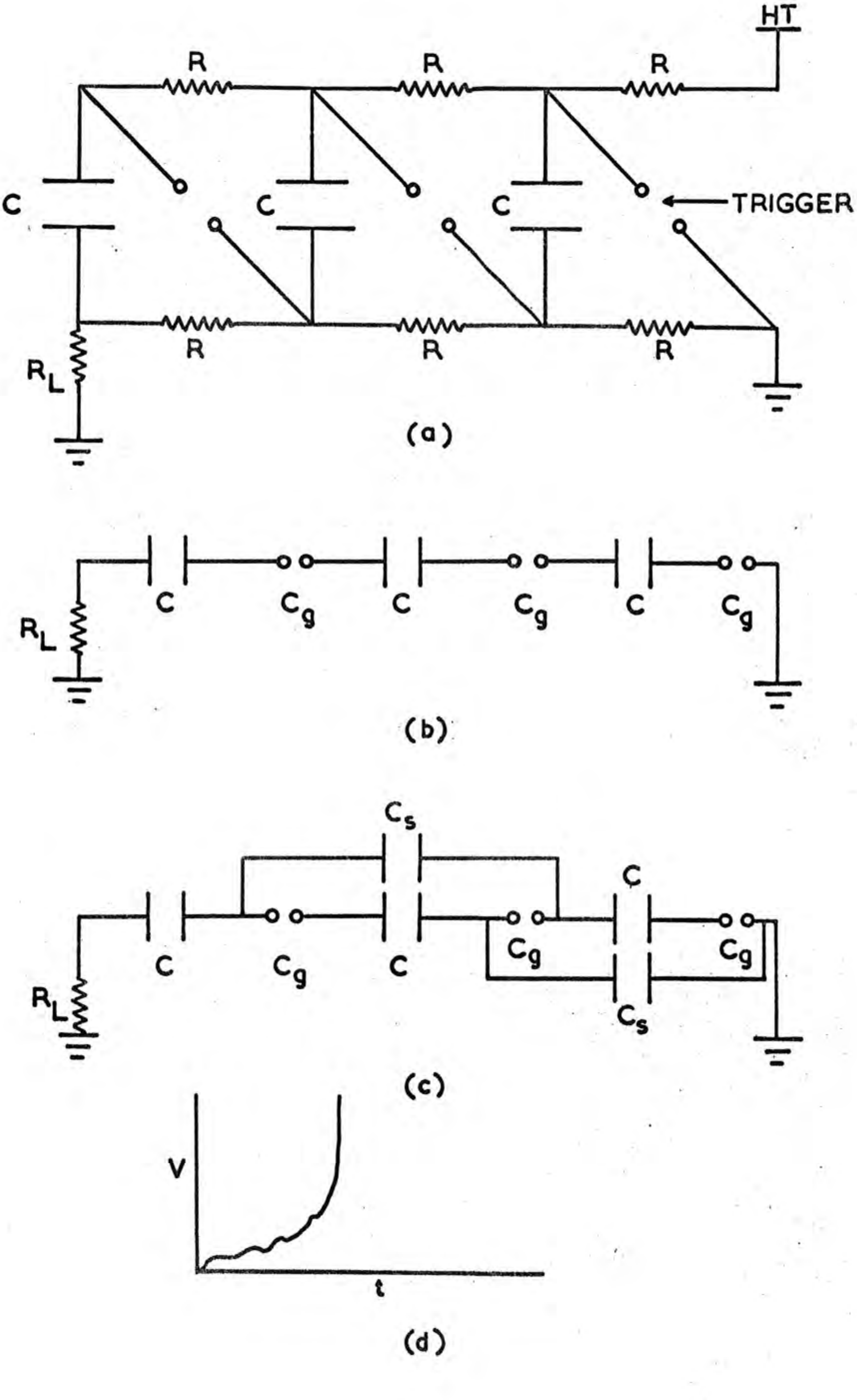

Figure 2.8 MARX GENERATOR OPERATION

n, of capacitors, C, are charged in parallel to a high voltage, U, via a chain of resistors R. By means of a series of switches, usually spark gaps, the capacitors are connected rapidly from parallel to series thus causing an output pulse of amplitude nU to be produced across the load R_L Figure 2.8b. Similarly the output capacity of the circuit is C/n. The operation mechanism is as follows:-

If the first switch is close by a trigger pulse a step pulse of amplitude U is applied across the remaining elements of the circuit and a pulse appears at the output with a decay time $\tau = R_L \frac{C_g}{n-1}$ where C_g is the capacity of one spark gap. This discharges the condensers C by a small amount and charges the remaining n-1 spark gap capacities by about $\frac{U}{n-1}$. Similarly if the first two gaps are triggered then the over voltage is about $\frac{2U}{n-1}$. Thus when only a few of the gaps of a generator with large number of stages have broken down, the over voltage of the remaining gaps will be small, and for large R_L, will take a long time to develop and the generator may even fail to operate. As more gaps breakdown the over voltage on the remaining gaps increases and the output voltage V increases accordingly Figure 2.8d. The introduction of coupling capacitors C_s Figure 2.8c, or resistors (14), produces a low impedance discharge path which allows the over voltage of the second gap by 100%, independantly of the number of stages if the first gap is broken down. For successful operation the condition $C_g \ll C_s \ll C$ must be satisfied. If the discharge is to proceed in an over volted gap an electron must be present in the high field region between the electrodes. Such electrons can be produced if the spark gaps are placed in line of sight allowing photoelectrons to be released from the electrode by ultra-violet photons from the gaps which have already fired. In very fast generators, where the transit time of the light is significant, electrons can be supplied by a corona discharge from a third sharply pointed electrode placed perpendicular to the line of the spark and maintained at a high voltage, usually about half that across the gap. Marx generators of this type have been used to drive streamer chambers directly (13, (15), however in order to obtain very short pulses the generator must be of small physical dimensions. This leads to a low output capacity and such generators are suitable for driving a high characteristic impedance (>100Ω) or low capacity. In order to drive the 30Ω electrodes described in the previous section a generator of higher output capacity is necessary. The increased inductance and capacity of such a system make the pulses produced too long to be useful in streamer production directly and a pulse shaping network is required to shorten them.

Many alternative, novel and ingeneous mechanisms have been developed for generating high voltage impulses, in particular by J.C. Martin (16) (AWRE) and by Fitch and Howell (17). These usually rely on the principle of electric vector inversion by which the Marx generator operates. The 'LC' Marx employs an LC resonance circuit in alternate stages and the stacked transmission line generator uses the termination effects of transmission lines to produce the necessary vector inversion. Triangular pulses of 750 kV have been produced from a 'spiral' generator with a volume of less than 10 litres. However, the conventional Marx generator is still the most reliable and widely used pulse generator.

2.5 Pulse Shaping

The simplest way to shape pulses from large Marx generators, and that used by the early workers in the field (18) is the shunt or 'crowbar' spark gap. Basically the generator is connected directly to the chamber and the pulse cut off, while it is still rising, by shunting it to ground with a spark gap which fires by simple overvoltage.

However the rise time of the generator is still long (15-25 nsec), and very short pulses of high amplitude cannot be generated by this method even if the shunting gap can remove the pulse within a few nanoseconds.

A more sophisticated pulse shaping system is the Blumlein line (8) a transmission line device originally developed for radar and flash X-ray work. The line may be charged from a D.C. supply or pulse charged from a Marx generator and produces a square pulse, equal in amplitude to the charging voltage, across a matched load. The length of the pulse is equal to twice the transit time of the line. Coaxial Blumlein lines have been used at SLAC, DESY and CERN but because of the size of such a device and the complexity of its construction a more compact easily made pulse shaper was designed for the streamer chamber which is the subject of this thesis.

2.6 Design of the Pulse Shaper

The method used to shape the pulse is that of the parasitic capacitor Cp. A very low inductance high voltage capacitor is charged from the output of the Marx generator and this in turn is discharged onto the electrodes by a series spark gap. The low inductance of the capacitor Cp and the high speed of the spark gap give the low rise times necessary for short pulse generation. Such a pulse shaping circuit is shown in Figure 2.9.

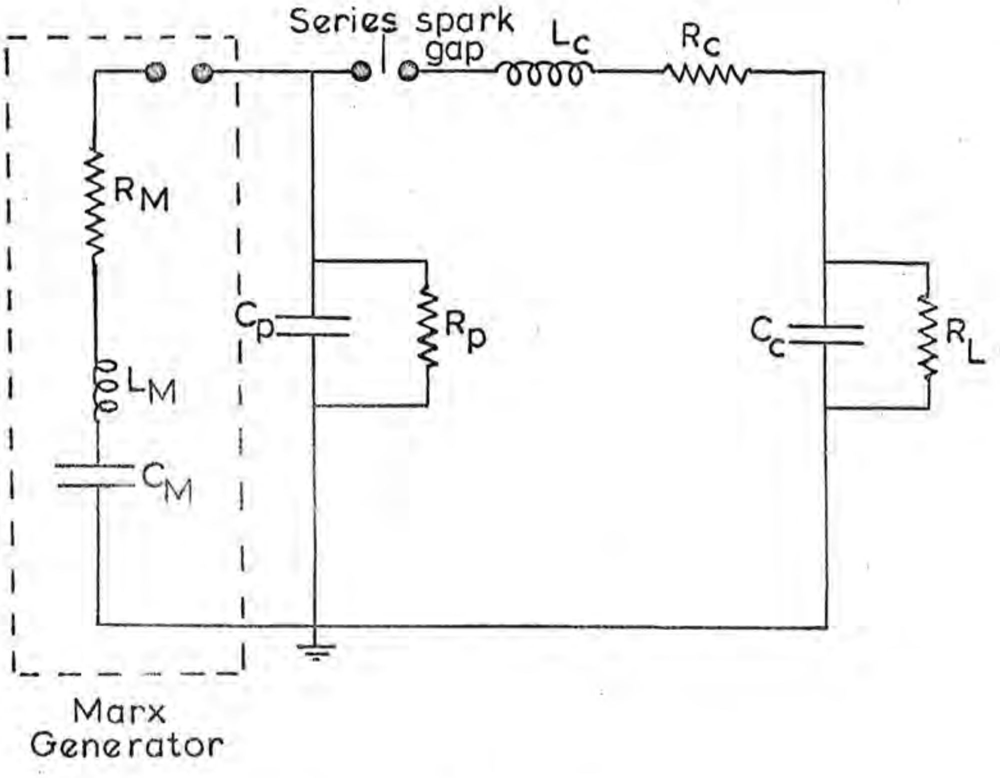

Figure 2.9

where C_m, L_m and R_m are the capacity inductance and resistance of the Marx generator respectively.

C_p and R_p are the capacity and leakage resistance of the parasitic capacitor.

C_c, L_c and R_c are the capacity, inductance and resistance associated with the discharge of the parasitic capacitor onto the chamber electrodes and R_L is the terminating resistance of the electrodes.

The values of C_p, C_m and the output voltage of the Marx generator V_m are decided by the energy and voltage transfer efficiencies from one capacitor to the next. If the charge due to a voltage V_m on C_m is shared by both C_m and C_p in parallel then, by charge conservation, the voltage V_p on C_p is

$$V_p = \frac{C_m V_m}{C_p + C_m} \qquad 2.3$$

Similarly for a voltage V_p on C_p shared by C_p and C_c in parallel the voltage on V_c is

$$V_c = \frac{C_p V_p}{C_c + C_p} \qquad 2.4$$

Combining equation 2.3 and 2.4 the voltage transfer efficiency from C_m to C_e is given by

$$\Delta V = \frac{V_c}{V_m} = \frac{C_p C_m}{(C_c + C_p)(C_p + C_m)} \qquad 2.5$$

The equation $V = f(C_p)$ has a maximum value at

$$C_p = \sqrt{C_m C_c} \qquad 2.6$$

This value of C_p is the most efficient in transferring voltage from the Marx generator to chamber electrodes using the circuit in Figure 2.9. As the capacities are fixed this is also the optimum value for energy transfer. Figure 2.10 shows the energy and voltage transfer efficiencies ΔE and ΔV from C_m to C_c using the optimum value of C_p given by Equation 2.6. It can be seen that the energy transfer efficiency has a broad maximum at $C_c/C_m = 1.0$ i.e. $C_c = C_p = C_m$. This is the condition for

TRANSFER EFFICIENCIES v C_c/C_m - DOUBLE LOOP

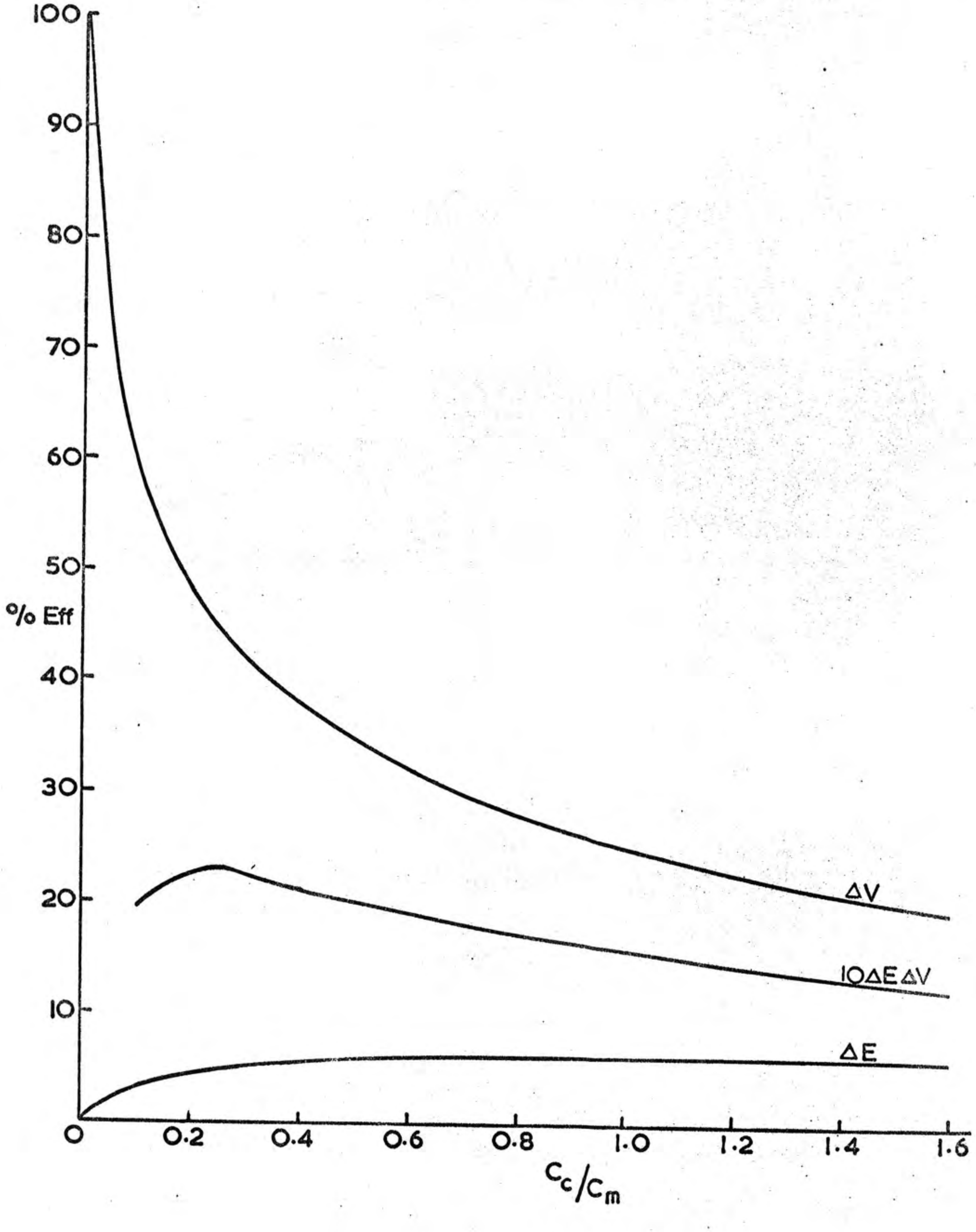

Figure 2.10

the most efficient energy transfer and corresponds to the Marx with the least number of capacitors necessary to drive the streamer chamber. Unfortunately ΔV at this point is only 0.25 and for a 300kV pulse across C_c would require an output voltage of 1.2MV from the Marx generator. This is considered inconveniently high. The alternative of maximising the voltage transfer efficiency ΔV would require an infinitely large C_m and C_p. As a compromise the product of the energy and voltage transfer efficiencies was maximised. A graph of this parameter against $\frac{C_c}{C_m}$ is also shown in Figure 2.10 and is marked $10\Delta E\Delta V$. The scale is multiplied by 10 for convenience of display. The maximum of this curve lies at $\frac{C_c}{C_m} = 0.25$. ΔE is now down by 30% but ~~their~~ there is a corresponding increase of about 80% in ΔV. Using the value of 200pf for C_c obtained earlier we find for V_c=300kV

$$C_p = 400\text{pf} \quad V_p = 425\text{kV}$$
$$C_m = 800\text{pf} \quad V_m = 666\text{kV}$$

As errors in the value of C_p may easily arise when constructing capacitors to withstand such high voltages, the effect of the departing from the optimum value given by Equation 2.6 is shown in Figure 2.11 for $C_m = 4C_c$.

In the above discussion only the 'static' transfer of charge from one capacitor to another has been considered. In the streamer chamber this will be done within a few nanoseconds and the actual voltages produced depends on the transient response of the circuit. For the purpose of analysis the circuit in Figure 2.9 can be split into two loops. The first is that involving the transfer of charge from C_m to C_p the second that from C_p to C_c. Both circuits are of the type shown in Figure 2.12a. The solution for the voltage across C on/closing switch S for an initial voltage V_o on C' has been obtained (3), (19), but the equation is long and difficult to handle. The main features of the transient may be obtained from the analysis of two simpler circuits Figure 2.12b & c. The solutions for the voltage across C enclosing switch S are given below their respective circuits. Less than critical

TRANSFER EFFICIENCIES v C_p/C_c - DOUBLE LOOP

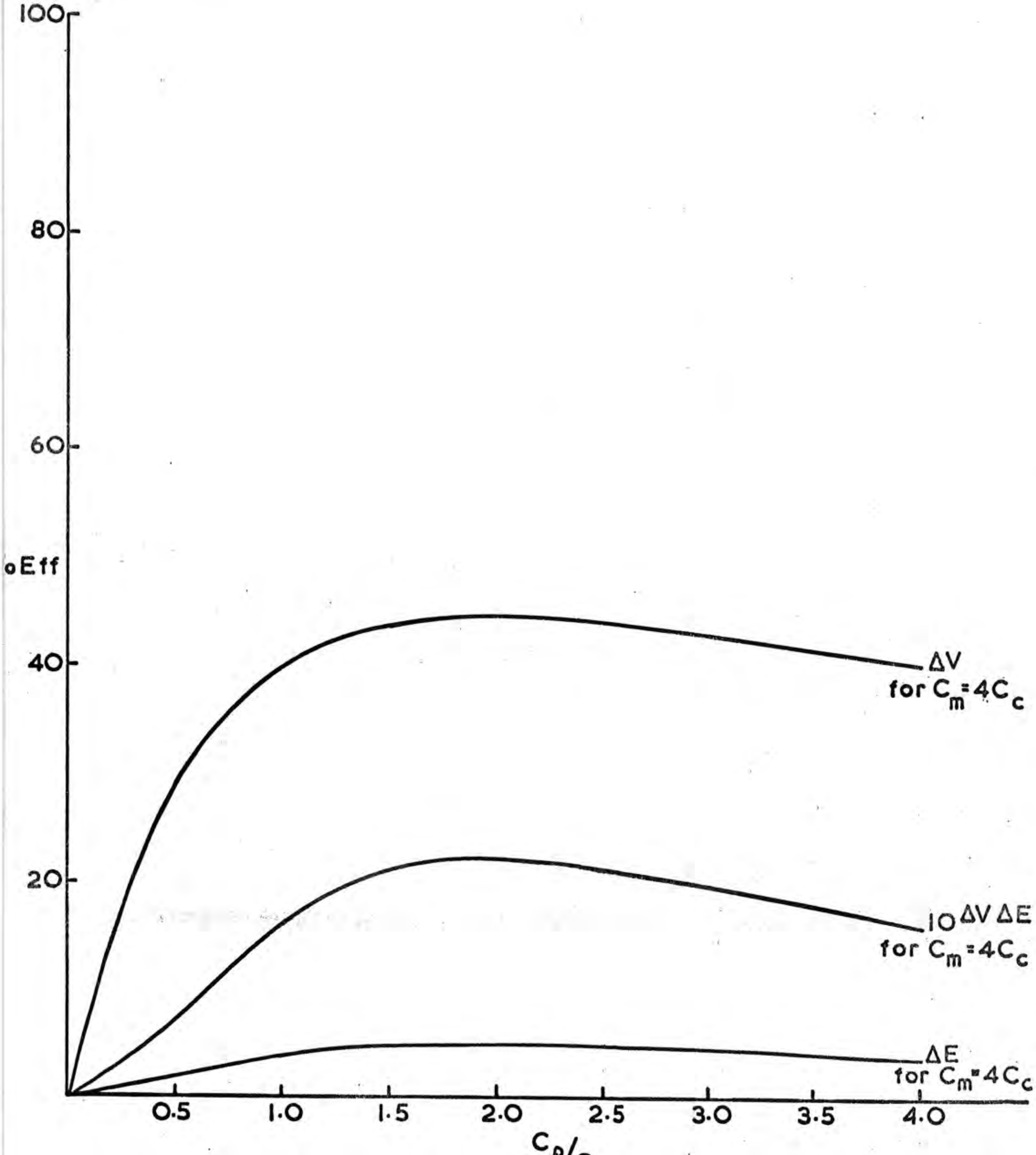

Figure 2.11

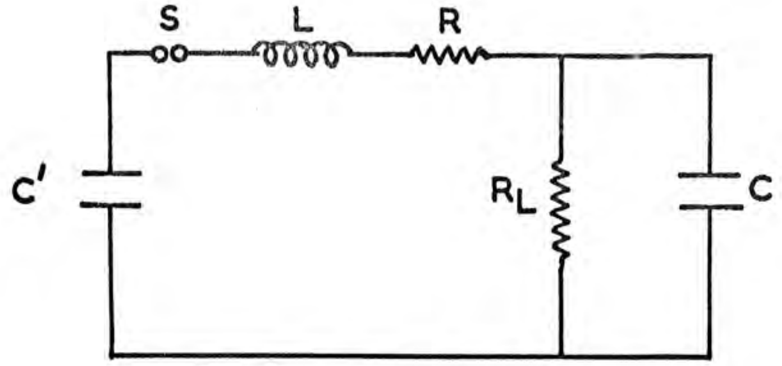

a)

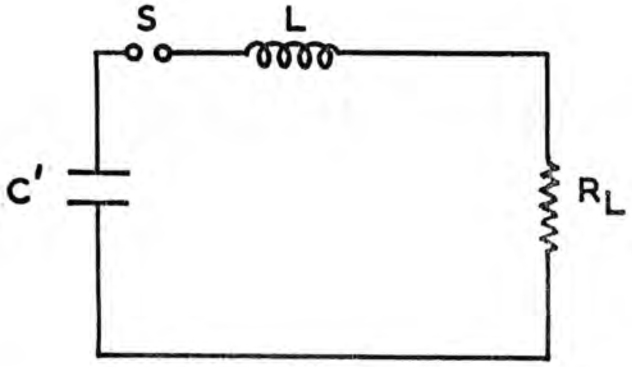

b) $$V = \frac{V_0 \frac{R}{2l}}{\sqrt{\frac{1}{LC'} - \frac{R^2}{4L^2}}} \mathrm{SIN}\left(\sqrt{\frac{1}{LC} - \frac{R^2}{4L^2}}\; t\right) \exp\left(\frac{-R}{2L}\right)$$

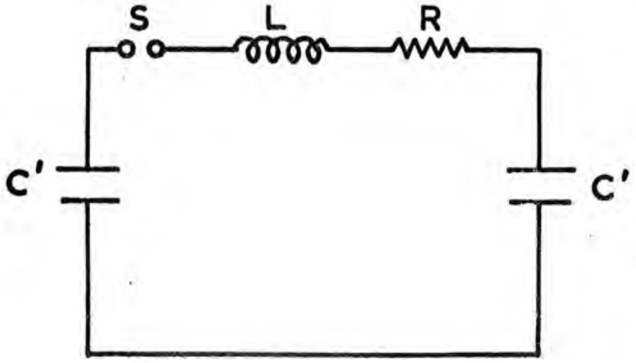

c) $$V = \frac{V_0 C'}{C+C'}\left[1 - \exp\left(\frac{-Rt}{2L}\right)\left(\mathrm{COS}\left(\sqrt{\frac{(C+C')}{LCC'} - \frac{R^2}{4L^2}}\; t\right) + \frac{\frac{R}{L}}{\sqrt{\frac{(C+C')}{LCC} - \frac{R^2}{4L^2}}} \mathrm{SIN}\left(\sqrt{\frac{(C+C')}{LCC'} - \frac{R^2 t}{4L^2}}\right)\right)\right]$$

Figure 2.12 TRANSIENTS IN RESONANCE CIRCUITS damping is assumed in both cases. The solution for greater than critical damping for b is found by replacing sin with sinh in the equation given. Circuit b is equivalent to the voltage transfer from C_p to the electrode structure if their characteristic impedance were the dominant parameter and circuit C is equivalent to the voltage transfer from C_m to C_p if the leakage resistance of C_p is large. This solution is a damped oscillation about a mean value of $\frac{V_m C_m}{(C_p + C_m)}$ which was used in Fig. 2.1. If L is large or R small the peak value of this oscillation approaches twice this value and so a separate inductance of 10 μH is added between the Marx generator and the parastic capacitor C_p. This increased inductance also slows down the rise time on C_p and relaxes the restrictions on the firing time of the series spark gap if a consistent firing voltage is to be maintained. The expected waveform across C_p on firing the Marx generator is shown in Figure 2.13 ($R=9\Omega$). Also shown is the expected loss of charge through the leakage resistance of the capacitor C_p used. For maximum efficiency the series spark gap is set to fire on the first peak of the oscillation and the pulse which drives the chamber is produced by the decay of the charge on C_p through R_L. Even if the spark gap does fire on this peak there still remains, for cases other than $C_m = C_c$, a finite voltage on the Marx generator. Figure 2.14 shows that $\frac{V_m}{3}$ still remains for $\frac{C_p}{C_m} = 2.0$ and as zero damping is assumed this figure will be an underestimate. As this surplus charge decays through R_L via the 10 μH inductance an undesirable long after-pulse is developed across the streamer chamber. This pulse must be removed by a second 'shunt' spark gap connected directly across C_c which fires by overvoltage during the fast pulse from the parastic capacitor.

The increase in the voltage transfer efficiency produced by the use of a 10 μH inductor allows the use of a Marx generator of lower output voltage. Hence the parameters of the pulsing system may be summarised thus:-

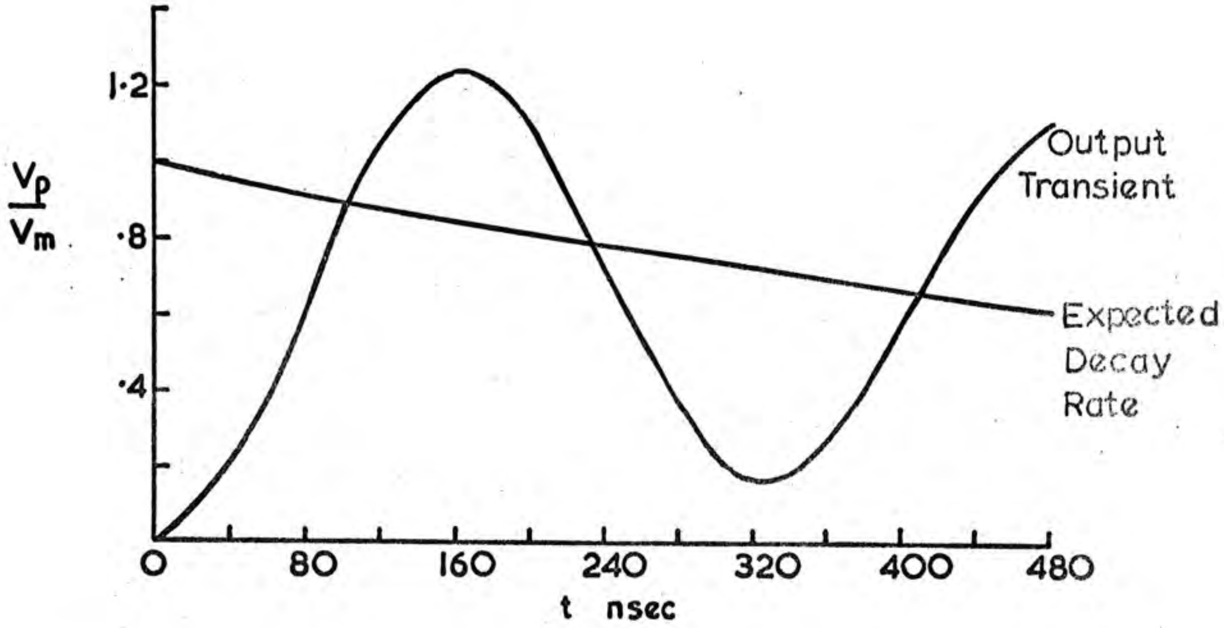

Figure 2.13 EXECTED WAVEFORM ON THE PARASITIC CAPACITOR.

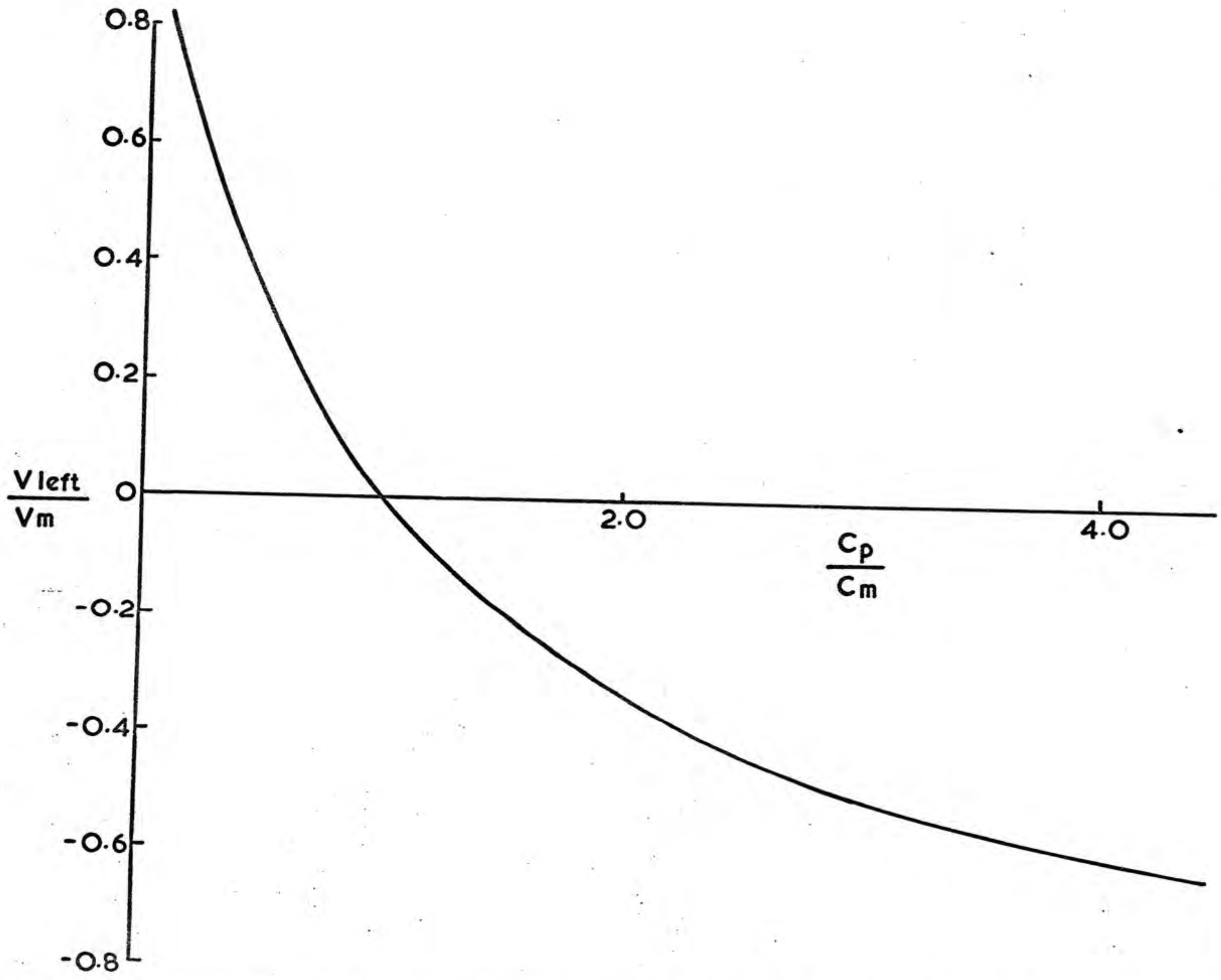

Figure 2.14 VOLTAGE REMAINING ON MARX GENERATOR AT PEAK OF TRANSIENT ON C_p.

$C_m = 800 \pm 100\text{pf}$ $V_m \Rightarrow 450$ kV

$C_p = 400 \pm 50$ pf $V_p \Rightarrow 400$ kV

$C_c = 200 \pm 100$ pf $V_c = 300 \pm 50$ kV

The requirements of a streamer chamber pulsed by a pulse shaper of the parastic capacitor type of network have been discussed and in the next Chapter the construction of such a device is described.

REFERENCES

1. RAETHER.H., Electron Avalanches and Breakdown in Gases, Butterworths Press, 1964.
2. von ENGEL, A., Ionised Gases. Oxford Clarendon Press, 1965.
3. TAN, B.C., TC-L/INT 70-7 CERN.
4. KRUITHOF, A.A., Physica, IV 6 (1937) 430.
5. MEEK and GRAGGS, Electrical Breakdown of Gases, Oxford Clarendon Press (1953).
6. DAVIDENKO, V.A., Sov. Phys. JETP, 28 (1969) 227.
7. DAVIDENKO, V.A., Nuc. Inst. Methods 75 (1969) 277.
8. BULOS, F., S.L.A.C. report No. 74 (1967).
9. Handbook of Physics and Chemistry. Chemical Rubber Publishing Co., Cleveland, Ohio.
10. VOLODIN, V.D., Prib. Tekh .EKSP., 5 (1971) 62
11. CRAGGS and MEEK, High Voltage Laboratory Technique, Butterworth 1954
12. MARX, E., Deutsches Reichspatent No. 455933.
13. GYGI, E and SCHNEIDER, F., CERN 64-46
14. MARTIN, C.J., SSWA/JCM/704/49.
15. GOLUTVIN, I.E., Prib. Tech. Eksp 3 (1967) 74.
16. GOODMAN, M.J., A.W.R.E. News.
17. FITCH, R.A. and HOWELL V.T.S, Proc. I.E.E. 4 (1964) 849.
18. CHIKOVANI, G.E., Nuc. Inst. Methods, 29 (1964) 261.
19. FLETCHER, R.C., Phys. Rev. 20 (1949) 861.
20. MOHLER, Phys. REV. 28 (1926) 46.
21. LOZANSKII, E.D. SOV. Phys. TECH. Phys. 13 (1969) 1269.

CHAPTER THREE

CONSTRUCTION

3.1 Introduction

In the preceding chapter the design of the streamer chamber has been described and the parameters of its various parts calculated. The following pages will show how these ideas were put into practice.

3.2 The Marx Generator

The Marx Generator comprises eight capacitive stages each capable of being charged to 60kV giving a static output voltage of +480kV. For an output capacity of 800pf therefore, a stage capacity of 6400pf is required. The most convenient way to store energy at this voltage is to use barium titanate capacitors which, because of the high relative dielectric constant of this material ($\geqslant 3000$), combine high capacity with low volume. Many types are available commercially and those used were manufactured by Steatite and Porcelain Products Ltd. of Worcestershire U.K.. Each has a capacity of 1800pf at zero voltage and room temperature, and has a working voltage of 30kV. The required stage capacity and working voltage are achieved by using the capacitors in two, parallel banks of eight, connected in series. The resultant capacitor is charged to ± 30kV via chains of $2M\Omega$ resistors and the centre tap is grounded via a similar chain to avoid an asymetric voltage distribution caused by dissimilar leakage resistances in the two halves of the stage. A circuit diagram of the Marx generator is shown in Figure 3.1. The stage capacity given above results in a theoretical output capacity of 900pf but this must be reduced by ~ 10% as the dielectric constant of barium titanate is a decreasing function of applied voltage, age and frequency.

The capacitors for each stage are mounted between three brass plates which then become the positive, earth and negative electrodes for that stage. The plates used are large enough to accommodate sixteen capacitors in each half stage should a generator of higher output capacity be required for some later experiment. The brass plates slot

MARX GENERATOR MARK II

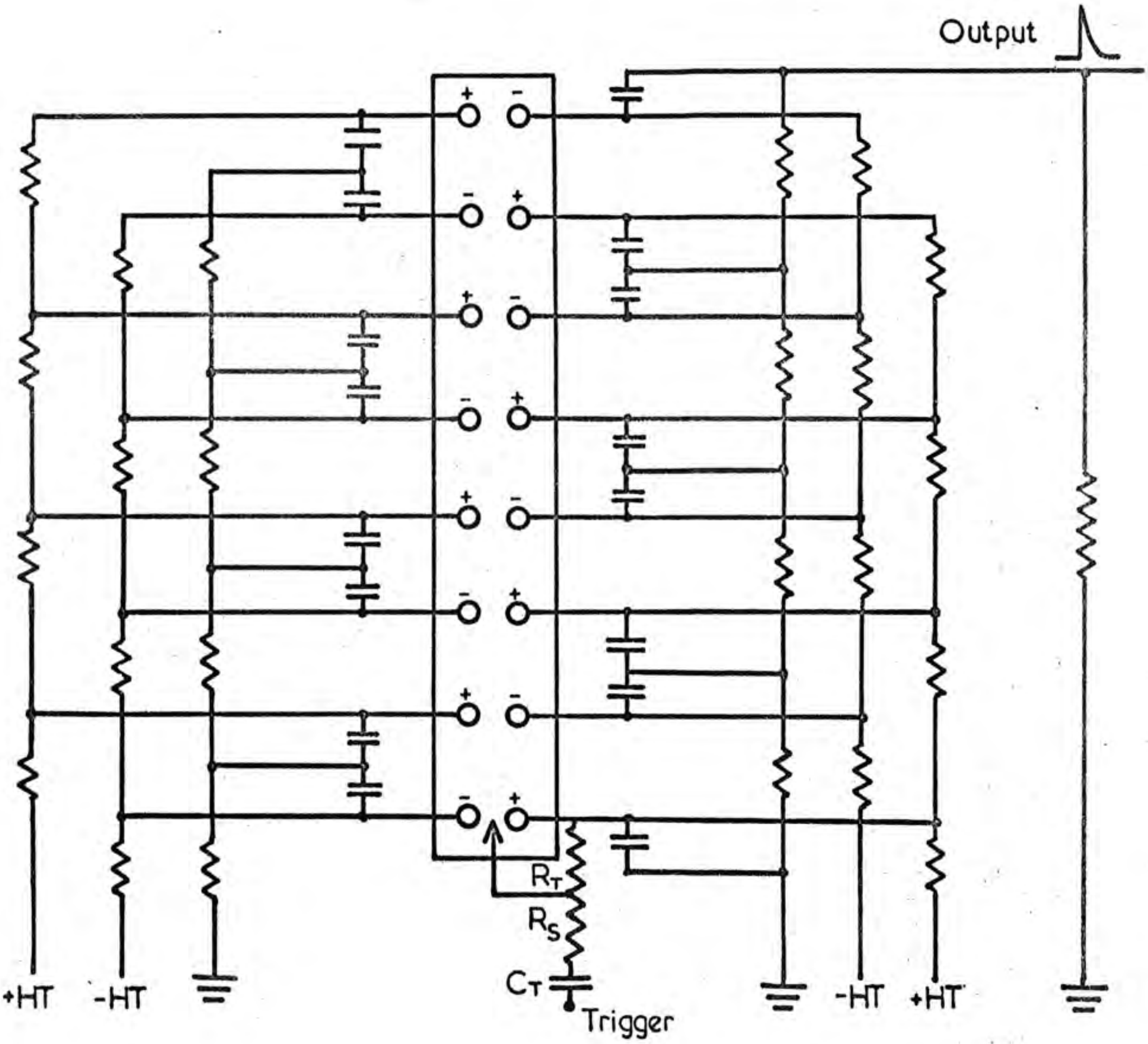

Chain resistors $2M\Omega, R_L = 500\Omega$, $R_T = 1M\Omega$, $R_S = 100\Omega$,
Each capacitor approx. 14000pf, $C_T = 500$ pf,

Figure 3.1

into grooves in the 2cm thick perspex support frames. By comparing Figure 3.1 with Figure 3.2 which is a photograph of the actual generator one can see that the component layout is as in the circuit diagram. The positive plate of the nth stage is immediately below the negative plate of the (n+2)th stage. This gives a coupling capacity between these stages of 40pf and is sufficient to allow the redistribution of charge described in section 2.3 necessary for reliable operation.

The charging resistors must withstand the stage charging voltage (60kV) during the firing of the Marx generator but for this application need not dissipate a continuous high power as the H.T. supply units used are only capable of <1mA of current at ± 30kV. The resistors used are 1MΩ 2 Watt carbon types connected in pairs and insulated from the body of the Marx generator by enclosure in PVC tubing. There is a resistance of 30M in the charging line between each HT unit and the input to the Marx generator which limits the current drawn to within the rating of the H.T. units.

The stage capacitors stand either side of a vertical spark gap column and each is connected to its respective spark gap by copper braid. The spark gap electrodes are 16mm brass rods with a hemispherical stainless steel tip of 8mm radius. This tip limits the spark erosion which would alter the breakdown voltage of the gap after many discharges. Elkonite has been used for this purpose by other workers (1), but the reliable performance of the steel over two years indicates that it is not necessary at the low repetition rates used here (<2/min). Each spark gap electrode is sealed by an 'O' ring into the wall of a 10 cm diameter cylindrical perspex pressure vessel. The spark gap separation is fixed at 13mm, a distance which was decided by experiments on a single test spark gap and gives breakdown over the desired range of voltage. The perspex cylinder is sealed at each end by an 'O' ring and a perspex cap. Nitrogen gas is supplied to the column through a ~~nozzel~~ nozzle in the

FIGURE 3.2

THE MARX GENERATOR

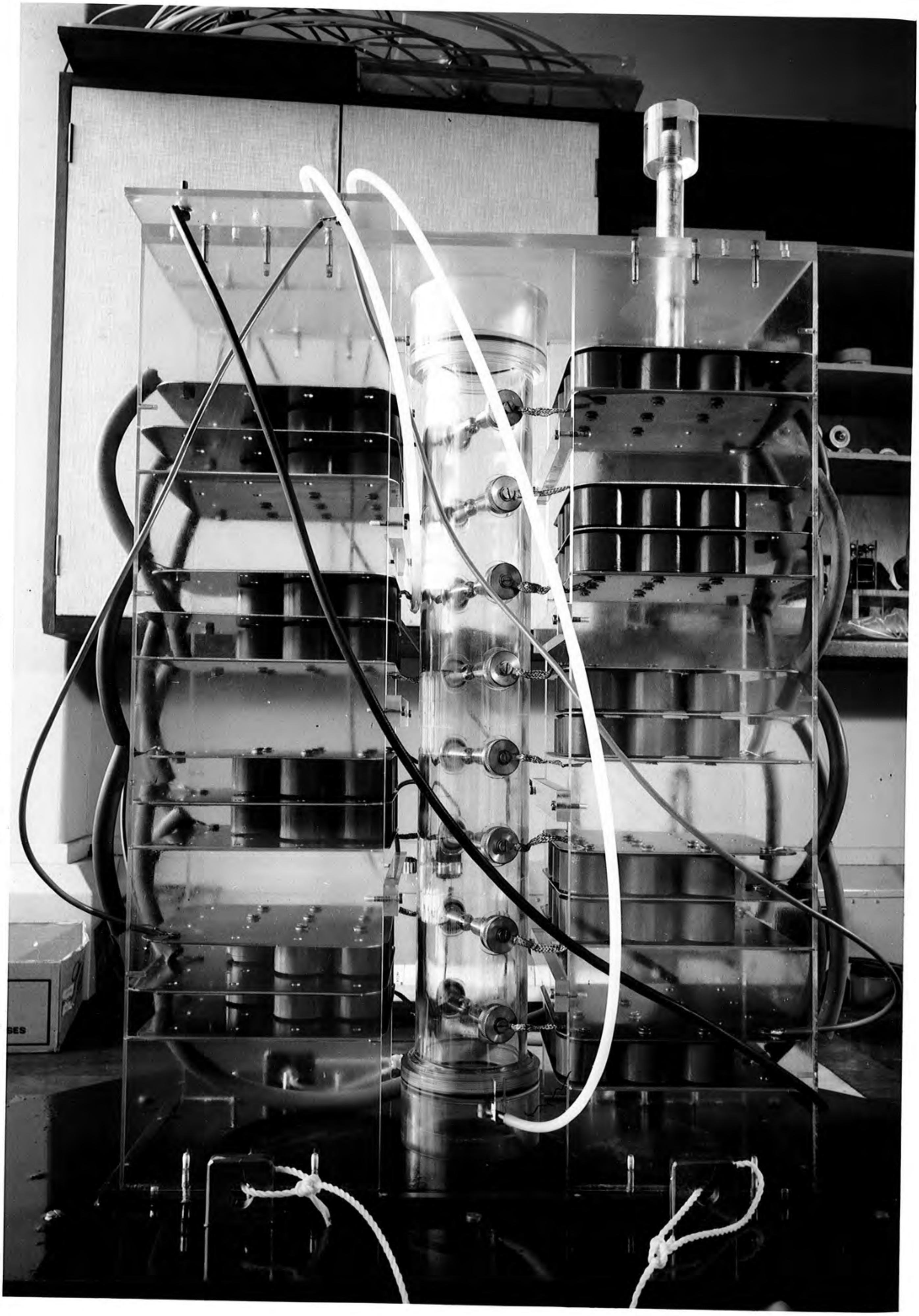
SES

lower cap and exits through a similar nozzel in the top. The column can be pressurised to 3 atmospheres (absolute) of nitrogen (oxygen free) and the breakdown voltage of the gaps controlled accordingly. This arrangement of the spark gap allows their direct illumination by U.V photons from those gaps which have already broken down (section 2.3).

The Marx generator is triggered by a trigatron type spark gap in the first stage of the generator. An insulated tungsten pin passes through a hole in the centre of the positive H.T electrode, the end of the pin being flush with the end of the electrode. To trigger the Marx generator a 15kV pulse is applied to the pin causing breakdown to the surrounding electrode at its tip. The resulting plasma then drifts into the gap between the main electrodes and breakdown of the first gap, and consequently the generator as a whole ensues. As the trigger electrode is charged to the positive H.T. voltage prior to firing it is decoupled from the triggering circuits by a 500pf capacitor. This limits the amount of energy which can be dissipated in the triggering spark to that stored in the 500pf capacitor but no difficulty was found in triggering the generator by this method. The use of a separate triggering spark gap (1), triggering pulses applied directly to the first spark gap (3) and the triggering of more than one stage are considered unnecessarily complex for this application.

All feeds to the Marx generator are taken via couplings on its upper surface to ease disconnection from supplies and the 18mm 'Tufnol' base board is fitted with steel eyes for connection to a hoist which is used to lift the generator into and out of its insulating tank of oil. The tank measures 90 x 60 x 90 cms and contains 450 litres of transformer oil. A clearance of more than 15 cms is allowed on all sides of the generator giving greater than 50% safety margin against breakdown to the side of the tank through the oil.

The output of the Marx generator is directly from the last stage and is taken via the top plate of the support frame by a 10 μH inductor (section 2.5). One of the inductors used is shown in Fig. 3.3. Heavy gauge copper wire is wound around a length of nylon tubing (6 mm bore) and supported down the centre of a second PVC tube (25 mm bore), the ends of which are sealed by the brass connectors. The outer tube is filled with transformer oil to provide insulation. A solution of copper sulphate was also used and gave superior insulation as the high dielectric stresses in the solution are relaxed by its high conductivity but the transformer oil was prefered as the possibility of contaminating the oil in the Marx generator tank by leakage from the inductor was eliminated.

3.3 The Parasitic Capacitor

The requirements of the parasitic capacitor, i.e. high working voltage (500kV), relatively high capacity (500 pf) and minimal inductance are difficult to realise using solid dielectrics. Experiments with these showed that unless special techniques are used to bond the electrodes to the dielectric, breakdown of the latter is inevitable, using convenient thicknesses of dielectric (~1cm), by discharges which originate in air pockets between it and the electrodes. The low relative dielectric constant of common solid materials ($2.0 < \epsilon r < 8.0$) requires that a capacity of 400pf has a large surface area ($\sim 1m^2$) a characteristic incompatable with low inductance and rapid discharge. High pressure gas dielectric capacitors do reduce the breakdown problems but the low dielectric constant of gases ($\epsilon r \sim 1.0$) makes them inconveniently large. The third alternative, that of a liquid dielectric, provides a satisfactory answer. In general they have high dielectric strength (> 100kV/cm), are self repairing if breakdown does occur and like gases flow to fill completely the space between the electrodes thereby eliminating air pockets from which breakdown may originate. Several liquids have the desired high relative dielectric constants which are maintained to high frequencies (1GHz) noteably glycerin(ϵr=43) and water (ϵr=80.36 at 20°C). The latter was chosen because, unlike glycerin, it is readily available is easy to handle and has a low leakage resistance, the self discharge

FIGURE 3.3

A TYPICAL HIGH VOLTAGE INDUCTOR
($10 \mu H$)

time for water being $\sim 8\ \mu$sec. Using the circuit in Figure 2.9 the discharge time τ_p of C_p will be greater than $8\ \mu$sec as its capacity is effectively greater than that of the water alone by an amount equal to the output capacity of the Marx generator C_m. Hence $\tau_p = R_p(C_m+C_p)$. By adding a contaminant such as tap water to the pure water this time constant can be reduced and by making it smaller than the breakdown time of the electrically 'weakest' part of the system, the dimensions of the pulsing unit may be reduced. A lower limit is of course set by the rise time of the voltage pulse on C_p (~170 nsec) and if τ_p approaches this value there will be a serious loss of pulse height. The decay time used was shown in Figure 2.13 and is due to a leakage resistance of $1k\Omega$,($\tau_p = 1.2\ \mu$sec).

By the inclusion of both the series and the shunt spark gap in the container holding the water all the slowly changing parts of the circuit are effectively insulated. Extra insulation of the circuitry between the spark gaps and the terminating resistors of the electrodes is not necessary due to the very short duration of the pulse in this region. The layout of the components in the water tank is designed to achieve the following points. Firstly to produce a low inductance, symmetrical geometry which will couple easily onto the electrode structure, Figure 2.5, and produce an isotropic pulse distribution. Secondly to produce an electric field distribution in the water which protects the areas most sensitive to breakdown, i.e. the plates of capacitor C_p are mounted between the spark gaps thereby shielding the pressure vessels from the high field which would be produced in them by their proximity and low dielectric constant compared with the surrounding water. Thirdly to minimise the stray capacities in the tank which easily arise using water. Such strays would increase the value of C_p to greater than 400pf thus departing from the optimum condition $C_p = \sqrt{C_c C_m}$ and increase the capacity of the electrodes C_c where they pass into the tank for connection to the spark gaps resulting in inefficient voltage transfer and longer rise times. The latter stray capacity is reduced by dividing the tank into two compartments so that an insulant of low dielectric constant can be used in the output section if required.

The value of C_p and the stray capacities may not be measured using conventional a.c. bridge techniques as the leakage resistance of the water ($\sim 1\mathrm{k}\Omega$) is much less than the reactance of these capacities at the operating frequencies of commercial bridges ($\leqslant$10kcps). However the desired quantities may be obtained by an analogue technique.

Now $$D = \epsilon_o \epsilon_r E$$

By Maxwells equation div $\epsilon_o \epsilon_r E = 0$ 3.1

Ohms' law may be expressed as $I = \sigma E$

From the law of conservation of current for steady currents within the medium div $J = 0$

$$\therefore \mathrm{div}\, \sigma E = 0 \qquad 3.2$$

where the symbols have their usual meaning.

Thus from Eq. 3.1 and Eq. 3.2 the electric flux and current flux in the medium are synonymous and the bulk effects of a quantity of liquid follow a simple proportionality. Hence a measure of the leakage resistance of C_p, when compared with the leakage resistance of a known capacity in the same dielectric, is also a measure of its capacity. Polarization of the dielectric precludes the use of a multimeter or similar low voltage d.c. device and an alternating voltage which is symetrical about zero must be used. The circuit is shown in Figure 3.5 where C_K and R_K are the known capacity and its leakage resistance. The leakage resistances are found by comparing the voltage dropped across them with that dropped across a known resistance. An error is introduced into the measurement of C_p by the partition in the tank which insulates one section from the other, but comparison with results taken in a tank without such a partition show them to be negligible. Two brass plates

15 x 15 cms with a 5 cm separation, expected to have a capacity of 400pf, had a measured capacity of three times this value due to the effect of strays. Their dimensions had to be reduced to those shown in Figure 3.4 to obtain a value of 375pf. The upper plate measures 30 x 7.5 cms, the lower 7.5 x 7.5 cms and their separation is 5 cms. Both plates have a 0.5 cm diameter brass bar soldered around their edges and the lower, high voltage, plate is curved downwards where it is overlapped by the earth plate to reduce dielectric stress in these regions. The stray capacity on the output side of the tank using this arrangement was less than 100pf.

3.4. The Spark Gaps

Both spark gaps, the series and the shunt, are built to the same design. They can be seen in position in the water tank in Figure 3.4 and a single gap is shown drawn in Figure 3.6. The pressure vessel is machined from a single block of perspex and measures 15 cms in diameter and 12.5 cms in length. The cavity is of circular cross section for maximum strength and minimum field distortion, and the wall has a minimum thickness of 2.5cms. The brass inserts are screwed directly into the pressure vessel and each is sealed by a single 'O' ring. Stainless steel hemispheres, 5 cms in diameter, form the electrodes and these are connected to the inserts by spacers of variable thickness which are used to control the gap separation. The distance between them may be varied from 0 to 2.5 cms. Unless otherwise stated the electrode separation of the series gap was 1.6cms and that of the shunt gap 1.3cms. The breakdown voltages of both gaps were controlled by pressurising them with up to 10 atmospheres of oxygen free nitrogen, a pressure above which the Paschen curve is non-linear giving a smaller increase in breakdown voltage for a given increase in pressure.

As was stated in Chapter 2 it is necessary for an electron to exist between the electrodes before breakdown can occur and when electrons were not supplied from some external source the spark gaps were extremely

FIGURE 3.4

THE WATER TANK HOUSING THE SPARK GAPS AND THE PARASITIC CAPACITOR.

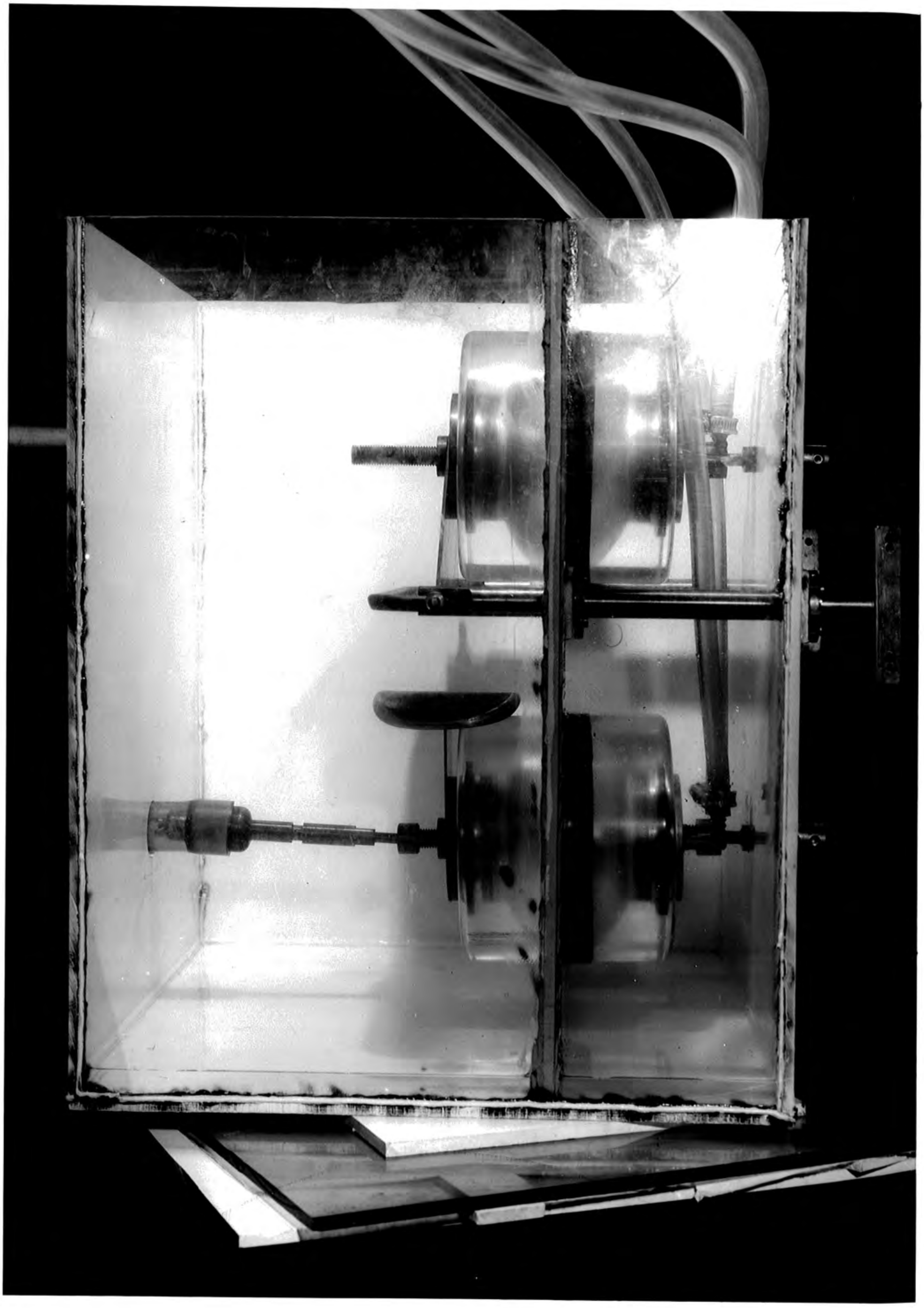

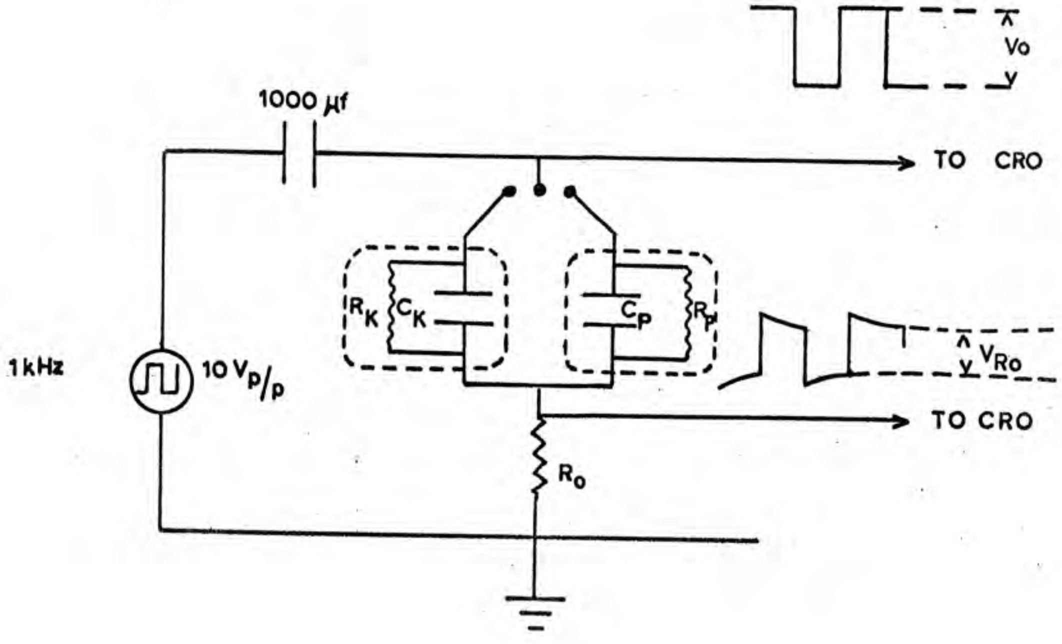

Figure 3.5 Cp Measuring Circuit

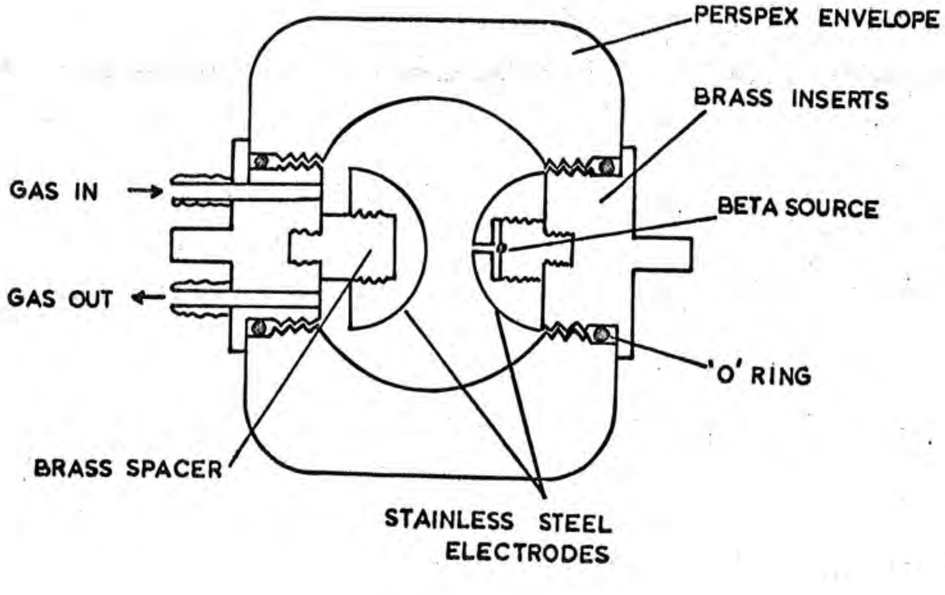

Figure 3.6 Spark Gap

unreliable often failing to operate even when highly overvolted. The effect of not supplying an initiating electron has been used by Schneider (4) in the design of a very fast pulsing system with sub-nanosecond rise times. The most convenient way of supplying electrons is from a radio active source. A 2mC sealed foil of strontium 90 is placed behind a 2mm hole in the centre of one of the electrodes of each gap. Each source provides 7.4×10^7 beta particles per second about 10% of which escape into the gas between the electrodes where they produce approximately 300 ion pairs/centimeter of path in the nitrogen at 10 atmospheres pressure. This results in a mean rate of electron production in excess of 10^9 electrons per second and the probability of not finding an electron within the gap, during the peak of the output of the Marx generator (~10 nsec) is considered negligible. More efficient use of the source can be made by placing it on the inner surface of the pressure vessel, but this was found to distort the electric field to a degree sufficient to produce sparks from the electrodes to the source.

The electrodes are connected to the parasitic capacitor by 1.6 cm diameter brass tubing. A lower intrinsic inductance could probably be obtained by using metal sheets but this would increase the stray capcity in the tank and lead to a need for more complex water seals at the tank boundaries than the 'O' ring arrangement used for the tubing.

3.5 The Electrode Structure and Terminating Resistors

The design of the electrode structure has already been described in section 2.2 and in reality differs little from that shown in Figure 2.5. The completed structure is shown in Figure 3.7. The earth electrodes are 6.3mm aluminium sheets screwed onto 19mm soldered aluminium angle frames. The heads of the screws are all countersunk into the inside surface of the sheet and sealed to remove any sharp points which may lead to spurious breakdown. The high voltage electrode is a single 2mm thick brass plate and like the front earth plate has a 60 x 60 cm

FIGURE 3.7

THE COMPLETED ELECTRODE STRUCTURE

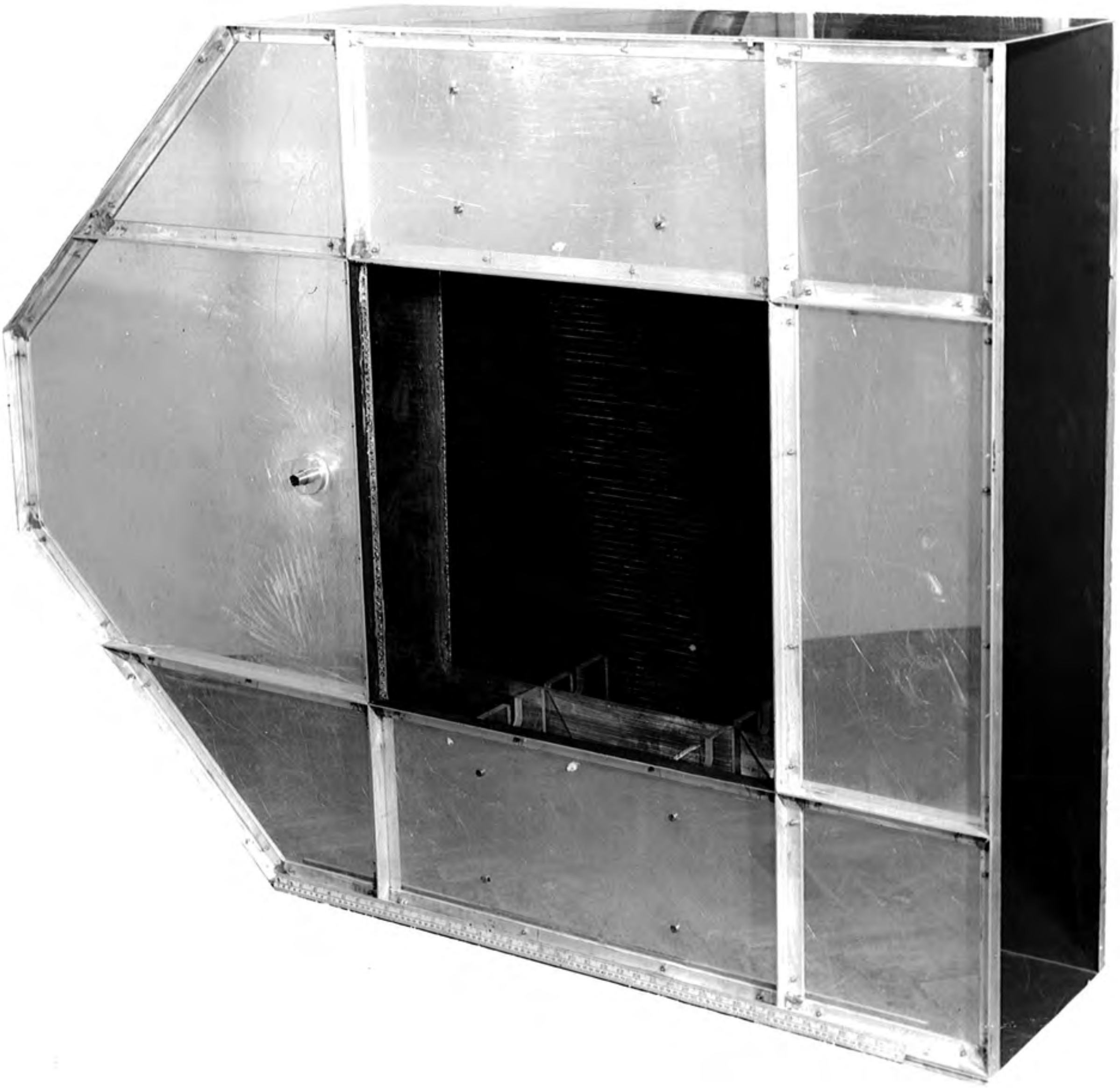

hole cut from its centre to permit photography. The holes are the direction of pulse propagation with 22 swg tinned copper wire giving an optical transparency of 95% at each electrode. A corona guard is fitted to the edge of the high voltage plane to reduce the high fields produced in this region. The guard is a 16mm brass tube, split along its length to allow insertion of the edge of the electrode to which it is soft soldered. The heat used in the soldering process produced severe buckling of the brass sheet but such distortions were removed by strategically cutting the plate, to remove excess metal, and then re-soldering. The high voltage electrode is supported to within ± 2 mm of the mid point of the two earth planes by a series of perspex supports which also act as strengtheners for the electrode structure as a whole. The interior surface is painted matt black to reduce reflections of the particle tracks.

The wide end of the electrode structure is fitted with holes to take the terminating resistors. Standard two watt carbon or wire wound resistors have been used and considered reliable by some researchers (5) but more than 10/chain are necessary to withstand the 300kV pulse, and as the peak power dissipation in the termination is above 3 x 10^9 watts, their long term stability must be uncertain. When using carbon resistors individual ones were found to burn out after only one or two pulses creating an effect which was not immediately noticeable but produced a significant change in the performance of the system. Also the impedance of most carbon or wire wound resistors tendsto become reactive at the frequencies in use here (10^8Hz).

A more reliable termination was found to be the electrolytic resistor. These are simply made to the individual requirements of the system and consist of a flexible tube (e.g PVC) filled with an aqueous solution of copper sulphate. Each end of the tube is sealed with a rubber bung through which a 5 cm length of phosphor bronze rod is inserted to make the electrodes. The required connectors may then be soldered to the ends of these rods. The resistors used here are 15 cms long, 5 cms in diameter and are filled with ~ 0.1 saturated solution of copper sulphate. Such a resistor should be capable of dissipating over 1kJ (6), well in excess of the 90 Joule output of the Marx generator. Four such resistors connected symetrically across the end of the electrode structure are used to provide the necessary termination and have a combined resistance of $35\,\Omega$. As with the water dielectric of the parasitic capacitor measurements of the resistance of the copper sulphate are complicated by polarization and contact phenomena and a similar technique to that described in section 3.3 was used to overcome them. The linearity of the resistance of the termination at high voltage was checked by measuring the decay constant of a known capacity charged to 10kV as it discharged through the electrolytic resistors. The resistance so found was the same as that at low voltage to within an experimental error of 5%. Despite disturbing discolourations of the copper sulphate solution and the PVC envelope, the resistors were found to be stable to within 5% over many months of operation.

3.6 The High Voltage Probe

A copper sulphate resistor in the form of a potential divider was used in an attempt to measure a high voltage pulse but without success as the attenuation ratio required, $\sim 3000/1$ necessitated either a very long high resistance section or a very short low resistance section. This is because the resistivity per unit length of the copper sulphate in both sections must be equal if their stray capacities are to attenuate in the same ratio as their resistances, thereby giving a linear response at high frequencies (>100 Mcps). Reactive compensation is of course possible but largely ineffective where the attenuator is situated in an electric potential distribution produced by surrounding objects which differs from that produced by the current in the probe. Much greater success was experienced with a transmission line probe Figure 3.8, (7). A third electrode is placed between the parallel plates of the electrode system. When a high voltage pulse is applied to the outer electrodes a similar pulse is induced on the probe. This pulse is smaller than the

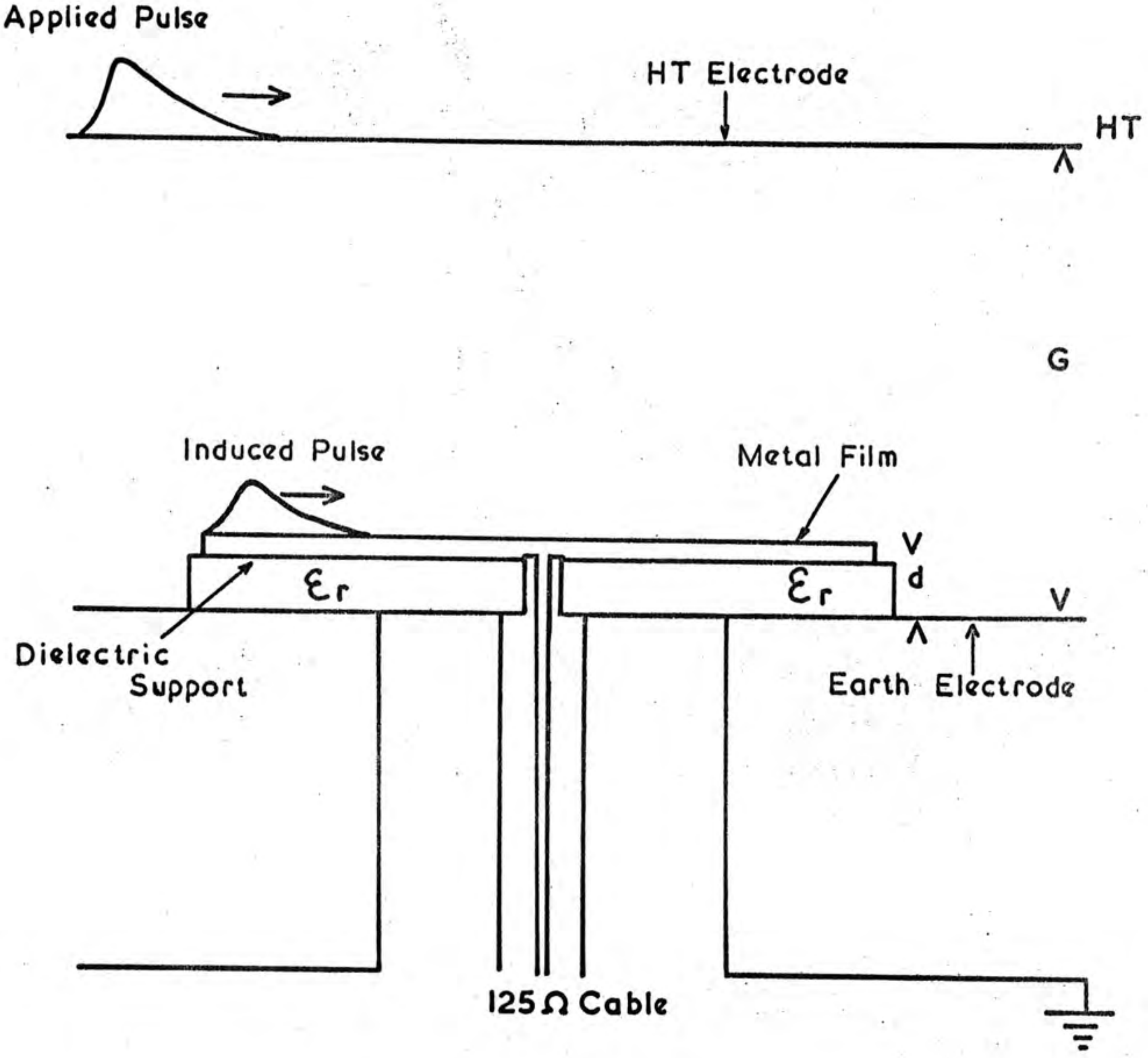

The High Voltage Probe

Figure 3.8

applied pulse by an amount equal to the ratio of the H.T. and probe electrode separations from the earth electrode where the dielectric constants of the intervening materials are the same. The probe electrode is directly connected to the input of a C.R.O where the pulse may be displayed.

There are two main factors which guarantee fidelity of response. Firstly the decay time constant of the capacity of the probe, C, through the input resistance of the C.R.O, R, must exceed the longest time constant of the pulse to be measured or a frequency dependant attenuation factor will result. Secondly, to prevent oscillation of the probe, its surface resistivity r must exceed the reactive component due to its inductance ωL, at the highest frequency used. However a value of r large enough to cause a non-uniform voltage distribution across the surface of the probe, as it decays through R with time constant RC, is unacceptable. This leads to the restriction.

$$\omega L < r < \frac{Rb}{L} \qquad 3.3$$

where b is the breadth of the probe and L the length.
Simple probes of this kind have been used (1) but the probe electrode must be thick to achieve self support and is hence under damped. Also to achieve adequate insulation between the probe electrode and ground only a small attenuation ratio may be used and a supplementary resistive divider is necessary.

These difficulties have been overcome by Schneider (3) who mounted the probe electrode, in the form of an evaporated gold film, on an insulating mica sheet. The separation of the probe from the earth plane is now much smaller and the attenuation ratio is further improved by a factor ϵr, the relative dielectric constant of the sheet. The film must be thinner than the skin depth Θ of the highest frequency used ω to produce the same speed of propagation of the pulse inside and outside the supporting sheet. Thus

$$d \ll \frac{2\rho}{\omega\mu} \qquad 3.4$$

where ρ is the resistivity of the film and μ the permiability of the support.

It was found that the inconvenience of producing evaporated thin films could be avoided by using aluminised mylar sheet, which is commerically available in almost any size and in 50 and 120 μm thicknesses. This film has all the required properties for probe construction. The probe developed for the streamer chamber has the following parameters:-

Length L = 10 cms

Breadth b = 50 cms

Thickness =120 μm relative dielectric constant ϵ_r=3.0 at 1MHz

Surface resistivity r $\approx$1Ω/square

Capacity C = 10,000 pf

Film thickness = 250Å cf skin depth in aluminium at 1GHz =2000Å.

Input resistance of CRO (Tektronix type 519) = 125Ω

The probe was glued with lacquer to the inside surface of the earth electrode immediately in front of the wired section, Figure 3.7, and its edges protected with adhesive tape. The leakage resistance of the probe to ground was more than $10^8\Omega$ and considered negligible. Contact was made to the probe by a General Radio Connecter glued to the outside of the earth plate with silver doped epoxy resin.

The probe was calibrated against a Tektronix high voltage probe, type P6015 at 50Hz (attenuation factor 1000/1 ± 1%) using a type 7704 oscilloscope calibrated to within 2%, Figure 3.9. The high input resistance of the CRO ($10^7\Omega$) lengthens the time constant of the probe to 0.1 seconds such that it still exceeds that of the calibrating frequency which is 4.0 msec. The performance of this type of probe was checked at higher voltages and frequencies by applying a pulse of known height (10kV) and decay constant to the electrodes and no change in the calibration factor could be found.

The attenuation factor of the probe used is 3700/1 and when used with a 125 Ω,X5 attenuator and a CRO deflection factor of 9.5V/cm gives a resultant display calibration factor of 176±5.0kV/cm. Long term drift

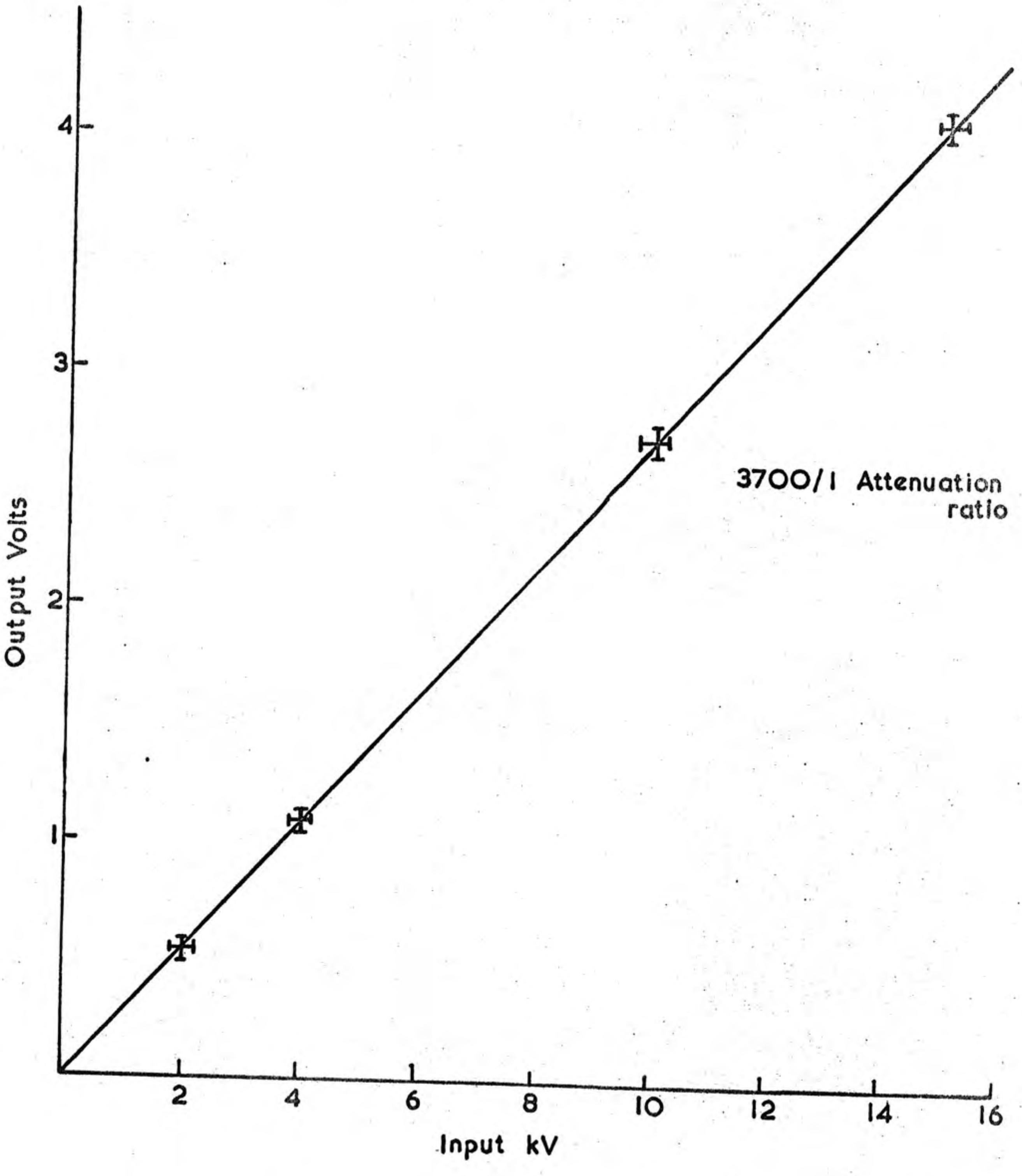

Figure 3.9 Probe Calibration Curve.

was found to be small and such probes have been used continually over a year without need of adjustment.

3.7 The Chambers

Two types of chamber were tried. Originally the system was designed around a pair of sealed chambers 60 x 60 x12.5cms in size. These were made from $\frac{1}{4}$" soda glass glued together with epoxy resin. Each was baked under vacuum at 150°C for >8 hrs before filling with 98% neon and 2% helium at 760 Torr. When new they performed well and excellent tracks could be produced in them but the structure proved to be mechanically unsound and after some months the gas became contaminated with air.

More reliable operation was achieved using a gas cycling system and chambers consisting of a support frame and Melinex windows. Both polyurethane and perspex frames were tried, but work was abandoned on the polyurethane when hermetically sealing in the windows to the frame was found to be difficult. The perspex frames were 1.2cm thick 14 cms deep and 60cms long, butt jointed and glued with perspex cement at the edges to give the required shape. The corners of the resultant structure were strengthened with triangular cross section inserts. The melinex windows, 50μm or 120μm, were stretched using a pneumatic frame technique and attached to the frame using double sided adhesive tape. The gas is supplied to the chambers through ports in the upper side and leaves through the lower side. Connection is made to the cycling system through rubber hose.

3.8 The Gas Cycling System

The gas purification system is shown in Figure 3.11 and is in two identical halves. One half is in use while the other is regenerated or repaired. The active agents are type A5 molecular sieve and 250 gms of activated charcoal which is cooled to 175°C in a cryostat of liquid nitrogen, the level of which is maintained from a master dewar. The charcoal is regenerated by heating it to 150°C under vacuum. The neon helium mixture is driven through the system by a small diaphragm pump

GAS PURIFICATION UNIT

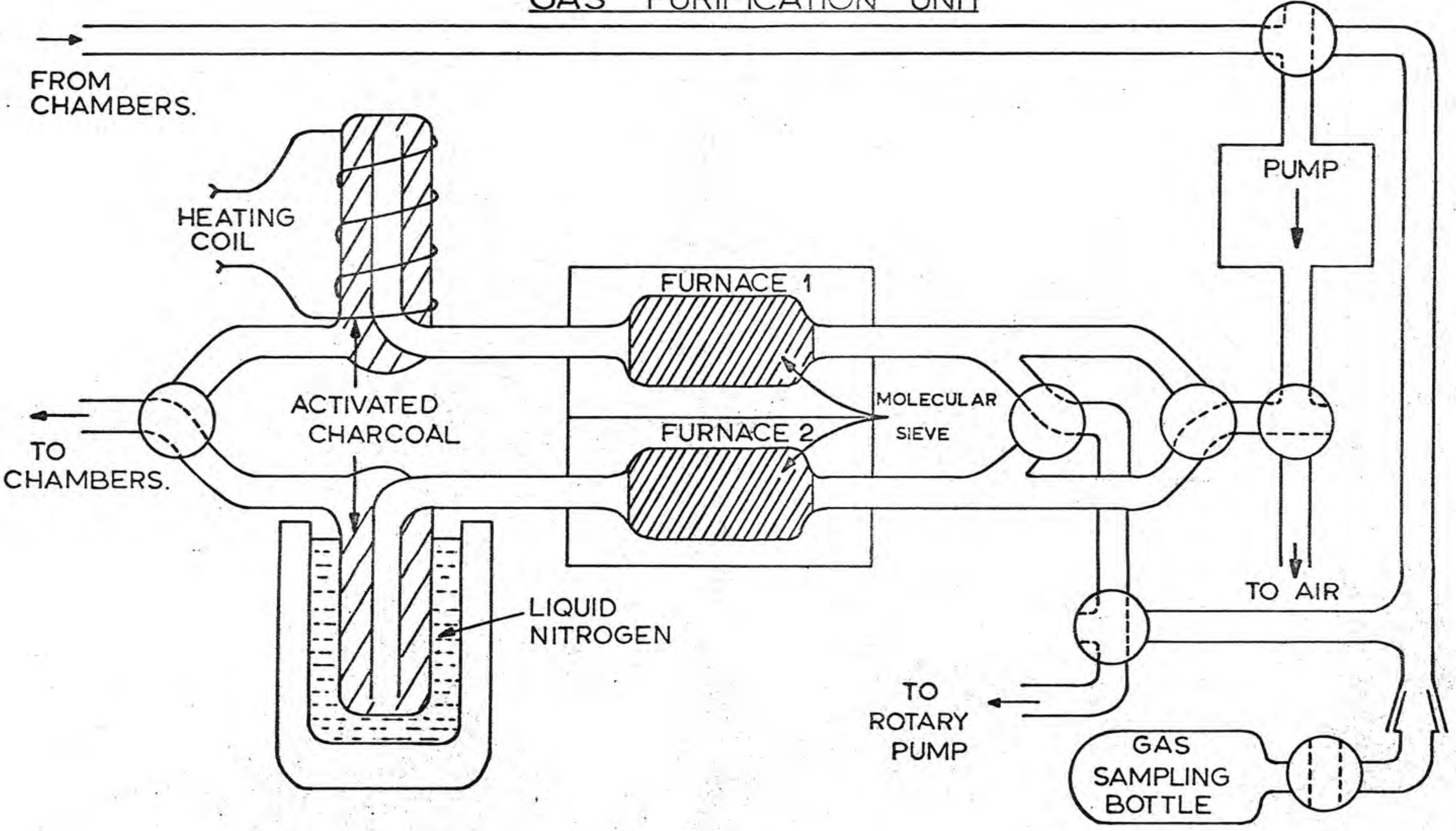

Figure 3.10

capable of pumping 5 litres/minute but normally run at about 20% of this rate. The capacity of the streamer chambers is 80 litres.

An analysis of the gas taken from the streamer chamber after several months of operation showed the fraction of helium in the gas to be smaller than the 30% contained in the master bottle. This loss is probably due to the preferential loss of the helium through the melinex walls of the chambers and other 'weak' parts of the cycling system. The exact percentage of helium in the chambers at anytime is therefore not known but is taken to be between 10 and 20%.

Attachment of electrons to electronegative impurities in the gas, in particular oxygen and water vapour, will vary with the purity of the gas which could not be constantly monitored but such effects were found to be negligible using pulse delays of less than 200μsec when compared with the loss of electrons from the chambers by spurious electric fields. This feature is discussed in chapter six.

3.9 The Triggering Logic

As we saw in section two of this chapter, to fire the Marx generator, a 15kV pulse must be supplied to the trigger electrode of its first spark gap. To be able to limit the diffusion of the electrons released by the particle to be detected as it traversed the chamber, the minimum delay between its passage and the application of the high voltage pulse must be short ($<1\ \mu$sec).

Plastic scintillators in a variety of arrangements are used to detect cosmic rays traversing the chamber Figure 3.12, and after time delay compensation, are wired in conventional manner to discriminators and simple AND and NAND logic gates. After the introduction of a controlled delay, a logic pulse is derived from these gates of amplitude -700mV and 10nsec duration and is amplified by a specially designed high voltage, avalanche pulser (DP5) to 5kV within 60nsec of the input pulse. This circuit is described in detail in Appendix B.

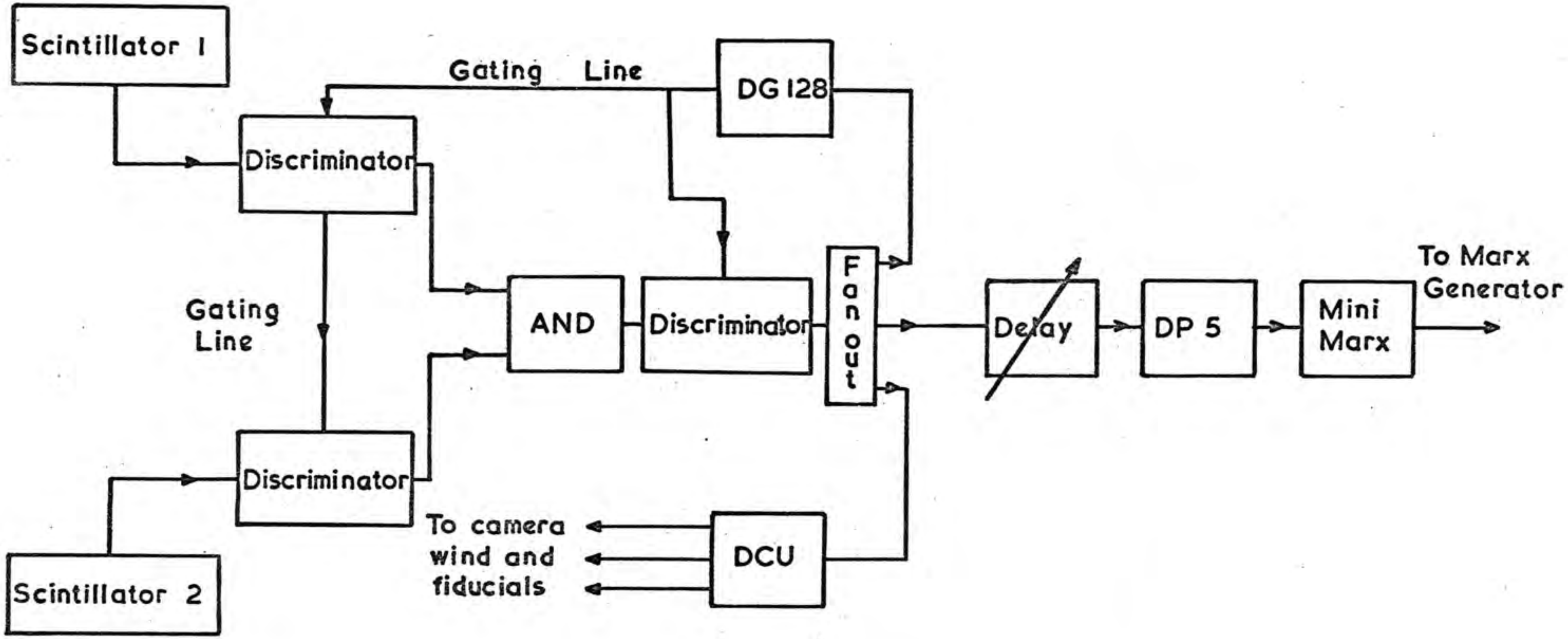

ASSOCIATED ELECTRONICS LOGIC DIAGRAM

Figure 3.11

A small three stage Marx generator (the Mini Marx) of 5kV/stage and output capacity 660pf then amplifies the signal to the 15kV necessary to drive the large Marx generator. The Mini Marx also acts as a buffer between the main high voltage system and the more sensitive logic circuitry and is housed in a separate screened enclosure between the two.

As the rate of triggers from the logic is usually much greater than the 2/minute maximum rate of the Marx generator power supplies, the logic is paralysed during this time by a gate generator (DG128). This generator is triggered by a standard logic pulse and produces a paralysis gate of 0.1 to 1280 seconds duration. A more detailed description is given of this device in Appendix B.

3.10 Component Layout

One of the most important features of any high voltage system and in particular a pulsed system such as a streamer chamber, is the positioning of each part of the circuit with respect to the next and to surrounding objects. In this case the layout was designed to achieve the following ends.

a) To protect personnel from the high voltage sources,

b) To provide dark conditions for photography,

c) To minimise the possibility of spurious breakdown,

d) To minimise the pulses which may be many kilovolts, which travel back down the triggering leads when the system fires, resulting in damage to the low voltage logic circuitry.

e) To reduce radio frequency radiation from the device which would disrupt the triggering logic and electronics associated with neighbouring experiments.

f) To permit the connection of a high sensitivity CRO (10V/cm) to the high voltage probe without it being destroyed by the high voltage pulse.

The arrangement used is shown in Figure 3.12. The apparatus is

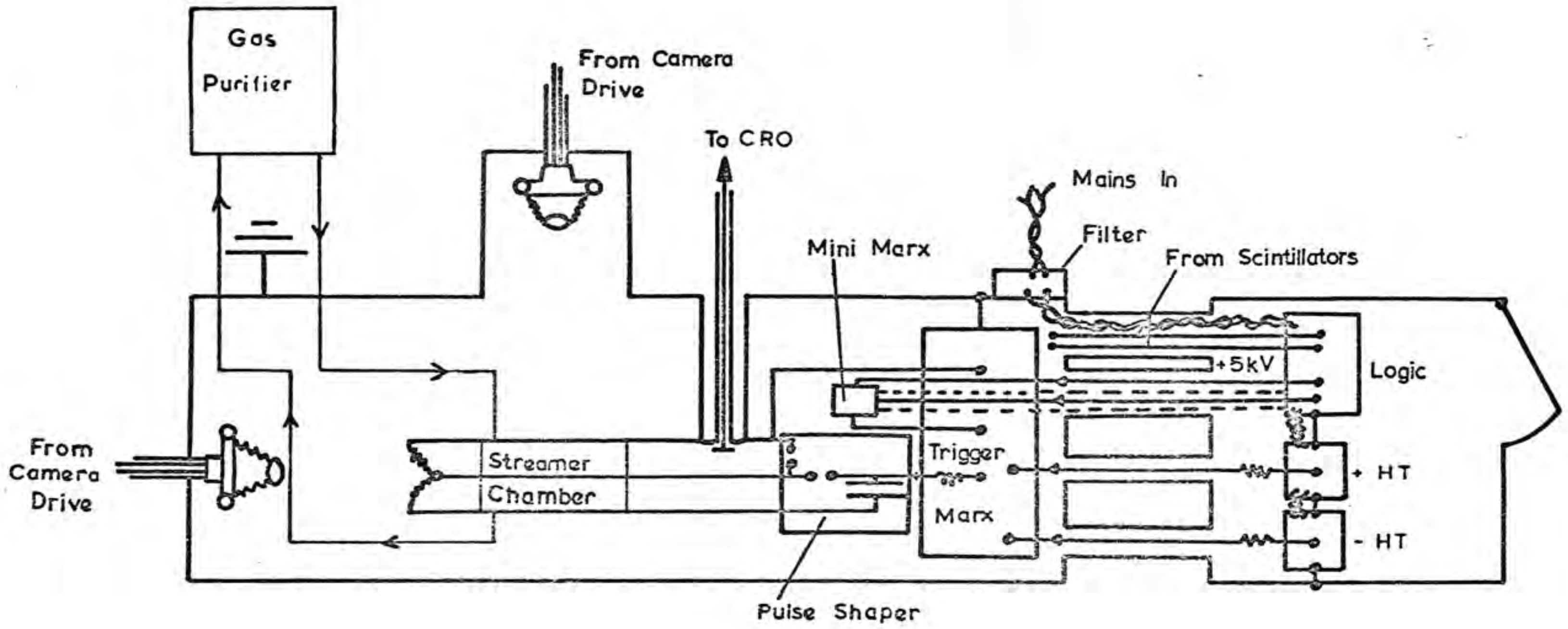

Figure 3.12 Component Layout

enclosed in two specially constructed steel enclosures. Each is made from 18 gauge steel, spot welded onto 2cm steel angle to form sections 1.2 metres square. The sections are bolted together with a layer of brass mesh between the joints and with the bolts parallel to the surface of the enclosure, thereby avoiding r.f leakage. The mini Marx, the Marx generator and the pulse shaper are all housed in one enclosure measuring 3.6 x 2.4 x 1.2m painted black inside to limit reflections. All the associated electronics is housed in a smaller room 1.2 x 2.4 x 1.2m placed at the end of the larger one. The interconnecting cables pass through four, 5cm diameter conduits between the rooms.

The power from themains is via an r.f filter which attenuates by 100dB frequencies up to 1GHz. Only live and neutral are connected here, the earth being via copper braid to a lug welded to the steel wall.

The ancillary electronics is mounted in racks which are insulated from the floor and earthed only through a single connection to the metal wall near the mains input filter. As the outputs of the H.T generators do not float they are connected to the Marx generator by single unscreened wires; the return path is via the steel wall. This is undesirable but as this part of the circuit does not carry fast transients (<1 msec) they do not represent a serious source of interference. Any transients which do occur will find the 30MΩ charging resistors in the HT line and a negligible impedance in the return path through the steel wall, resulting in a very small potential drop along the wall.

When the Marx generator fires it would, if left to itself, erect symmetrically about earth, as the earth point is connected more than 1 metre away from it. This is prevented by the addition of the $10\mu H$ inductor which forms a bridge with the low inductance return braid, the mid point of the two being earthed to the steel wall via the outer electrode of the streamer chamber. The result is that only a few kV is dropped along the return line and the majority of the output is across the conductor and the charging parasitic capacitor.

The discharge of the parasitic capacitor is symmetrical and as there is no added inductance and little resistance, only the exact point where the electrodes are connected to the steel wall can be regarded as earth. This is of vital importance when measuring the high voltage pulse.

The screen of the 125Ω cable carrying the signal from the probe to the CRO represents a second earth and if this and the true earth are even only a few centimetres apart on the electrode structure, large currents will flow in the screen causing considerable interference on the CRO display. The main symptons of this were sparks from the CRO trolley feet to the floor, an extremely distorted CRO trace involving apparent time reversals and loops and occasional flash over from the signal leads to the power leads inside the oscilloscope. These effects could not be overcome by moving the CRO to the next screened laboratory, which indicates that direct radiation of radio frequencies was playing little part in the phenomenon.

The problem was completely solved by making the earth connection from a copper pipe 6cms in diameter,Figure 4.6. One end of the pipe is screwed by a flange to an aluminium ring glued with silver doped epoxy resin to the earth electrode. The other end is bolted by a similar flange to a 6cm hole in the screened enclosure wall. The 125Ω cable from the probe is supported down the centre of the pipe, where it rests in a completely earthed,field free environment. The resulting CRO traces were now 'clean' enough to see the effects of direct radiation which were eliminated by closing off all access hatches and camera mounts with steel covers.

Other essential supplies which are external to the screened room are the three nitrogen cylinders for pressurising the spark gaps and the neon purification system. Connecting hose to and from these are all taken via loose couplings, designed to minimise r.f leakage, mounted in the steel wall.

3.11 Photography

Two cameras are used, one to photograph streamers parallel to the other perpendicular to the applied electric field. Both are Cossor motor driven types 1431 and each is fitted with a Nikko 'O', f2.0, 35mm lens. The cameras are wound on during the paralysis time by a logic triggered cycling unit, the DCU, which is described in Appendix B. This unit also powers the fiducials. Fibre optics is used to carry light from a quartz halogen lamp located in a small screened enclosure to known positions on the electrode structure. Directly powered light sources near the streamer chamber electrodes present considerable problems of interference in the drive unit.

A demagnification of 40:1 is used making the largest angle subtended at the chambers 20° thus producing negligible distortion in the image field (0.2mm in 60cm.) The lens apertures most frequently used are f2.0 and f2.8. The latter is found preferable for most applications as the slight loss of light is well compensated for by increased definition and depth of field. Photography perpendicular to the field requires the greater depth of field, ± 30 cms at a range of 125cms from the lens. Figure 3.13 shows the apparent size of an object, which moves across the required depth of field, using an aperture of f2.8. The linearity of the line over most of the field shows that the actual object sizes may be calculated from the image sizes by the use of a simple range dependent magnification factor.

Two types of film are used, the first Kodak 2475 for most of the photography and the second the less readily available Kodak 2485 when higher contrast and sensitivity were required. However it is thought that some detail of the streamer may be lost when using such high contrast films. Both the films have a very high speed (>1500ASA), extended red sensitivity which is suited to the photography of neon discharges, and have been widely accepted for this type of photography (1) (8). The

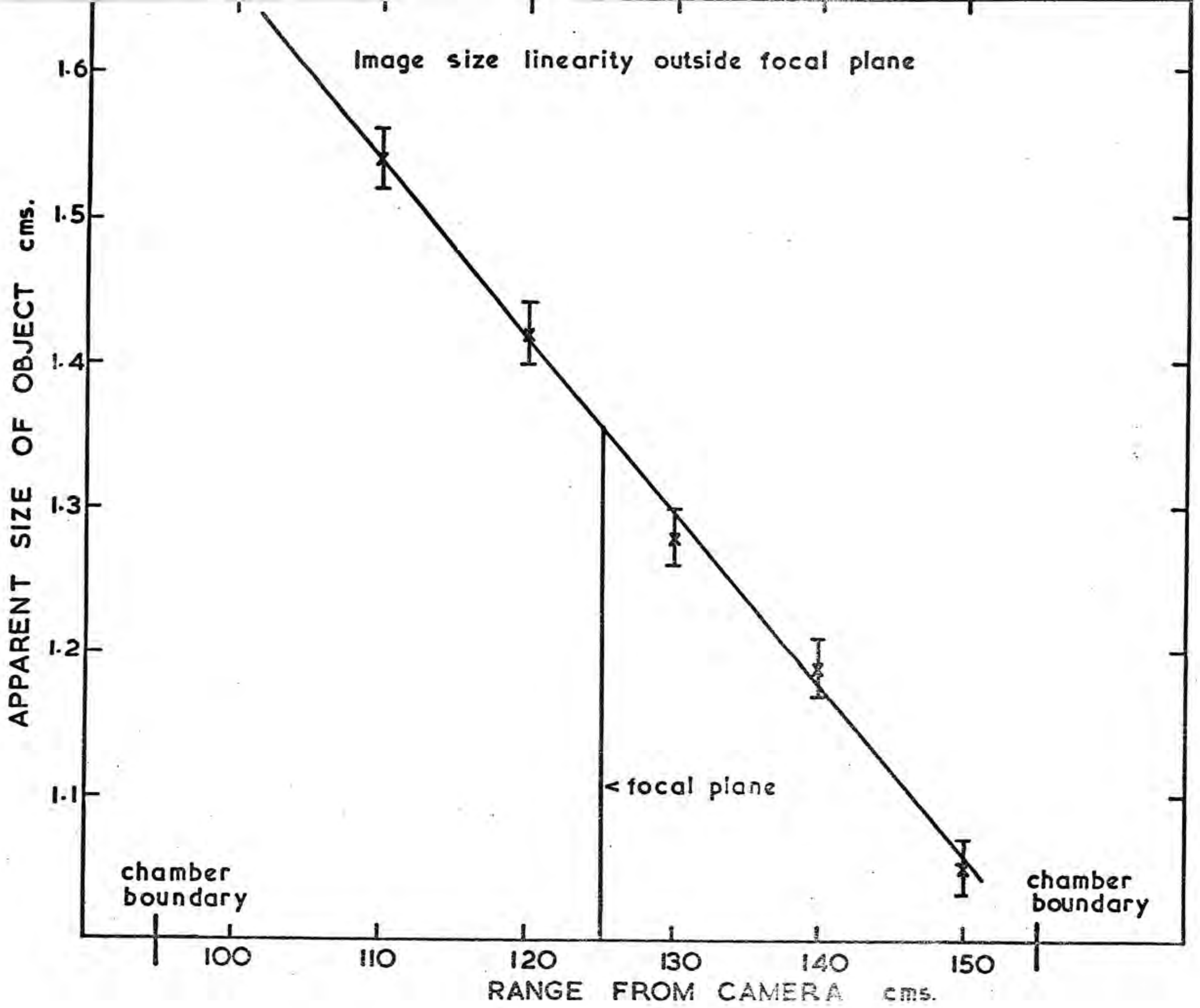
Image size linearity outside focal plane
APPARENT SIZE OF OBJECT cms.
1·6
1·5
1·4
1·3
1·2
1·1
< focal plane
chamber boundary
chamber boundary
100
110
120
130
140
150
RANGE FROM CAMERA cms.

Figure 3.13

2475 was hand developed in DK50 at 20^{o}C for 8 minutes and the 2485 in MX857 at 35^{o}C for 3 minutes.

The circle of confusion for the above optical system is about 0.1mm and is much smaller than all the objects photographed and is therefore neglected as a source of error.

In this chapter the construction of the extensive array of equipment necessary to generate useful streamer tracks has been described. The following chapters are a detailed account of its performance and characteristics.

REFERENCES

1. BULOS, F., S.L.A.C. Report No 74. (1967)
2. SLETTEN, A.M. and LEWIS, T.J. IEEE Monograph 193 (1956) 53.
3. GYGI E., and SCHNEIDER F, CERN 64-46.
4. SCHNEIDER, F. CERN ISR/GS/71-17.
5. ECKART, V and LADAGE, A., Int. Symp. on Nuc. Elect. Versailles 1968 6 III P10.1.
6. MARTIN, C.J., SSWA/JCM/704/49.
7. FLETCHER, R.C., Rev. Sci. Inst. 20, (1949) 861.
8. ECKARDT, V., Private communication.

CHAPTER FOUR

OPERATION

4.1 Introduction

The following chapter is a brief account of the performance of the component parts of the system and the streamer chamber as a whole.

4.2 The Marx Generator

When the generator was first assembled its operation was erratic and it displayed no usable working range. Each stage was added to the generator separately and operated several times (~ 20) until it became stable and in this way reliable performance of the whole generator was achieved. The resultant operating characteristics are shown in Figure 4.1. The pressure of nitrogen in the spark gap column is used to control the breakdown voltage of the gaps from 25kV to > 60kV. The upper line, the maximum hold-off voltage, is the highest voltage, at a particular pressure, to which the generator could be charged for > 2 minutes without breakdown. The lower line, the minimum triggerable voltage, is the lowest voltage which would give five consecutive successful triggerings, each after charging the generator for twenty charging time constants. The region between the lines is the working range of the generator and has proved stable over two years of use. However, unless the gas in the spark gap column was being constantly changed its breakdown voltage did increase by a few percent after ten to twenty firings, probably due to the formation of nitrides in the spark gap column. A continuous flow of gas is also essential for the pressure reduction valve and meter on the gas cylinder to function correctly. It is probable that the voltage range over which the generator will trigger at a particular pressure is determined by the working range of the trigatron spark gap in its first stage rather than the performance of the generator as a whole.

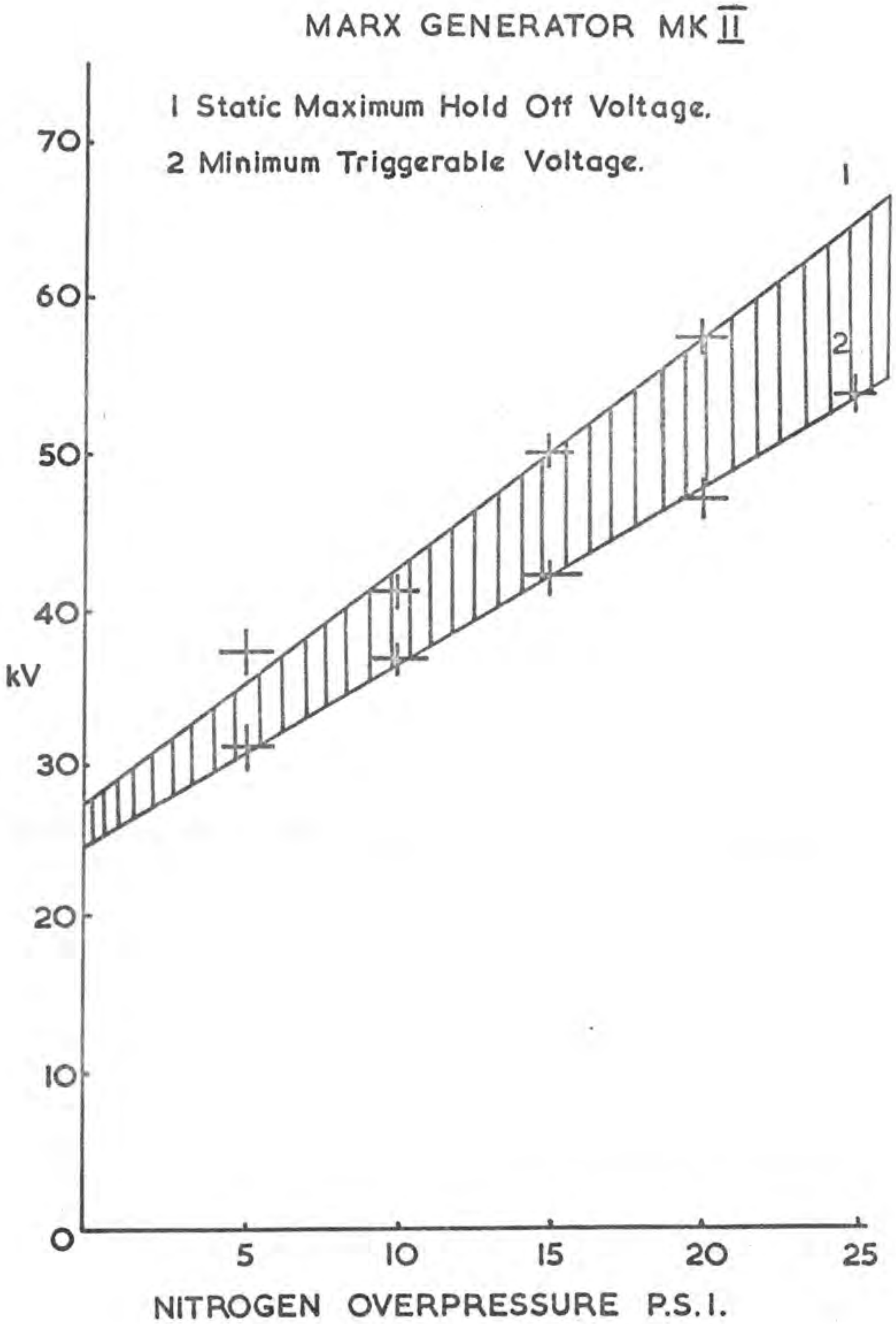

MARX GENERATOR MK II
1 Static Maximum Hold Off Voltage.
2 Minimum Triggerable Voltage.
1
2
kV
70
60
50
40
30
20
10
0
5
10
15
20
25
NITROGEN OVERPRESSURE P.S.I.

Figure 4.1

4.3 The Spark Gap Performance

The spark gaps were tested by discharging the output of the Marx Generator to ground via each spark gap in turn and the pressure of nitrogen in each, necessary to hold off a particular voltage, was noted. Gap separations of 1.8cms and 0.8cms were used and the characteristics of both gaps are shown in Figure 4.2. Changes of pressure produce linear changes of voltage over the range considered and a simple proportionality exists between hold off pressure and electrode separation. The voltage scale in Figure 4.2 is the charging voltage per stage of the Marx generator and although proportional to the voltage across the spark gap, this voltage is unknown due to the resonance of the discharge circuit.

As with the Marx generator it was found necessary to change the nitrogen gas in the spark gap between discharges to maintain a constant breakdown voltage.

4.4 The Parasitic Capacitor Waveform

The voltage waveform across the parasitic capacitor is interesting but not easily displayed due to the difficulty of constructing submersible half megavolt probes. However this waveform may be displayed by a novel technique using the high voltage probe already mounted on the streamer chamber electrodes.

The series spark gap is pressurised above the maximum breakdown pressure of the voltage being used. Under these conditions it acts like a pure capacity of 25 ± 5pf. The voltage waveform on the parasitic C_p now appears on the high voltage electrode of the streamer chamber attenuated by an amount equal to the ratio of the electrode capacity to the spark gap capacity. It is necessary to remove the terminating resistors of the electrodes during this exercise to produce a time constant in this section of the attenuator which greatly exceeds the time constants of the waveform on C_p. The waveform on the high voltage electrode may now be displayed on an oscilloscope (Tektronix type 519) using the high

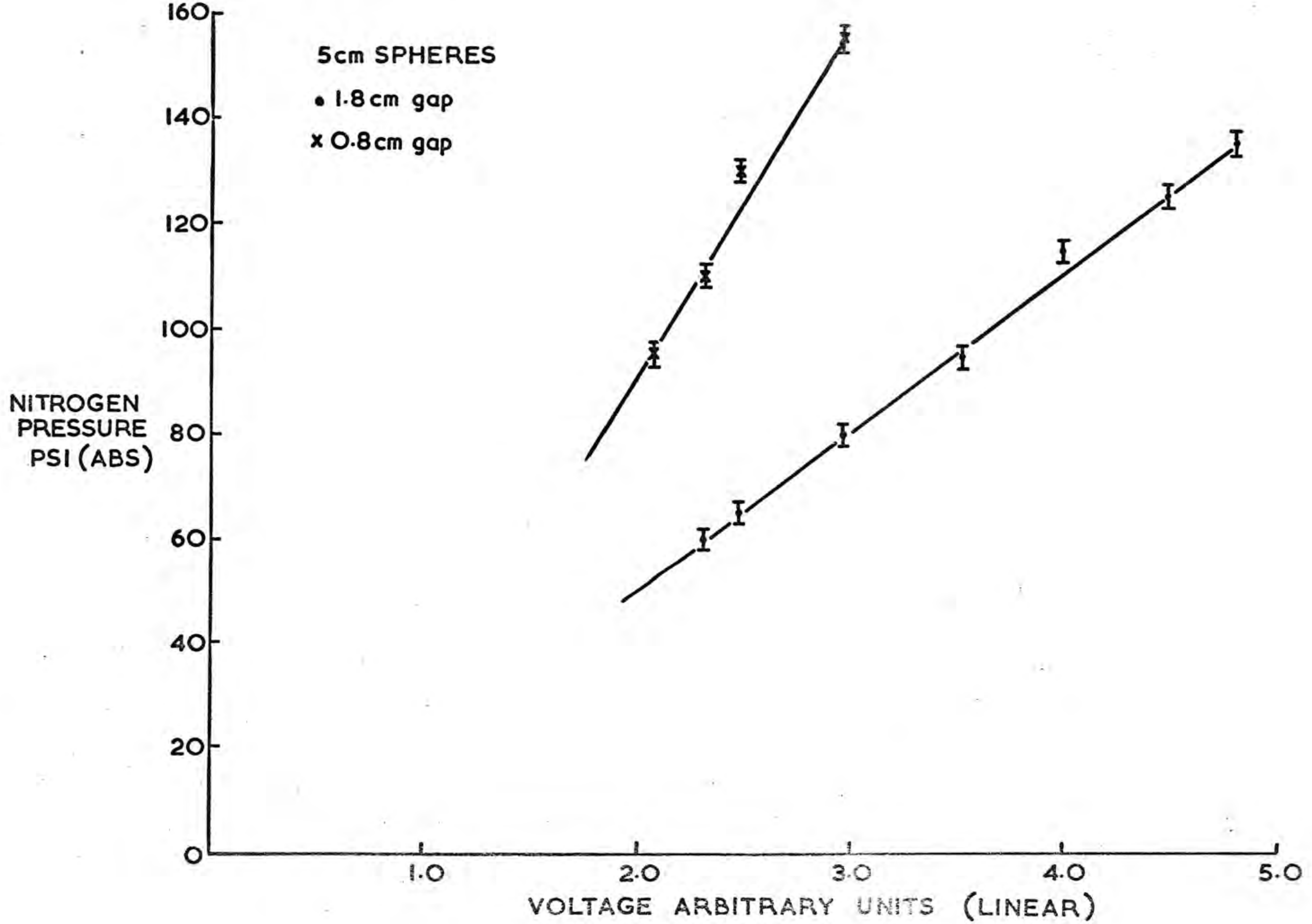
160
140
120
100
80
60
40
20
0
NITROGEN PRESSURE PSI (ABS)
5cm SPHERES
• 1.8cm gap
x 0.8cm gap
1.0
2.0
3.0
4.0
5.0
VOLTAGE ARBITRARY UNITS (LINEAR)

Figure 4.2

voltage probe described previously in section 3.6. This whole attenuating system cannot be accurately calibrated due to the uncertainty in the capacity of the spark gap and the time constant effects produced by the finite leakage resistance of the water in the tank but a vertical sensitivity of 350 ± 50kV/cm is estimated. Also the time constant of the transmission line divide probe is 1.25μsec which is similar to the expected decay constant of the pulse to be measured (section 2.6). This will produce a modification of the waveform as seen on the oscilloscope. A typical waveform is shown in Figure 4.3 and was produced with a Marx generator stage voltage of 34kV, an output inductance of $10\mu H$ and a parasitic capacity of 375pf. The leading edge of the waveform should be compared with the expected waveform which was shown in Figure 2.13, and both rise times can be seen to be 165nsec. The slight undershoot in Figure 4.3 at $>1.5\mu$ sec is caused by the short probe time constant mentioned above.

4.5 The Water Dielectric

When the tank housing the parasitic capacitor and the spark gaps is filled with pure deionised water, the decay time constant of the pulse on C_p is long and this is shortened by the addition of tap water. The leakage resistance is usually adjusted to between 1kΩ and 2kΩ. After several weeks of operation the water becomes contaminated with dissolved impurities from the tank contents and various unidentified life forms. These do not seriously impa~~re~~ir the operation of the device but do result in a slow decrease in the resistivity of the water. This can easily be compensated for by a corresponding increase in the Marx generator charging voltage (< 5%) but after a few months of operation the water is usually changed in order to reduce the stress on the generator's capacitors.

Occasionally bubbles are formed in the water which collect on the under surface of the earth plate of C_p. These are a potential source of breakdown and must be removed. Their origin is not known but possible sources are: the release of dissolved air from the water, the production of gases during possible partial breakdown of the water, electrolytic

FIGURE 4.3

TRANSIENT WAVEFORM ON THE PARASITIC CAPACITOR

VERTICAL SENSITIVITY 350 ± 50 kV/cm

HORIZONTAL SENSITIVITY

TRACE	1) 1 μ sec/cm
	2) 500 nsec/cm
	3) 200 nsec/cm
	4) 100 nsec/cm
	5) 50 nsec/cm

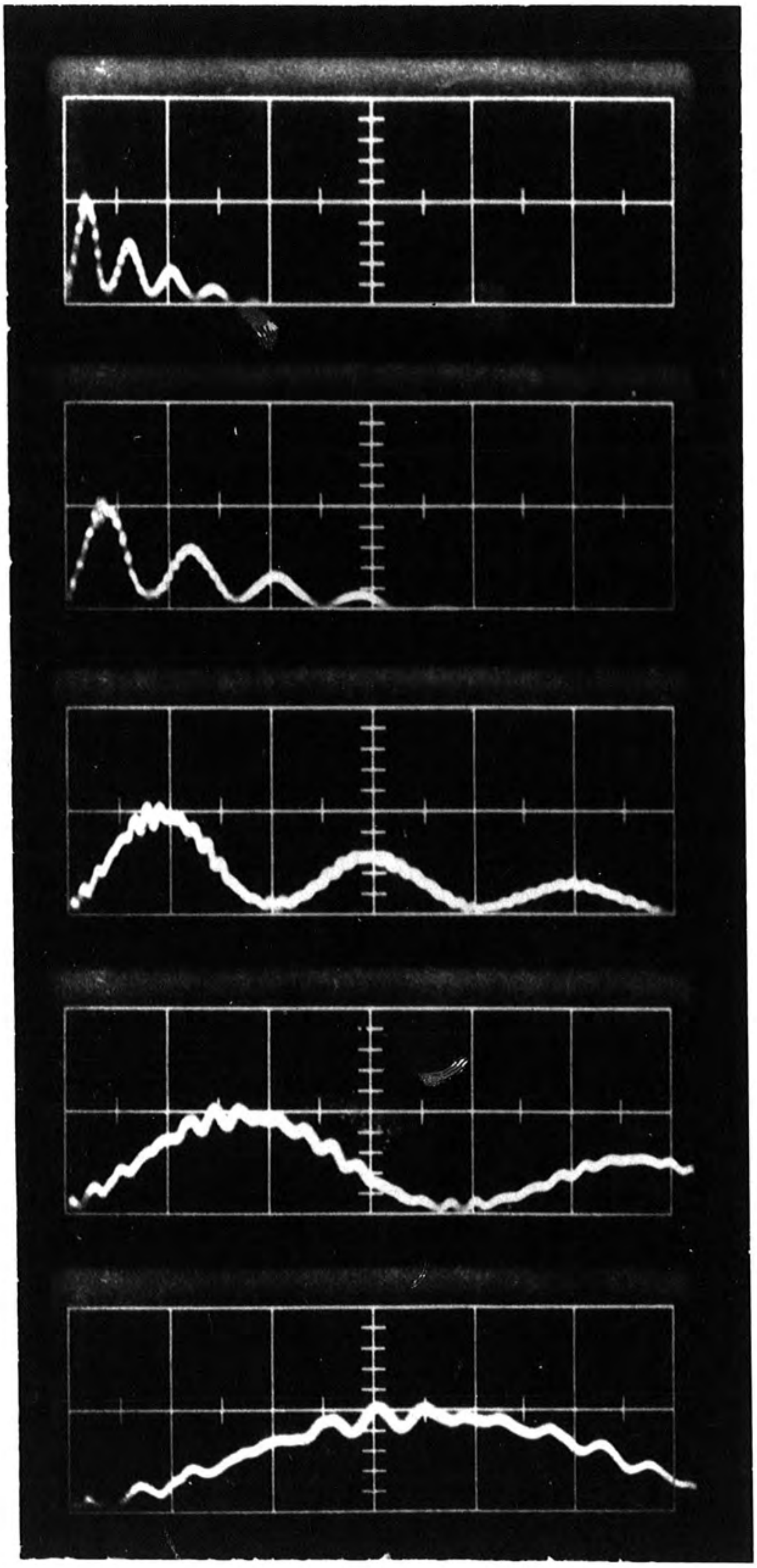

action in the water and the release of gas by micro-organisms. The second two are the most probable but no perturbations of the produced pulse, attributable to breakdown of the water, have been observed.

4.6 Matching the Electrode Termination

The terminating resistors of the streamer chamber were matched to the characteristic impedance of the electrode structure empirically. The criteria used to indicate adequate matching were a uniform streamer luminosity throughout the chamber and the critical damping of the waveform produced when the shunt spark gap fired. It is not possible to use the accepted methods of pulse reflection measurements to achieve matching as the pulse length exceeds the pulse transit time of the electrodes. If the termination is too low the streamer brightness decreases towards the termination and the decaying pulse, as seen using the probe, approaches zero volts rather slowly. If the termination is too high the intensity variation of streamer brightness reverses its direction and the pulse develops a negative overshoot and a subsequent oscillation about zero. Photographs of cosmic ray showers as detected by the streamer chamber have proved very useful in demonstrating brightness anisotropies. The best match was found using a 35Ω termination which compares well with the theoretical characteristic impedance of the electrode structure which is 30Ω. A variation of $\pm 2\Omega$ in the terminating resistance can easily be tolerated.

4.7 Generation of the Pulse

When a low dielectric constant, insulating material is used in the output side of the pulse shaper tank, a smooth R.C pulse can be generated on the electrodes by the discharge of C_p using the series spark gap. Such a pulse has a rise time of 5 nsec and a decay constant of $(C_p+C_c)R_L$. On firing the shunt spark gap, to remove the surplus energy from the Marx generator, the RC pulse is clipped at its peak and the energy which was contained in the tail of the pulse appears in the form of an oscillation which is $\frac{1}{3}$ of the amplitude of the main pulse and of similar time constant.

This oscillation decays in about 300 nsec. Such a pulse is of course unsuitable for streamer generation because of its long tail and its ill defined height and width.

It was found that if water is used in the output side of the water tank there are beneficial changes in the pulse shape which outweigh any disadvantageous losses of efficiency due to the increased stray capacities. The effect is probably due to less critical damping of the discharge pulse produced by the increase of these very strays. A series resonance is stimulated between C_p and C_c, the first oscillation of which approaches zero about 22nsec after the start of the pulse. The second peak of the oscillation never reaches any significant height due to its rapid decay through the load resistance R_L. The result is a single symmetrical pulse. Figure 4.4a shows a number of such pulses generated using a constant Marx generator output voltage. No shunt gap is used but the pressure in the series gap is varied between traces. The exact conditions are shown on the fly sheet to the figure. The ratio of initial pulse height to the tail height, which is produced by direct charging of the electrodes from the Marx generator, increases as the pressure in the series spark gap increases and it fires nearer the top of the output waveform from the Marx generator on C_p. Figure 4.3. In the example shown in Figure 4.4, for 100psi in the spark gap, the tail is very small but is still finite and must be removed by the shunt spark gap. The variation of pulse height with series gap pressure is shown by the centre curve of Figure 4.5. The effect on the pulse shape shown in Figure 4.4a trace 5, of the shunt gap firing at various pressures, is shown in Figure 4.4b. When the shunt gap fires early during the pulse the energy is dissipated, as before, in the form of an oscillation. However, the pulse has a fast fall time and is of the order of the formative time of the shunt spark gap. This can therefore be made to fire late in the pulse resulting in little perturbation of the original pulse and the removal of the surplus energy from the Marx generator as required. The

FIGURE 4.4

PULSE PRODUCTION IN THE STREAMER MODE

	(A)	(B)
VERTICAL SENSITIVITY	176 ± 5kV/cm	176 ± 5kV/cm
HORIZONTAL SENSITIVITY	20nsec/cm	20nsec/cm
MARX GENERATOR VOLTAGE	36kV/stage	36kV/stage
PARISITIC CAPACITY	375pf	375pf
TERMINATION	38 Ω	38Ω

		SERIES GAP PRESSURE	SHUNT GAP PRESSURE
TRACE	(1)	15 psi	15 psi
	(2)	40 psi	40 psi
	(3)	65 psi	65 psi
	(4)	90 psi	90 psi
	(5)	115 psi	120 psi

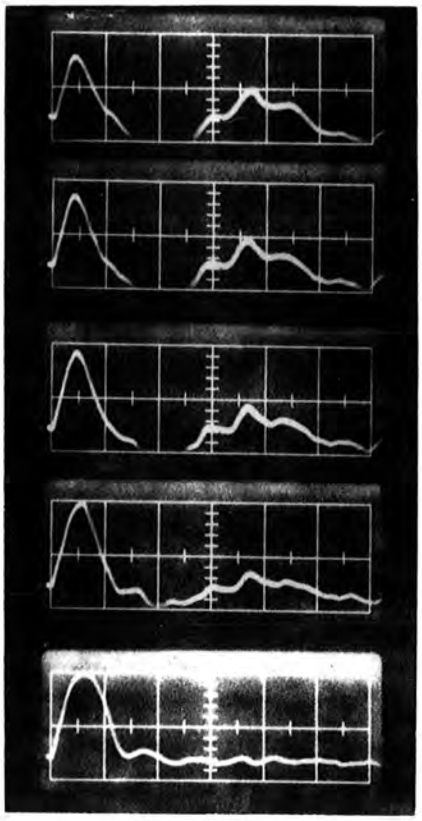

(B)

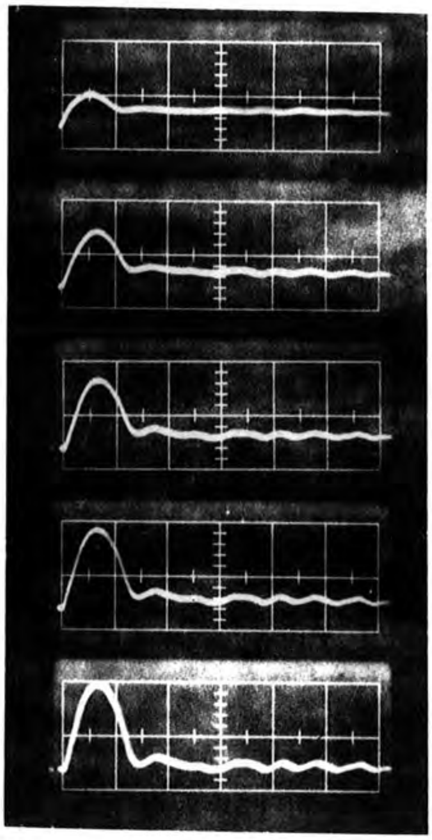

(A)

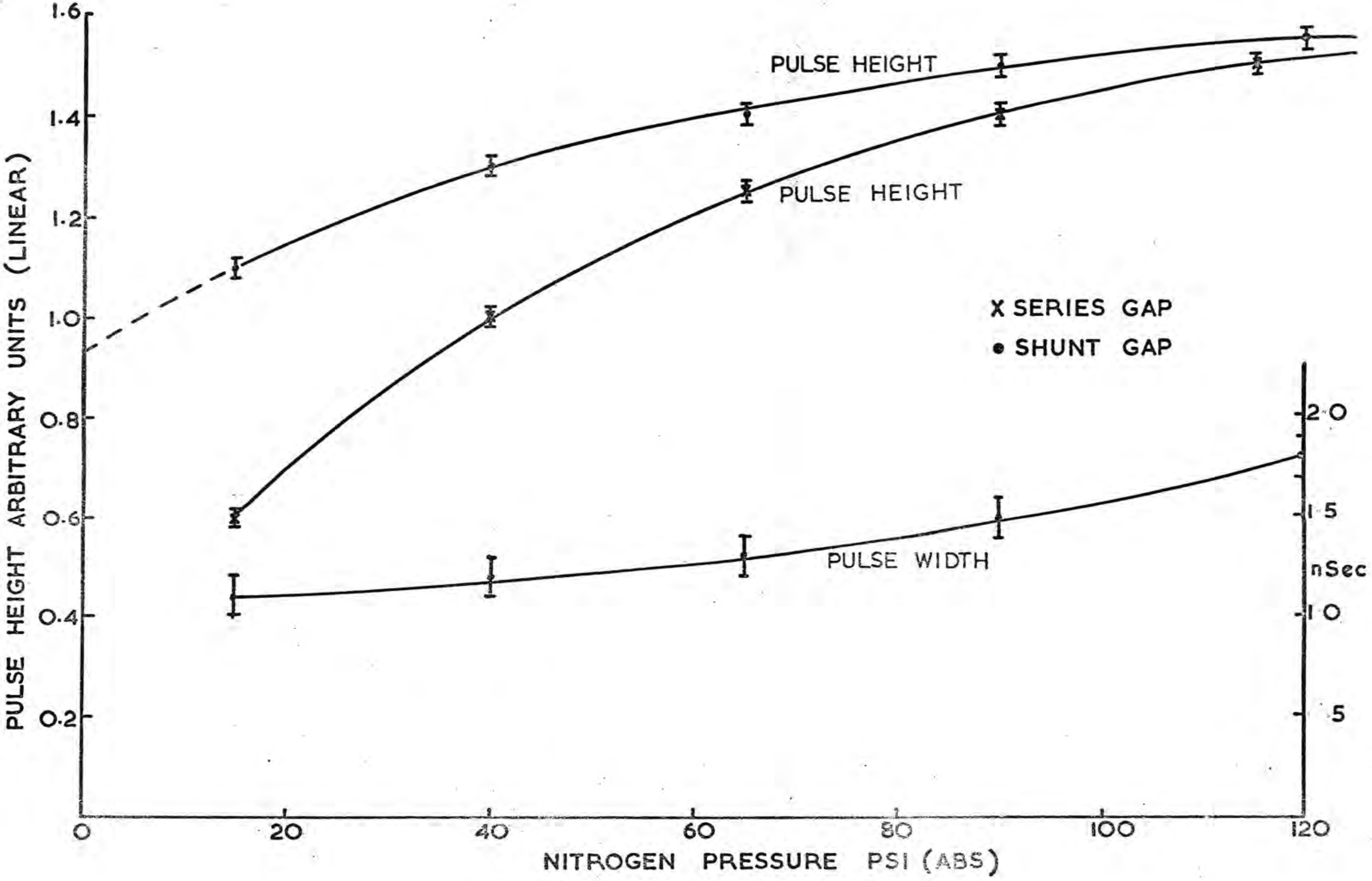

1.6
1.4
1.2
1.0
0.8
0.6
0.4
0.2
PULSE HEIGHT ARBITRARY UNITS (LINEAR)
PULSE HEIGHT
PULSE HEIGHT
X SERIES GAP
● SHUNT GAP
PULSE WIDTH
2·0
1·5
nSec
1·0
5
0
20
40
60
80
100
120
NITROGEN PRESSURE PSI (ABS)

Figure 4.5

upper curve of Figure 4.5 shows the variation of pulse height, and the lower curve the variation of pulse width (FWHM), with the pressure of nitrogen in the shunt gap. The change of this pressure gives satisfactory control over the pulse width in the range 13.5 to 17nsec. The maximum length of pulse is governed by the natural resonance of C_p and C_c through the inherent inductance which is 75nH and also the necessity for precise shunt operation, Figure 2.12c. The minimum length of the pulse is determined by the generation of the unwanted tail oscillations produced when the shunt gap fires to cut off the pulse. Over the range of pulse widths which can be generated in this manner the pulse height varies by only 5%,a change which can be easily counteracted by an increase in the generator output voltage. The maximum pulse height is limited by spurious breakdown of the air around the electrodes, in particular near the input and along the corona guard of the high voltage electrode. These effects limit the maximum pulse height to ~ 20kV/cm i.e. 300 kV but this could be increased by reducing the field distortions in these regions.

By extrapolating the pulse amplitude against shunt gap pressure curve back to zero pressure, where it may be considered to have 'zero' breakdown voltage, the formative time of the spark may be estimated and is found to be 6nsec.

Stability of the amplitude and duration of the applied pulse is of great importance because of the high velocity of streamer propagation $>10^8$ cm/sec, and the strong dependance of streamer velocity on applied field, Figure 2.3. Five consecutive pulses are shown in Figure 4.6. The rise time is 8nsec and varies very little over the whole range of possible pulses. The top of the pulse is fairly flat and extends from 3 to 7nsec depending on pulse length. The fall time of the pulse is similar to the rise time. The amplitude is constant, for constant operating conditions to within ± 0.1 kV/cm. and the width (FWHM) to within 200psec. Most of the apparent time jitter shown in Figure 4.6 is attributable to trace starting errors caused by statistical fluctuations

FIGURE 4.6

FIVE CONSECUTIVE STREAMER CHAMBER PULSES

VERTICAL SENSITIVITY 176 ± 5kV/cm

HORIZONTAL SENSITIVITY 10nsec/cm

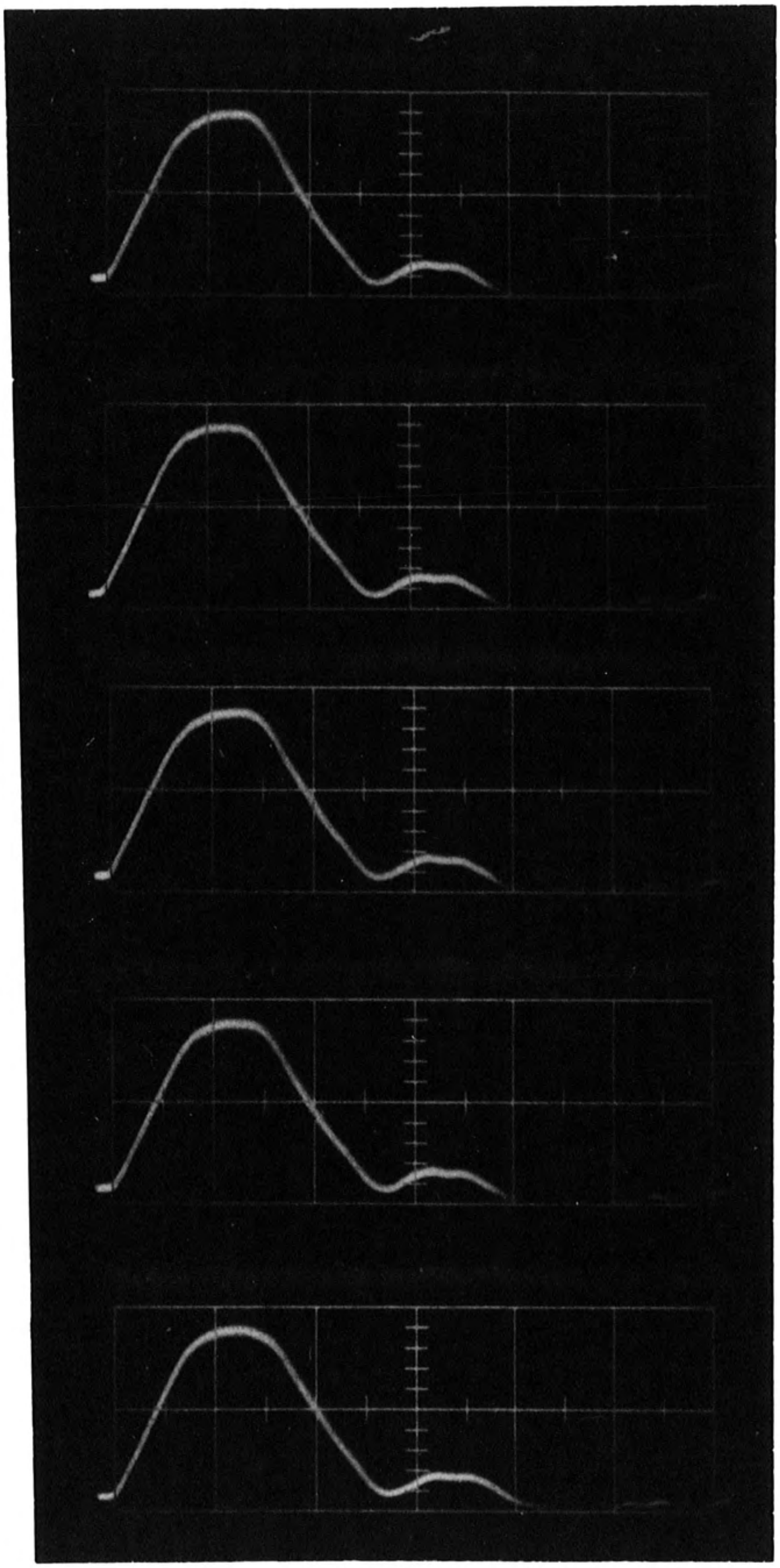

in the CRO triggering circuits. The oscillograms were obtained using 10.000 ASA Polaroid film in a standard camera and the pulse parameters were measured using a travelling microscope. The long term stability has already been discussed in section 4.5 and to counteract small changes in the pulse it was monitored daily and the system adjusted accordingly. No changes in the performance of the spark gaps have been observed since construction.

4.8 Pulse Generation Delay

The delay between the passage of the triggering cosmic ray particle and the application of the high voltage pulse to the streamer chamber depends upon many parameters, for example the operating pressures and voltages of the various spark gaps. Measurement of the delay under all conditions is therefore impractical. A representative graph of total delay as a function of the Marx generator pressure, the most significant controlling parameter, is shown in Figure 4.7. A charging voltage of 50kV/stage was used as it is typical of normal operation. This graph should be compared with the Marx generator characteristics in Figure 4.1. The full range of pressures at 50kV/stage cannot be used as the Marx generator, in accordance with normal practice, was only allowed to charge for 40 seconds when producing the results shown in Figure 4.7 and the delay becomes infinite at 19 psi. The error bars in Figure 4.7 represent ± one standard deviation of the statistical fluctuation of the delay time. No account has been taken of scintillator, photomultiplier, and cable transit times in this figure and for the simple detection arrangements used here a further 70nsec should be added to the delay times shown. The total minimum delay time, over the range of pressure used for taking results, is assumed to be constant at 600nsec and the statistical fluctuations are considered negligible.

The variation of delay with series gap pressure was found using the circuit in Figure 4.8. The circuit is that normally used to drive spark chambers. When the spark gap fires an exponentially decaying

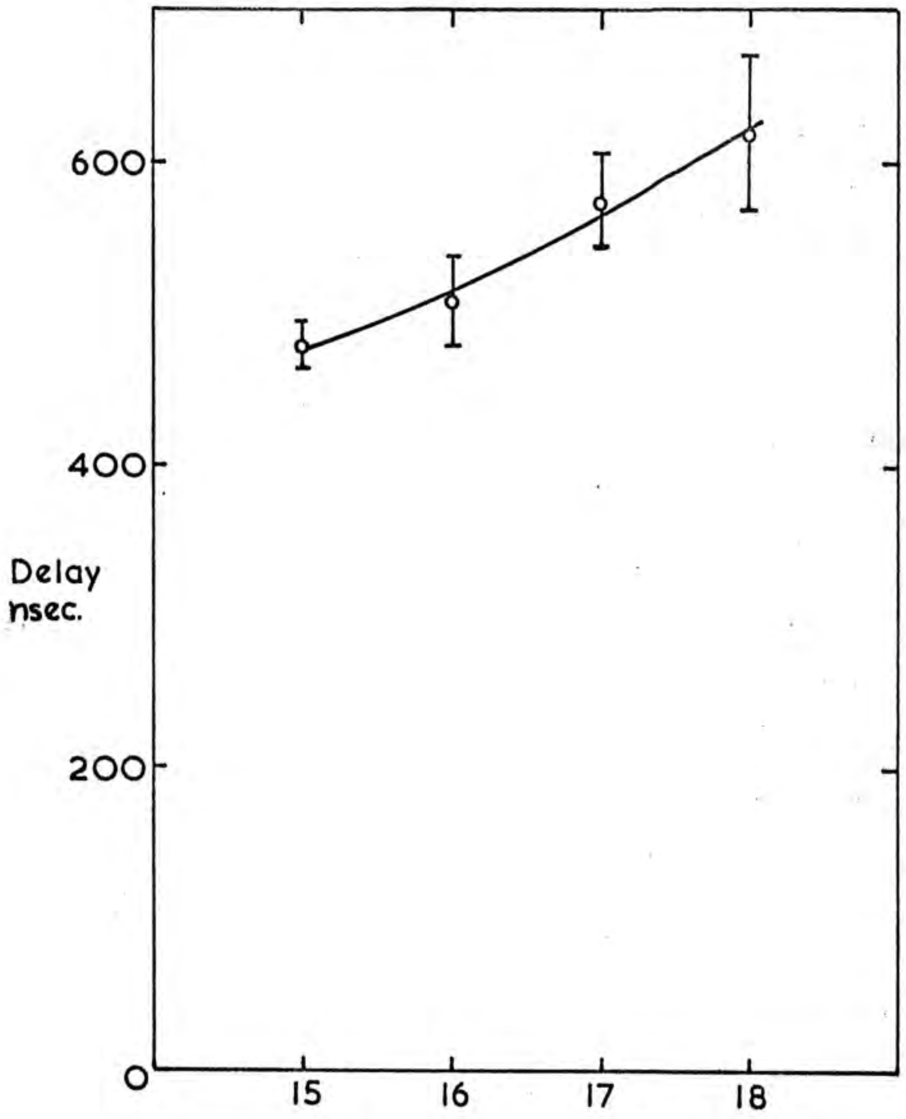

STREAMER CHAMBER DELAY

Figure 4.7

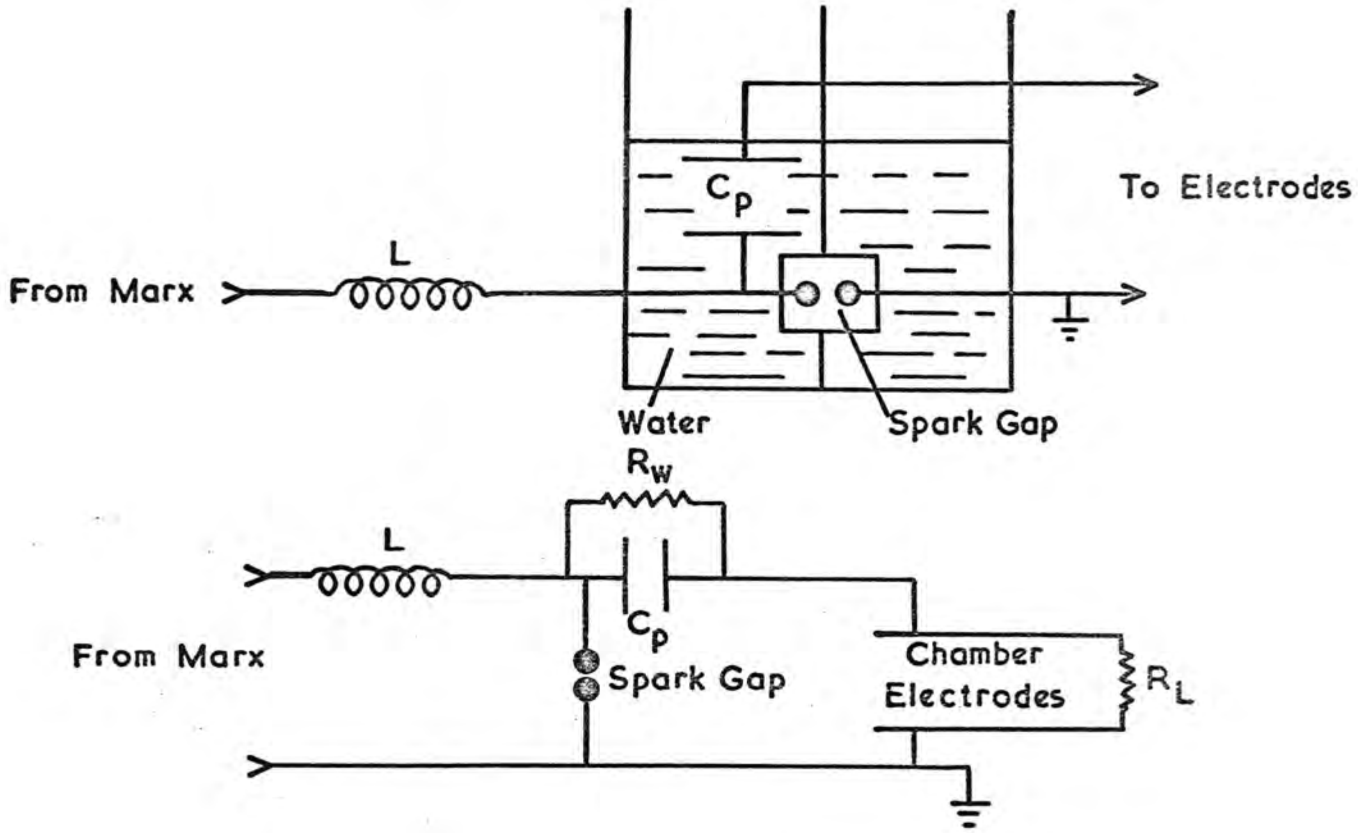

'SPARK CHAMBER' TYPE PULSING SYSTEM

Figure 4.8

pulse, opposite in polarity to the Marx generator output voltage, is produced across the electrodes and the remaining charge in the generator is shunted to ground. The Marx output current transient also appears on the electrodes as the parastic capacity charges through the terminating resistors of the streamer chamber. Hence the length of this transient, before the firing of the spark gap, may be determined. This is shown in Figure 4.9. The shape of the curve is a product of the 'sinusoidal' output voltage of the generator and the nonlinearity of the Paschen curve in nitrogen at pressures > 100 psi. The maximum change in delay time which can be produced by a change in the series spark gap pressure is 90nsec and amounts to only 30 nsec over the range of pressures actually utilised.

4.9 Streamer Generation

Photographable streamers can be generated in the neon helium gas mixture with the range of pulse heights between 17.5 and 20kV/cm and the range of pulse lengths 13.5 to 17nsec (FWHM) using the streamer chamber here described.

Intermediate pulse parameters proved the most satisfactory for example 18.8kV/cm and 15nsec. Typically streamers so generated have lengths, parallel to the field, between 0.3 and 1.8cm. The majority of streamers are < 0.8cms long and appear as roughly cylindrical streaks showing little change of width along their length. These diameters are in the range 0.05 to 0.3cms. The longer streamers tend to have the larger central diameters and where these streamers extend beyond the shorter ones there is a rapid increase in diameter. Some of these develop lobes of almost spherical shape and have diameters approaching 1cm. The boundaries of such streamers are diffuse and a radial finger-like structure is occasionally visible.

A typical 90° stereo photograph of a cosmic ray track taken in the streamer chamber is shown in Figure 4.10. The driving pulse parameters and scale of the picture are given on the fly sheet.

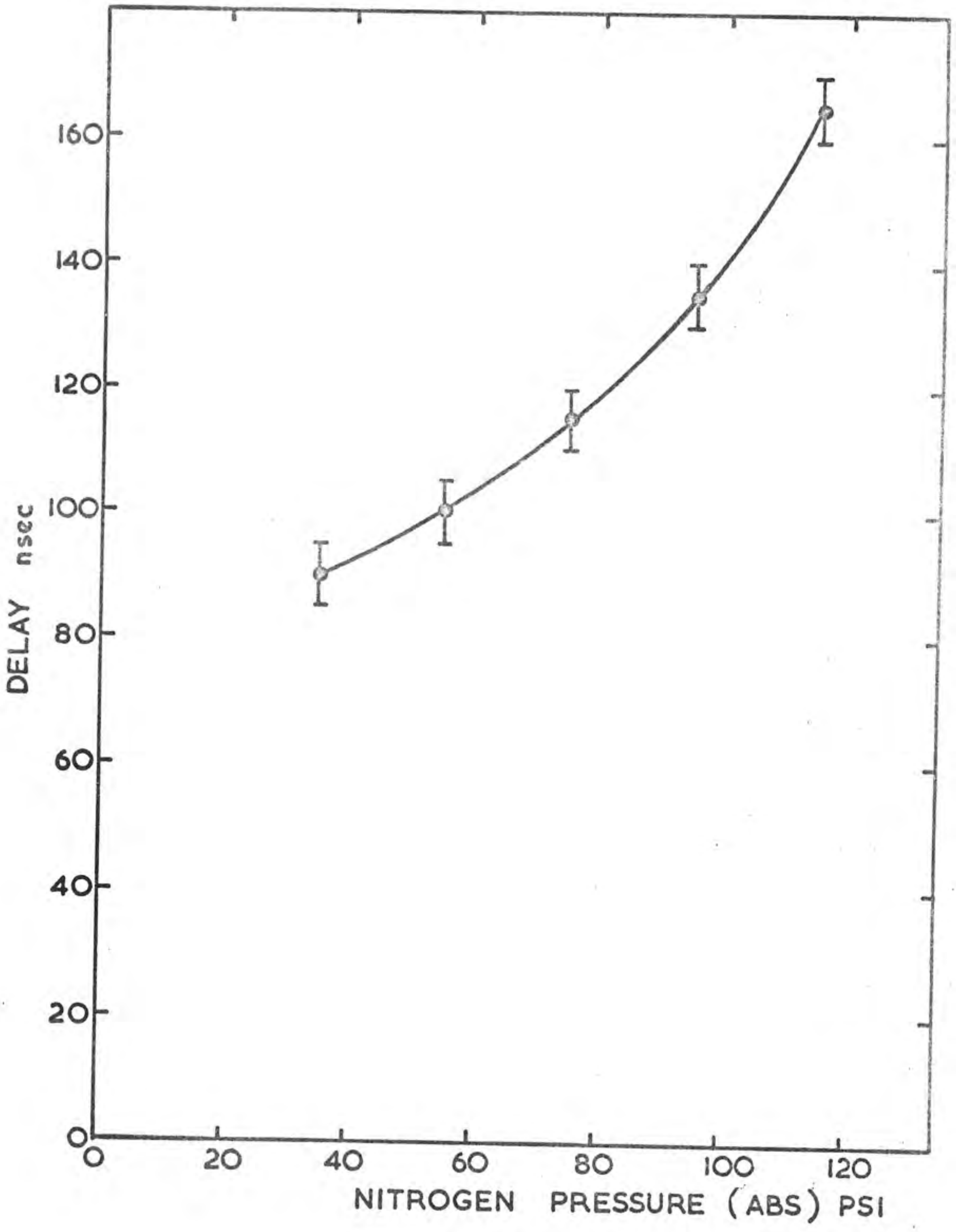

DELAY nsec
0
20
40
60
80
100
120
140
160
0
20
40
60
80
100
120
NITROGEN PRESSURE (ABS) PSI

Figure 4.9

FIGURE 4.10

90° STEREO PHOTOGRAPH OF A TYPICAL COSMIC RAY TRACK

MAGNIFICATIONS OF EACH VIEW ARE SIMILAR BUT NOT IDENTICAL ABOUT 50cm OF TRACK IS SHOWN IN EACH CASE

PULSE PARAMETERS 18.8kV/cm for 15nsec (FWHM)

PULSE DELAY 600nsec

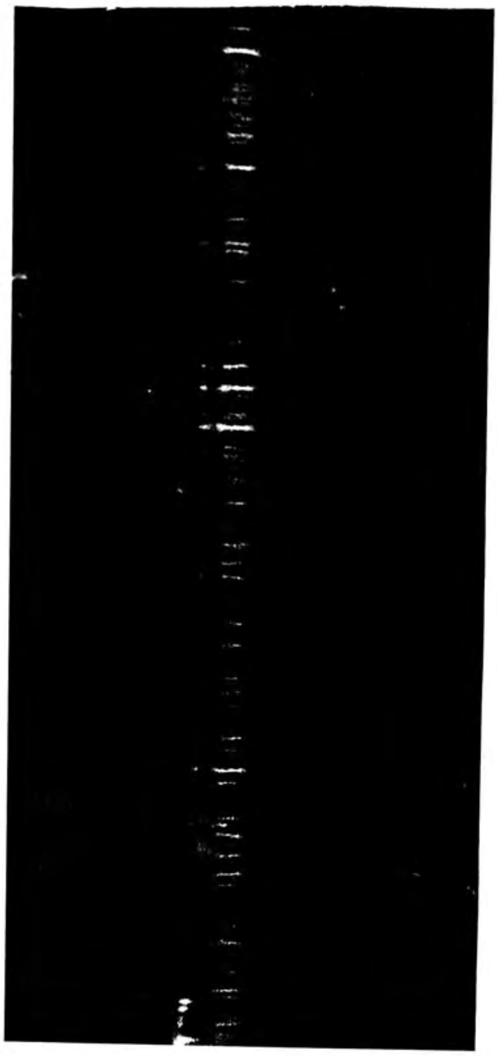

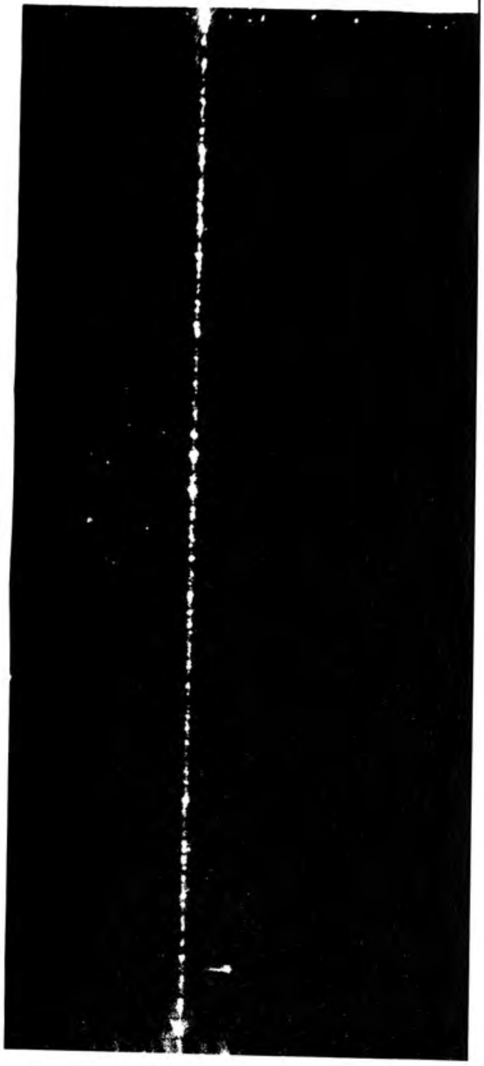

Streamer chambers are of course not completely isotropic in their performance. When particles traverse the chamber at small angles to the electric field vector, the streamers tend to join together at their centres and may even generate a complete spark between the electrodes The angle at which the streamers coalesce is dependant upon the operating conditions. Using mean streamer lengths of 0.8cms the longer streamers show signs of joining at track angles to the electric field as large as 60° but in general this angle is less than 40°. With angles less than 20° little of the structure of the original streamers can be seen. When using the chamber to detect cosmic rays the majority of such highly angled tracks are due to δ rays which create a higher ionisation density in the gas than a typical 2 GeV cosmic ray muon. This will doubtless give an underestimate of the isotropy in this case.

A decrease in streamer length, or an increase in pulse delay time has only a small effect on the joining of streamers over the range considered (1). The effect is reduced as the formative time of the spark increases. In the former case this is due to the increased distance one streamer must travel to meet the next. In the latter case due to the greater spatial dispersion of the streamers after diffusion of the electrons released by the particle.

For tracks making angles less than 20° with the electric field a highly conducting channel is created and where the discharge strikes the melinex windows of the streamer chamber it spreads out over the surface to form a disc. Such discs vary in diameter from 1 to 6 cms with occasional ones growing to 12cms in diameter. Such phenomena are less frequent at longer delays again due to the increased formative time of the spark. These discs often display radial structure and must propagate over the melinex surface with velocities approaching 10^{9}cms/sec if they are to occur during the pulse.

It was found that sparks generated parallel to the field, either along tracks, or by spurious breakdown, were capable of puncturing the melinex windows producing undesirable leaks in the system. The

50μm melinex was virtually useless because of this and the 120 μm was found to be more suitable. A greater thickness of melinex would be preferred but more than 150 μm of melinex has poor optical transmission.

The spurious breakdown which causes many of the melinex damaging sparks is mainly produced near the walls of the chambers where the dielectric interface gives rise to distortions of the electric field (2). These distortions are lessened if the chambers are made from a material of low dielectric constant and the walls are as thin as possible. At the time of writing, chambers with 6mm perspex walls are being constructed to replace those in use.

Discharges in the chamber gas also occur where the melinex windows make contact with the wired section of the electrodes. This takes the form of a diffuse glow which causes little damage but obscures the tracks. This can be avoided by operating the chambers at a very small under-pressure such that the melinex walls become concave, thereby producing a space between the gas and the wires sufficient to take the gas out of the distorted field region.

The brief outline of the performance of the streamer chamber given in section 4.9 will be expanded in the following chapters where detailed results are given and comparisons of these with various theories made.

REFERENCES

1. ZHANKOV, I.K., Prib. Tech. Eksp 2 (1968) 56.

2. BREARE, J.M., Nuc. Inst Methods 100 (1972) 281

CHAPTER FIVE

RESULTS I

5.1 Introduction

For the purposes of this thesis the properties of the chamber have been divided into two sections. In this chapter the performance of the streamer chamber parallel to the electric field will be examined and some theoretical explanations for the obtained results will be made. In chapter six a similar treatment will be given to the characteristics of the system as seen perpendicular to the field. The properties in these two directions are, of course, not independent and many of them will be shown to be manifestations of the same basic processes.

5.2 The Statistics of Streamer Development

In chapter two it was stated that the growth of an electron avalanche in a gas could be described by the equation

$$n = \exp(\alpha x) \qquad 5.1$$

where n is the number of electrons a distance x from the start of the avalanche and α is Townsend's first coefficient. Clearly however, such growth is a statistical process and the number of electrons contained in the avalanche is subject to considerable fluctuations. These fluctuations will predominate in the early stages of development as they will be magnified by later growth of the avalanche. An elementary account has been given of these effects by Wijsman (1) and Furry (2) and the resultant electron number distribution is known as the Furry distribution.

Let $P(n,x)$ be the probability that an electron, starting at $x = o$ causes an avalanche of n electrons after drifting a distance x under the influence of an electric field. The probability that no ionisation will take place in this distance is given by the Poissonian distribution to be

$$P(1,x) = \exp(-\alpha x) \qquad 5.1$$

Similarly the probability of one ionisation between o and x is

$$P(2,x) = \exp(-\alpha x)\,(1 - \exp(-\alpha x)) \qquad 5.2$$

Hence it is found that

$$P(n,x) = \exp(-\alpha x)(1 - \exp(-\alpha x))^{n-1} \qquad 5.3$$

The mean number of electrons at x is given by

$$\bar{n} = \exp(\alpha x) = \sum_{n=1}^{\infty} np(n,x) \qquad 5.4$$

Thus $$P(n,x) = \frac{1}{\bar{n}}\left(1 - \frac{1}{\bar{n}}\right)^{n-1} \qquad 5.5$$

and as $\bar{n} >> 1$ equation 5.5 may be written approximately as

$$P(n,x) = \frac{1}{\bar{n}} \exp\left(\frac{-n}{\bar{n}}\right) \qquad 5.6$$

Which is the required Furry distribution

The probability of getting $N > n$ electrons is

$$\int_{n}^{\infty} \frac{1}{\bar{n}} \exp\left(\frac{-n}{\bar{n}}\right) dn = \exp\left(\frac{-n}{\bar{n}}\right) \qquad 5.7$$

Throughout this derivation the value of α has been assumed constant In fact for n greater than 10^7 α is reduced by space charges and during the early stages of avalanche growth the electron energy, and hence α, may be dependent on x. However a discussion of these effects is postponed until the concluding chapter of this thesis and they will be assumed negligible throughout the following theory. The differential probability derived from equation 5.7 where $M = \frac{n}{\bar{n}}$ is

$$P_1(M,x)\, dM = \exp(-M)\, dM \qquad 5.8$$

Now in the streamer chamber an avalanche may start from many electrons. For an avalanche starting from Z electrons the number of electrons in the avalanche is

$$n_z = \sum_{i=1}^{z} n_i \quad \text{also} \quad M_z = \sum_{i=1}^{z} m_i$$

Supposing an M_i distribution according to equation 5.8 then a differential probability of

$$P(M_z,x)\,dM_z = \frac{1}{\Gamma(z)}\, M_z^{z-1} \exp(-M_z)\, dM_z \qquad 5.9$$

is obtained, The probability $W_z(n,x)$ that the avalanche with z initial electrons contains, after travelling a distance x, a number of particles equal to or larger than n is given by

$$W_z(n,x) = \frac{1}{\Gamma(z)} \int_{n/\bar{n}}^{\infty} M_z^{z-1} \exp(-M_z)\, dM_z$$

$$= \frac{1}{\Gamma(z)}\, \frac{1}{2^{z-1}} \int_{\sqrt{\frac{2n}{\bar{n}}}}^{\infty} t^{2z-1} \exp\left(\frac{-t^2}{2}\right) dt \qquad 5.10$$

The right hand side of equation 5.10 is the function representing the χ^2 distribution.

In chapter two it was indicated that an avalanche will transform into a streamer when the number of electrons in it reaches 10^8. Equation 2.1 shows that this occurs when $\alpha x = 20$. Therefore the probability $F_z(L)$ that, after an avalanche has covered a distance L it will transform into a streamer is

$$F_z(L) = \frac{1}{\Gamma(z)}\, \frac{1}{2^{z-1}} \int_{s}^{\infty} t^{2z-1} \exp\left(\frac{-t^2}{2}\right) dt \qquad 5.11$$

where $s = \left(2 \exp\left(20\left(1 - \frac{L}{L_m}\right)\right)\right)^{\frac{1}{2}}$

and L_m is the Meek length, the mean distance through which one electron initiating an avalanche must travel before the avalanche streamer transition occurs.

5.3 The Basic Model for Track Formation

In the previous section only single avalanches initiated by one or more electrons were considered but along the track of an ionising particle there may be many closely spaced electrons. This will result in the interaction of neighbouring avalanches. Chikovani has outlined a statistical model which can be used to describe the formation of a particle track which passes perpendicular to the electric field in a streamer chamber (3).

The area, perpendicular to the electric field, which is covered by the electrons is first divided into cells Ro x Ro where Ro is defined as the linear size of the area within which the development of the avalanches is suppressed by the streamer due to space charge effects. The arrangement of the cells is chosen so that track axis divides the central cell into halves. Only one streamer may develop in each cell.

The cells are each divided into subcells $R_1 \times R_1$ where R_1 is the linear size of the area within which the electrons all go to form one avalanche. Each cell therefore contains $S = (\frac{R_o}{R_1})^2$ subcells. This is shown in Figure 5.1. The subcells are arranged so that the line passing through the centre of a cell parallel to the track divides the central subcells into halves.

In the original model developed by Chikovani the distribution of electrons across the track is assumed to be uniform to simplify the calculation. The width b of the distribution is chosen to contain 80% of these electrons.

Let S_i be the number of subcells in the ith cell which are covered by the track and d_i the average density of electrons in each subcell. Then the number of subcells in the ith cell which are occupied by at least one electron is, from the Poissonian distribution, given by,

$$j_i = S_i \ (1 - \exp\ (-d_i)) \qquad 5.12$$

The average number of electrons in the occupied subcell is therefore

$$k_i = \frac{d_i S_i}{j_i} = \frac{d_i}{(1-\exp(-d_i))} \qquad 5.13$$

According to equations 5.11, 5.12 and 5.13 the average number of streamers per unit track length is given by the expression

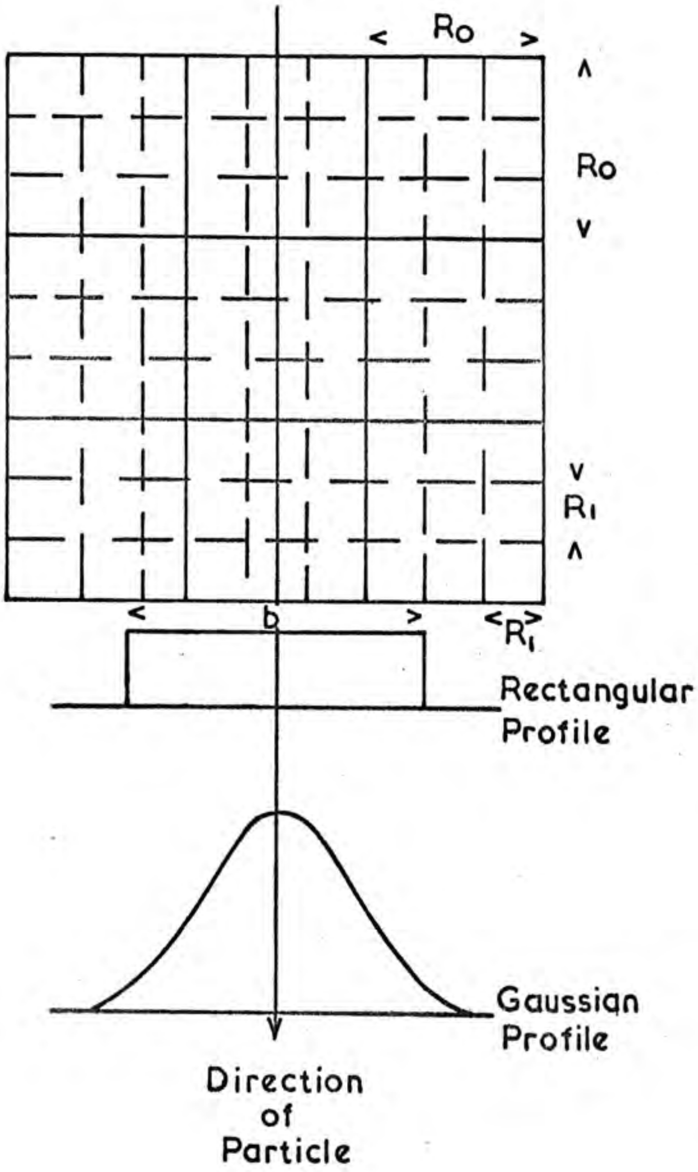

MATRIX FOR STREAMER GENERATION MODEL

Figure 5.1

$$No = \sum_{i} (1-\exp(1-S_i(1-\exp(-d_i)\, F_{k_i}\, (L/L_m)))) \qquad 5.14$$

Where the summation is performed over all the cells covered by the track.

A computer programme was written to generate the number of streamers per centimeter which would be expected on a particle track for various values of $\frac{L}{L_m}$ using the above theory. This model performs well but is not wholly satisfactory. The distribution of the electrons across the track is taken to be uniform and the choice of its width as say $8\sqrt{Dt}$, where D is the diffusion constant and t is time, must be considered arbitrary and cannot be expected to be correct for all values of t as the actual electron density at the chosen cut off point will vary with delay time. Also when, with increasing time, the edge of the rectangular electron distribution crosses a cell boundary, discontinuities in the programme output occur which are unacceptable.

5.4 The Improved Model

The most obvious improvement to the model is the replacement of the rectangular distribution with one of the Gaussian, normal type to describe the electron distribution across the particle track. Rather than calculating the mean electron density across the track, the electron density may now be evaluated independently in each column of subcells parallel to the track.

Thus the electron density in any subcell is given by

$$Ed = 0.5 \times I_o \times R_1(\mathrm{erf}(X_2) - \mathrm{erf}(X_1)) \qquad 5.15$$

where I_o is the most probable number of ion pairs created per centimeter by the passage of a particle through the chamber gas.

$X_2 = \frac{x_1}{\sqrt{4Dt}}$ and $X_1 = \frac{x_2}{\sqrt{4Dt}}$ where x_1 and x_2 are the coordinates of the subcell edges.

---

ie
bed
l
he
GAUSS
equati
of a
nt over
he mode.
track
e to th
bution
anged
n the
icle
umber of
d value
its
0.67cm
optical
the
value
is mode
makes

this difference negligible.

The value of I_o depends upon three main factors. The first of these is the delay time of the high voltage pulse. The primary ionisation in neon is given by Charpak et al (5) to be about 12 cm^{-1} for a minimum ionising particle. However, these electrons will decelerate in the gas by ionising and exciting collisions to energy levels below the ionisation potential of neon in less than the minimum value of delay obtainable with the streamer chamber. Therefore the required value of I_o is taken to be the secondary ionisation density. This is given as 37 cm^{-1} (5).

The second important factor is the energy of the detected particle. The results of Eyeions et al (6) and Jones et al (7) indicate an increase of 47% in the energy loss of a cosmic ray muon in neon from minimum ionising momenta (300 MeV/c) to plateau momenta (100 GeV/c) and a 'typical' cosmic ray muon of momentum 2 GeV/c shows an increased energy loss of about 20% over a minimum ionising particle.

The third factor which influences I_o is the gas composition. In the gas mixture the presence of helium will effectively reduce the ionisation to around 3ocm^{-1} as the primary ionisation in helium is only 3.5 cm^{-1}(8). Therefore, as will be seen, the performance of the model has been examined for values of I_o in the range 20 to 40 ion pairs/cm in the gas mixture used.

The number of streamers per centimeter as a function of delay time τ_D, for various values of L/L_m was calculated using the model GAUSS. The relevant parameters used were; R_o = 0.65cms, R_1 = 0.15cms and I_o = 28cm^{-1}. The results are shown in Figure 5.3. Significant numbers of streamers are generated at short time delays for L/L_m = 0.9 where the number of electrons starting each avalanche will exceed unity. At longer delays however, values of L/L_m greater than unity are needed to develop all possible streamers as, due to the statistical fluctuations in avalanche production, the probability of an avalanche starting from a single electron, transforming into a streamer within the Meek length, is less than 40%. Using values of L/L_m of 1.2 nearly all possible streamers have developed and the curves reach saturation.

It is of course important to note that, because the photographic sensitivity requires the growth of avalanches beyond the transition point, the values of L/L_m which may be inferred from gathered data will be less than the values actually used by an amount equivalent to this extra growth.

The sensitivity of the streamer density to changes in ionization in the range 20 to 40 ion pairs/centimeter for various values of L/L_m and delay times is shown in Figure 5.4. The figures were generated using the model GAUSS.

For both large and small values of L/L_m the parameter is almost saturated at all values of delay but there does exist a region of moderate sensitivity in the centre of each range. This sensitivity is greatest at longer delays (100 μsec) for values of L/L_m from 0.94 to 1.0 where a change in streamer density of over 50% exists for a change in ionisation from 20 to 40 ion pairs/cm.

To test these theoretical ideas, experiments were conducted with the streamer chamber using cosmic rays of energies selected by a range telescope.

5.5 The Range Telescope

Using the energy loss curves of Sternheimer (9) and the range energy curves of Rossi (10), for muons in air and lead, a simple range telescope was constructed to select cosmic rays of known energy and is shown diagrammatically in Figure 5.2.

A three scintillator system is used, each being separated from the next by 10 cm of lead. Thus for a coincidence of type $A+B+\bar{C}$, muons of momentum in the range 240 MeV/c to 360 MeV/c are selected. These traverse the chamber between scintillators A and B and are of energies which will produce minimum ionisation in the chamber gas. Errors in the energy selection due to the finite angular acceptance of the system and the effects of multiple scattering in the lead are assumed negligible. The energy lost in the streamer chamber itself is estimated to be less than 10 MeV for such

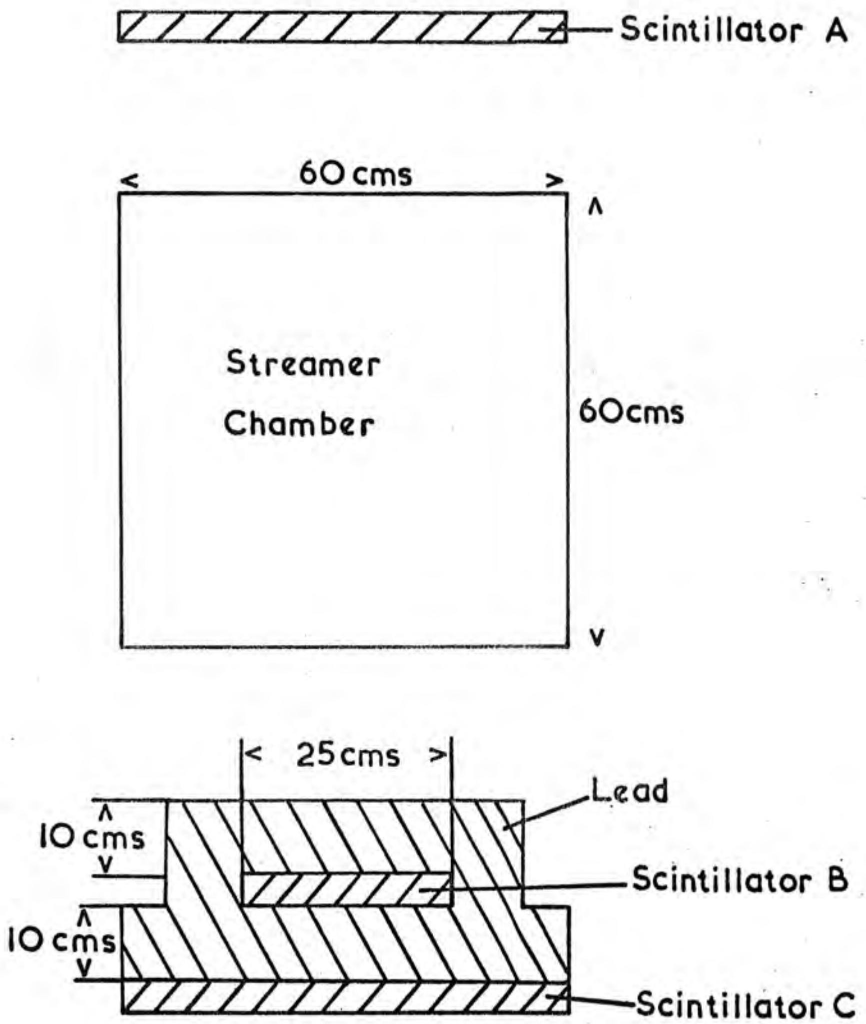

Cosmic Ray Range Telescope

Figure 5.2

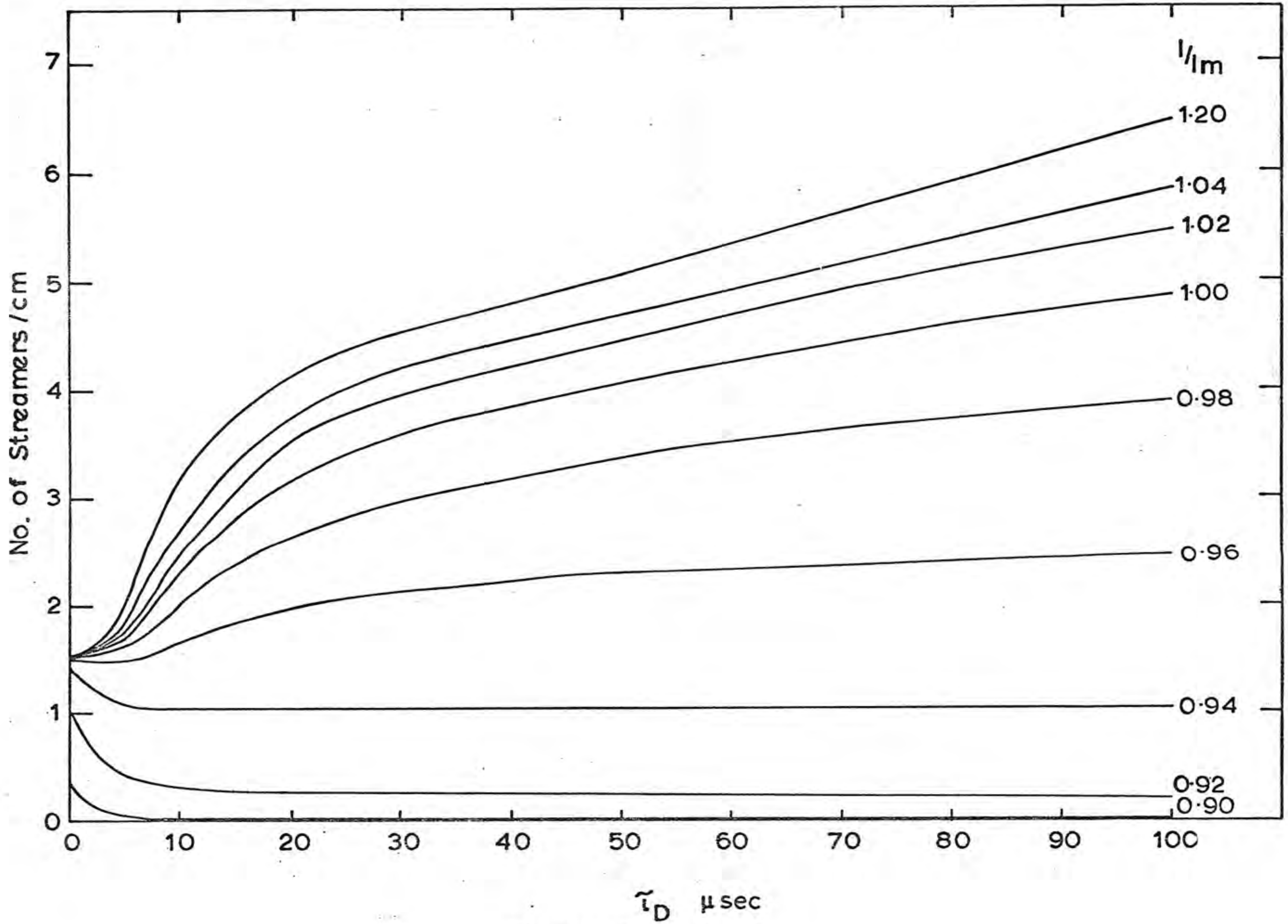
Streamer Generation Model Gauss

Figure 5.3

Streamer Generation Model Gauss

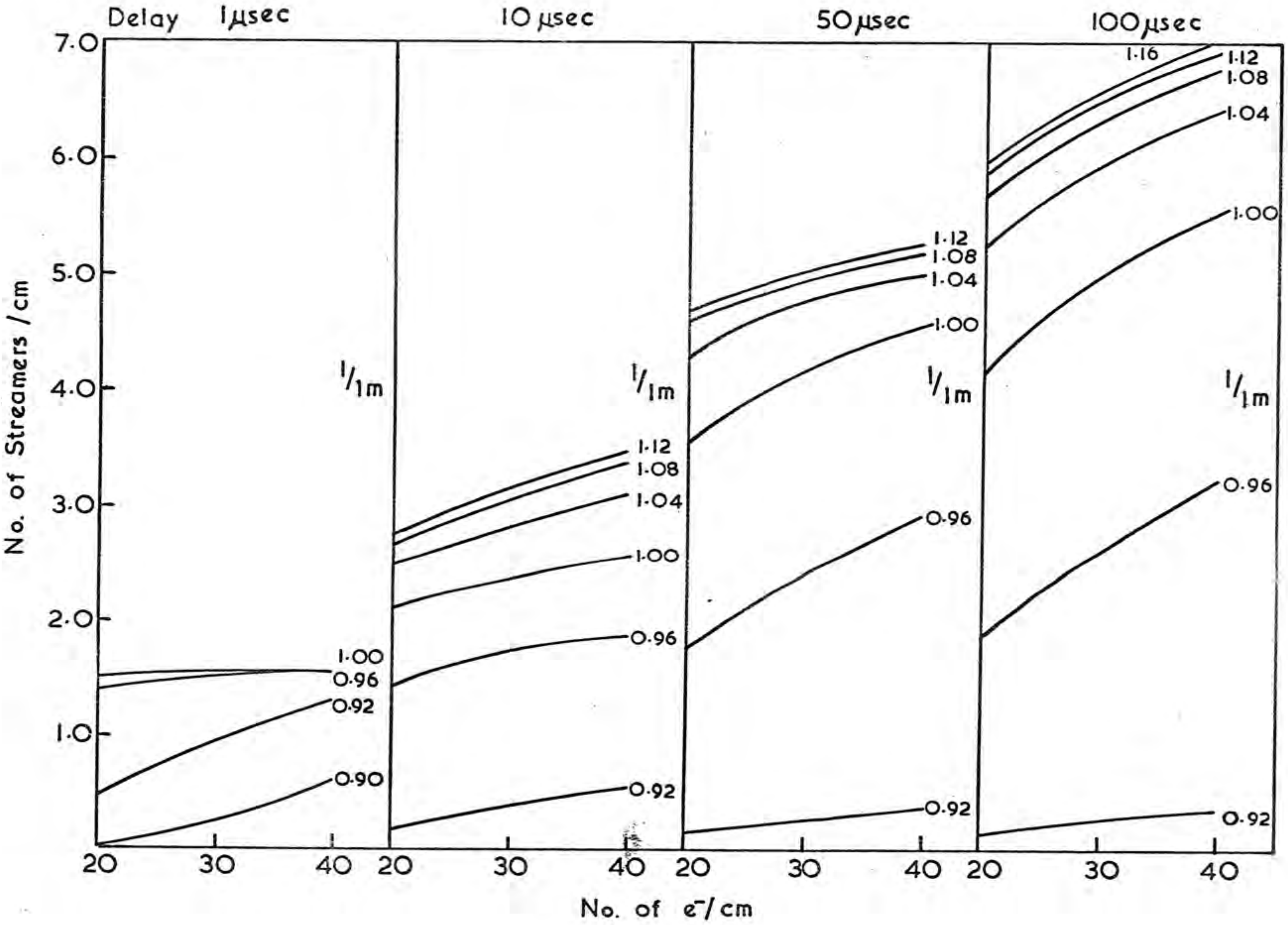

Figure 5.4

particles.

By using a coincidence of the A+B+C variety it is possible to select cosmic rays with energies great enough to penetrate both thicknesses of lead and hence obtain particles with momenta greater than 360 MeV/c. As the cosmic ray muon spectrum is peaked at about 2 GeV/c this is taken to be the most probable energy of particles selected using this type of coincidence.

5.6. The Streamer Density

Using the range telescopedescribed above,the streamer chamber was used to produce tracks of particles of minimum ionising cosmic ray muons. These were photographed using the cameras described in chapter three on Kodak 2475 film using an f number of 2.0. The event rate was about 0.5/ minute and the delay of the high voltage pulse was varied between 600nsec and 200 μsec. The pulse height was 18.8± 0.1kV/cm and two widths were used, 15.0 and 15.9± 0.2nsec (FWHM). A graph of streamer density as a function of delay for the two pulses is shown in Figure 5.5. Comparison of these curves with the output of the model, shown in Figure 5.3, yields several interesting features.

In general there is very good agreement between the streamer densities using the 15nsec pulse and the model output for $L/L_m = 0.98$. However, the model fails to produce the dip in the streamer density at $\tau_D = 1\mu$sec although drops are produced for lower values of L/L_m. These are produced as the electrons along the track diffuse out over the first few avalanche radii away from the track centre,thereby reducing the number of electrons which start each avalanche and hence increasing their mean formative time.

Comparison with the results using the longer pulse reveals a similar agreement for delays less than 20 μsec but at values greater than this, the actual number of streamers generated exceeds the saturation values generated by the model. There are two possible reasons for this. Firstly, the area dominated by a single streamer has been assumed to be a square of side R_o whereas the streamers are in fact of circular cross-section

Streamer Density for Minimum Ionising Particles

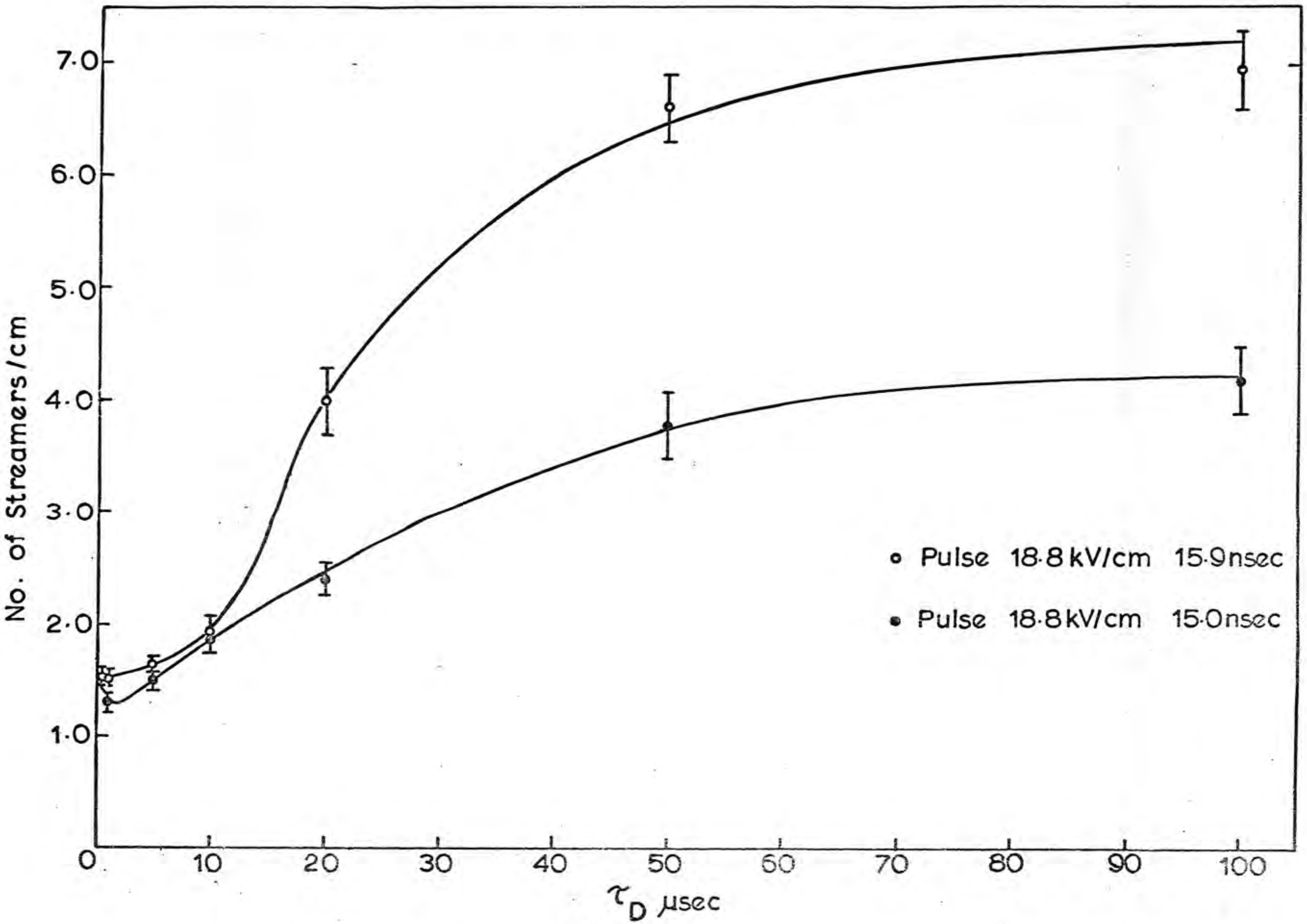

Figure 5.5

and therefore capable of occupying the area available in a close packed structure. This would give a possible increase in streamer density of $\frac{\sqrt{3}}{2}$ and bring the value at 100 μ sec within the predicted range. There is, however, still a discrepancy at 50 μ sec.

For time delays greater than 100 μ sec, a significant number of electrons may have diffused, parallel to the field, distances greater than the final streamer length and hence streamers may develop behind the forbidden gaps between other streamers. For very long delays therefore, the upper limit to the observed streamer density is the optical streamer radius.

The above experiment was repeated using particles selected by the A+B+C coincidence system which were expected to produce 20% greater ionisation in the chamber gas than the minimum ionising particles. The results of the model shown in Figure 5.4 indicate a maximum change in streamer density of 11% at delays of 100 μsec and $L/L_m = 0.98$. All other delays produce a smaller effect. The experimental results are shown in Figure 5.6. The streamer densities are, within the error of 5%, the same as those obtained using minimum ionising particles which were shown in Figure 5.5. The errors shown are experimental as the statistical errors were reduced below these values by averaging the results over several tracks. Better experimental accuracy may reveal differences, but to obtain sufficient statistical accuracy for ionisation measurement of a single particle, track lengths in excess of 1 meter will be required.

5.7 The Streamer Density Distribution

Davidenko et al (11) using image intensifier techniques have shown that, in helium at 0.4 atmospheres, the number of streamers per unit length of track obeys the Poissonion distribution for delays of less than 5 μ sec which is in accordance with the distribution of the primary ionisation. For longer delays the secondary electrons diffuse outside the streamer radius and the distribution becomes Landau.

Streamer Density for Greater than Minimum Ionising Particles

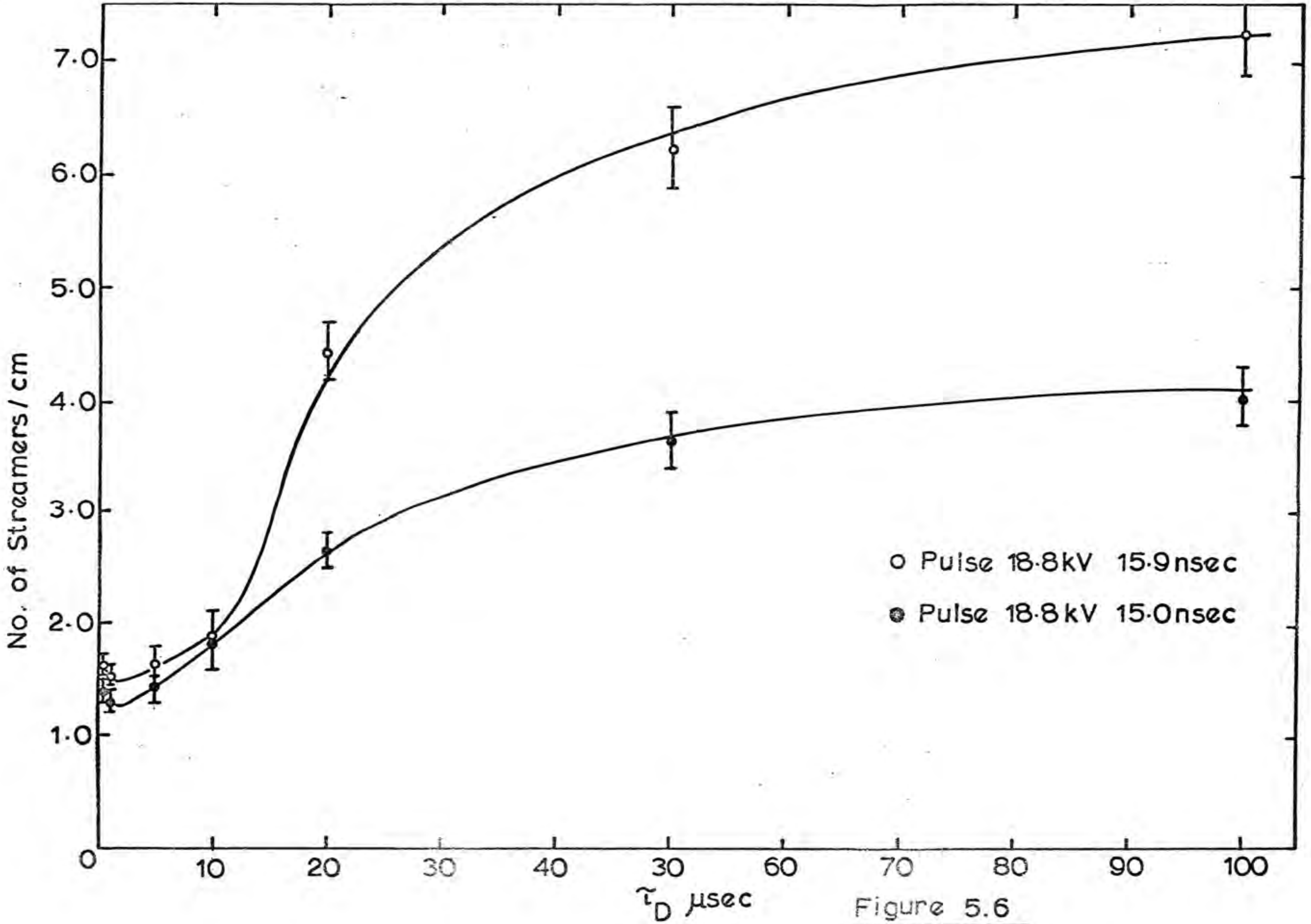

Figure 5.6

The number distributions of streamers in the neon helium mixture in the streamer chamber were measured for delays between 1 μsec and 200μsec using pulses of 18.8kV/cm and 15nsec duration. These are shown in Figure 5.7. For delays of 50μsec or less the data is in 5cm bins, whereas for 100μ sec or over bins of 2.5cm are used to improve the statistics. It is clear that the distributions are essentially symmetrical and for shorter delays tend towards a delta function. This may be explained as follows. Consider the ionisation density to be distributed with variance σ^2 then the number in any sample of that ionisation, for example the number of electrons on 5cm of track, will be distributed with a reduced variance dependent on the length of track sampled. If, as at short delays, this information is in the form of a streamer, then the finite width of the streamer represents a lower limit for the bin width and further reduces the sensitivity of the measurement.

Figure 5.8 shows the effect of rebinning the data, taken using a 15.9nsec pulse at a delay of 200 nsec. The histogram using 1cm bins does show signs of asymmetry, however further development of this is limited by a second factor.

This second factor may be described as a lack of dynamic range. Using low L/L_m values only, avalanches of high multiplicity transform into visible streamers and the tail of the Landau distribution will be generated. If higher L/L_m values are used most of the avalanches starting from single electrons will transform but the streamers of high multiplicity, which formed earlier, will attain greater lengths and tend to coalesce, thereby destroying the information connected with the tail of the distribution. This was clearly the case when taking the measurements shown in Figure 5.8, as there were many regions on the track consisting of groups of unresolvable streamers.

5.8 The Streamer Diameter

The diameter of the streamers has already been mentioned in connection with the choice of parameter R_1 in the streamer model GAUSS and in the brief

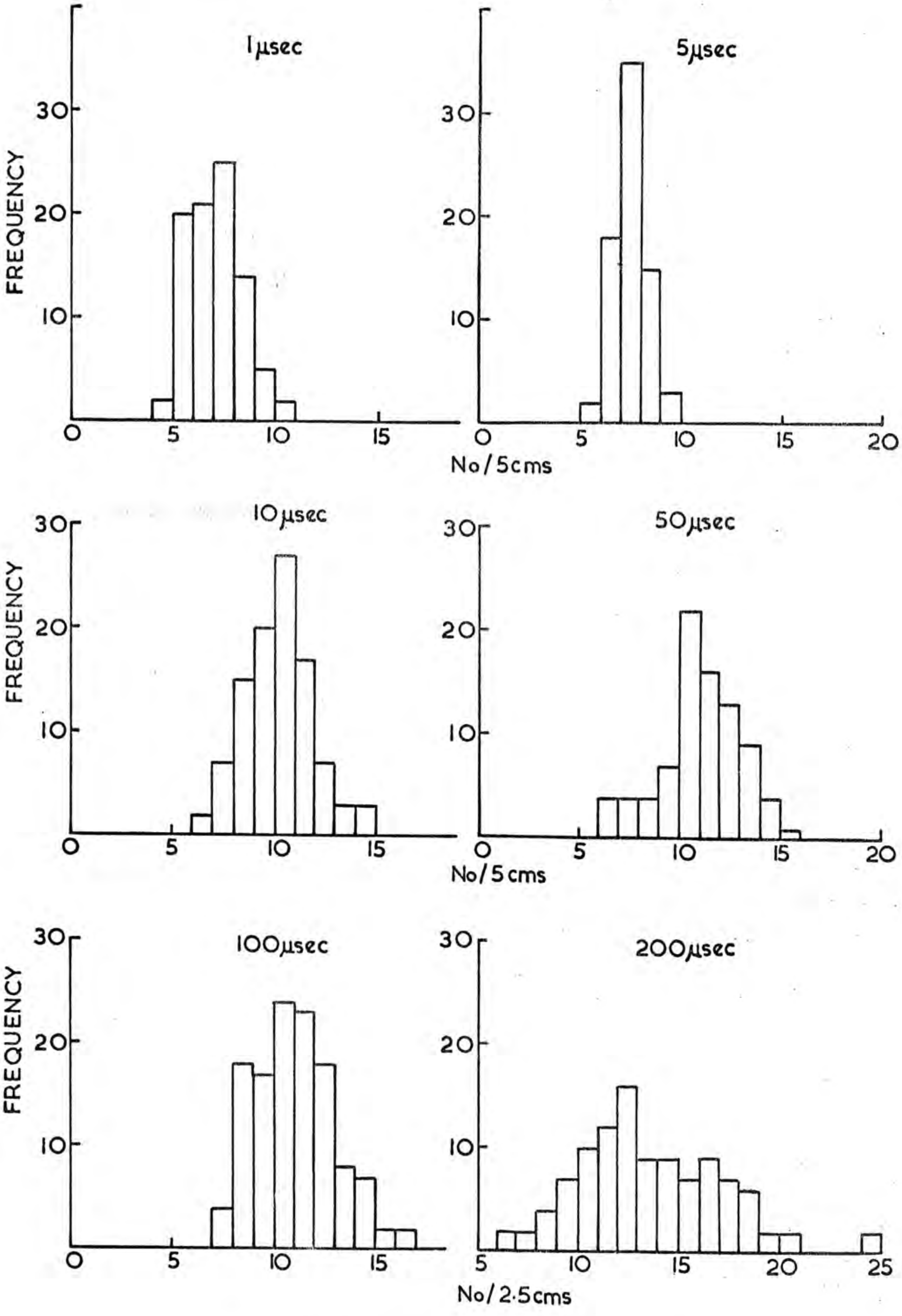

STREAMER NUMBER DISTRIBUTIONS

Figure 5.7

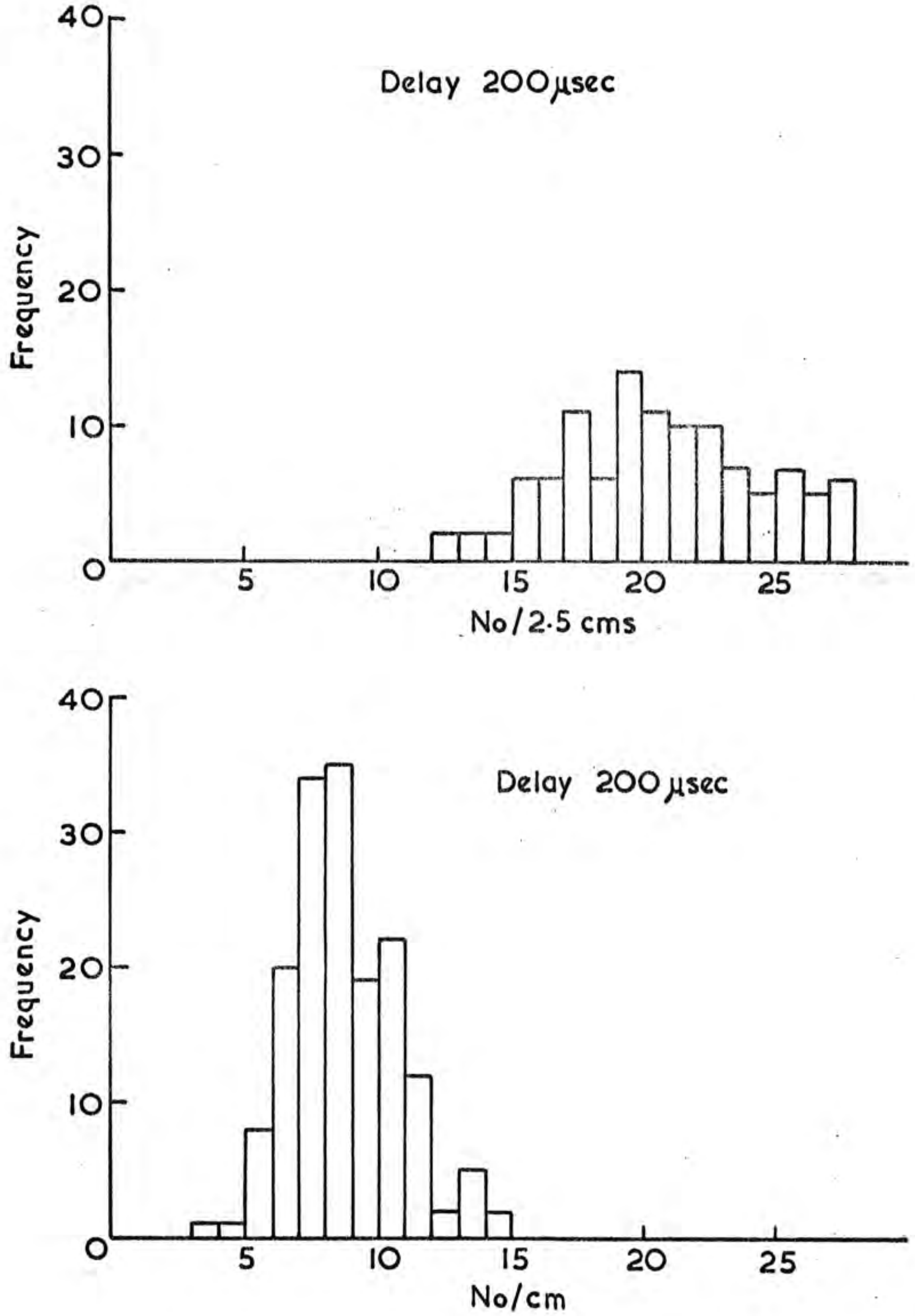

STREAMER DENSITY DISTRIBUTION

Figure 5.8

description of track formation at the end of chapter four.

The results obtained were in closer agreement with those of Chikovani (3) than those of Davidenko (12) who, by means of an image intensifier was able to photograph very young streamers. The latter work was performed in neon at 0.8 atmospheres pressure and gave a mean streamer diameter of 1 mm. Chikovani reports a mean diameter of 1.6mm at a delay of 1 μsec which is in better agreement with the 2 mm obtained here.

The diameter distribution is concentrated towards the smaller values at 1 μsec delay as can be seen in Figure 5.9 but the tail of the distribution increases with delay inaccordance with the results of Chikovani (3). However, this tail reaches a maximum at 20 μsec and decreases at longer delays until the distribution is again concentrated around the smaller values at 100 μsec. As would be expected,the shorter streamers produced at longer pulse delays, due to the increasing formative time of the avalanches, do have smaller diameters and the mean diameter was found to decrease to 1.6mm at delays of 100 μsec. However reducing the duration of the applied field by 6%, and hence the streamer length by about 2mm, produced no significant change in the streamer diameter distributions. Davidenko (12) has indicated that, in accordance with elementary diffusion theory, the variation of diameter d as a function of length L is of the form $d \propto L^{\frac{1}{2}}$ but as the change in diameter is less than 30% over the whole range of lengths from 2 to 12 mm,the results obtained here are not incompatable with this relationship.

The reason for the increase in the tail of the streamer diameter distribution at a delay of 20 μsec is thought to be related to a maximum in the electrical interference between streamers occuring at this delay, causing them to join into groups of larger diamter.

5.9 Electron Diffusion

As the delay between the passage of the particle through the streamer

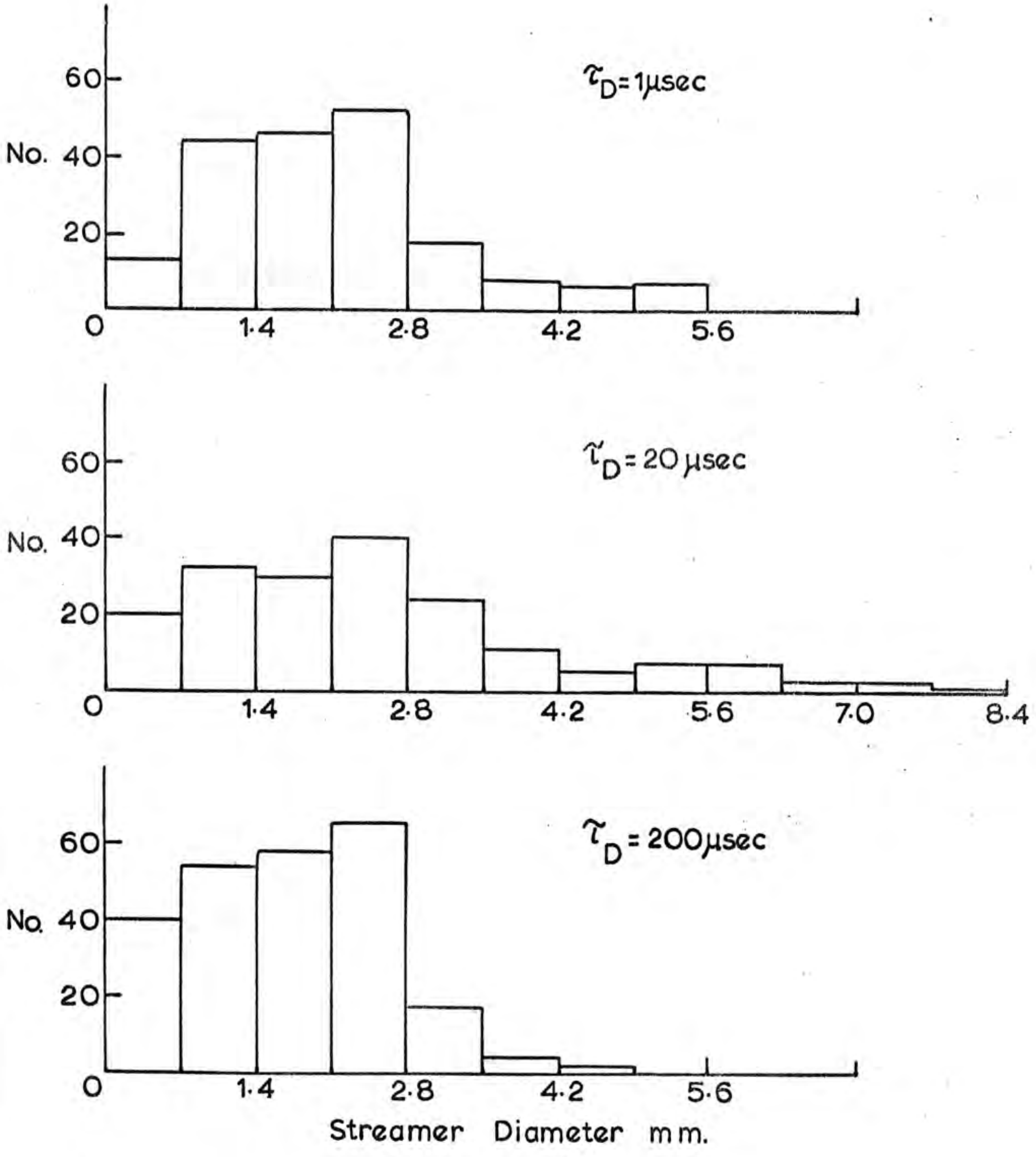

Streamer Diameter Distributions

Figure 5.9

chamber and the application of the high voltage pulse increases from zero to 200 μ sec, the electrons which constitute the track diffuse from their original positions. They form a band which, from Fick's law of diffusion, has a projected variance σ_D^2 where $\sigma_D^2 = \sqrt{4Dt}$ where D is the diffusion constant of the electrons and t is time.

There are several reasons why the deviation of streamers produced on such tracks should differ from that given by the accepted diffusion constant for the gas, which for neon is 1800 ± 200 cm^2/sec at NTP. Davidenko et al (11) have shown that the addition of small quantities of molecular gases (1Torr) to neon greatly reduces the diffusion constant and that this reduction may be as much as a factor of three for the 'technically pure' gas. Also addition of water vapour will reduce the value of D to as little as 40 cm^2/sec.

The value obtained here was 630 ± 20 cm^2/sec and is shown graphically in Figure 5.10. An 18.8 kV/cm field of 15.9nsec duration was used and D is in close agreement with the results of Davidenko (11). Chikovani (3) attributed this effect to the fact that only avalanches starting from large numbers of electrons near the centre of the track were transforming into streamers at small delays but found agreement with the expected diffusion constant of ~ 1800 cm^2/sec at delays of 200 μ sec. However, this appears to be in disagreement with his statement that there was no variation in the deviation of the streamers when the field was increased from 10kV/cm to 20 kV/cm, when presumably avalanches of lower multiplicity, near the edges of the track, would transform into streamers.

To test these ideas, the value of σ_D was measured using the reduced pulse length of 15.0nsec. The measured value of σ_D was now 480 ± 20 cm^2/sec, a significant decrease on the previous curve, showing that the value of σ_D is indeed pulse dependent, though the maximum obtainable value is doubtless less than that for the pure gas (11) as the value of σ_D at 200μsec delay shows no increase over the values at shorter delays.

STREAMER DIFFUSION.

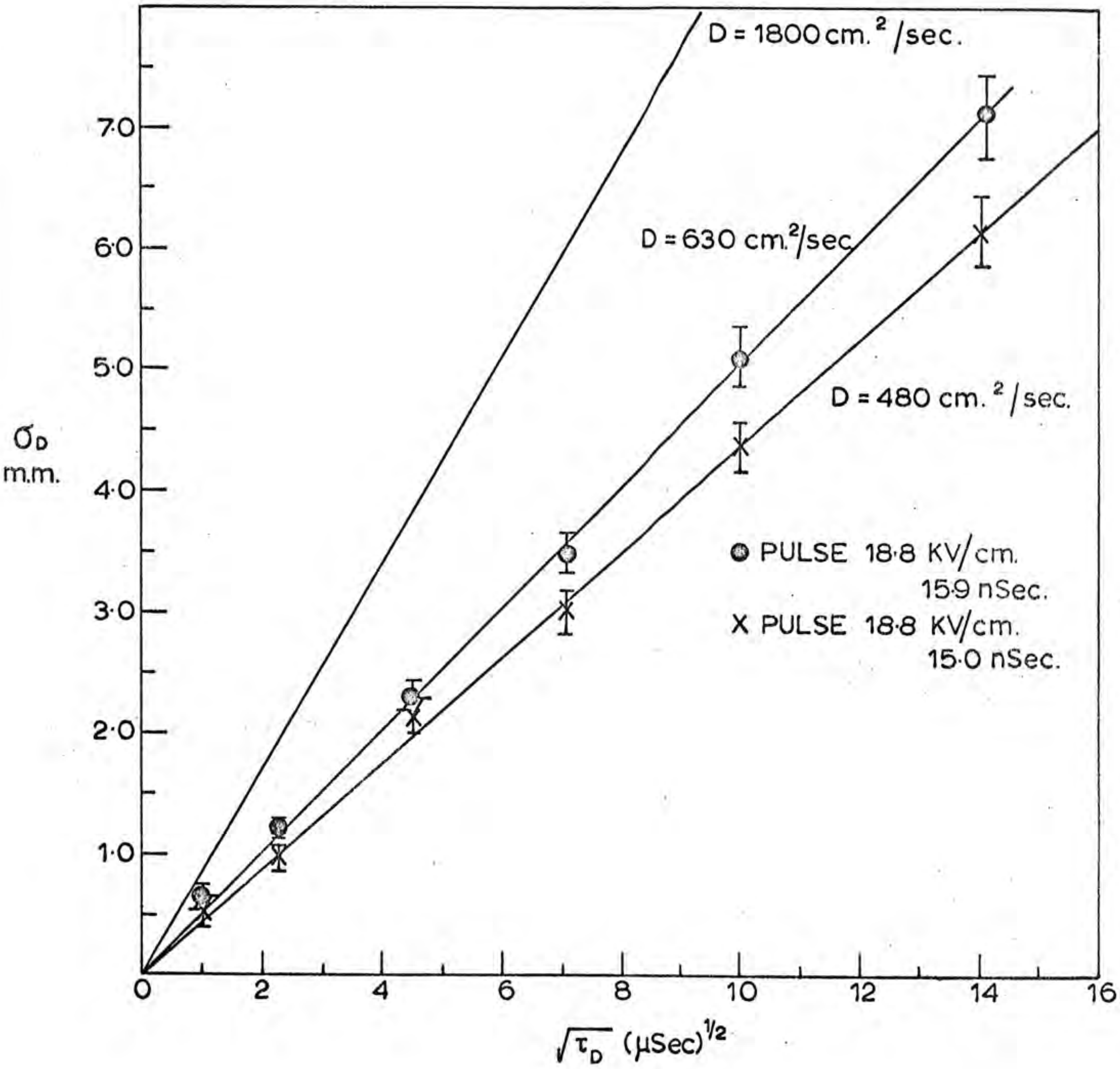

Figure 5.10

It should be noted that, as the streamers in the chamber described in this thesis have a group of electrons as their source, they will tend to take on the average position of the group. This will produce a small reduction in the value of D over the value given in reference (11). This will occur even under ideal conditions of pulse shape and gas purity as the streamers used to generate the results in reference (11) incorporated fewer initial electrons due to the decreased streamer dimensions.

There will also be an effect due to the presence of helium but this is considered small compared to the effect of molecular impurities.

The slight departure from the straight line of the points at 1μ sec in Figure 5.10 may be due to the thermalisation distances of the primary electrons adding to the effects of diffusion.

Calculations (13) show that the electrons may take up to 1 msec to completely thermalise from energies just below that of the first excited state of the containing gas, but it has also been shown (14) that molecular impurities will considerably reduce this time. Thus the high values of σ_D at 1μsec are probably due to the limited accuracy in determining the centre of the track,from which position the displacements are measured, as any error in this position will lead to an increased value of σ_D.

5.10. Locational Accuracy

The accuracy of particle track location in a direction looking parallel to the applied electric field was determined by the hand fitting of straight lines to the tracks formed by minimum ionising particles. Ten independent lines were fitted to each of four tracks at each delay time. The total spread of the lines about their mean position was taken as being $\pm 3 \sigma_{/\!/} \frac{n}{n-1}$, where $\sigma_{/\!/}$ is the locational accuracy in this direction and n is the number of lines drawn in taking the measurement. The mean value of the four determinations is plotted as a function of delay time in Figure 5.11. The errors shown are one standard deviation of the scatter of the obtained values,rather than the error on the mean which would be a factor of three smaller than this.

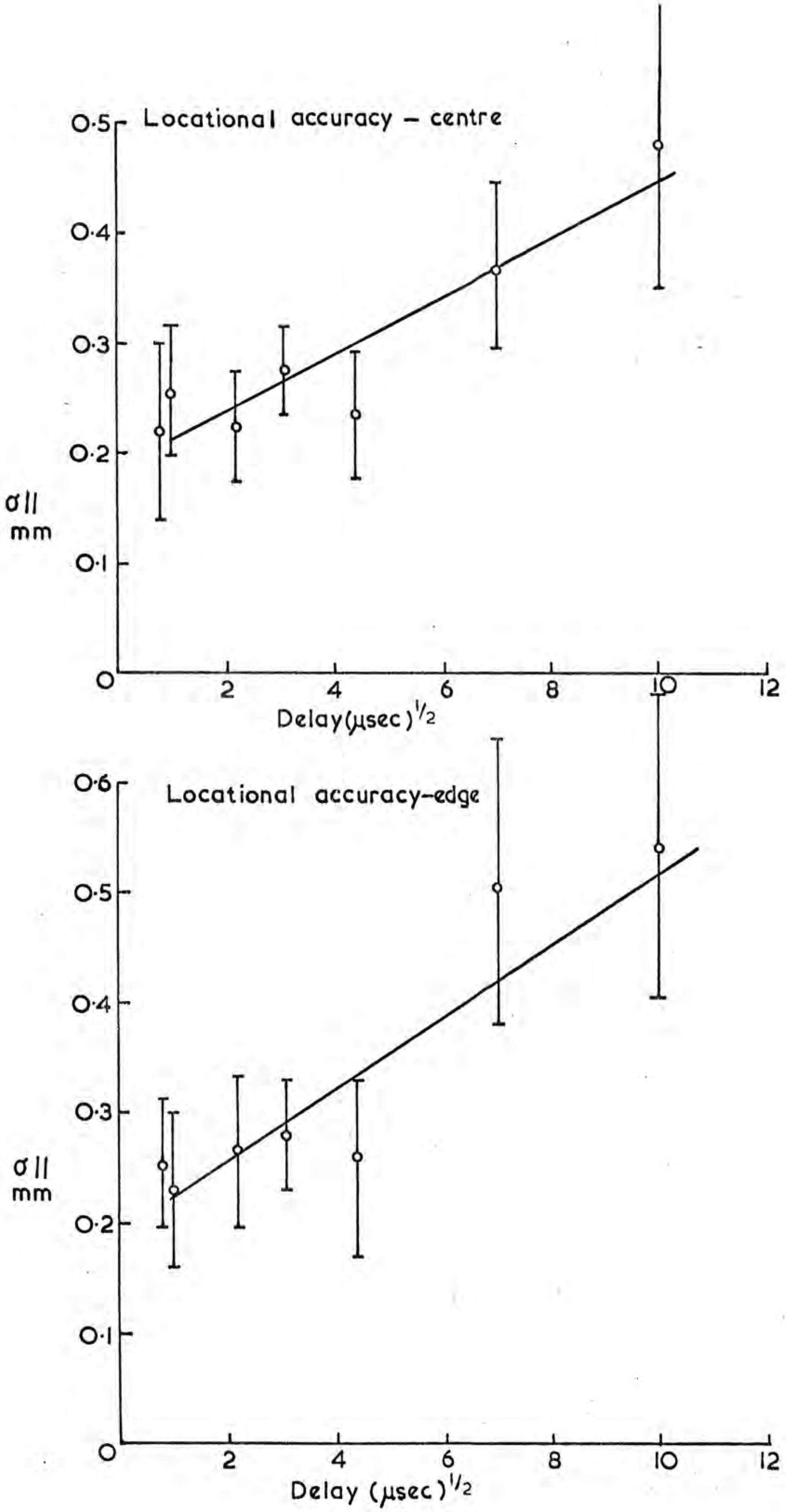
Locational accuracy – centre
0·5
0·4
0·3
0·2
0·1
O
σ||
mm
2
4
6
8
10
12
Delay(μsec)^1/2
Locational accuracy–edge
0·6
0·5
0·4
0·3
0·2
0·1
O
σ||
mm
2
4
6
8
10
12
Delay (μsec)^1/2

Figure 5·11

Two curves are shown. The upper one is the accuracy at the centre of a track 50 cm long, whereas the lower is that at the end of such a track where errors due to the rocking of the fitted line about the centre of the track and optical distortions are greatest.

The errors introduced by this method of measurement were found, by fitting to a 'perfect' straight line, to be ~ 0.07mm. This will be of negligible consequence when dealing with the values obtained here.

Three main factors affect the accuracy of the streamer chamber. At delays less than 10μ sec the finite optical streamer diameter is dominant and limits the accuracy to 0.25mm. This is in excellent agreement with the results of Bulos et al (15) and Meyer (16) who used scanning machines. For delays longer than $10\,\mu$sec the diffusion of the electrons, as described in the previous section, widens the track beyond the streamer radius and the accuracy decreases in approximate proportion to $(\sigma_D)^{\frac{1}{2}}$. In principle this agrees well with the results of (15) but as can be seen, the effective diffusion constant found here in Figure 5.11 is considerably less than the value of 412 cm^2/sec quoted by (15). This is probably due to the different methods of measurement.

At delays of $100\,\mu$sec and over, the effects of random spurious electric fields in the chambers caused the tracks to become bent and produce large variations in the measured accuracy from track to track. This is reflected by the large error bars on these points. As the effect of the spurious fields was greater on streamers when viewed perpendicular to the applied field discussion of them will be left to the next chapter.

5.11 Spatial Resolution.

Without the aid of a particle accelerator the resolution of the streamer chamber cannot easily be measured directly due to the inconvenience of waiting for cosmic ray pairs with small enough opening angles. However, the resolution may be inferred from other data.

It has been stated in connection with the parameter R_o in the streamer generation model GAUSS, that the effective size of a streamer is 0.65x0.65cm and that only one streamer may form inside this region. This therefore, must represent the closest separation of two particles, using pulses of short delay times (< 5 sec), that will form two independent tracks in the chamber. At separations less than this the streamers will coalesce and only a single track will be formed.

At longer delays the track width exceeds the electrical width of a single streamer due to the diffusion of the electrons left by the ionising particle. A simple approach would therefore be to define two tracks as being just resolved if their centres are separated by two standard deviations of the normal distribution of the electrons across the tracks. Thus the resolution R as a function of time would be

$$R = 2\sqrt{4Dt} \qquad 5.16$$

where D is the diffusion constant of the electrons in the chamber gas. It has been shown in section 5.8 however, that the diffusion constant for the streamers generated on the track depends on the operating conditions of the streamer chamber. It is therefore reasonable to suppose that the resolution should also be dependent upon these conditions and that this parameter may be improved at long delays if the 'diffusion' constant is reduced by the use of pulses with low L/L_m values. There may of course be effects due to the higher multiplicity of avalanches, forming where the tracks overlap, causing them to transform into streamers early and hence obscure the region between the tracks but such effects cannot be investigated at present.

A second factor affecting resolution is also present. Because of the nature of track formation, which has already been described, the distribution of the streamers across the track, unlike the initial electrons, may not be Gaussian. Figure 5.12 shows this distribution for a delay of 200μsec using the results from Figure 5.10 and it is clear that the departure is negligible.

Thus the best estimate of the spatial resolution of two adjacent tracks, as seen parallel to the field, is that given by equation 5.16 using the value of D obtained for the particular pulsing conditions employed. For short

Streamer Diffusion Distribution

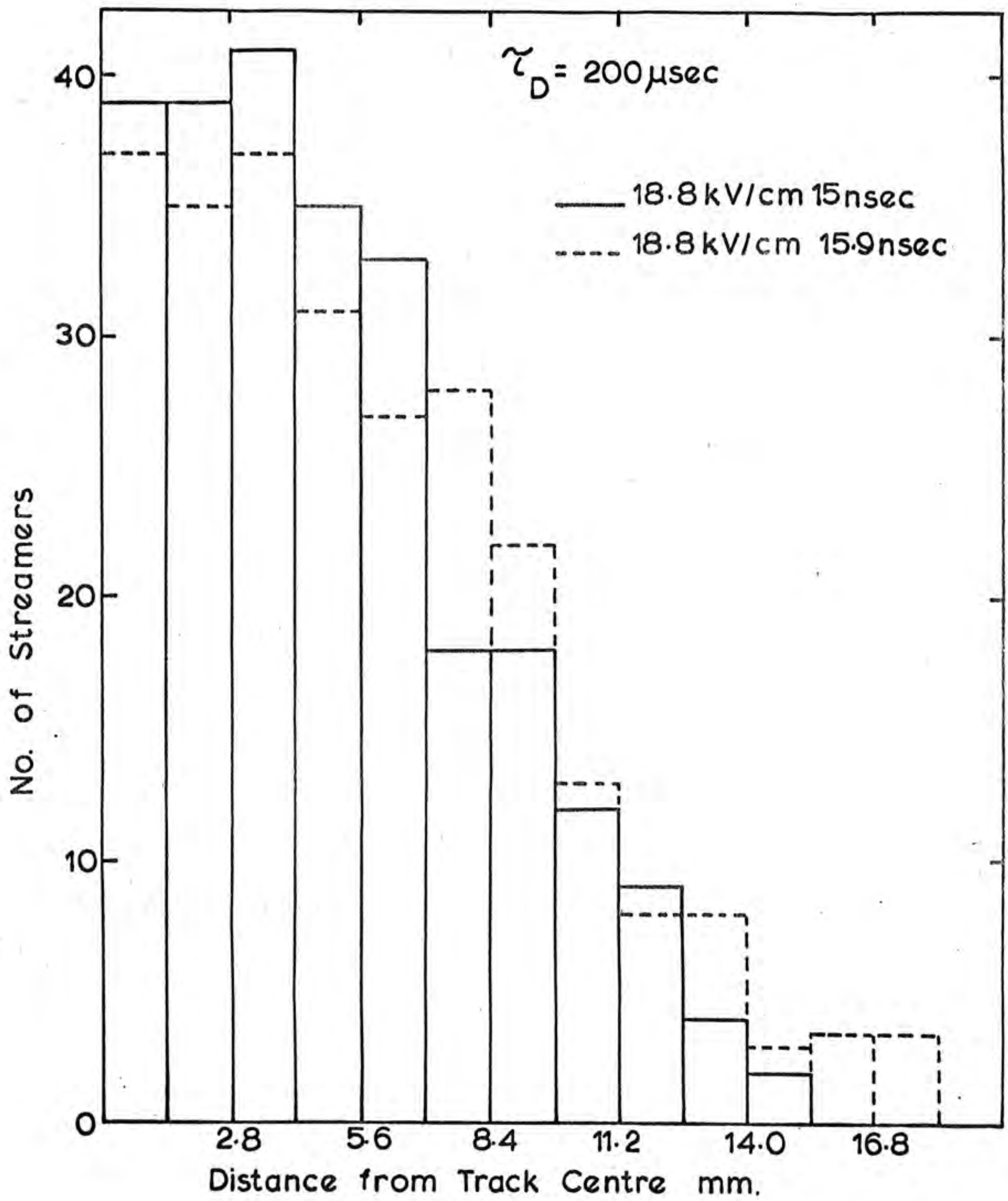

Figure 5.12

delayswhere the track width is less than the electrical streamer diameter, this represents the maximum resolution of the system and is taken here to be 0.65 cm.

5.12 Conclusion

In this chapter we have seen how the operating mechanisms and conditions of the streamer chamber affect its characteristics as seen parallel to the applied field and define the limits of the device as a useful tool. A more detailed assessment of this performance is left to the concluding chapter of this thesis.

REFERENCES

1. WIJSMAN, R.A., Phys. Rev. 75 (1949) 833.
2. FURRY, W.H., Phys. Rev. 52 (1937) 569.
3. CHIKOVANI, G.E., Nuc. Inst. Methods 29 (1964) 261.
4. LANDAU, L., Sov. J. Phys. 8 (1944) 201.
5. CHARPAK, G., Ann. Rev. Nuc. Sci. 14 (1964) 323.
6. EYEIONS, D.A., Proc. Phys. Soc. A. 68 (1955) 793.
7. JONES, D.G., Proc. Phys. Soc. 81 (19) 1237.
8. DAVIDENKO, V.A., Sov. Phys. J.E.T.P 29 (1969) 1.
9. STERNHEIMER, M., Phys. Rev. 115 (1959) 137.
10. ROSSI, B., High Energy Particles, Prentice Hall (1952).
11. DAVIDENKO, V.A., Nuc. Inst. Methods, 67 (1969) 325.
12. DAVIDENKO, V.A., Nuc. Inst. Methods 75 (1969) 277.
13. BRAGLIA, G.L., Comitato Nazionale Energia Nucleare RT/F1(65)61.
14. DAVIDENKO, V.A., Sov, Phys. JETP., 30 (1970) 49.
15. BULOS, F., S.L.A.C. Report No. 74 (1967).
16. MEYER, H., DESY F1 72/4 (1972).

CHAPTER SIX

RESULTS II

6.1 Introduction

In this chapter the performance of the streamer chamber perpendicular to the applied electric field will be described and the model GAUSS, which was developed in chapter five, used to explain its properties where applicable.

The discussion of the effects of spurious clearing fields in the chamber, mentioned in section 5.9, has been left to this chapter because of its greater effect on the steamers as seen perpendicular to the applied field. This will be undertaken first.

6.2 The Bending of Tracks

When the chambers with perspex frames and melinex windows were used to detect particles, the streamer tracks showed considerable deviations from the expected straight path produced by the majority of cosmic rays in a gas at NTP. The effect was found to be dependent upon the delay time of the high voltage pulse τ_D and the distortions were usually greater in the direction of the applied field.

The dependance of the effect upon delay time indicates that a spurious electric field is present in the chambers, which displaces the electrons from the path of the particle being detected. To estimate the magnitude of the field, straight lines were fitted through the obtained tracks and the maximum deviation of each line from its track was measured. The mean maximum displacement for all tracks is plotted as a function of delay time, for displacements parallel and perpendicular to the field, in Figure 6.1.

The considerable departure of the curves from the expected straight lines at time delays greater than $10\,\mu$Sec is attributable to the preferential loss from the chambers of electrons which have moved through distances large

Average Maximum Track Displacement v Delay

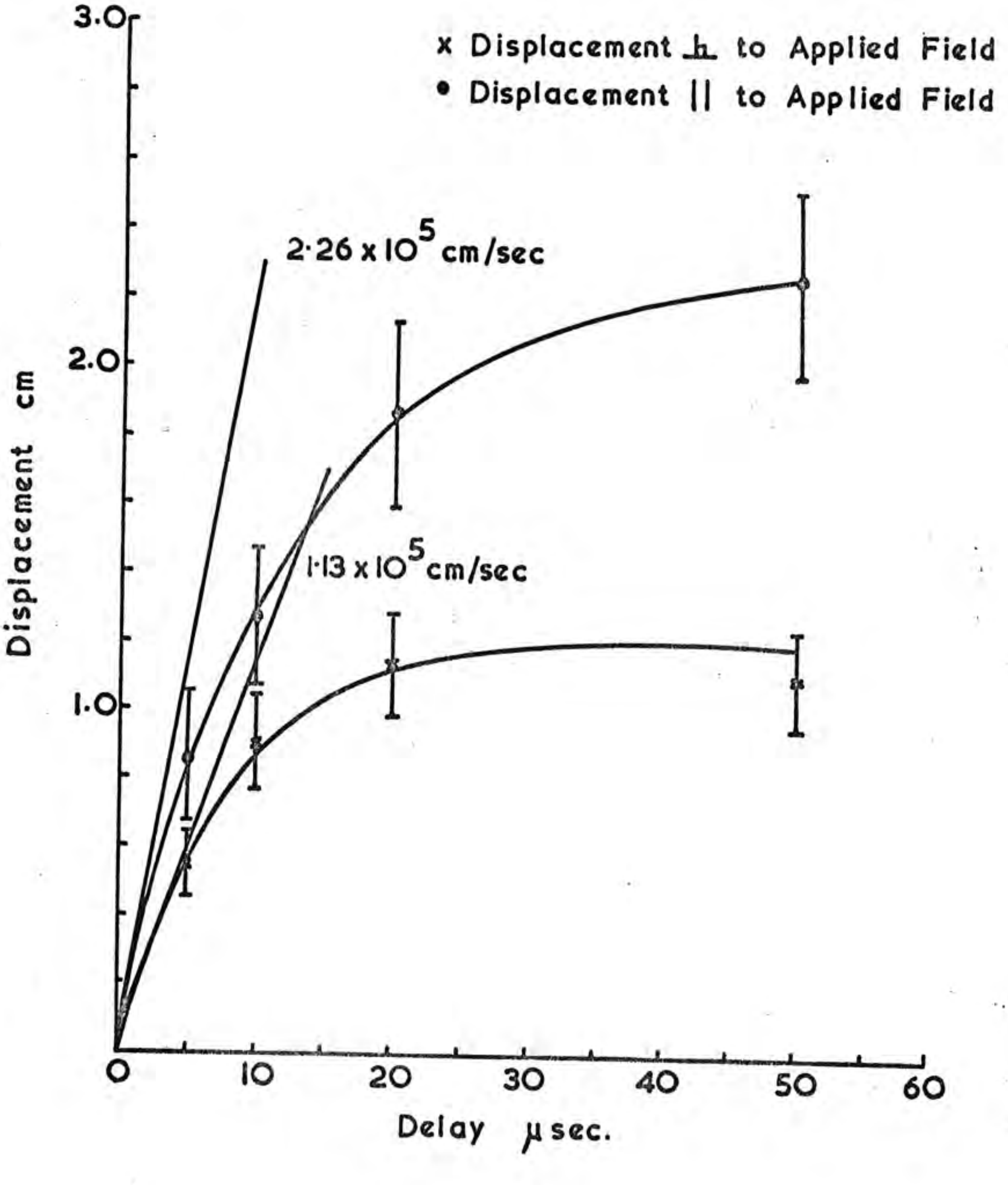

Figure 6.1

enough to reach the walls of the chamber. Hence in the case shown in Figure 6.1 at delays exceeding 50μsec the efficiency of the system is seriously affected by the clearing field.

By drawing tangents to the curves in Figure 6.1 at $\tau_D = 0$ it is possible to estimate the maximum drift velocity experienced by an average electron on the track. The values are 2.26×10^5 cm/sec parallel to the applied field and 1.13×10^5 cm/sec perpendicular to it. Using the results of Bowe (1) these may be converted into field strengths which are 14.5V/cm and 5.7V/cm respectively.

The presence of fields tangential to the electrodes and the fluctuations of the field, both in strength and direction, throughout the chamber suggest that it may be caused by highly localised charges on the chamber walls. Figure 6.2 shows qualitatively the field produced by a charge placed asymetrically between the electrodes of the streamer chamber, for example on the melinex windows. The regions of the chamber marked A are experiencing a field tangential to the electrodes, while regions marked B are in a field opposite in direction to that in the centre of the chamber.

It has been suggested that the spurious fields may be produced by streamers intersecting both walls of the chambers (2) and clearing fields have been shown to exist in sealed spark chambers (3) and flash tubes (4) where the discharge completely crosses the gap between the walls of the device. The fields experienced by these workers were found to be small and decayed with a few seconds. To test this hypothesis the mean maximum streamer displacement was measured as a function of the time between triggers and using a pulse delay of 20 μsec. The results in Figure 6.3 show that there is no significant reduction in the effect even using triggering rates more than 100 times slower than the workers in reference (2).

A second experiment was performed. The streamer chamber was left unused for three days and the distortions of the first few tracks produced after this time compared with that produced after many hours of use. Again no difference could be found. It was therefore concluded that the field

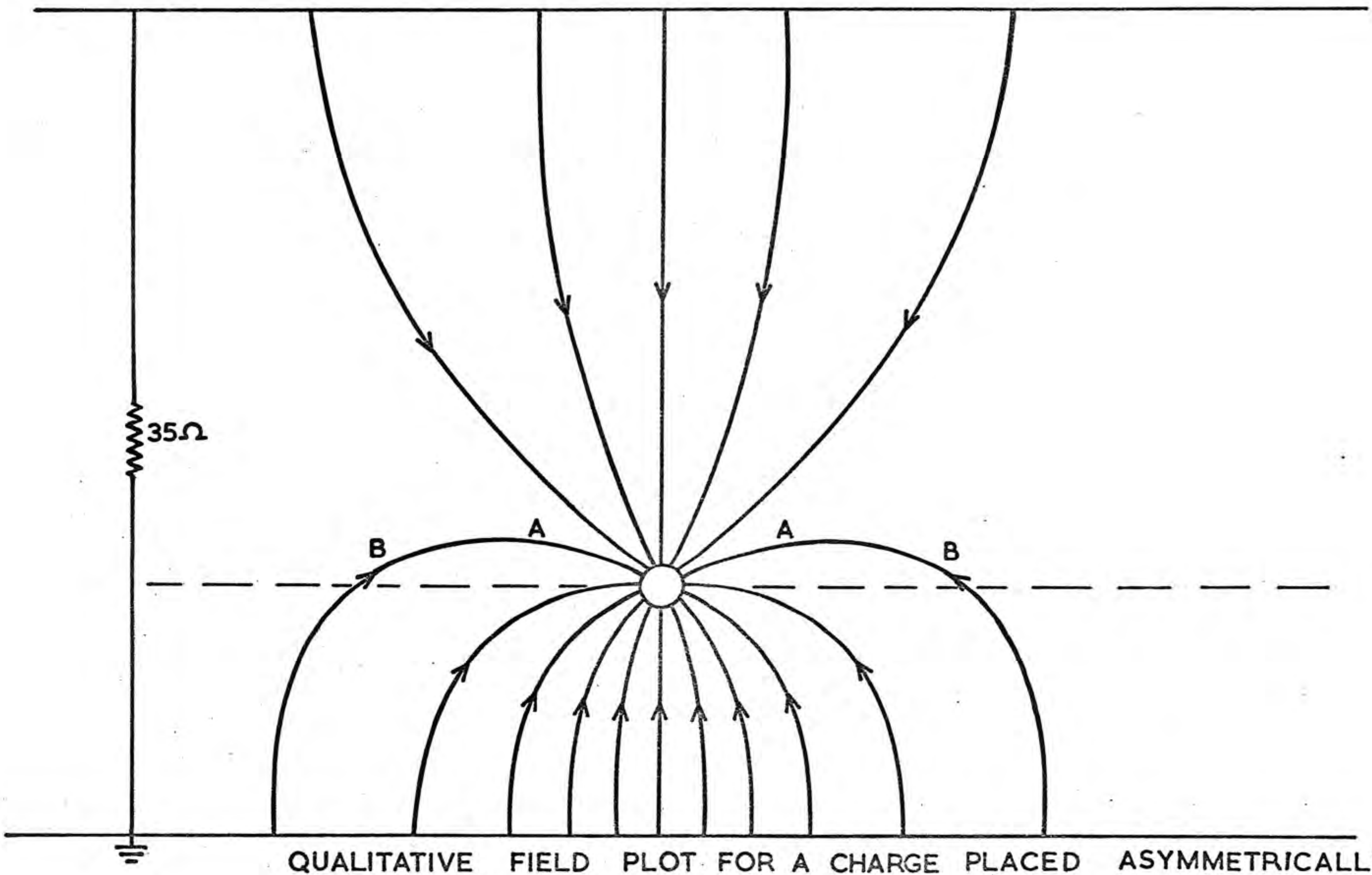

QUALITATIVE FIELD PLOT FOR A CHARGE PLACED ASYMMETRICALLY BETWEEN TWO FLAT ELECTRODES

Figure 6.2

MEAN MAXIMUM DEVIATION FROM FITTED LINE Vs TIME BETWEEN TRIGGERS

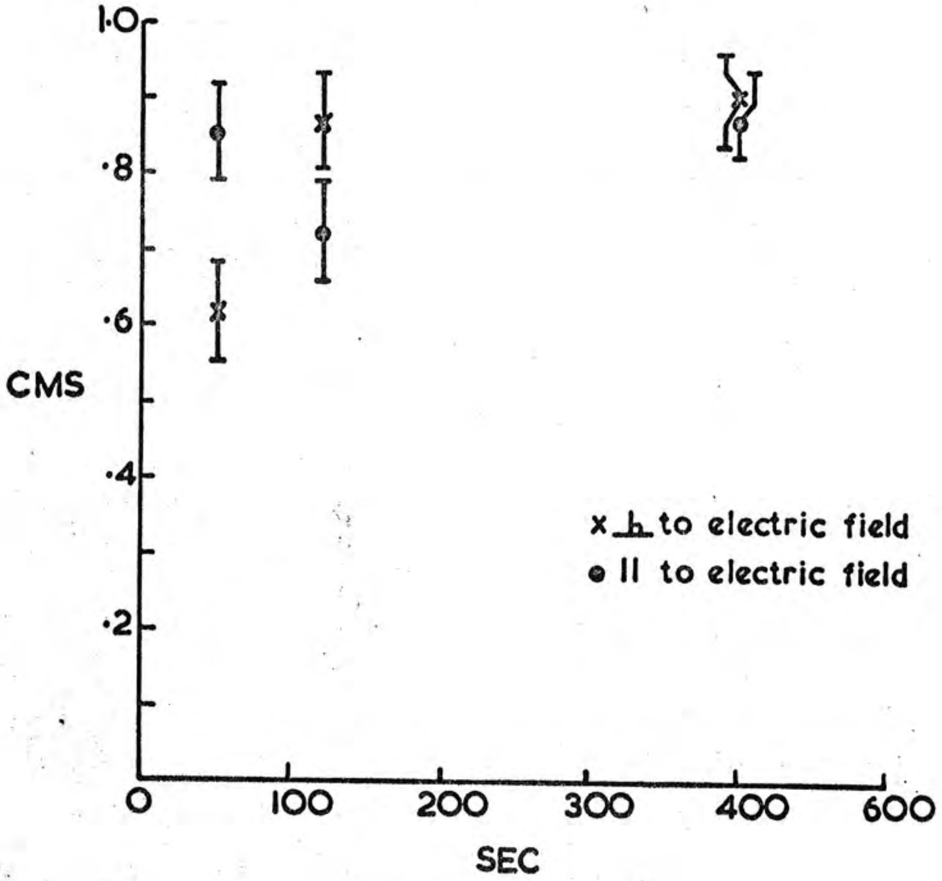

Figure 6.3

present here were independent of track formation. Zichy (5) has shown that electrostatic charges may become trapped in polymer surfaces in the form of a film electret, which displays a very long decay time. It is considered that the fields occuring in the streamer chamber are produced by such trapped charges. It was found that the magnitude of the field did decrease over a period of several weeks and after three months the effects of the field became negligibly small. The origin of the field is therefore associated with the manufacture of the chambers and the charges are probably attached to the surface of the melinex windows by the action of cleaning and polishing.

Once the random field had decayed and tracks could be generated with delay times exceeding 200μ sec the effects of a second type of clearing field became visible. This field produced the bending of each end of a 'vertical' cosmic ray track towards the negative electrode. The origin of this field is undoubtedly the edge breakdown, which was mentioned in section 4.9, depositing charge on the melinex windows. The high surface resistivity of the melinex ($10^{13}\Omega$) confines the charge to the edge of the chambers producing a clearing field in this region. Improvements in the design of the chambers should eliminate this effect.

6.3 The Streamer Length Distribution

Throughout this section measurements of the streamer length will be presented. As the streamers, in particular the long ones, have diffuse edges, the end of the streamer is defined as that point at which the recorded photographic density falls to half its maximum value.

(a) The Basic Shape

A typical streamer length distribution, using a pulse delay of 600 sec, is shown in Figure 6.4. The applied field was 19.5 ± 0.1 kV/cm for 13.6 ± 0.2nsec and the streamers were photographed on Kodak 2485 film using an aperture of f2.8. The most probable length is 0.42 ± 0.03cm and the mean

A Typical Streamer Length Distribution

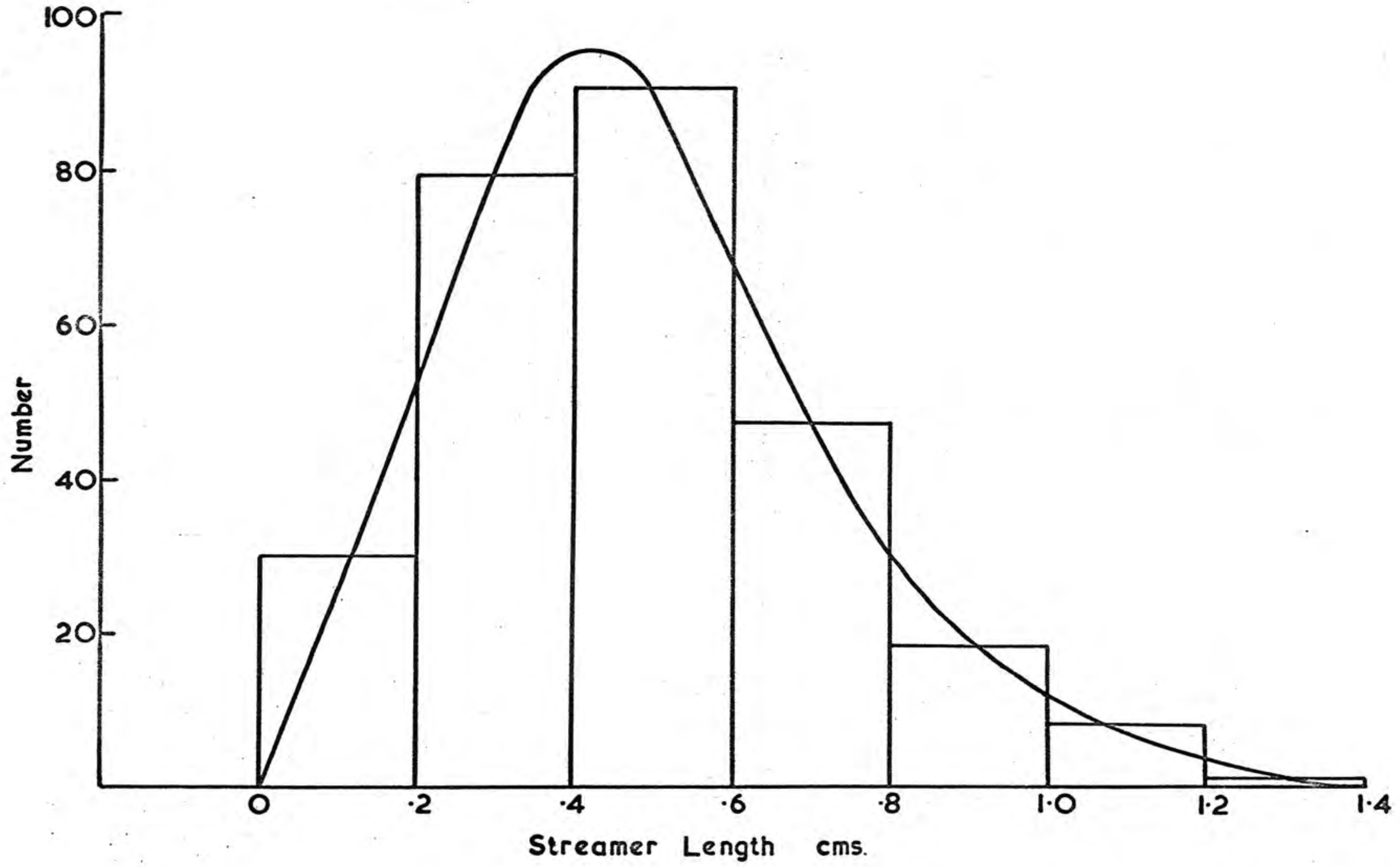

Figure 6.4

length is 0.48 ± 0.02 cm. The difference in these figures indicates the asymmetry of the curve. The distribution is very similar to one obtained by Davidenko et al (6) using a similar streamer length and an image intensifier camera to photograph the streamers which were in neon at 0.8 atmospheres pressure. Considering that the field strengths used by Davidenko are only half that used here and that no electric interaction between streamers occurs in his system, this distribution shape appears to be stable over a very wide range of conditions. It also suggests that few of the dimmer streamers have been lost from the distribution in Figure 6.4 during photography as all the streamers should be photographed using the image intensifier techniques described by Davidenko (6).

(b) The Theoretical Shape

The length distribution of the streamers under fixed external conditions is related to the value of L/L_m at which the individual avalanches transform into streamers. If the actual applied pulse is given the value of L/L_m to which it is equivalent, say 1.0, then the quantity $(1-L/L_m)$ for a particular streamer, is a measure of the relative time it has spent in the streamer phase at the end of the applied pulse. It is therefore an estimate of its length.

The streamer generation model GAUSS was used to generate the number of streamers which will develop from avalanches within particular intervals of L/L_m. Intervals of L/L_m of 0.02 were used over the range of 0.88 to 1.2 and, for delays from 600 nsec to 200 μsec, histograms of streamer number against $(1-L/L_m)$ were plotted. An example is shown in Figure 6.5. The delay is 600nsec and the most probable ionisation is taken as 28cm^{-1}. Comparing the theoretical curve with the actual one in Figure 6.4 reveals a reversal of the asymmetry, the tail of the theoretical curve being towards shorter streamer lengths. Three factors are responsible for this. Firstly the energy loss of a particle passing through the chamber will not be constant but will vary according to the Landau distribution. This gives a finite

Streamer Generation Model Gauss

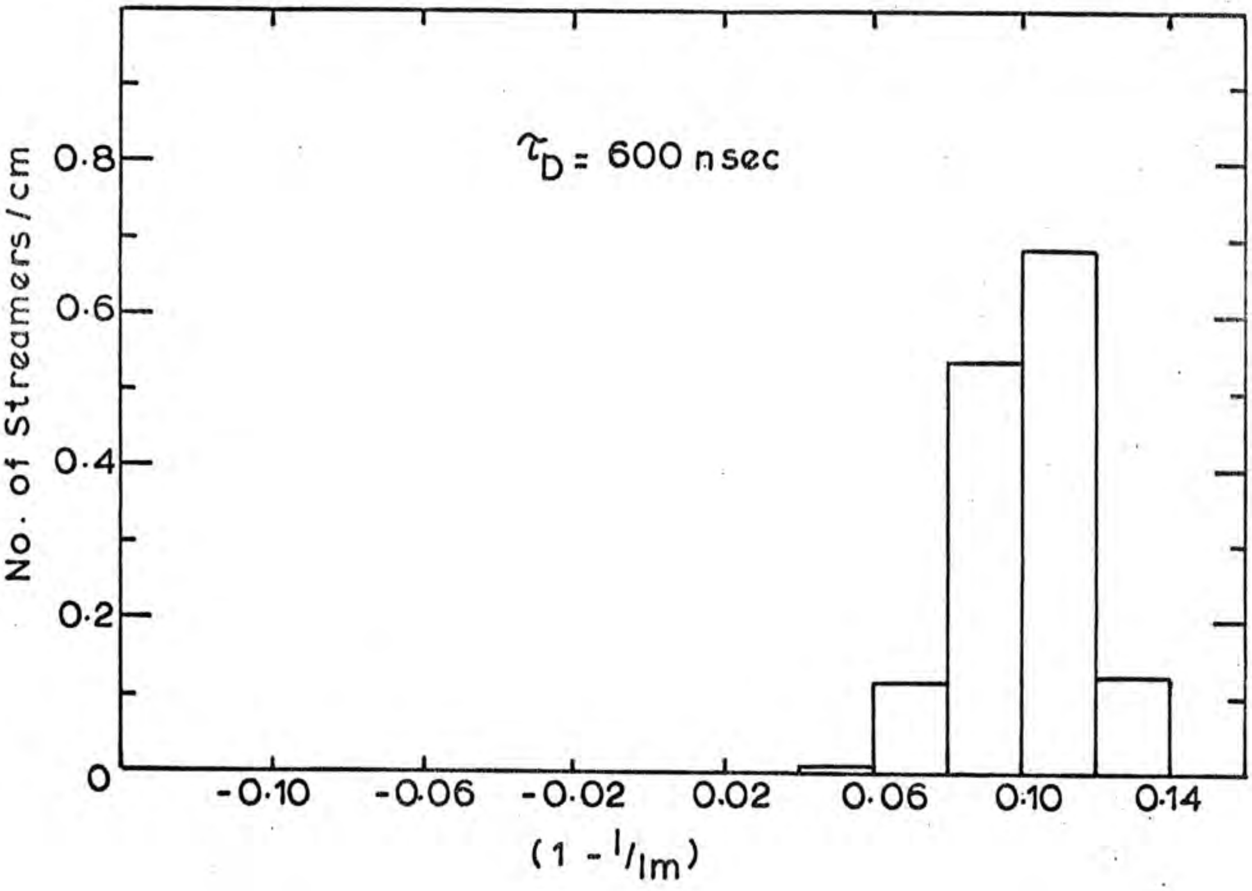

Figure 6.5

probability to energy transfers, and hence ionisation densities, many times the most probable value. Streamers which form on such clusters will have very short formative times and hence produce longer streamers. This will increase the tail of the length distribution. Secondly the velocity of the streamers has been shown to be dependent upon the length of the streamer, Figure 2.4, and upon the electric field strength, Figure 2.3. Streamers which form at small values of L/L_m will experience high velocities in their later stages of growth while newly formed streamers will propagate with much smaller velocities. Also streamers which form during the fall time of the high voltage pulse will propagate, in their early stages, with an even slower velocity than those which transformed during the peak of the pulse. Both these factors will increase the tail of the streamer length distribution towards the higher values, however at present, there is insufficient data available concerning streamer velocities in neon, using fields of 20kV/cm, to permit the calculation of the expected distribution. Thirdly, if some streamers do not achieve lengths and hence brightness, to register on the film, they will be lost from the length distribution. This will tend to reduce the size of the tail at the low value end of the distribution and impose a profile upon it which is related to the sensitivity of the film. This effect however, does not seem to be dominant if the comparisons made at the end of subsection (a) of this section, with the results of Davidenko, are valid.

Many of these features become more apparent as the pulse delay time is increased.

(c) The Effects of Delay

As the pulse delay increases theory predicts a shortening of the streamers and the theoretical distribution of streamer lengths becomes more skew A plot of $(1-L/L_m)$ against streamer number for a delay of 20 μsec, as generated by the model is shown in Figure 6.6.

Streamer length distributions were measured for a variety of field strengths and durations, and delay times. A typical set of results, for

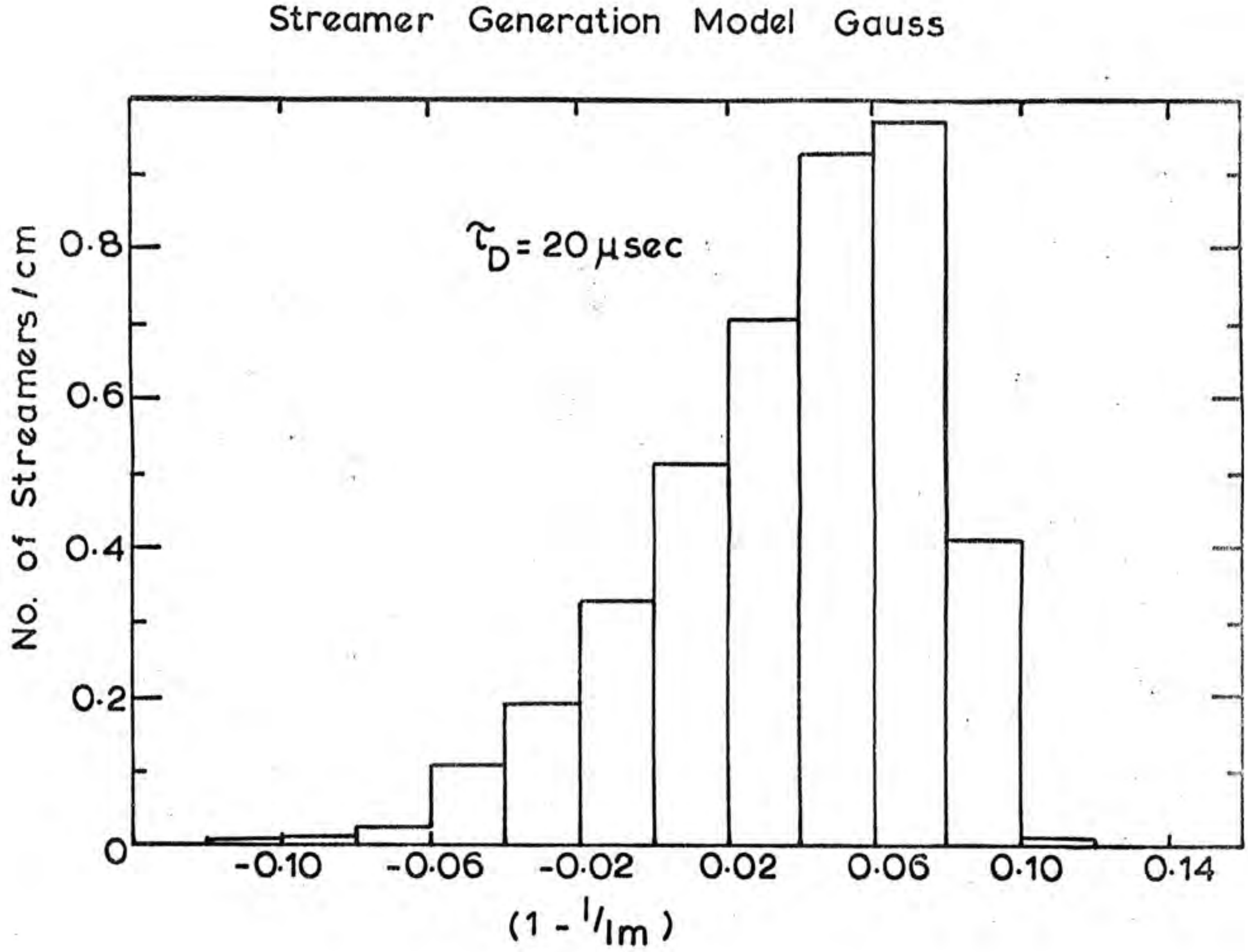
Streamer Generation Model Gauss
τD = 20 μsec
No. of Streamers / cm
0
0·2
0·4
0·6
0·8
-0·10
-0·06
-0·02
0·02
0·06
0·10
0·14
(1 - I/Im)

Figure 6.6

a pulse height of 18.8 kV/cm and length 16.0 nsec, is given in Figure 6.7 a and b. The agreement between the theoretical and experimental shapes deteriorates at long delays. Some reasons for this have been given above, but for delays exceeding 5μsec the generation of streamers longer than 1.8cm requires further explanation.

At longer delays, as the avalanches start from fewer electrons, the number of electrons which start each avalanche becomes a poorer sample of the electron distribution along the track and characteristics of the Landau distribution, in particular its long tail, are reproduced in the streamer length distribution. At shorter delays the details of the distribution are lost due to the large size of the samples which go to form each avalanche. One would expect however, that the tail would disappear at very long delays when each streamer tends to start from a single electron. Under these conditions the streamer number density would exhibit a sensitivity to initial ionisation much greater than has been found.

Reliable streamer length distribution at delays exceeding 20μsec are difficult to obtain as the electrons released by the particle diffuse to positions behind other electrons and streamers optically obscure one another. There is also a tendancy for two streamers which form along the same field line, but with their centres a few millimeters apart, to join at their ends and become indistinguishable from a single long streamer. This mechanism is thought to be the most probable cause of the increased tail of the measured streamer length distributions using delays greater than 5μsec.

The basic features of the streamer length distributions can be summarised by plots of the most probable and mean streamer lengths as a function of delay time. Figure 6.8 shows such plots for the length distributions shown in Figure 6.7. The mean values are calculated from the results and the most probable values of streamer length are obtained by hand fitting curves to the obtained histograms and then taking the most probable point on the curve.

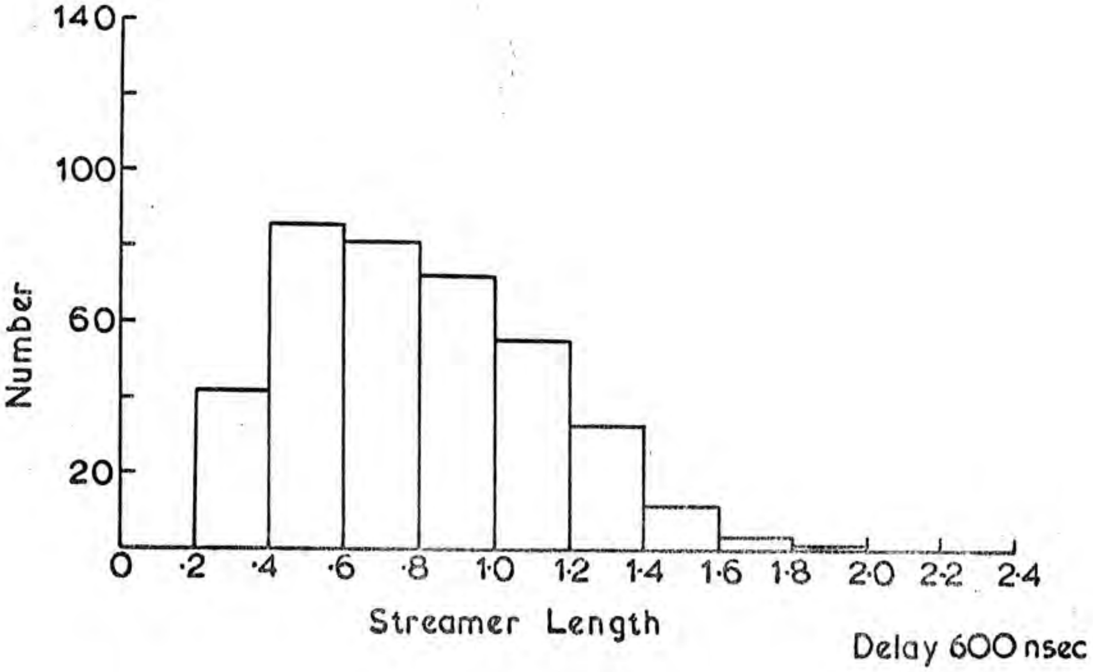
140
100
60
20
Number
0
·2
·4
·6
·8
1·0
1·2
1·4
1·6
1·8
2·0
2·2
2·4
Streamer Length
Delay 600 nsec

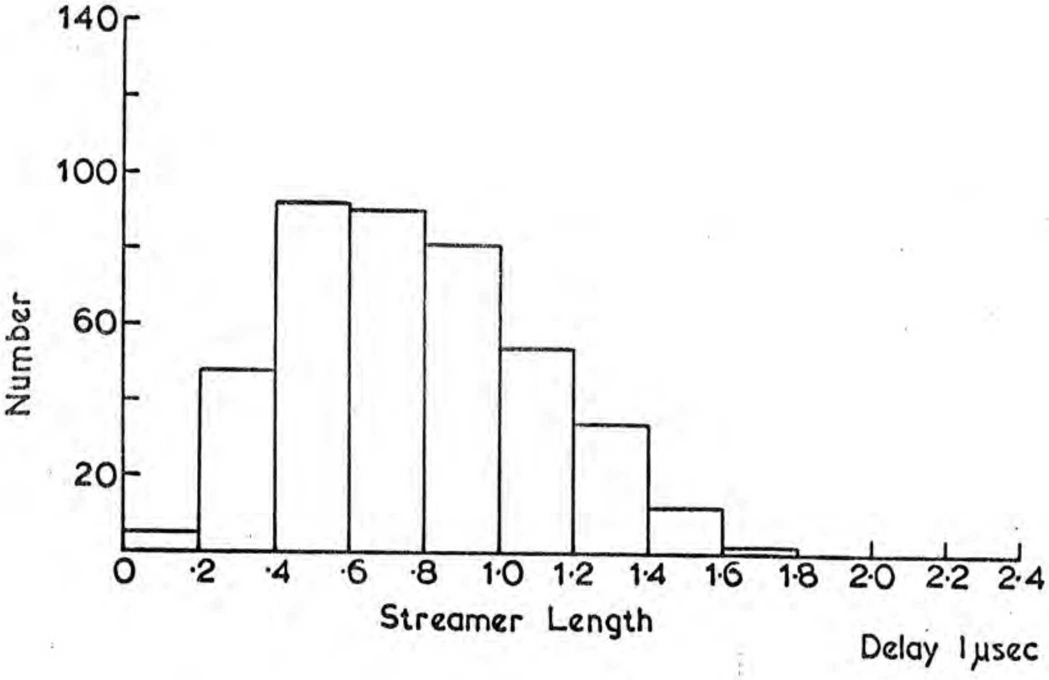
140
100
60
20
Number
0
·2
·4
·6
·8
1·0
1·2
1·4
1·6
1·8
2·0
2·2
2·4
Streamer Length
Delay 1 µsec

Figure 6.7a

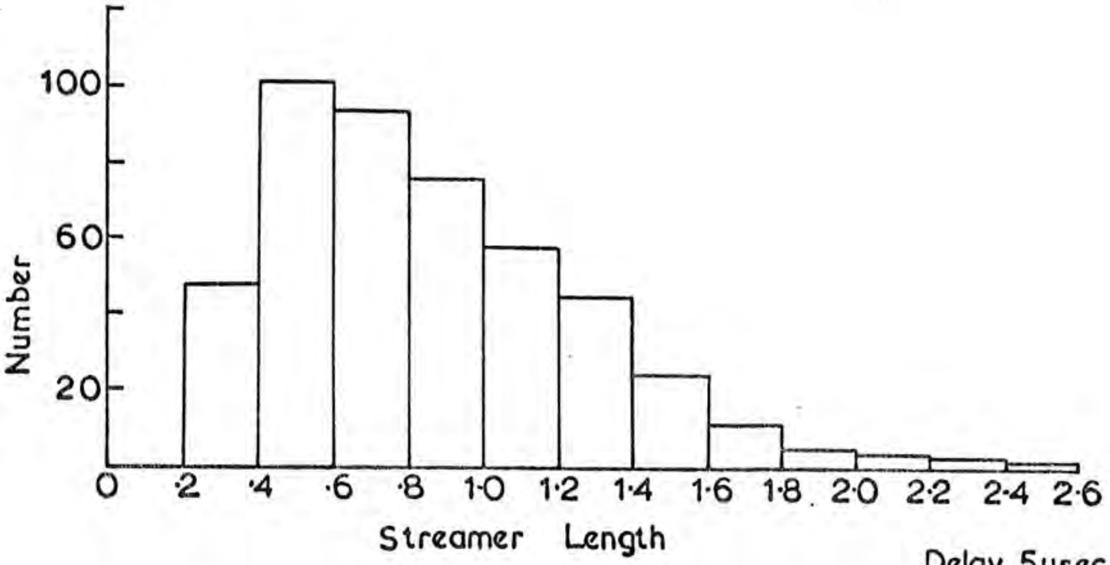

Delay 5 μsec

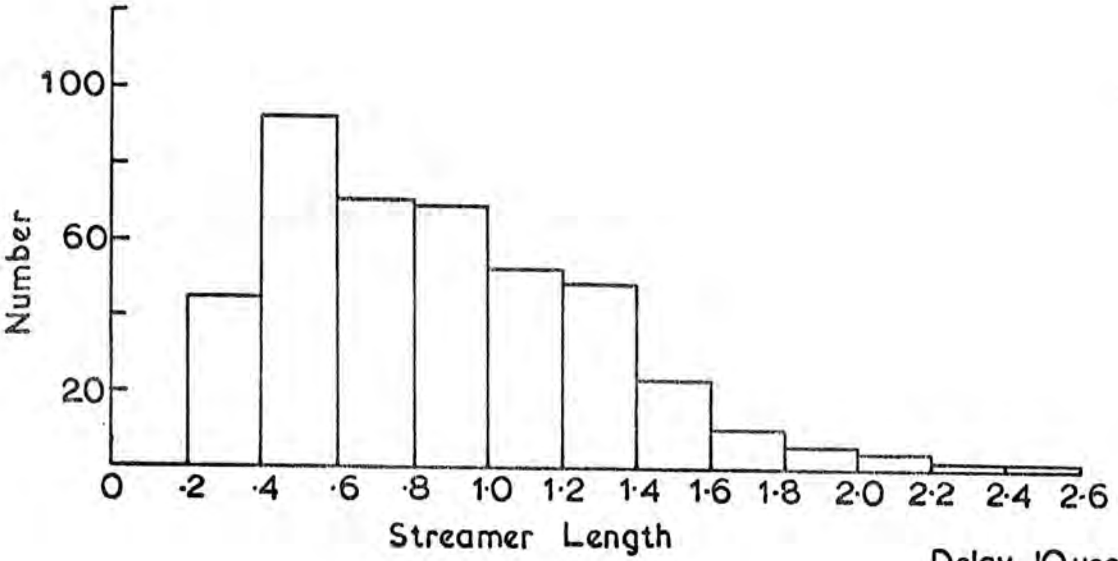

Delay 10 μsec

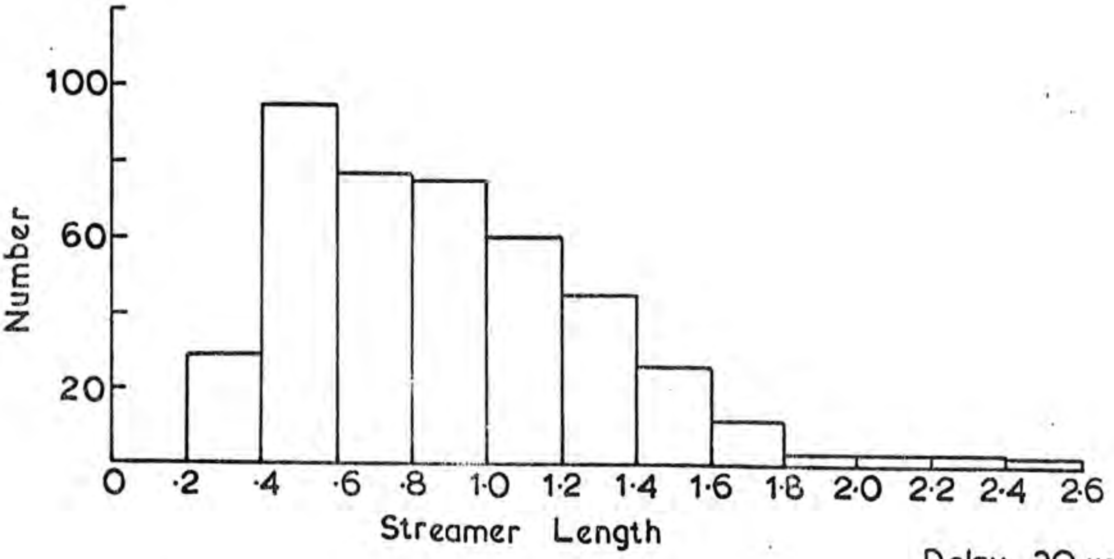

Delay 20 μsec

Figure 6.7b

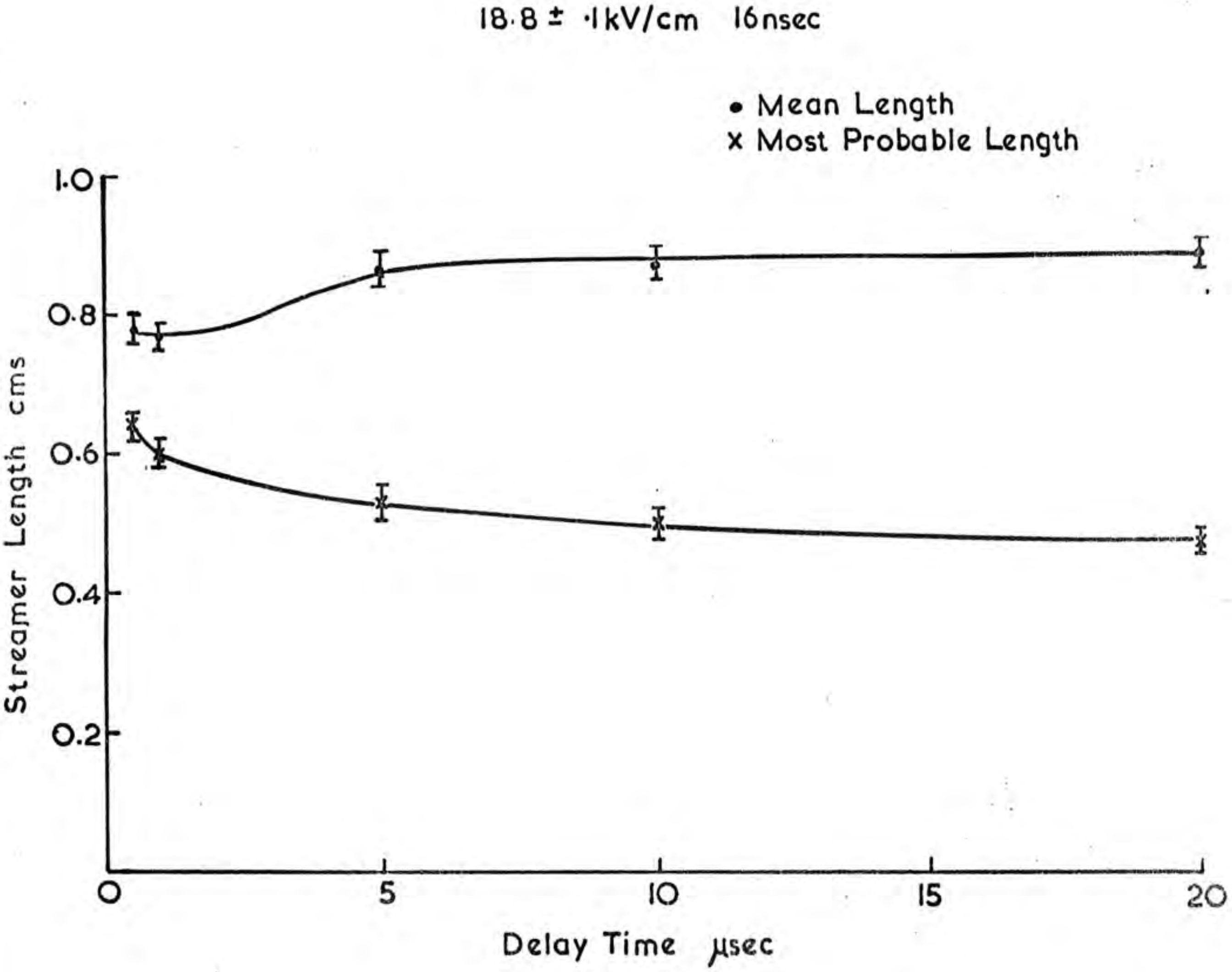
18·8 ± ·1kV/cm 16nsec
• Mean Length
x Most Probable Length
1.0
0.8
0.6
0.4
0.2
Streamer Length cms
0
5
10
15
20
Delay Time µsec

Figure 6.8

The most probable streamer length shows a characteristic drop between delays of 600nsec and 20μsec which is similar to the drop in the streamer number obtained theoretically for small values of L/L_m (C.92) and shown in Figure 5.3 In this case however, the pulse used was equivalent to a larger value of L/L_m ($\sim$0.98) and it is clear that the length distribution contains information concerning the spacial electron distribution which is lost by the saturation of the streamer density.

It is possible to generate a theoretical curve for the most probable length of streamers as a function of time delay using the model GAUSS. Figure 6.5 and 6.6 showed the differential transition probabilities of avalanches at various values of L/L_m and the peak of such a distribution may be taken as being equivalent to the peak of the streamer length distribution. The quantity ($1-L/L_m$ MAX) is plotted against pulse delay time, for three values of ionisation density in Figure 6.9. There is good agreement, in basic shape, with the experimental curve shown in Figure 6.8.

The experimental plot of mean lengths, shown in Figure 6.8 follows the drop of the most probable length curve at 1 μsec delay but this drop is soon counteracted by the development of the long tail of the length distribution and so the mean value shows little change over the whole range of delays up to 20 μsec.

Similar constant values were obtained for the mean length generated using other field strengths and durations. For a field of 19.5 ± 0.1kV/cm the following mean lengths were obtained using delays in excess of 5 μsec.

Pulse length	Mean Streamer Length
15.85 ± 0.2nsec	0.95 ± 0.05 cms
14.8 ± 0.2nsec	0.75 ± 0.05 cms

The most probable streamer lengths were also measured for three pulse lengths using a field of 19.5 kV/cm and the results are plotted as a function of time delay in Figure 6.10. The curve produced using the 15.85 nsec pulse

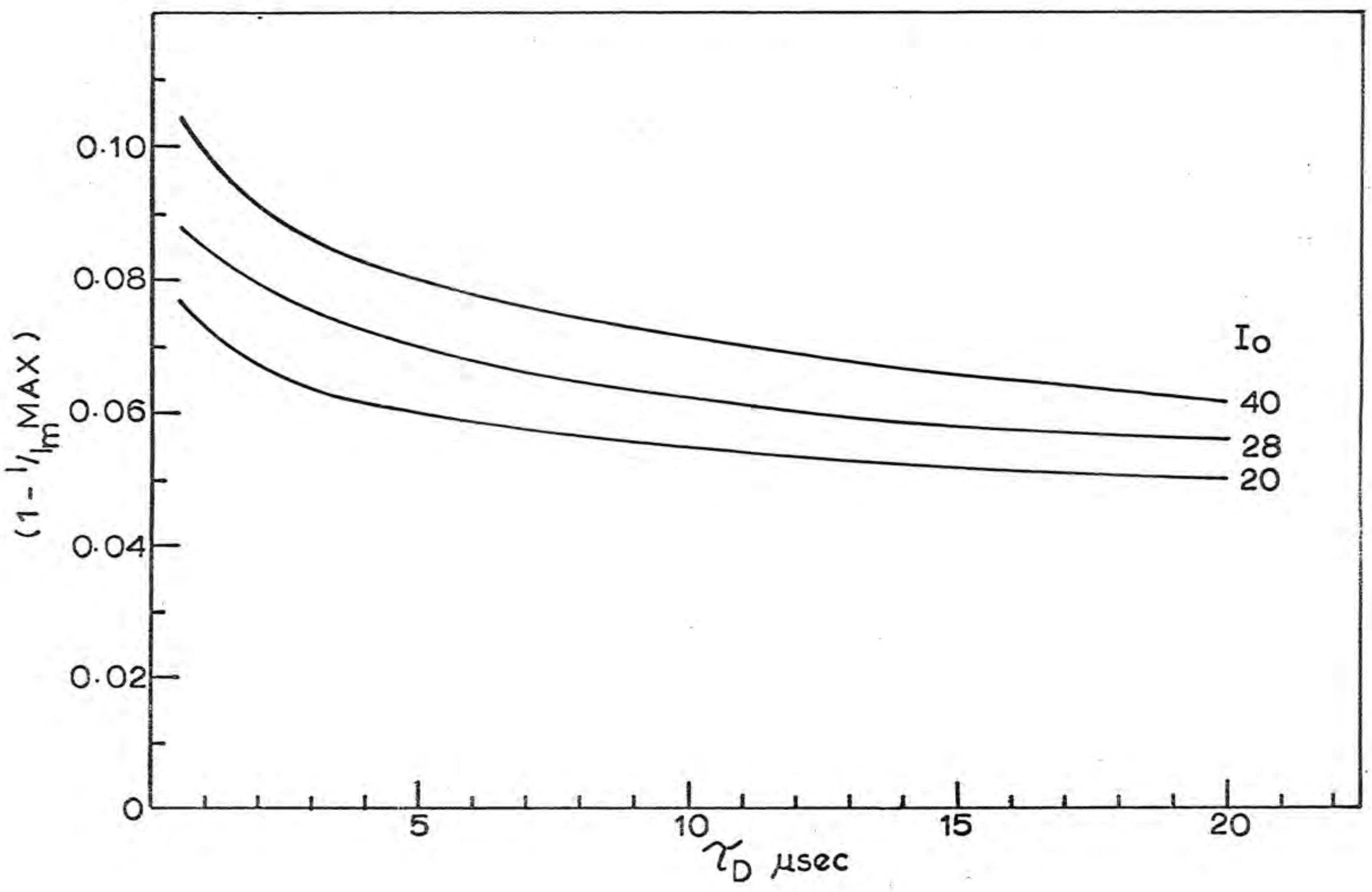
Streamer Generation Model Gauss

Figure 6.9

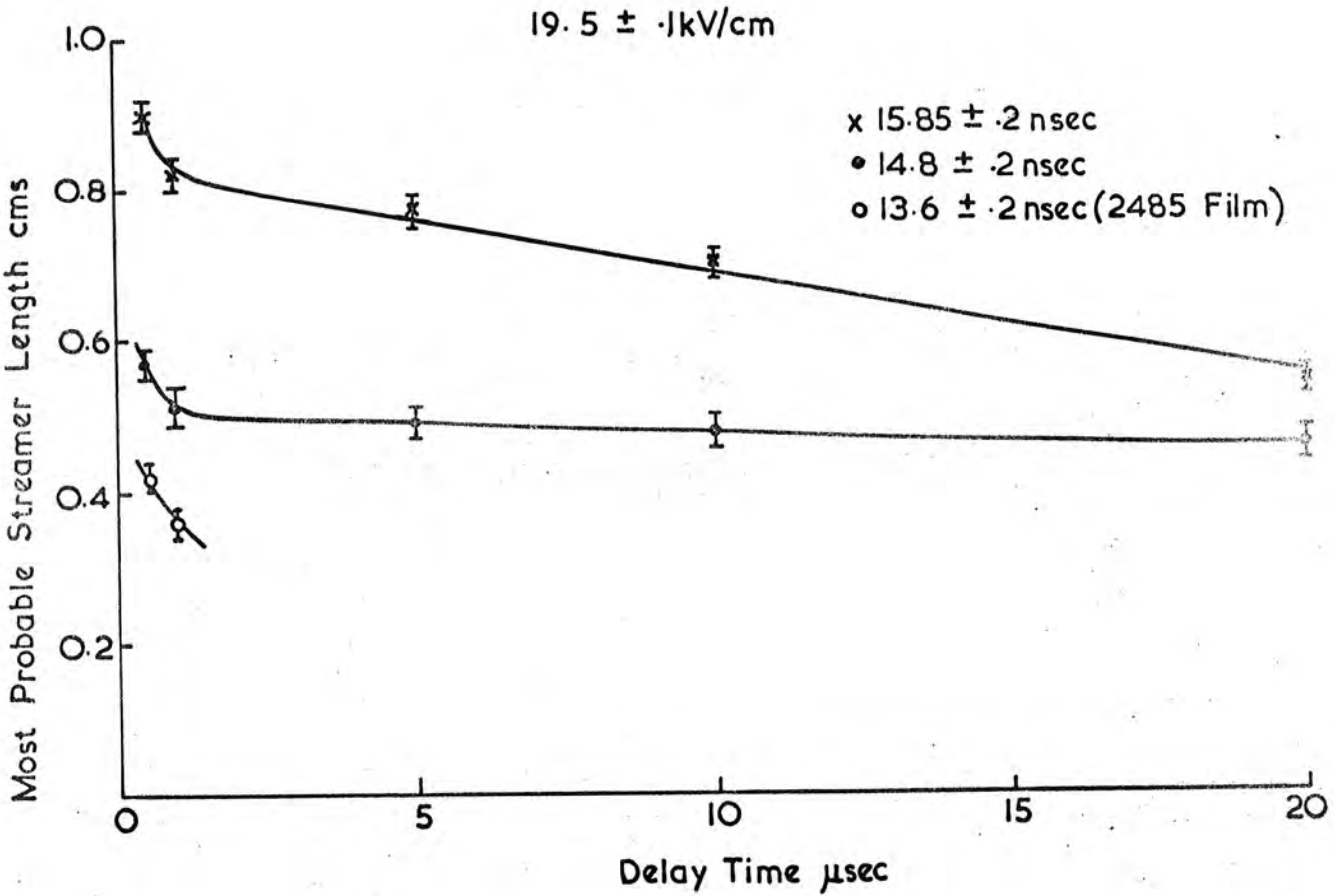
19.5 ± ·1kV/cm
x 15.85 ± ·2 nsec
• 14.8 ± ·2 nsec
o 13.6 ± ·2 nsec (2485 Film)
Most Probable Streamer Length cms
1.0
0.8
0.6
0.4
0.2
0
5
10
15
20
Delay Time μsec

Figure 6.10

is in excellent agreement with that obtained theoretically, for an ionisation density of 28 cm^{-1}, shown in Figure 6.9 and gives the same percentage drop in length over the delay times covered by the curve. The experimental curve does depart slightly from the smooth theoretical curve in the 5μ sec region but the departure is bearly outside the experimental error. The error bars shown on Figure 6.10 are those produced in estimating the peaks of the length distributions. The curve for a pulse length of 14.8nsec shows greater departure from the theoretical curve becoming much flatter towards longer delays. This is attributable to the loss of the shorter streamers from the photographs, due to the lack of sufficient photographic sensitivity. Thus for very short streamers the most probable value of streamer length will tend towards the shortest phorographable length. For Kodak 2475 type film, under the conditions used here, this length appears to be around 4mm but some streamers of length shorter than 4mm are photographed as can be seen in the length distributions shown in Figure 6.7.

No streamers could be photographed on the 2475 type film when using a 13.6nsec long pulse and a field of 19.5kV/cm but it was possible to obtain length distributions, at delays of 600nsec and 1μsec, using type 2485 film. The streamers were again beyond photographic cutoff however, at 5μ sec delay.

6.4 The Streamer Velocity

By means of an electronic shutter and an image intensifier with a gain of 10^7, Davidenko et al (7) have measured the streamer velocity in neon for streamer lengths from 2.5 to 6.5 mm and using applied fields from 10 to 17 kV/cm. A summary of these results was given in Figure 2.3 and 2.4.

For long streamers, where the shape of the length distribution is not significantly affected by photographic cut off effects, it is possible to obtain a measure of the streamer velocity for fields approaching 20kV/cm. If the most probable streamer length is assumed to be independent of such distribution distorting effects and dependent only on field strength, its duration, and the pulse time delay, then the results given in Figure 6.10 may be used in such a determination. The only points on the graph which may be regarded as being free from distorting effects are the 600nsec and 1μsec delay points for the 15.85 and 14.8 nsec pulse lengths. By considering the change in the most probable length of the streamers, on increasing the pulse length by 1.05nsec, one obtains

Streamer Length	Velocity
0.74 cm	$3.2 \pm 0.7 \times 10^8$ cm/sec
0.67 cm	$2.95 \pm 0.7 \times 10^8$ cm/sec
0.5 cm	1.46 10^8 cm/sec

The last result was taken using a 13.6nsec pulse length and the effects of photographic sensitivity limitations cannot reasonably be neglected. The streamer lengths quoted above are the mid points of the lengths through which the streamers grew during the time considered.

The above results, for streamer lengths of 0.74 and 0.67 cms are in good agreement with the results of Davidenko et al if they are extrapolated to the streamer lengths and field strengths used here and it seems probable that the small quantity of helium present in the streamer chamber alters the velocity of the streamers by an amount within the experimental error.

The results of Davidenko et al (7), for fields of 10kV/cm and streamers 0.45cm long, show that the negative and positive streamer velocities are equal and the negative velocity is equal to twice the positive at 18kV/cm. Particle tracks produced in the streamer chamber using a field of 18.8kV/cm were examined and the lengths of the positive and negative directed streamers compared. Best fit lines were drawn through the tracks using the geometrical centres of the shortest streamers as a reference. The extentions of streamers, exceeding 1 cm in total length, on each side of the line were then measured. Figure 6.11 shows

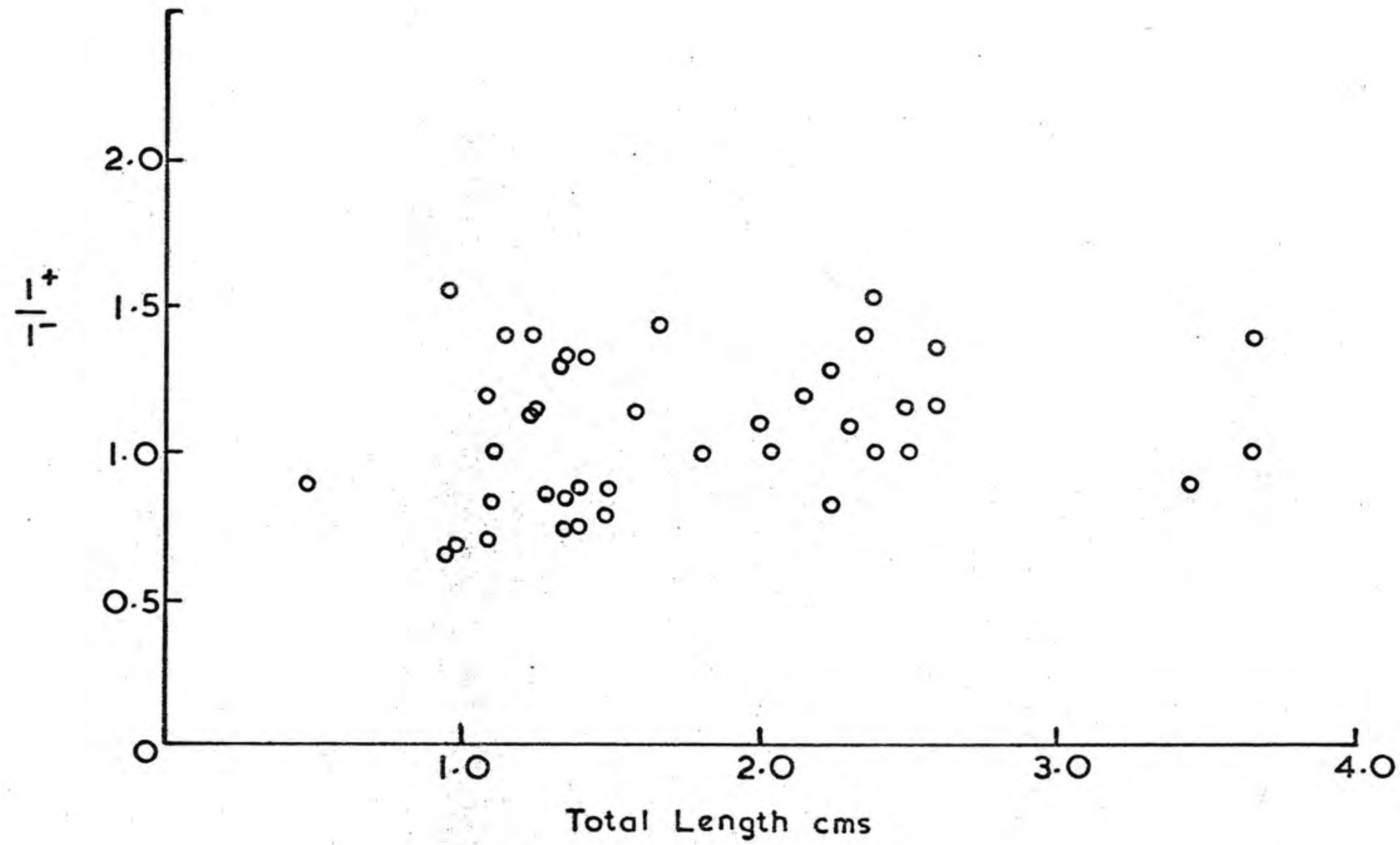

Ratio of l^+/l^- as a Function of Total Streamer Length

Figure 6.11

a scatter diagram of the ratio of the measured positive to negative length as a function of total length.

Only one obvious trend is shown by the results. The positive length exceeds the negative length by about 25% in most cases but the apparent lack of variation in the length ratio as the total length changes suggests that this may be only a zero effect. The positive streamer simply starts to grow first.

The above hypothesis is in direct contradiction with Davidenko. His results were obtained using single streamers and the presence of a large number of closely packed streamers, along the track of an ionising particle, may so modify the local field around any one streamer as to mask the effects he described (7). If the streamer lengths in the positive and negative direction are dependent upon the local environment, in particular the electric field distortions produced by neighbouring streamers, then this may be sufficient to explain the random nature of the points in Figure 6.11.

6.5. The Streamer Density

The streamer density as a function of time delay seen perpendicular to the electric field is similar to that seen parallel to the field and is shown in Figure 6.12. The reduction in the streamer density, seen at delays of 5μsec, is identical to that shown in Figure 5.5 and 5.6. The reasons for the decrease have already been discussed in chapter five and are attributable to the diffusion of the electrons outside the first avalanche radius.

The main feature of the graph in Figure 6.12 is that the 'zero' delay streamer density is 1.8 compared with 1.5 as seen parallel to the field. It may be expected that more streamers will be below the photographic cut off in the perpendicular view where the photon flux emitted by the streamers is least but this is compensated for by a geometrical effect. Streamers which would be obscured in the parallel view by the large end diameters of the longer streamers, become visible in the perpendicular view between the thinner central dimensions of such streamers.

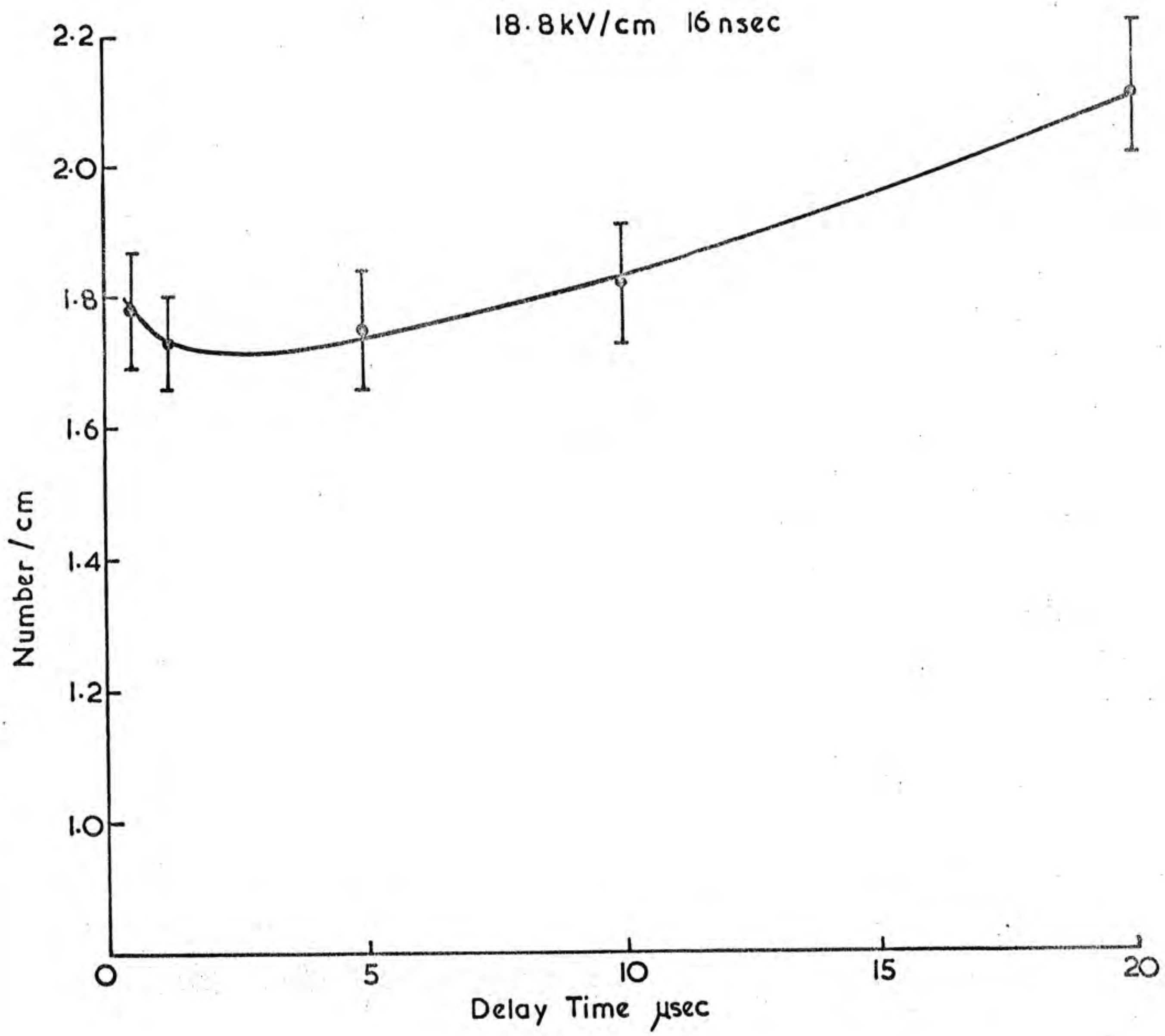
18·8kV/cm 16nsec
Number / cm
2·2
2·0
1·8
1·6
1·4
1·2
1·0
0
5
10
15
20
Delay Time μsec

Figure 6.12

As the electrons along the track diffuse apart the streamer density increases. In the perpendicular view there is a limit to the maximum number which can be seen. Each streamer represents a dead zone behind which streamers may form and not be seen. Thus considering long streamers and a mean optical diameter of 2mm, the maximum streamer density which will be seen is 5/cm and represents an asymptotic upper limit for the streamer density shown in Figure 6.12.

6.6 The Streamer Centre Displacement

(a) Some Theoretical Considerations

In Chapter two it was stated that a streamer starts its growth from the head of the avalanche when the avalanche has attained the Meek length. Thus the centre of a streamer is displaced from the position of the initiating electron and will introduce a systematic error into the location of elementary particle tracks through the chamber.

This distance may be estimated as follows:-

The applied pulsed field, as shown in Figure 4.6, may be described approximately by the following equations

$$E = E_{MAX} \frac{t}{9\times10^{-9}} \qquad \text{for} \quad 0 < t < 9 \times 10^{-9}\ \text{sec} \qquad 6.1$$

$$E = E_{MAX} \qquad \text{for } 9\times10^{-9} < t < 15.6\times10^{-9}\ \text{sec} \qquad 6.2$$

$$E = E_{MAX}\left(1 - \frac{t}{9\times10^{-9}}\right) \text{for } 15.6\times10^{-9} < t < 24.6\times10^{-9}\ \text{sec} \qquad 6.3$$

Where E is the field and t is time.

Equation 2.1 indicates that an avalanche will attain the Meek length when the product αVt approaches 20. The time into the pulse at which this occurs may be obtained by integrating this product over the shape of the pulse. It is necessary to insert values of α and v which are both functions of field. The data of Hughes (8), for α as a function of field in 90% Neon and 10% Helium, may be approximated by the following equation.

$$\frac{\alpha}{p}\left(\frac{E}{p}\right) = 0.016\left(\frac{E}{p} - 6.25\right)\ \mathrm{cm}^{-1}\ \mathrm{Torr}^{-1} \qquad 6.4$$

where the symbols have thier usual meanings.

The value for the drift velocity of the electron is taken to be given by the equation

$$v = (15 + 2.44 \times 10^{10}t)\ 10^{5}\ \mathrm{cm\ sec}^{-1} \qquad 6.5$$

which is a simple interpolation of the data of von Engel (9). The value of the integral,

$$n = \int_{0}^{T} \alpha\ \left(\frac{E}{p}\right)\ v\left(\frac{E}{p}\right)\ dt \qquad 6.6$$

Using a peak field E_{MAX} of 20kV/cm and performed over the rise time of the pulse, gives a value of $\ln(n) = \alpha v\ t = 15.2$ where n is the number of electrons in the avalanche.

To obtain a value of 20 for the product $\alpha\ v\ t$ the integration must be continued into the flat top of the pulse where the value of α is 312 cm^{-1} and the drift velocity is 2.35×10^{7} $\mathrm{cm\ sec}^{-1}$. A further 6.55×10^{-10} sec of the pulse increases ln(n) to the required value of 20 and at this point the avalanche attains the Meek length. The total elapsed time is now 9.65nsec. No account has been taken of the reduction of the field in the avalanche by the space charge of the electrons which may tend to increase this time slightly.

The Meek length may now be calculated by integrating the drift velocity of the electrons in the avalanche, given as a function of field by equation 6.5, over the formative time. This gives the value of the Meek length, using a pulse of the type shown in Figure 4.6, as 1.22mm.

In the above discussion the avalanche has been taken to start from only one electron but as was seen at the beginning of chapter five the avalanche may be initiated by several electrons and this number will vary along the length of a particle track. The most probable fraction of the Meek length at which the avalanches along a track will transform into streamers may be found using the model GAUSS. The actual displacements of the centres of the streamers from the position of the original electron was calculated using the value of the Meek length obtained above and is shown plotted as a function of pulse delay time and ionisation density in Figure 6.13. The effect on the displacement of the two parameters is only about 5% and for most purposes the streamer centre displacement can be regarded as 1.13mm.

(b) An Experimental Investigation

To investigate the ideas expressed in the previous sub section, streamer tracks which were produced by particles which traversed the chamber at angles of about 30° to the vertical were studied. Such particles passed through the streamer chamber on both sides of the high voltage electrode as is shown in Figure 6.14. The streamer centre displacement, which is towards the positive electrode, is now equal and opposite on either side of the central electrode thus facilitating a determination of this distance. Such a measurement was seriously limited in its precision by the locational accuracy of the particle track viewed perpendicular to the applied field. The accuracy will be discussed further in the following section. No significant dependence of the offset on delay could be found and so the data taken under all conditions was averaged and the value of the displacement was found to be 2.9 ± 0.4mm. This figure exceeds the experimental value of 1.13mm by an amount well outside the experimental error. Possible sources of this extra displacement are as follows.

(1) In section 6.4 it was stated that the reverse streamer velocity may exceed the forward velocity by almost a factor of two, under the operating conditions used here (7), hence the geometrical centres of the streamers may appear displaced towards the cathode. This displacement however, would be in the opposite direction to that observed and should also be noticable where streamers of various lengths appear on the tracks. It has also been shown in section 6.4 that no significant difference between the velocity of the

Streamer Generation Model Gauss

Theoretical Streamer Centre Displacement

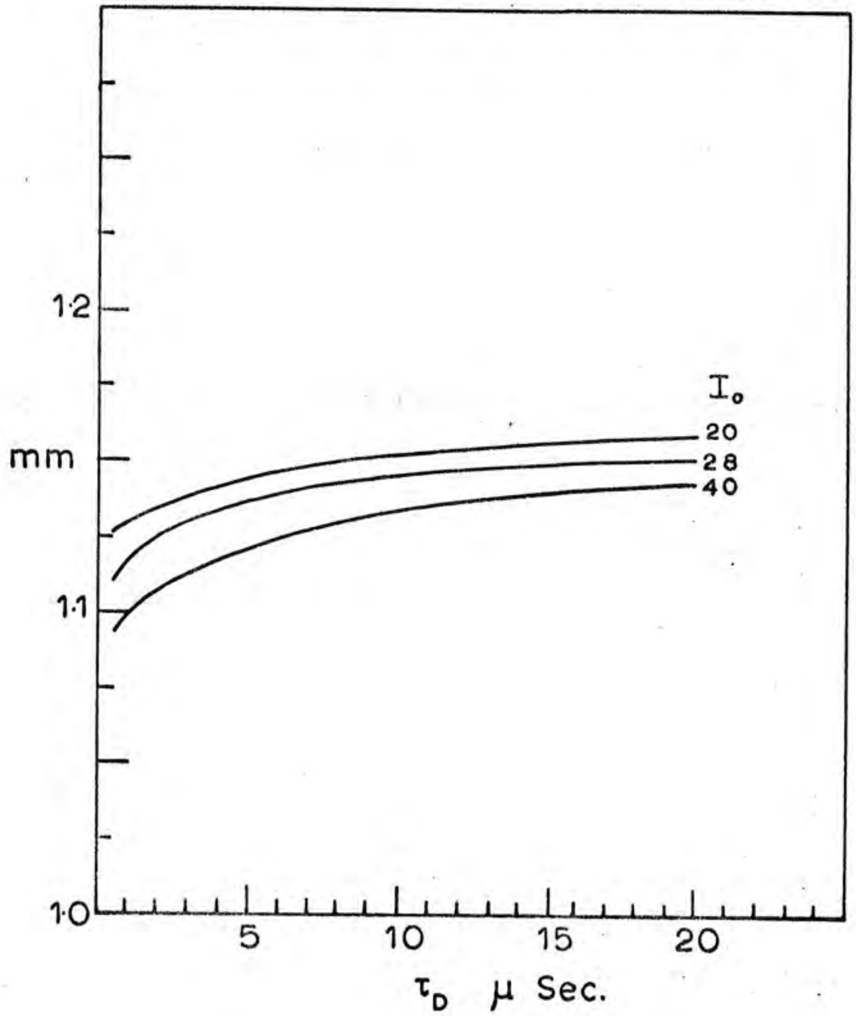

Figure 6. 13

FIGURE 6.14

A STREAMER TRACK LOOKING 90° TO THE APPLIED FIELD SHOWING THE STREAMER DISPLACEMENT.

PULSE PARAMETERS 18.8kV/cm FOR 16nsec.

PULSE DELAY 5μsec

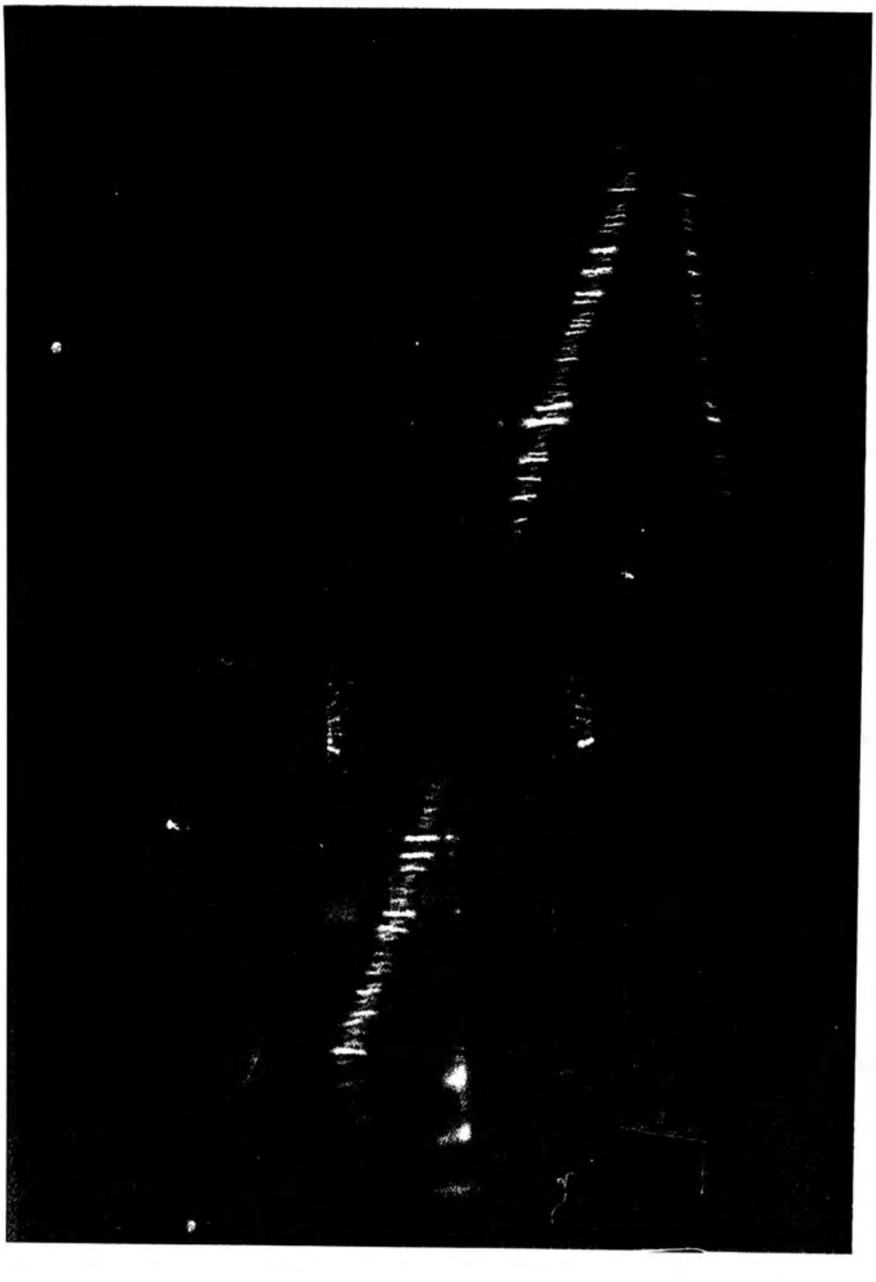

positive and negative streamers have been found and so the contribution produced by this effect to the streamer centre displacement is considered negligible.

(2) A homogeneous electric clearing field in the chamber could produce a track displacement of the magnitude observed but the displacement produced by such an effect would depend on the pulse delay time. It also contradicts the actual nature of the field which was described in section 6.2 as varying in both strength and direction throughout the chamber.

(3) Photography perpendicular to the applied field is via 1.2cm of perspex which will introduce an optical distortion of the streamer position. The maximum angle subtended at the camera by any streamer is only 16° making such distortions negligibly small compared with the observed displacement.

(4) During the discharge of the Marx generator, before breakdown of the series spark gap 165 nsec into the transient, the charging current waveform of the parasitic capacitor appears on the electrode structure by capacitive coupling through the series spark gap. This pulse is similar in form to the prepulse produced by a Blumlein line. The height of the transient can be estimated from the capacity of the spark gap (25pf) and the terminating resistance of the electrodes and has been confirmed by measurements using the high voltage probe to be 7± 1 kV under typical operating conditions.

The results of Bowe et al (1) show, for the values of E/P used here, the drift velocity of electrons in neon may be described by the equation

$$v = 1.3\sqrt{\frac{E}{P}} \times 10^{6} \text{ cm sec}^{-1} \qquad 6.7$$

The first 165nsec of the transient waveform may be considered as the first half cycle of a sine wave and so the distance drifted by the electrons, before the discharge of the series spark gap, is given by the integral

$$d = \int_{0}^{\tau/2} 1.3\text{x}10^{6} \sqrt{\frac{E}{P} \sin \frac{2\ t}{\tau}}\ dt \qquad 6.8$$

This integral may be solved in terms of eliptic integrals and these in turn expressed by Gaussian hypergeometric series. The approximate summation of these series gives the electron displacement as

$$d = 0.51\,\tau\sqrt{\frac{E}{P}} \times 10^{6}\ \text{cm} \qquad 6.9$$

Thus for a 7kV prepulse, lasting 165nsec and of sinusoidal form, the displacement of the initial electron before the start of avalanche growth is 1.32 mm.

Adding this value to that obtained for the most probable avalanche length gives an expected streamer displacement of 2.45 mm which agrees reasonably well with the measured value. The prepulse is thought to be the dominant agent in producing the increased streamer offset but the other processes, in particular the Townsend ionisation coefficient being reduced by space charges are probably important.

6.7 Locational Accuracy

The factors affecting the locational accuracy looking perpendicular to the applied field are essentially the same as those already described in the previous chapter with respect to the view parallel to the field. A procedure, identical to that outlined in Chapter six,was used to measure the locational accuracy and the results, found using tracks 50cm long, are shown for points near the track centre in Figure 6.15 and near the edge in Figure 6.16. The finite length of the streamers plays a significant part in the limitation of the locational accuracy and, at the centre of the track, completely dominates the effects of diffusion. The accuracy is between 0.3 and 0.4 mm over all delays up to 100μsec. The dependence of accuracy on streamer length is further illustrated by its considerable increase when the streamer length is reduced from 6.0 to 4.0 mm, Figure 6.15.

Again the results of spurious clearing field are indicated by the size of the error bars and are much greater near the edge of the track. Here the particle approaches the wall of the chamber where the clearing field, the optical distortions, and the curve fitting errors are greatest. The

Locational Accuracy Centre

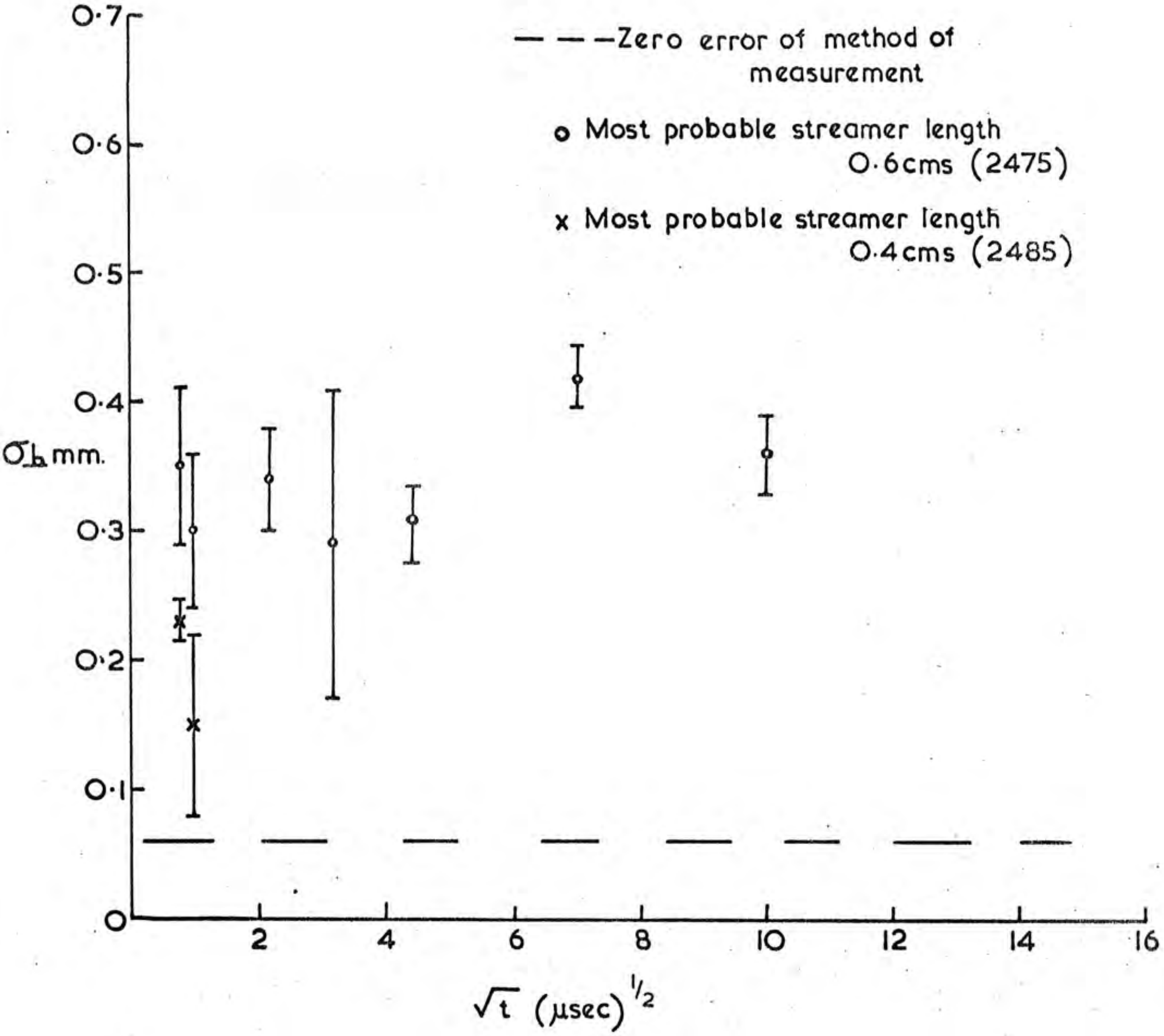

Figure 6.15

Locational Accuracy Edge(Lower)

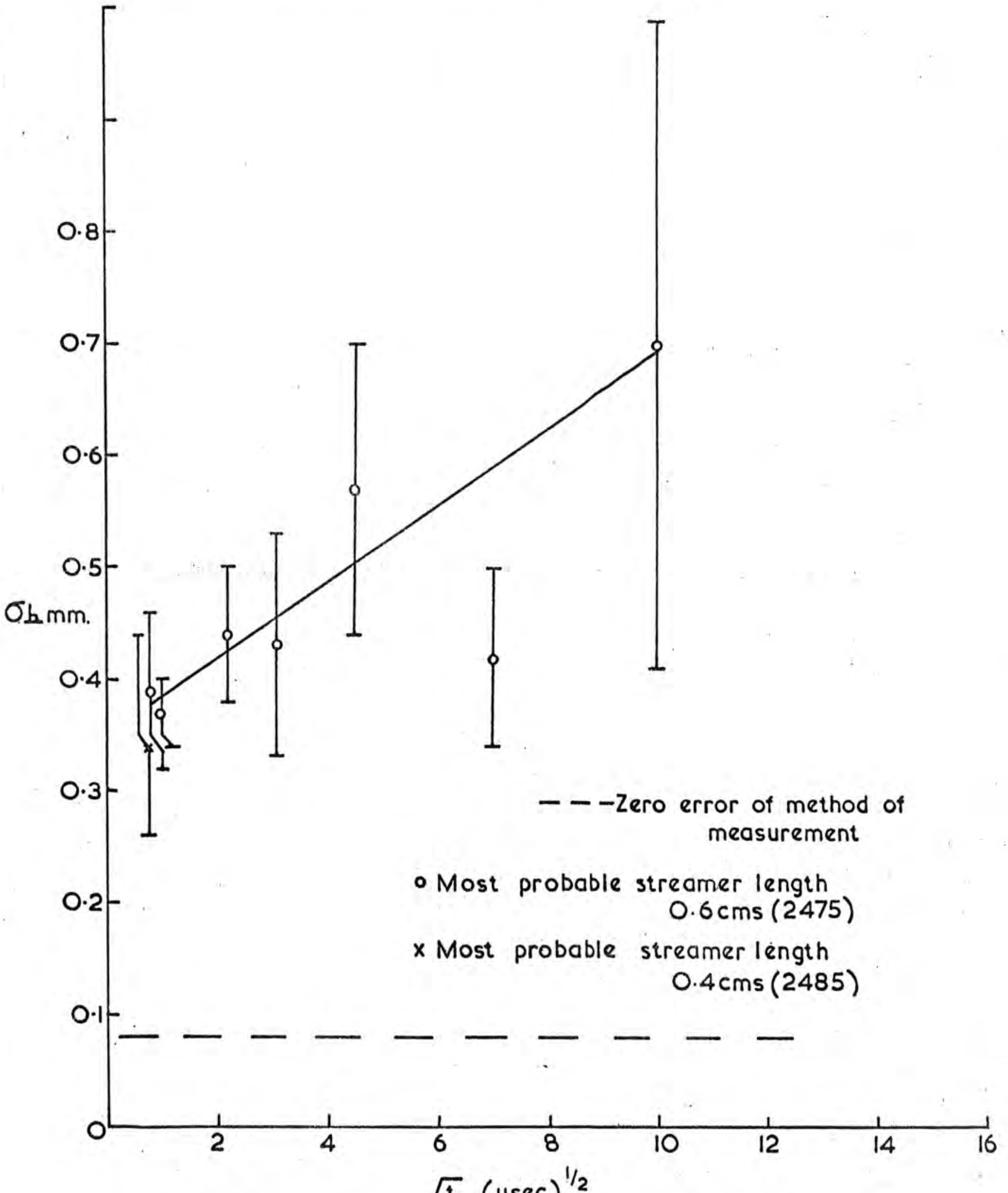

Figure 6.16

zero errors, attributable to the method of measuring, are shown on the diagrams.

6.8 Spatial Resolution

The resolution as seen perpendicular to the applied field is also limited by the streamer length. Avalanches growing on two independent tracks, within one streamer length of each other, will join together and their individuality will be lost. The limit to which the streamer length may be reduced is set by the electrical streamer interaction distance. This was $R_o = 0.65$cm in the parallel plane and must be a similar value here. It is probable that a reduction of the streamer length beyond 0.5cm will not greatly reduce the resolution. The effect of diffusion upon resolution will be more masked in this direction than looking parallel to the field as the streamer length invariably exceeds its diameter.

Chapters five and six have been an account of the basic properties of the streamer chamber. In the final chapter these properties and the operation of the system as a whole will be discussed, and its limitations and capabilities investigated.

REFERENCES

1. BOWE, J.C., Phys. Rev. 117 (1960) 1411.
2. VILLA, F., Int. Symp on Nuc. Elect. Versailles 1968 P7-1.
3. STUBBS, R.J., BREARE, J.M., Acta. Physica. Academiae Scientiarum, Hungaricae 29 (1970) 473.
4. HOLROYD, F.W. and BREARE, J.M., Proc. Int. Conf. on Cosmic Rays Hobart (1971).
5. ZICHY, E.L., Static Electrification Conference (1967) P52.
6. DAVIDENKO, V.A., Nuc. Inst. Methods. 75 (1969) 277.
7. DAVIDENKO, V.A., Sov. Phys. JETP., 28 (1969) 227.
8. TAN, B.C. TC-L/INT 70-7 CERN.
9. von ENGEL, A., Ionised Gases, Oxford Clarendon Press 1965.

CHAPTER SEVEN

DISCUSSION AND CONCLUSION

In this, the final chapter, an assessment will be made of the streamer chamber design and any improvements and extensions of its basic operating principles which may be useful will be made. The limitations of the streamer generation model GAUSS and the implications of the results produced by it will be considered. The experimental results, which were presented in the previous two chapters outline the boundary of usefulness of the streamer chamber as a tool of Physics and these properties will be compared with their equivalents as exhibited by other particle detectors, in particular the bubble chamber.

7.1. The Design

The preceding chapters have shown that the principle of using a water dielectric capacitor as the energy storage element in the fast discharge circuit used to drive a streamer chamber is viable. The size of this part of the circuit has been successfully reduced to about one tenth the size of an equivalent Blumlein line.

The system is very reliable and the produced pulse shows little sign of short term drift, the height being stable within ± 0.1kV/cm and the length within ± 200psec. The stability of the pulse is perhaps best represented by the two streamer diffusion curves shown in Figure 5.10. The only difference between the two curves is 900psec in pulse length. The results were taken over a period of two weeks for each curve and the closeness of the points to the fitted line is indicative of the control of the pulse possible over this sort of time scale. Changes in the characteristics of the water used as a dielectric in the parasitic capacitor are more of a problem and the water must be replaced after 2 or 3 months use. This problem could be overcome however, by cycling the water through a purifier or by using a flushing system.

The control over the length of the high voltage pulse was quite adequate but less than that hoped for, although any control is an improvement over the Blumlein line system in which different lines must be used to produce different pulse lengths. Attempts to produce pulses of lengths outside those used to obtain the results in this thesis, that is less than 13.6 nsec and longer than 17.0nsec, tended to alter the basic shape of the pulse and make a reasonable comparison of data taken using such pulse lengths impossible.

The change in shape occurs when the flat top of the pulse is eliminated and the pulse becomes triangular rather than trapesium shaped. A decrease in the rise time of the pulse will therefore extend the range of possible pulse durations.

The need to use two high pressure, high voltage spark gaps makes the layout of the components in the water tank far from ideal although a close approximation to a coaxial design has been achieved. Some of the above problems should be solved by the second generation streamer chamber pulsing system described below. It is based on the same principles as the first streamer chamber and utilises a parasitic capacitor with a water dielectric.

7.2. A proposed second generation Streamer Chamber

The main aim in designing the improved version of the streamer chamber was to eliminate the need for two spark gaps and to improve the geometry of the component layout,with a coaxial system as the ideal.

In Figure 2.14 we saw plotted the voltage remaining on the Marx generator capacity C_m when the peak of the transient on C_p is reached. If the series spark gap fires during the peak,then this voltage is that which must be removed from the Marx generator by the shunt spark gap. There is one point on Figure 2.14 where this voltage and hence energy is zero. There is no residual voltage on the Marx generator if the parasitic capacity is equal to the Marx generator capacity, and, as was assumed in calculating the data for Figure 2.14, they are ideally coupled with no resistive damping. If this condition can be achieved the shunt gap may be eliminated. The pulsing system may now be constructed using a coaxial component layout and such a design is shown in Figure 7.1. The cylindrical parasitic capacitor, a single spark gap and, if small enough, the Marx generator may all be housed inside a single metal cylinder. The diameters of the central and outer conductors are chosen to minimise breakdown, while the value of C_p may be controlled by simply varying the length of the water filled section.

By making the parasitic capacity equal to the Marx generator capacity it may be necessary to depart from the optimum condition of $C_p = \sqrt{C_c C_m}$, as the only way to achieve the condition is by making the chamber capacity C_c and parasitic capacities C_p equal. This leads to the need for generators with inconveniently high output voltages. It is probably more convenient to use a lower value of $\frac{C_c}{C_p}$ than that given by the above relationship. This would result in an inefficiency in the energy transfer from C_m to C_c. As can be seen in Figure 2.10 and Figure 2.11 the situation in which $C_m = C_p = 4C_c$ would give a decrease of 36% in this energy transfer efficiency but there would be a corresponding increase of 60% in the voltage transfer efficiency which would leave the product of the two largely unchanged from the situation in which $C_m = C_p = C_c$. This is considered acceptable as the voltage transfer efficiency is more important than energy transfer when concerned with such systems operating in the megavolt region.

It should be simpler to control stray capacities with the arrangement shown in Figure 7.1 than in the present system but the variation of the dielectric constant of barium titanate with voltage may cause departures from the condition $C_p = C_c$ at times during the pulse but such effects will probably be small and could be completely removed by using paper-

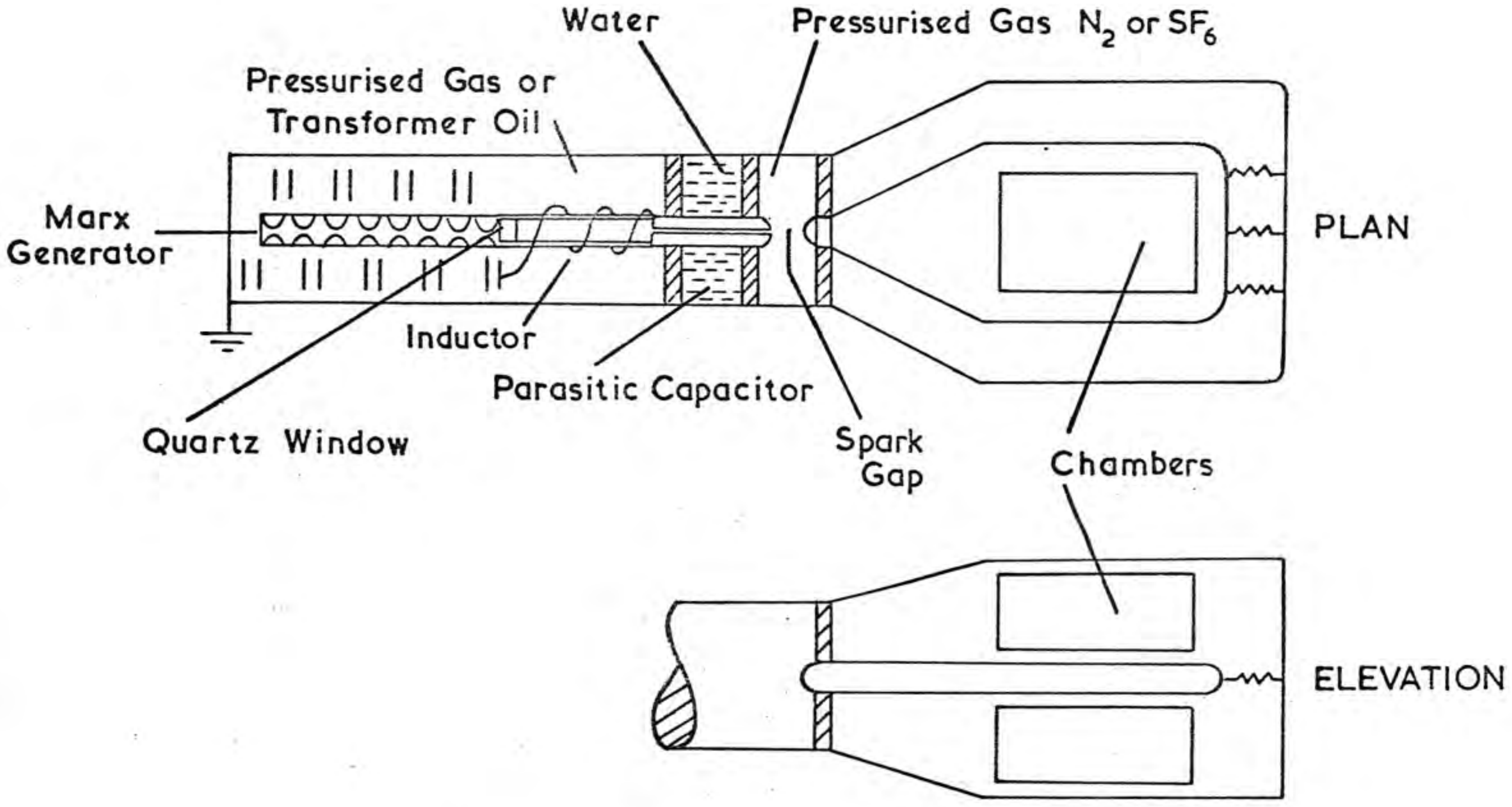

Proposed Streamer Chamber Pulsing System

Figure 7.1

oil type capacitors in the Marx generator.

If the central conductor can be made hollow, ultra violet light from the Marx generator spark gap may be used to illuminate the series spark gap, thereby allowing the removal of the radio-active source which produced the electrons necessary to initiate breakdown. Such a hole should be sealed by a quartz window to maintain the desired pressures in various parts of the system.

The pulse produced on the electrodes by this system should be of the pure 'RC' type. The loss of the shunt gap precludes any active control over the pulse length but for small systems, where the effects of a slight electrode termination mismatch can be neglected, a limited control may be achieved by varying the value of the terminating resistor.

The pulse length itself should be even more stable than when a spark gap is used to produce its trailing edge as its length will be determined by passive components only.

Water filled Blumlein lines have been considered but they will be much more complex in their design and construction than the system described above and have been avoided as the use of a square pulse is not essential for most applications.

7.3 Comments on the High Voltage Probe

The values of the electric field intensity in the streamer chamber quoted throughout this thesis were measured using the transmission line probe described in chapter three. The calibration factor was measured as 176 ± 5kV/cm but the effect of using frequencies much greater than the calibrating frequency has not been considered. Little difference was found between calibrating the probe with 50Hz sine waves and megacycle high voltage pulses between which frequencies the dielectric constant of the melinex probe support decreases by 6%. A similar rate of decrease would lead to an overestimate of the calibration factor by about 9%. The repercussion of such an effect on the results presented here is not great. Never need the field strength be known accurately, the important thing being the detection of changes in that field. This was achieved quite adequately using the probe. The difference in the shapes of the pulses employed by various workers far outweigh errors in pulse height measurement in their effect on the comparison of results. Empirical relationships produced from such data, although practically useful, must be of considerably less physical significance.

7.4 The Streamer Generation Model GAUSS

The behaviour of the model GAUSS has already been compared with the actual behaviour of the streamer chamber in preceding chapters. The model has proved particularly useful in predicting the shape of the graph of streamer density as a function of time delay and the effects of delay on the most probable streamer length. Better control of the relevant parameters, such as the variation of the streamer interaction distance with streamer length, will doubtless lead to closer agreement between the model's predictions and experimental results.

It was found difficult to produce streamer length distributions which compared favourably with those measured but in this case much data concerning the variation of the streamer velocity with electric field intensity, the length of the streamer, the environment produced by its location on the track of an ionising particle and the nature of the photographic response near its limit of sensitivity, which is unavailable at present, is needed to transform the output of the model into the same form as an actual distribution.

Further improvements may be made to the model by considering in greater detail the statistics of avalanche growth. In chapter five the probability that an avalanche, started by one electron, will grow to a size between n and $n + \delta n$ electrons, at a distance x from its start, is given by the Furry distribution.

$$p(n,x) = \frac{1}{\bar{n}} \exp\left(-\frac{n}{\bar{n}}\right) \qquad 5.6$$

This relationship has been confirmed by the linear shape of the $(\ln(p(n,x)),n)$ plot by Schlumbohm (1), Cookson and Ward (2), and Cookson, Ward and Lewis (3). At high values of $\frac{E}{p}$ Schlumbohm (4) found departures from the above equation in the shape of a maxima at low values of n. He attributed this to the failure of the condition necessary to establish the Furry distribution, namely that each electron has the same probability α x of an ionising collision, in the interval δx, at a distance x from thestart of the avalanche and that this probability is independent of the distance travelled from the previous ionising collision. This condition fails when α^{-1} the average distance between ionising collisions, is not much greater than $\frac{Vi}{E}$, the minimum distance over which an electron may gain the ionisation potential Vi. Schlumbohm has shown that the value of the quantity $H = \frac{E}{Vi}$ determines the type of distribution. The value of H used here is typically less than 5 and is below the value of 12 above which the Furry distribution holds.

The statistics of avalanche growth, for values of H less than 12 have been treated by Legler (5) and Byrne (6) and are summarised by Cookson and Lewis (7). The peaked distributions are found to be of the Polya type and may be obtained in a manner similar to that for the Furry distribution by considering that the ionisation coefficient is a decreasing function of avalanche size n and is of the form

$$\alpha' = \alpha \left(1+ \frac{a}{n}\right) \qquad 7.1$$

where α is the limiting value of α' for large n which is normally about 100 and a is a parameter dependent upon the type of gas. Byrne (6) has shown that this assumption leads to a Polya distribution for n of the form

$$q(n,x) = \frac{b}{\bar{n}} \quad \frac{1}{(b-1)!} \quad \left(\frac{bn}{\bar{n}}\right)^{b-1} \quad \exp \quad \left(\frac{-bn}{\bar{n}}\right) \qquad 7.2$$

where $b = (1+a)$.

The limiting cases are $b \rightarrow 1$ and $b \rightarrow \infty$ leading to the Furry and Poisson distribution respectively. If the electrons in an avalanche growing on a particle track do obey this type of peaked distribution rather than the Furry distribution as was used in equation 7.2, then this may be a further reason for the discrepancy between the differential plot of streamer number produced on a particle track as a function of L/L_m, and the experimentally obtained streamer length distributions, where L is the distance through which the avalanche has drifted when the avalanche transforms into a streamer and L_m is the Meek length. It is most likely however, that the electric field perturbations and the photon flux from neighbouring streamers on the track, will have a greater effect on track formation than the above mentioned corrections to the electron number distribution of the avalanches.

7.5 The Limits of Track Location

Most applications of the streamer chamber will rely on its ability to delineate the track of an elementary particles in space. Any errors which the device may introduce into such measurements are of vital importance and can be divided into two groups.

(a) Random Errors

These limit the precision with which the centre of the line of streamers may be located and are the source of the locational accuracy as shown in Figures 5.11, 6.15 and 6.16.

At short pulse delays the accuracy is limited by the finite streamer dimensions and to a much smaller extent by the distance the electrons travel from their original positions while thermalising. Experiments requiring the maximum locational accuracy must use the shortest pulse delay and the smallest streamers possible. Using the shortest photographable streamers which were about 0.4cm long in this case the measured locational accuracy is about 0.25mm both perpendicular and parallel to the applied field at the centre of a 50cm track (sections 5.10 and 6.6).

Increasing the delay allows the effects of diffusion and spurious fields to considerably increase this value. It is possible to partially reduce both effects. The deviation of the streamers from the centre of a particle track has been shown to be dependent on the size of the applied pulse and, by selecting the areas with a high electron density, only the centre of the track need be made visible. The effect of spurious clearing fields is more troublesome. Fields produced by edge breakdown and friction can be eliminated by careful construction but the effect of sparks produced by particles travelling along the field lines can only be removed by eliminating the insulating material between the chamber gas and the electrodes. Internal wires or meshes must be closely wound to minimise field distortions in the gas and will reduce the optical transmission of the chambers and so a conducting thin film may offer a better solution.

(b) Systematic Errors

That the position of the centre of the streamer track, when it has been located with the maximum accuracy obtainable, may not be the position of the particle track is, in some experiments, even more important than the effects of random errors. These systematic errors result in the total displacement of the display to one side of the actual event.

In the streamer chamber described here there are two main sources of such aberrations. The first is the displacement due to the Meek length. The pulses used here produce theoretical Meek lenths of 1.13mm in the neon helium gas mixture and a similar figure will apply to all streamer chambers which work on the same principle. A small reduction could be obtained by shortening the rise time of the pulse and by using pulses of higher amplitude. A 20kV/cm pulse with an infinitely short rise time would give a Meek length of not less than 0.6mm and this is probably the lower limit.

The second source of systematic error is a device effect but one which is common to several types of pulsing system. The waveforms produced in the slow discharge parts of the circuit, for example the discharge of the Marx generator onto the parasitic capacitor or Blumlein line, are coupled through to the rapid discharge parts of the circuit. This pulse causes the electrons left by the ionising particle to be displaced and a systematic error is introduced.

Here the charging current wave form of the parasitic capacitor is coupled to the electrodes by the capacity of the series spark gap The resultant electron displacement was given, in chapter five, to be 1.32mm. This can be reduced by minimising the capacity of the spark gap and a decrease by a factor of two or three should be possible with careful design. The shape of the waveform is controlled by the charging inductance between the Marx generator and the parasitic capacitor. As the total amount of charge being transferred to the capacitor is constant, for fixed operating conditions, then the area under the transient will be constant and any attempt to reduce its length will result in a corresponding increase in height. The displacement of the electrons, at the field strengths considered here, was shown in chapter five to be given by

$$d = 0.51\,\tau\sqrt{\frac{E}{p}} \times 10^{6}\text{cm} \qquad 6.8$$

Thus the dependence of d on $(E)^{\frac{1}{2}}$ means that a decrease in the duration of the transient will result in an overall reduction of the error.

7.6 Secondary Information from Streamer Tracks

The ability of a detector to yield more information about a particle than its location in space is an obvious advantage for any instrument. The degree of ionisation produced is of prime importance. Even though an expected change of 20% in the ionisation density could not be resolved by changes in the streamer density, this is by no means an indication of the impossibility of ionisation measurements using this gas mixture. According to the output of the model GAUSS such a change should be just resolvable if the accuracy of the measurements can be improved even further.

Another way to investigate ionisation in the 70% neon gas mixture would be by measuring the streamer lengths or parameter which, unlike the streamer density, does not become saturated as the streamer length increases. The model GAUSS was used to produce the expected relationship between the most probable length and the ionisation density. This is shown in the form of a plot of $(1 - \frac{L}{L_m} \mathrm{MAX})$ against ionisation density, for delays of 600nsec to 20 μsec, in Figure 7.2. The sensitivity is no greater than that shown by the streamer density but does extend into regions of delay at which the density can not be used, thus allowing the use of minimum delays and hence higher spatial accuracy.

The use of different gas fillings to reduce the ionisation density has been attempted by some workers. Helium and hydrogen offer both a low ionisation and a useful nucleus to use as a target (9). By allowing the electrons to diffuse apart streamers may form on each individual electron and the ionisation measured directly. Komarov et al (10) produced photographable streamers in helium with 15kV/cm pulses of 50nsec half width and in hydrogen with pulses of 20kV/cm for 100nsec. There are problems however, associated with the use of these gases. Firstly the electric fields are large and are usually applied for a long time (100nsec) thus requiring the need for large energy sources for a system of useful volume. This is incompatable with the production of fast rising pulses and easily managed systems. As was found using the 70% neon 30% helium mixture, the helium did tend to be lost through porous materials in the system, and the gas may be more difficult to keep pure than the neon mixture. The third problem is that of the poor emitted light intensity from both helium and hydrogen. Photographable streamers in helium tend to be long and even cross the gap between the electrodes. Falomkin et al (11) made the centres of such streamers more luminous than the rest of the streamer by contaminating the gas with hydrocarbons which reduced the light output from areas of lower electron density than the streamer centre. Image intensifiers can be used (9) but limit the size of such systems because of their poor resolution. In hydrogen, fields up to 40kV/cm

Streamer Generation Model Gauss

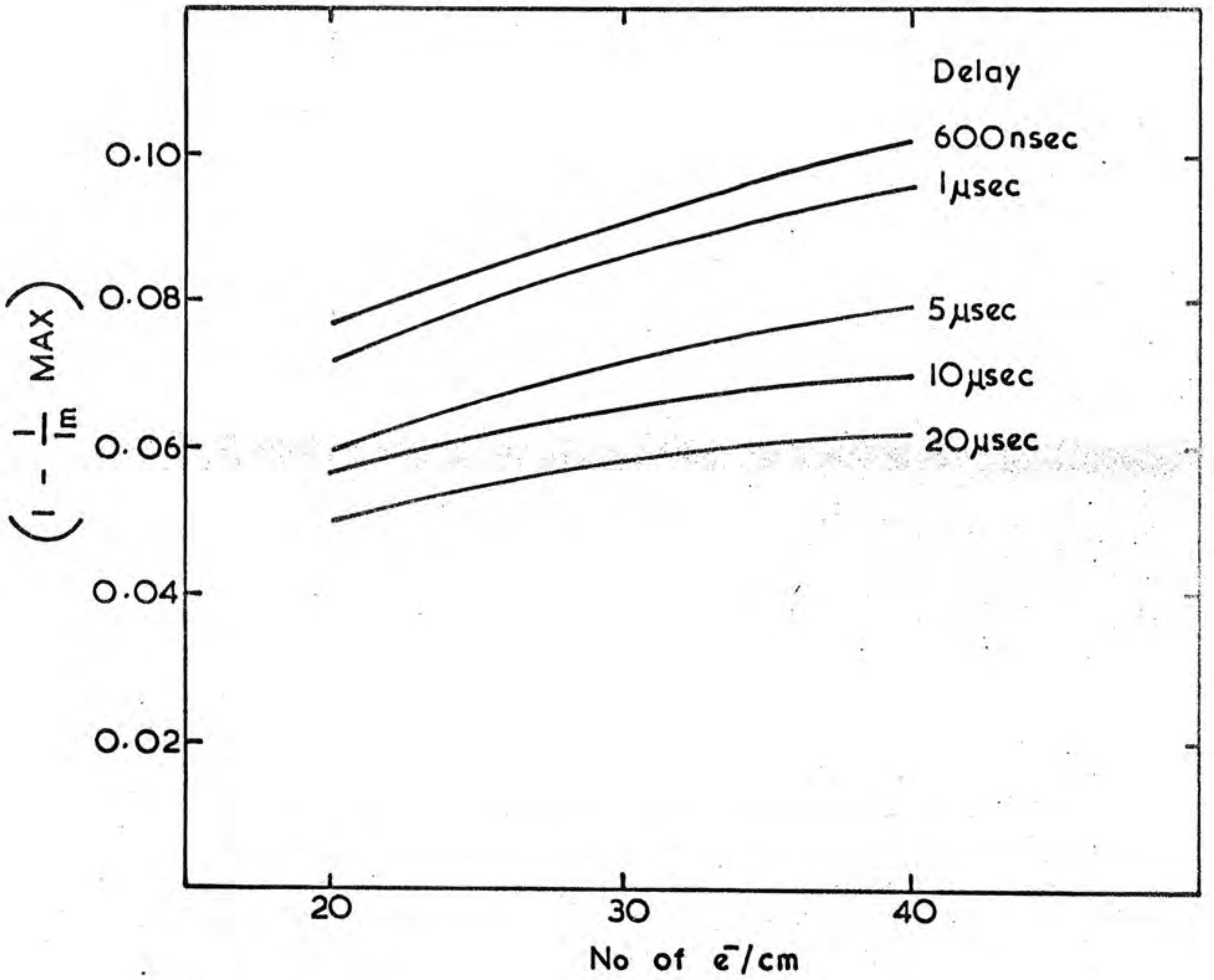

Figure 7.2

have been used with pulses of only 6nsec duration (12) but photographable streamers still crossed the gap. Such intense fields are difficult to produce, particularly in large systems and mixtures of gases may provide a solution. For example helium may be used with the addition of a few percent of neon, sufficient to increase the luminosity of the streamers to the level necessary for photography but not enough to seriously increase the ionisation density in the gas. The second generation streamer chamber described earlier in this chapter would provide the flexibility necessary for such work.

The most probable streamer length also shows a useful sensitivity to the time between the passage of the particle and the application of the high voltage pulse. Such an effect was shown in Figure 6.8 and 6.10 and may be of great use in the study of cosmic rays where the time of arrival of particles is often important. The results obtained here show a possible time resolution of better than 1 μsec for small delays but it was not possible to make a study using delays less than 600nsec because of the inherent delay in the streamer chamber system. There is good agreement between the experimental and the theoretical shape of the curve and so the model output may be used in such regions to predict the chamber's behaviour.

7.7 A Comparison with other detectors

As a means of particle track visualisation, the streamer chamber is a member of the same group of detectors as the bubble and cloud chambers. Its behaviour is largely that of its progenitors however, and the streamer chamber has more in common with the spark and proportional chamber than the bubble chamber, a device it may eventually replace in many regions of nuclear physics.

The basic accuracy of the bubble chamber is greater than that obtained with a streamer chamber. Data analysis programmes such as 'Thresh' give rms deviations in space of 0.1mm for bubble chambers (13) compared with 0.25mm for the streamer chamber (8), for typical 9 point fits to particle tracks. The accuracy of the bubble chamber is limited by the optics as the Airy disc is usually larger than the bubble diameter, whereas in a conventional streamer chamber the dimensions of the streamer themselves are the limiting factor. Image intensifier systems allow the use of much shorter streamers but the rather poor resolution of such devices precludes their use in photographing the size of chambers normally involved in nuclear physics experiments. The bubble chamber also offers better spatial resolution, it being about ten times greater than in a streamer chamber which was shown in chapter five, to be about 0.65cm looking parallel to the field.

For most purposes a separate target, usually liquid hydrogen, is used in a streamer chamber, making the interaction vertex invisible but Meyer (8) reports no difficulty in its reconstruction. Below are compared the typical errors involved in reconstructing such a vertex in a streamer chamber and a liquid hydrogen bubble chamber.

Streamer Chamber	Bubble Chamber
$x = \pm 0.5$mm	$x = \pm 0.04$ to 0.1mm
$y = \pm 0.5$mm	$y = \pm 0.04$ to 0.1mm
$z = \pm 2.0$mm	$z = \pm 0.4$ to 1.0mm

The streamer chamber does escape the multiple scattering found in the liquid filled bubble chambers which can amount to 1% in 80cm for a 1GeV pion and the energy loss in the streamer chamber is typically fifty times less than in the bubble chamber where it is about 20MeV/M. This advantage of the streamer chamber will be less significant at very high energies (300GeV) when both scattering and energy loss in the detector are less important.

Some secondary sources of error which are not found in a streamer chamber are:- the track displacement caused by the fluid motion during the expansion cycle, the effects of thermal convection and the variation of refractive index in the bubble chamber liquid due to turbulence. These are replaced by similar ones in the streamer chamber which are caused by spurious electric fields and the track displacements, caused by the

Meek length shift and prepulses. The former can be controlled to within acceptable limits by careful design of the chambers and the latter can probably be determined accurately enough to be corrected for in calculations.

The result of such effects in determining the masses of particles produced in a hydrogen target in a streamer chamber has been reported by Meyer and the errors on the masses compare well with bubble chamber data. For example:-

Particle	Streamer Chamber	Bubble Chamber
ω	$\Delta M_{\omega} = 35$MeV	20MeV
n	$\Delta M_{n} = 220$MeV	100MeV

In chapter five it was shown that a change in ionisation density from minimum to 1.2minimum ionising could not be detected but the model GAUSS indicates that a change of 30 to 40% should be measurable and the 20% change may just be resolvable if the errors on the measurements can be reduced to about half. These figures are typical of bubble chamber sensitivities to ionisation but the bubble chamber does give about 12 bubbles/cm^{-1} allowing a build up of better staistics than in the streamer chamber where the streamer density is only about 2cm^{-1}. This figure could be improved in the streamer chamber by the use of different gas mixtures involving helium and hydrogen. The streamer chamber does have the advantage of forming its tracks on the electrons produced by the detected particle in a manner which is more direct than in the bubble chamber and greater control over the performance of the device by using techniques traditionally applied to spark chambers is possible.

The sensitive time of a basic streamer chamber is governed by the diffusion of the electrons to the wall of the device and this usually takes about 1msec. Long before this occurs the track becomes too diffuse to be useful and so the maximum useful sensitive time is about 50μsec. This figure may be greatly reduced, by the addition of very small quantities of electronegative gases ($\sim$1ppm) for example SF$_6$, to less than 1μsec. A very high particle flux through the chamber may then be tolerated and the required events can be selected by external counters. An event rate of $2 \times 10^5 sec^{-1}$ in a 10cm liquid hydrogen target is possible but the data acquisition is limited by the camera transport time to about $2sec^{-1}$ which is typical of the repetition rate of current bubble chambers. Work on the SLAC rapid cycling bubble chamber (14) may offer repetition rates of $20sec^{-1}$ and the ultrasonicly driven chamber (15) may offer a kind of continuous sensitivity but the potential data output of the streamer chamber will far exceed this if the ancilliary equipment can be developed sufficiently. The performance of the streamer chamber at high repeition rates is also affected by its memory time which Eckardt has shown in experiments on track storage to be about 10msec (16) but the addition of electronegative gas to the chamber will reduce this to within the desired range.

The time resolution, as distinct from the sensitive time, where the difference in the time of arrival of two particles actually visualised is required has been shown in chapter six to be better than other track devices and is less than 1μsec a factor of 10^3 less than the bubble chamber.

7.8 Conclusion.

The streamer chamber is of similar versatility to the bubble chamber but has several advantages. Perhaps the greatest of these is the cost which, for detectors of equal active volume, is 10 to 100 times less than that of the equivalent bubble chamber. The work in this thesis has demonstrated that streamer chambers, considerably simpler than the typical bubble chamber and even simpler than the first streamer chamber, can be constructed within the material and financial resources of a university department. That such devices have a great future there can be no doubt but perhaps their greatest potential will be in providing research groups, who may not possess a bubble chamber or extensive spark chamber system because of financial limitation, with a sophisticated track detector.

The most rewarding avenues of research on streamer chambers are connected with the development of simpler systems using more advanced techniques and it is suggested that the second generation streamer chamber described earlier in this chapter will make a starting point for such investigations. The yield of secondary information from the device could be improved with a better understanding of streamer formation in various gas mixtures and an investigation of all the major rare gases is recommended. The low Z gases can be used for ionisation measurement and the high Z gases at high or low pressure may be used for X or γ ray conversion.

As to the future, some exciting experiments with Laser induced breakdown,highly localised around the electrons produced by the particle, are proceding (17). In principle the high electric field 1-10MV/cm produced by a pulsed CO_2 laser is used to accelerate the electrons. As the field is oscillating with frequency of 10^{14}Hz the electrons also oscillate about a fixed point and even though the electron density increases by ionisation the radius of the luminous centre is maintained below 100μm. Such a device obviously offers extremely high spatial accuracy and resolution but as yet is at the boundaries of present techniques. The main difficulties are in obtaining the enormous power densities required over a significant volume and in the triggering the system within a small enough time of the passage of the particle.

Such detectors, although highly complex and sophisticated will doubtless provide the solutions to many of tomorrow's problems as the energies of the particles involved in experiments reach 1000GeV and beyond.

REFERENCES

1. SCHLUMBOHM, Z angew Phys. 11 (1959) 156.

2. COOKSON, A.H. and WARD, B.W., Electron Letters, 1 (1965) 83.

3. COOKSON, A.H., Brit, J. Appl. Phys. 17 (1966) 891.

4. SCHLUMBOHM, Z Phys. 151 (1958) 563.

5. LEGLER, W., Z Naturf 16a (1961) 253.

6. BYRNE, J. Proc. Roy. Soc. EDIN 66A (1962) 33.

7. COOKSON, A.H., and LEWIS, T.J., Brit. J. Appl. Phys. 17 (1966) 1473.

8. MEYER, H.,DESY, F1-72/4

9. STETZ. A.W. and PEREZMENDEZ, V. Nuc. Inst. Meth. 73 (1969) 34.

10. KOMAROV, V.I., and SAVCHENKO, O.V., Nuc. Inst. Meth. 34 (1965) 289.

11. FALOMKIN, I.V., Nuc. Inst. Methods 53 (1967) 266.

12. GREY MORGAN, C., CERN TC-L-INST 70-10.

13. Bubble Chamber information, except where otherwise stated is by courtesy of HENP group Durham University.

14. BARNEY, H., Nuc. Inst. Meth. 74(1969) 345.

15. BROWN, R.C.A. and HILKE, H.J., Physics Bulitin 23 (1972) 215.

16. ECKARDT, V., Lettere Al Nuovo Cimento 1 (1971) 997.

17. SCHNEIDER, F. Private Communication.

APPENDIX A

THE SOLUTION OF POISSONS EQUATION BY RELAXATION

The basis of the method is the replacement of the derivatives in the differential equation by finite difference approximations and the subsequent approximate solution of the resulting algebraic equation.

Consider first the simple differential equation

$$\frac{d^2y}{dx^2} + F(x) = 0 \qquad (1)$$

with the two point boundary conditions $y = y_a$ when $x = x_a$ and $y = y_b$ when $x = x_b$ for $a < b$.

It is supposed that $F(x)$ is a function of x known at equally spaced intervals in the region (a,b). The solution in y corresponds to the known values of x.

Consider the region divided into equal intervals of width h and x_3, x_o, x_1 are consecutive points in the region

x increasing

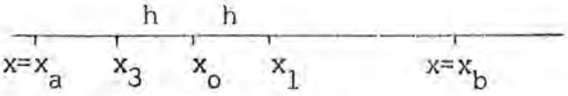

The Taylor expansion in the neighbourhood $x = x_o$ is

$$f(x) = y_o + (x-x_o)\left(\frac{dy}{dx}\right)_o + \frac{(x-x_o)^2}{2!}\left(\frac{d^2y}{dx^2}\right)_o + \ldots$$

Now $\quad x_1 = x_o + h$ and $x_3 = x_o - h$

Let $y = y_1$ when $x = x_1$

and $y = y_3$ when $x = x_3$

$$\therefore \quad y_1 = y_o + (x_1-x_o)\left(\frac{dy}{dx}\right)_o + \frac{(x_1-x_o)^2}{2!}\left(\frac{d^2y}{dx^2}\right)_o + \ldots$$

$$y_3 = y_o + (x_3-x_o)\left(\frac{dy}{dx}\right)_o + \frac{(x_3-x_o)^2}{2!}\left(\frac{d^2y}{dx^2}\right)_o + \ldots$$

$$y_1 = y_o + h\left(\frac{dy}{dx}\right)_o + \frac{h^2}{2!}\left(\frac{d^2y}{dx^2}\right)_o + \frac{h^3}{3!}\left(\frac{d^3y}{dx^3}\right) \ldots \qquad (2)$$

$$y_3 = y_o - h\left(\frac{dy}{dx}\right)_o + \frac{h^2}{2!}\left(\frac{d^2y}{dx^2}\right)_o - \frac{h^3}{3!}\left(\frac{d^3y}{dx^3}\right)_o \cdots \quad (3)$$

Adding 2 and 3 gives

$$y_1 + y_2 = 2y_o + h^2\left(\frac{d^2y}{dx^2}\right)_o + \text{terms in } h^4 \text{ and above}$$

Neglecting these higher order terms we can replace the differential equation (1) in the neighbourhood of $x = x_o$ by the algebraic equation

$$y_1 + y_3 = 2y_o - h^2 F(x_o) \text{ as } \frac{d^2y}{dx^2} = -F(x)$$

$$\text{or} \quad y_1 + y_3 = 2y_o + h^2 F(x_o) = 0 \qquad (4)$$

There is an algebraic equation of the form of(4)at each point of subdivision. Hence we get a set of simultaneous algebraic equations to solve of which equation(4)is typical.

We write $R_o \equiv y_1 + y_3 - 2y_o + h^2 F(x_o)$ is the residual at $x = x_o$.

A unit increment in the value of y at a given point (i.e. y_o) decreases the value of R_o by 2. But R_1 and R_3 each contain the term y_o and each of these residual is increased by 1 due to the increment. Thus for $\Delta y_o = 1$ the effect on the residuals can be represented by the pattern

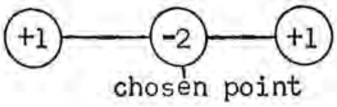

This holds for all points, except the first and the last.

For the first point

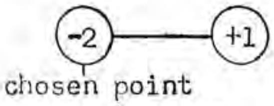

for the last point

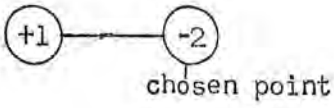

Procedure

a) the range $x = x_a$ to $x = x_b$ is subdivided such that $x_n - x_{n-1} = h$ and the values $y = y_a$ and $y = y_b$ inserted at the end points; quesses are then made for y at each point.

b) Using the guesses the residuals are then calculated for each point.

$$R_o = y_1 + y_3 - 2y_o + h^2F(x)$$

c) After obtaining all the residuals the largest is located and removed by a suitable increment in y at this point $y \approx \frac{\underline{Ro}}{2}$. This increment increases the residual of the neighbouring points by y. The process is thus repeated until the absolute value of the residuals is < 2 and the algerbraic sum of the residuals is ~ 0.

d) The resulting values of y_n are then the approximate solution of the given equation at points x_n.

The above method may be extended to solve Poissons equation in two dimensions

$$\frac{\partial^2 V}{\partial x^2} + \frac{\partial^2 V}{\partial y^2} + F\ (xy) = 0 \qquad (5)$$

with the values of V prescribed on the boundary of a given plane area.

The plane area over which integration is to be performed is subdivided by a uniform network and the values of the required function V are calculated at the nodel points of the network. A square network is usually used.

Let us consider the square network of side h.

We can write a finite difference approximation to equation (5) in terms of the values of V at the points labelled 0, 1,2,3

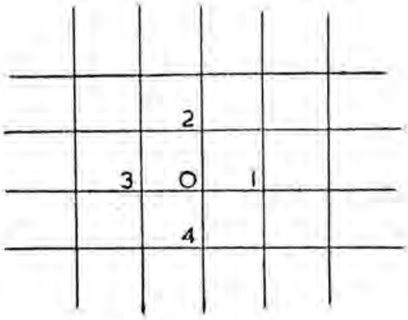

Following 4 we have

$$V_1 + V_3 = 2V_o = h^2 \left(\frac{\partial^2 V}{\partial x^2}\right)_o \text{- 6)}$$

Similarly $V_2 + V_4 - 2V_o = h^2 \left(\frac{\partial^2 V}{\partial y^2}\right)_o \quad \ldots 7)$

Adding -6) and -7) gives

$$\left(\frac{\partial^2 V}{\partial x^2}\right)_o + \left(\frac{\partial^2 V}{\partial y^2}\right)_o = \frac{1}{h^2} \left(V_1 + V_2 + V_3 + V_4 - 4V_o\right) \qquad \ldots (8)$$

This can be written using -5) as

$$V_1 + V_2 + V_3 + V_4 \quad -4V_o + h^2 F\,(x_o y_o) = 0 \qquad \ldots (9)$$

There is a similar equation at each nodel point and we get a set of simultaneous algerbraic equations.

The relaxation pattern for unit increments at each chosen point are thus:-

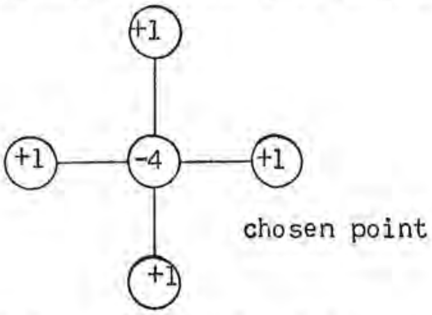

As before the values of V for each nodel point are guessed and their respective residuals calculated. The residual as are then systimatically reduced until they have an absolute magnitude of < 3. When the total of all the residuals is approximately zero and when individual positive and negative residuals are well distributed over the area of integration, the values of V at the nodel points tend towards the solution of the differential equation -5) at those points.

APPENDIX B

ANCILLIARY ELECTRONICS

(a) DP5

The DP5 is a pulse amplifier which generates, on receipt of an EG and G logic signal (-700mV; 50nsec; 50Ω) a 5kV pulse with a rise time of 20nsec and a delay of ~60nsec. The circuit is relatively immune to r.f. interference and the unit now driving the streamer chamber has run reliably for $> 10^6$ pulses.

The basis of the circuit is an avalanche Marx generator (1) (2) and the basic element of the Marx circuit is a 2N2219 transistor wired in the form of an avalanche diode, Figure B.1. About 75% of 2N2219's purchased will operate in this mode hence the transistors must be individually tested before use. If the collector emitter voltage V_{ce}, i.e. the applied voltage plus the input voltage, exceeds 250 volts, then the transistor will avalanche and the capacitor C which has been charged to E via R_1 and R_3, will be in series with the input voltage increasing its height by ~ 100V for $150 < E < 240$. The remainder of the voltage across the capacitor is dropped across the transistor. The time from input signal to output is determined by the quiescent current through the transistor. The nearer this is to that required to produce an avalanche the shorter will be the delay time. However, operating near this point the circuit is very unstable and susceptable to power supply drift and r.f. interference. Resistors R_1, R_2, R_3 are therefore chosen to give a suitable compromise between speed and stability. The average power dissipation depends upon the pulse repetition frequency and upon the value of the energy storage capacitor C. Additional power is dissipated because of the idling current and voltage.

In this circuit 14 such stages are used, Figure B.2. The first stage is base triggered from a low voltage transistor interface. It also has

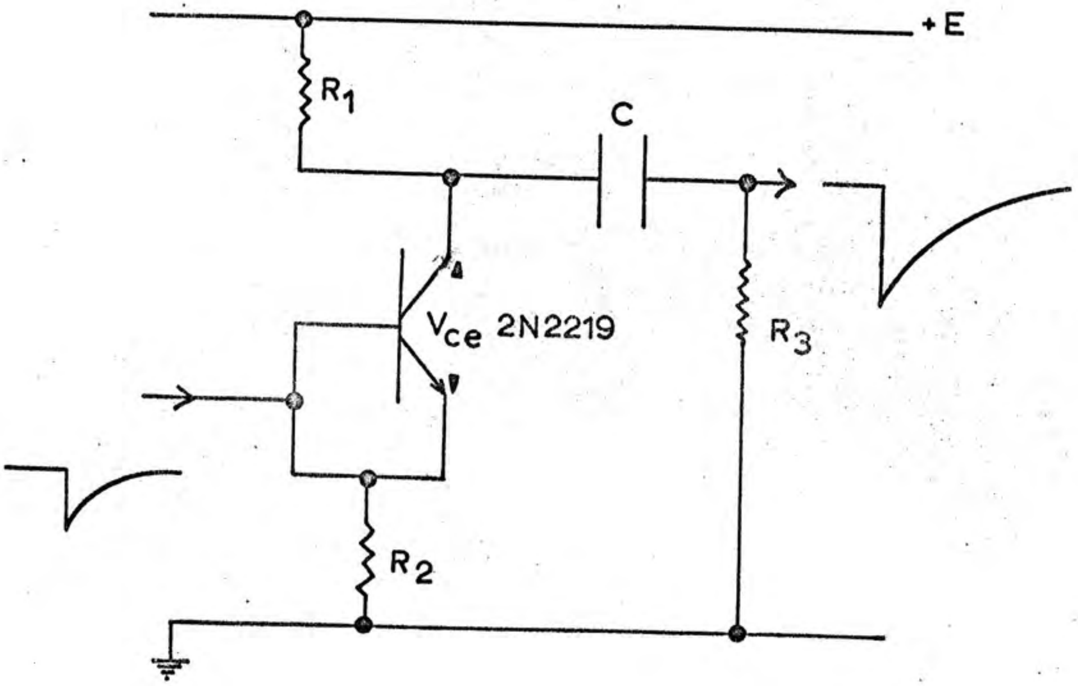

THE BASIC AVALANCHE CIRCUIT

Figure B.1

D.P.5. PULSE AMPLIFIER.

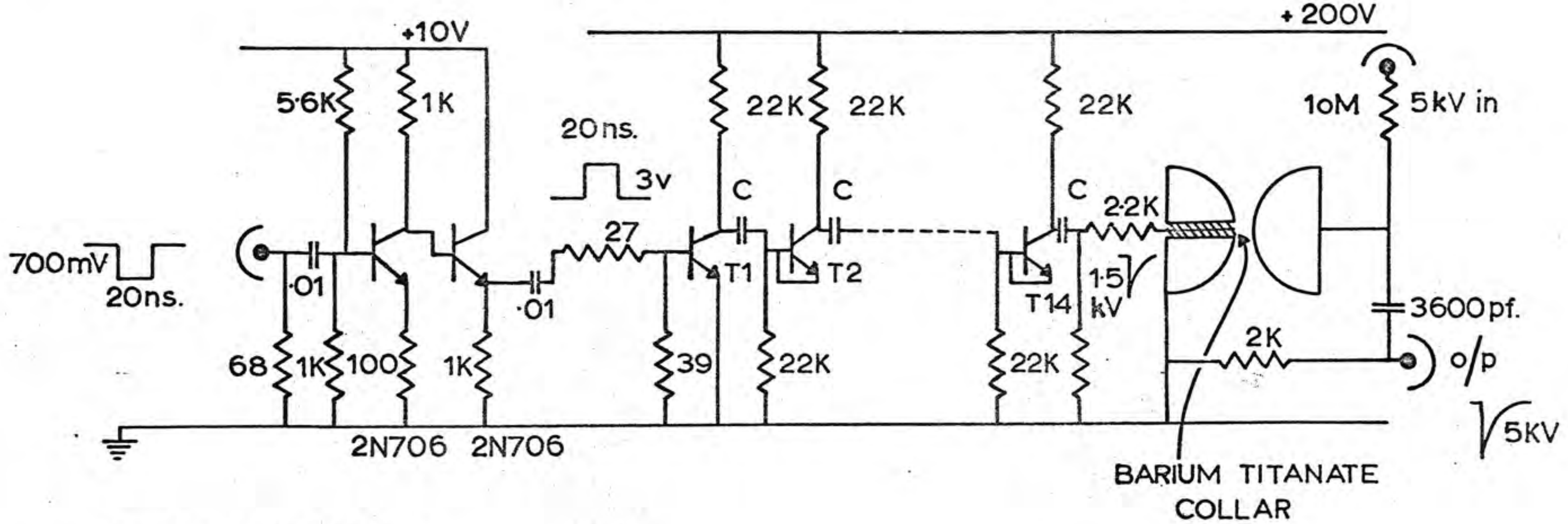

C=560pf. or 3600pf.

Figure B.2

its emitter connected to ground to minimise the resistance in the discharge path. This increases the heat dissipation of this stage and makes the use of a heatsink necessary. The delay between the receipt at the input of a 700mV logic signal and the output at the 14th stage of a 1.5kV pulse is 17nsec. The rise time is 1.5nsec. The rise time and delay are very dependent upon stray reactance and care must be exercised in reducing these quantities.

Amplification from 1.5kV to 5kV is performed by a trigatron spark gap (3). A barium titanate collar surrounds the central tungsten electrode to increase the electric field produced by the 1.5kV pulse at the electrode tip and hence allow operation of the spark gap at low triggering voltages. The output of the spark gap is a 5kV pulse with a rise time of 20nsec and constitutes the output of the DP5. Figure B.3 is an oscillogram of the sum of the input logic signal and the 5kV output pulse, showing its rise time and delay. The operating range of the spark gap is only a few hundred volts Figure B.4 and accurate adjustment of the gap is necessary for reliable operation. The unit is housed in a standard EG and G module which is powered by an M104 type bin wired to give 200 volts for the avalanche transistor circuit. The input interface is powered by the standard +10 volt line from the bin and the 5kV for the spark gap is supplied from an external source through the front panel.

The layout inside the module is designed to minimise back pulses, typically 200mV and self triggering. The spark gap is mounted with its axis on line with transistorised part of the circuit as the radiation from such a spark gap is least in this direction. The input interface is shielded from the rest of the circuit by mounting it in a brass enclosure on the side of the module. All internal connections are by carefully earthed screened cable.

FIGURE B.3

THE DP5 HIGH VOLTAGE PULSER ITS INPUT AND OUTPUT

VERTICAL SENSITIVITY INPUT 500mV/cm
OUTPUT 2kV/cm

HORIZONTAL SENSITIVITY 20nsec/cm

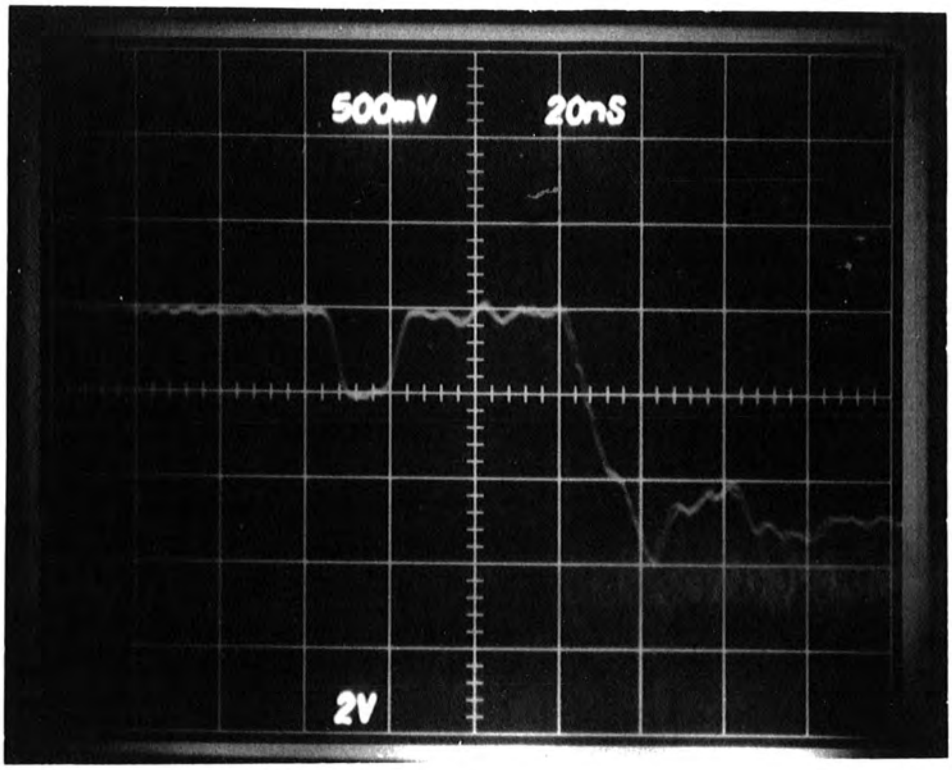
500mV
20nS
2V

DP5 SPARK GAP

WORKING RANGE

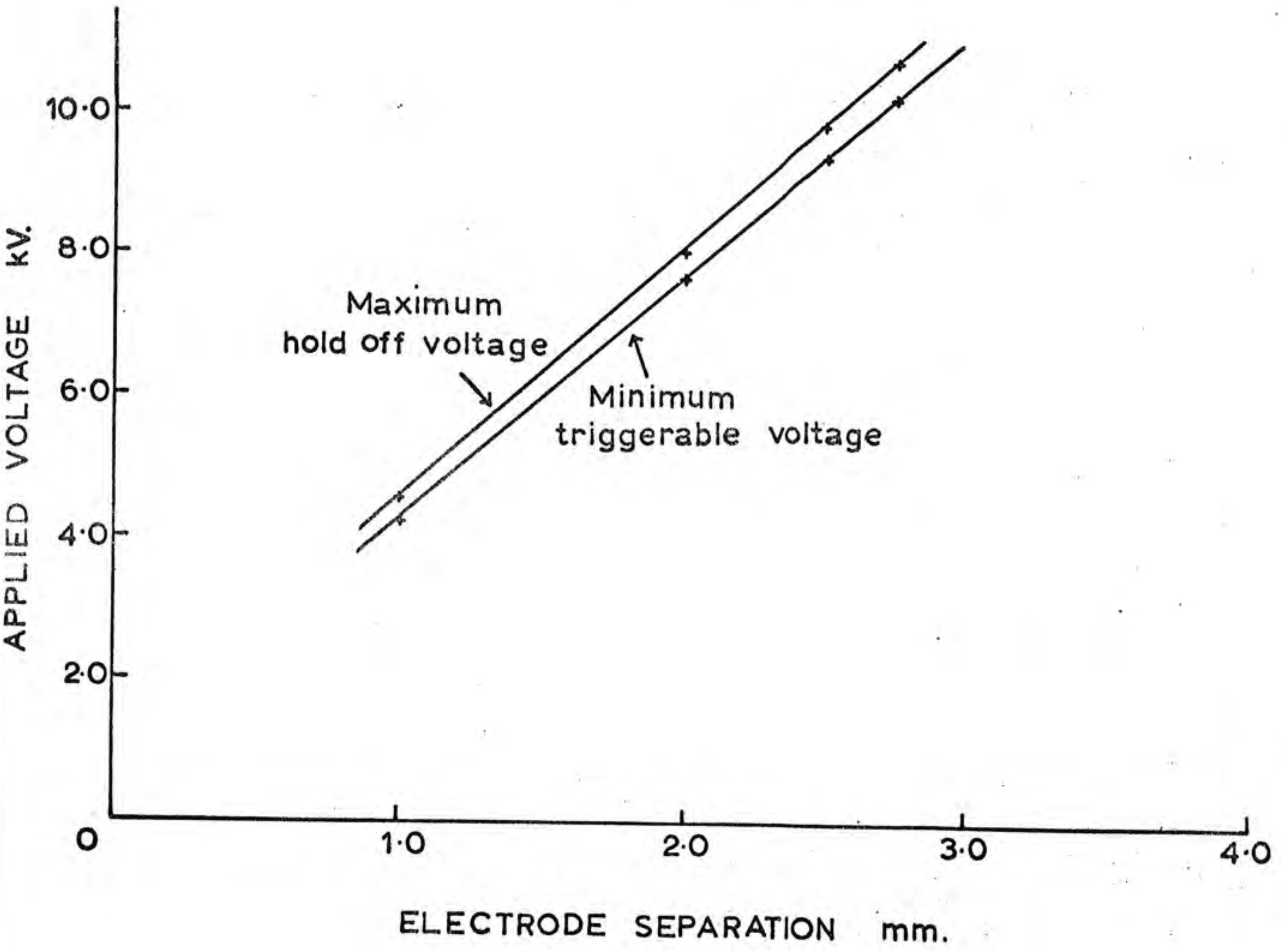

Figure B.4

(b) DG 128 Figure B.5

The DG128 is an EG and G compatible gate generator which produces, on receipt of a logic pulse (-700mV; 10 nsec; 50Ω) a + 20 volt gate of length 0.1 to 15.5 seconds in steps of 0.1, or 1 to 155 seconds in steps of 1.0 or 10 to 1550 seconds in steps of 10. There is a random error of ± 0.0125 seconds, ± 0.125 seconds and ± 1.25 seconds on each range respectively. There is also an error dependent on the accuracy of the clock in the DG128. The clock is a simple astable multivibrator, the tuning capacitors being switchable to give the three time ranges of the device. The basic frequencies are 40, 4 and 0.4 Hz; these can be adjusted by a trimmer potentiometer to within 1%.

The input signal, after amplification by a small transistor interface, sets a latch consisting of two of the NAND gates of an FJH 131. The latch then opens a gate allowing the output from the clock to pass into a ten stage asynchronous binary up counter (FJH 121's). The first two stages of the counter allow the clock frequency to be increased to four times the minimum time period of the device on each range and thence this reduces the starting error to +0.125 of this period.

The duration of the gate pulse is determined by the position of eight double pole, double throw switches. Each is fed by the output of one of the stages of the counter and also by 'one' and 'nought' logic levels. There are two outputs from each switch: one passes directly to one of the inputs of an eight input NAND gate FJH101, the other is inverted before passing to one of the inputs of a similar gate.

When a particular switch is depressed the respective counter output is fed directly to the first NAND gate and a logical 'nought' state to the inverter before the second NAND gate. If a switch is not depressed, then the first NAND gate is fed with the logical 'one' state and the respective counter output is connected to the inverter before the second NAND gate. Thus the first NAND gate will change state when the 'one' states corresponding to the number set by the switches occur and the second NAND gate will

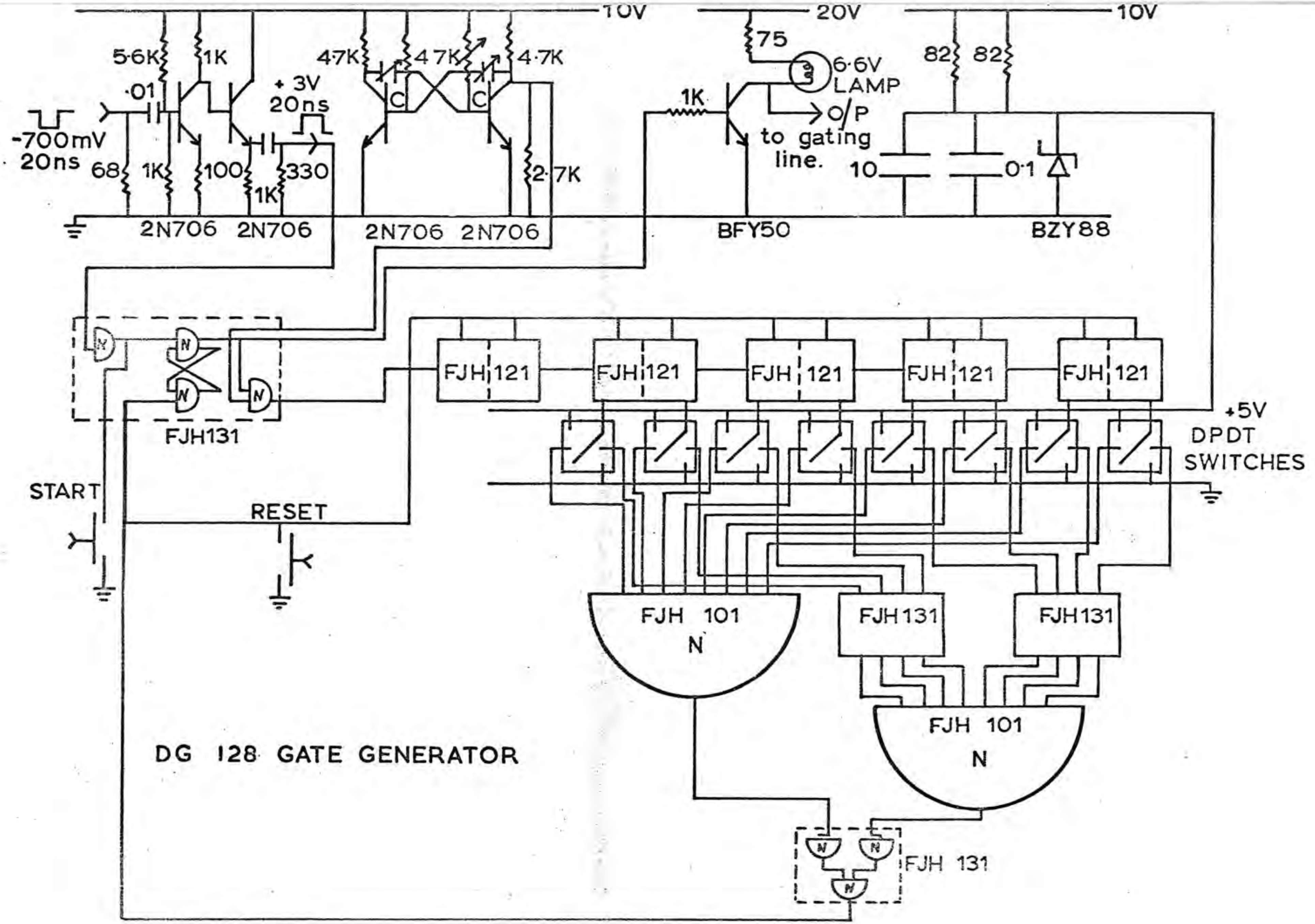
10V
20V
10V
5·6K
1K
·01
-700mV
20ns
68
1K
100
1K
330
+ 3V
20ns
2N706
2N706
47K
47K
4·7K
C
C
2·7K
2N706
2N706
75
6·6V
LAMP
1K
O/P
to gating
line.
BFY50
82
82
10
0·1
BZY88
FJH131
FJH 121
FJH 121
FJH 121
FJH 121
FJH 121
+5V
DPDT
SWITCHES
START
RESET
FJH 101
N
FJH131
FJH131
FJH 101
N
FJH 131
DG 128 GATE GENERATOR

Figure B.5

change state when all the 'noughts' occur. Hence a coincidence in the outputs of the NAND gates indicates that the counter has reached the number set by the switches. This is detected by a further two input NAND gate FJH131, the output of which operates the reset line of the counter and resets the latch, thus disconnecting the clock from the counter. The output from the latch is also amplified to +20 volts and represents the output of the DG 128. A small lamp is also operated by this part of the circuit, indicating when lit, the 'on' state of the gating pulse.

The whole circuit is housed in a standard EG and G module and powered by an M104 bin. The front panel contains the input socket, the timing switches, a start and stop buttons, the lamp and a clock frequency control. The output from the device is on pin 22 of the power socket at the rear of the module.

(c) DCU

The DCU is a self powered EG and G compatible cycling unit which on receipt of logic pulse (-700mV., 10 nsec, 50 Ω) is designed to supply power to six outputs for periods of 0 to 3 seconds at predetermined times during the cycling time of six seconds. The outputs are controlled by microswitches which are closed and opened by preset cams on the shaft of a synchronous motor. The motor is geared to give a shaft speed of 1/6 RPM.

The electronics which controls the motor are shown in Figure B.6 The EG and G logic pulse is amplified and inverted to a level sufficient to drive the first NAND gate of an FJH 131 which is used as a simple pulse shaper. The output from this gate sets a latch consisting of two more of the NAND gates of the FJH131 wired in the form of a flip-flop. The output of the latch which has now gone positive is then amplified by a single BFY50 and switches a relay which supplies power (240v ac) to the motor driving the cams. One of the cams driven microswitches is set to close after one revolution of the shaft and charges a 0.1μF condenser

PHOTOGRAPHIC CYCLING UNIT.

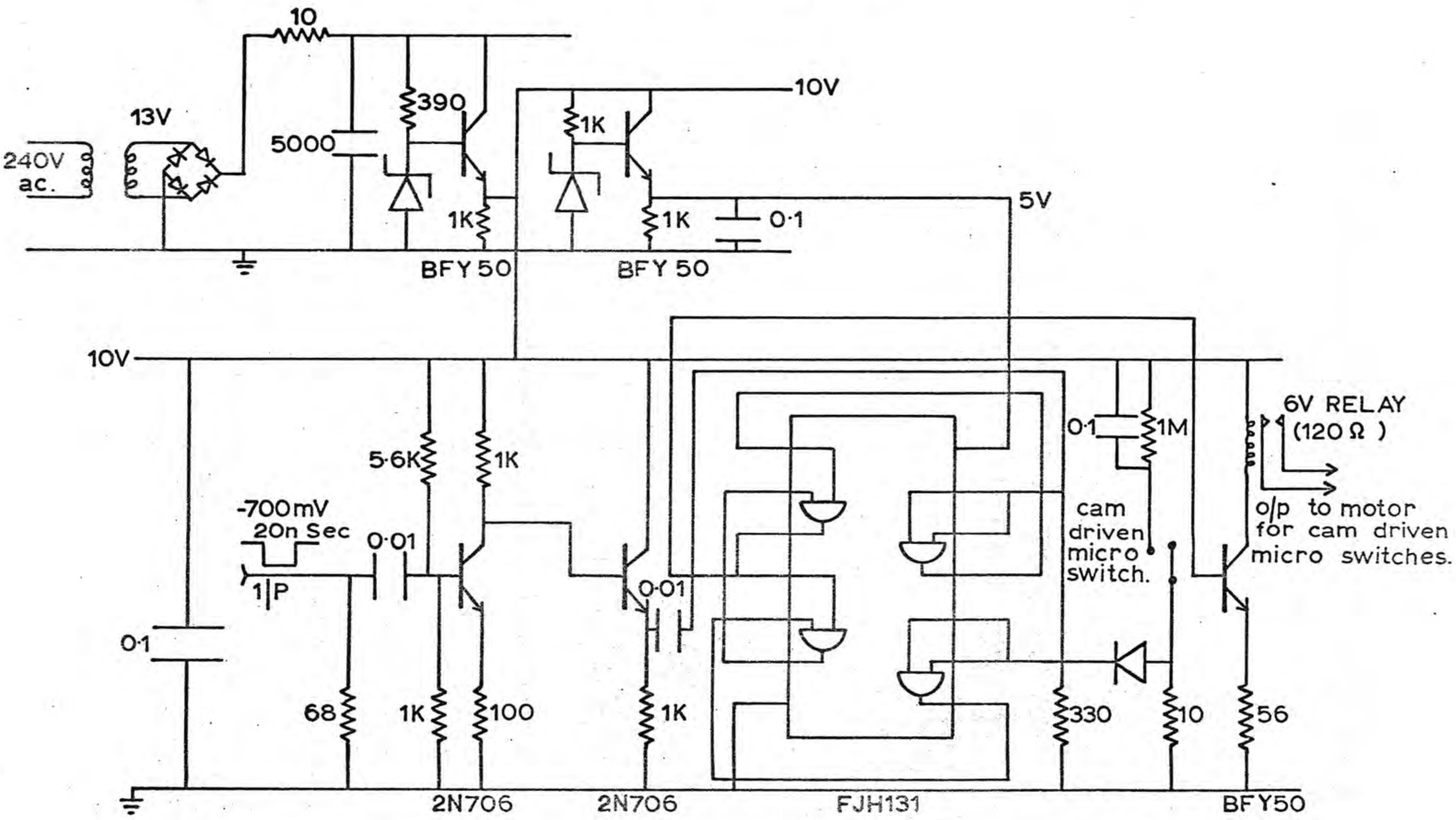

Figure B.6

via a 10 Ω resistor thereby generating a 1μ sec long pulse which, after shaping in the remaining NAND gate of the FJH 131, resets the latch and stops the motor. The motor may then be restarted by a further pulse applied to the input. The 0.1μF condenser then discharges itself via a 1MΩ resistor when the microswitch opens during the following cycle, ready to terminate the cycle again after one revolution. The discharge time constant is made long, 0.1 seconds, to avoid multiple pulsing when the contacts of the microswitch bounce on closure. The five remaining microswitches controlled by the cams are used to switch power in turn to cameras, fiducials, etc. as required. Over-riding buttons are also used to drive each output independently. The two DC voltage levels required by the circuit are 10 V for the transistors and 5V for the IC. These are generated internally by two single transistors zener controlled regulators which are driven by a bridge rectifier. High frequency smoothing is performed by ceramic condensers on all power lines. The whole device is housed in a screened, rack mounted enclosure. The electronics are in a compartment separated from the motor and the microswitches which are a source of switching transients and are individually suppressed by simple RC networks.

Power is supplied through screened cable to the device via a mains interference filter consisting of an LC π network on both the live and neutral lines. These filters are housed in a screened enclosure mounted at the rear. All internal wiring is also screened.

REFERENCES

1. JUNG, E.A., and LEWIS, R.N., Nuc. Inst. Methods 44, (1966) 224.

2. SCHMITT, F., Nuc. Inst. Methods 52 (1967) 1967.

3. SLETTON, A.M. and LEWIS, T.J., IEEE Monograph 193 (1956) 43.

ACKNOWLEDGEMENTS

The author wishes to thank Professor G.D. Rochester FRS for his support for the work and the use of his laboratory facilities, also Professor A.W. Wolfendale for many useful suggestions.

He is indebted to his supervisor Dr. J.M. Breare for his support and guidance, the members of the Nuclear Instrumentation group for their interest in the work and for many hazardous hours helping to operate the system, the technicians of the Physics department, in particular Mr. J. Webster who was always willing to turn his hand to anything, Mr. K.M. Al Hiti for his help in scanning the film, Mrs. D.A. Anson for the typing and Mrs. P. Russell for the diagrams.

He would also like to thank Mr.A.Robertshaw and his colleagues of the International Research and Development Company, Newcastle upon Tyne for making the early chambers and the gas cycling unit and Mr. M. Rousseau of Daresbury NPL for use of the lenses.

He is most grateful to his parents for their help and understanding particularly during the last three years.